UNIVERSITY OF LONDON THESIS

Degree PhD Year 2006 Name of Author BEHESTI, ISFAHANI, Hourinaz

An Analysis of the Regulation of Dorso-Ventral Patterning and T-box Gene Function in Early Eye Development

Hourinaz Behesti Isfahani

A thesis submitted for the degree of Doctor of Philosophy

University of London

2006

Developmental Biology Unit

Institute of Child Health

University College London

London

ProQuest LLC
789 East Eisenhower Parkway
P.O. Box 1346
Ann Arbor, MI 48106-1346

Abstract

Structural eye defects are often caused by aberrant mechanisms during the early stages of eye development. The underlying mechanisms of these defects are currently not fully known. The optic vesicle, which gives rise to the mature eye, is patterned by asymmetrical gene expression. The T-box transcription factors, *Tbx2*, *Tbx3*, and *Tbx5*, which are members of the evolutionarily conserved family of T-box genes, are expressed in the dorsal region of the developing eye. The expression of these genes overlaps with the expression of the secreted signalling factor Bone morphogenetic protein (Bmp) 4. Together, they represent the earliest dorsally expressed genes in the developing mouse eye and are co-expressed in several other vertebrate species. This thesis investigates the regulation of T-box gene expression by *Bmp4* in the developing mouse eye, and the importance of the regional expression of these genes for early eye development.

Bmp4 and Noggin coated bead implantation in combination with whole mouse embryo culture was performed to manipulate Bmp4 signalling during eye morphogenesis. Examination of gene expression revealed that manipulation of Bmp4 signalling alters the expression of the T-box genes as well as the ventrally expressed *Vax2* transcription factor, thus disrupting dorso-ventral (D-V) patterning. These changes resulted in reduced eye size and growth. Cell division was decreased globally and cell death induced in the dorsal neural retina. To directly investigate the role of *Tbx2* in eye development, mice with a targeted mutation of *Tbx2* were analysed, and gain of function experiments were carried out using *in ovo* retroviral gene delivery in the chick embryo. *Tbx2* was selected for further analysis, as it showed the largest change in expression in Bmp4 manipulated eyes. Both strategies resulted in reduced eye size. In the loss of function approach, establishment of the expression of D-V patterning genes occurred in the absence of Tbx2, but the maintenance of the expression of several of these was affected. Within the normal dorsal site of *Tbx2* expression, an increased trend in cell division was detected. Several abnormalities were also found outside of the *Tbx2* expression domain, including delayed formation of the ventral region of the eye, and abnormal lens and hyaloid vasculature defects. These findings suggest that *Tbx2* regulates eye

development both intrinsically and outside of its site of expression and that a Bmp-Tbx2 pathway regulates early growth and coordination of morphogenesis of the developing eye.

Acknowledgements

I am greatly indebted to my supervisor, Dr. Jane Sowden for her supervision throughout the course of my PhD and especially for her friendship. I would also like to thank Dr. Deborah Henderson, my subsidiary supervisor, for her insightful comments and Dr Andy Stoker for reading some of the material in this thesis. Many thanks also go to Professor Tim Cole for his guidance regarding the statistical analysis of data presented here and his patience in explaining ANOVAs and ANCOVAs to me. Thanks must also go to Dr Malcolm Logan and Babis Rallis for teaching me chick retroviral injections and for providing viruses for some of my studies, and to Dr Battersby for providing me with *Fgf15*$^{-/-}$ embryos. I would also like to thank my head of department, Dr. Patrizia Ferretti and the Dean of the Institute of Child Health, Professor Andrew Copp for their support throughout my time in the institute. I am particularly grateful for receiving a Bogue fellowship award to visit the states, and Professor Ginny Papaioannou for having me in her laboratory at Columbia University and for giving me access to the precious *Tbx2*$^{-/-}$ mice. I know their long story! I had such a memorable time in NYC, all owing to the fantastic people in the Papaioannou lab +1, and the fabulous i-house crowd.

Throughout it all, to my friends in the Developmental Biology Unit, the Neural Development Unit, and other parts of the institute, past and present, for their support. In particular, I'm forever indebted to Patimaporn Pungchanchaikul, Adam Swetloff and Noraishah Aziz for their constant encouragement and unconditional friendship, till the last minute of the very last hour. Special thanks also go to Deven Patel and Sofia de Noronha; your friendship has meant a lot. I am also grateful to Mrs Esta Adams, Mrs Diane Vaughn, Ms Katy Gardner, and Mr David Clarke for their kindness and provision of vital material throughout my PhD.

Finally, thank you from the bottom of my heart to my loving family; my dear mother for her patience, understanding, wisdom, and strength, my father for his constant support, though afar, and my brother for always managing to bring a smile to my face. You have been my pillars as always and given me the endless strength and encouragement for the completion of this thesis.

Table of Contents

List of Figures

List of Tables

List of Abbreviations

A	atria
aa	amino acid
AER	apical ectodermal ridge
ANR	anterior neural ridge
AP	alkaline phosphatase
bhh	banded hedgehog
bHLH	basic helix-loop-helix
Bmp	bone morphogenetic protein
Bmpr	bone morphogenetic receptor
bp	base pairs
BrdU	bromodeoxyuridine
BSA	bovine serum albumin
C	caudal
c.f.u	colony forming unit
CDK	cyclin-dependent kinase
CDKI	cyclin-dependent kinase inhibitor
CMV	cytomegalovirus
D	dorsal
D1	dorsal domain 1
D2	dorsal domain 2
DAB	diaminobenzidine tetrahydrochloride
DEPC	diethylpyrocarbonate
dH_2O	distilled H_2O
Di	distal
DIC	differential interference contrast
DIG	digoxigenin
DMEM	Dulbecco's modified Eagle's medium
DMSO	dimethyl sulphoxide
dNTP	deoxyribonucleotide triphosphate
dpc	days post coitum

Dpp	decapentaplegic
D-V	dorso-ventral
E. coli	*Escherichia coli*
EDTA	ethylenediaminetetraacetic acid
EGFP	enhanced green fluorescent protein
ES cell	embryonic stem cell
FCS	fetal calf serum
Fgf	fibroblast growth factor
FITC	fluorescein isothiocyanate
FL	forelimb bud
fl	fluorescein
g	gravity
Gas1	Growth arrest specific gene 1
GFP	green fluorescent protein
GPI	glycosylphosphatidylinositol
GST	glutathione S-transferase
H&E	Haematoxylin and Eosin
HH	Hamburger-Hamilton
Hh	hedgehog
HL	hyaloid vasculature
HNK-1	human natural killer-1
HRP	horseradish peroxidase
IRES	internal ribosomal entry site
kb	kilo bases
kDa	kilo Daltons
Ln	Log_e
MC	monoclonal
Min	Minute
Mitf	Microphthalmia associated transcription factor
M-L	medio-lateral
mm	millimetre
MN	mandibular process of the first branchial arch
msec	millisecond
Msx2	muscle segment homeobox 2

MX	maxillary process of the first branchial arch
N	nasal
NCAM	neural cell adhesion molecule
NE	neuroepithelium
NFL	nerve fibre layer
NP	nasal process
NR	neural retina
N-T	naso-temporal
OC	optic cup
OD	optic disc
od	optical density
OF	optic fissure
omb	optomotor blind
OS	optic stalk
OT.V	otic vesicle
OV	optic vesicle
P	proximal
PBS	phosphate buffered saline
PC	polyclonal
PCR	polymerase chain reaction
P-Di	proximo-distal
PECAM1	platelet endothelial cell adhesion molecule-1
PFA	paraformaldehyde
pH3	phosphorylated histone H3
Pre. RPE	presumptive retinal pigmented epithelium
Pres. NR	presumptive neural retina
R	rostral
RA	retinoic acid
RALDH	retinaldehyde dehydrogenase
RAR	retinoic acid receptor
RCAS	replication-competent avian leukemia virus with long terminal repeat, splice acceptor
RCASBP	replication-competent, avian leukemia virus long terminal repeat, splice acceptor, Bryan high-titre,

	polymerase
RGC	retinal ganglion cell
rhBMP2	recombinant human BMP2
rhBMP4	recombinant human BMP4
RPE	retinal pigmented epithelium
rpm	revolutions per minute
S	somite pairs
SDS	sodium dodecyl sulphate
SE	surface ectoderm
Sec	second
Shh	sonic hedgehog
SS	somite stage
T	temporal
TESPA	3-aminopropyltriethoxysilane
TGFß	transforming growth factor-beta
TUNEL	Tdt-mediated dUTP nick end labelling
TVL	tunica vasculosa lentis
UV	ultra violet
V	ventral
v/v	volume per volume
V3	ventral domain 3
V4	ventral domain 4
w/v	weight per volume

CHAPTER 1 Introduction

The eye develops through a series of interactions between distinct cell types. These give rise to several tissues which must acquire a precise size, shape, and orientation in relation to each other to collectively form the visual organ. Tissue interactions, which give rise to the eye, as well as the visual anatomy and function were already reasonably well-studied by developmental biologists and neuroanatomists half a century ago (Coulombre 1965). The genes and genetic interactions however, that direct tissue growth and interactions, as well as the crucial shaping of the different structures of the eye, remain largely elusive.

Congenital eye defects, which are present at birth and often cause blindness due to structural and/or functional impairment of the eye, are a significant cause of childhood blindness according to the World Health Organisation (www.who.int/blindness/causes). The underlying causes of congenital eye defects may be genetic and/or environmental. In particular, mutations in several genes encoding transcription factors and signalling molecules that are expressed during early eye development have been identified that cause structural congenital eye defects (see Table 1.1). However, the aetiology of these genetic defects are largely unknown. Elucidation of the genetic basis of eye development is therefore of great importance for the understanding of the mechanisms involved in the causation of congenital eye defects.

Visual impairment has devastating effects for children's development and their educational, employment, and social prospects in life (Rahi *et al.* 1999). This realisation has prompted the World Health Organisation's VISION 2020 initiative, which is a global partnership that aims to eliminate preventable blindness by the year 2020 (www.who.int/pbd/blindness/vision_2020/en/). Although the step from identification of genes and mechanisms that cause abnormal eye development to the treatment or prevention of congenital eye defects is today large, better understanding of eye development is necessary, which coupled with the advancement of technology encourages development of treatments or prevention of such defects in the future.

1.1 Overview of eye development and disease

The morphological descriptions that follow are based primarily on current knowledge of the development of the mouse eye, which is the model organism used in the majority of the experiments in this thesis. The corresponding chick and human eye developmental timelines are also given for comparative purposes. When appropriate, mouse eye development is contrasted to that of the chick embryo, which is the second model organism used in this thesis.

1.1.1 Optic cup formation

Three distinct cell types contribute to the formation of the eye: the neural ectoderm, the non-neural ectoderm, and mesenchymal cells, some of which are migrating cranial neural crest cells that originate from the dorsal portion of the neural tube, others originate from the paraxial mesoderm (Coulombre 1965; Gage *et al.* 2005). The morphogenetic processes involved in eye formation are generally believed to be conserved among vertebrate species. Eye formation initiates during neurulation, the process of neural tube formation, from a population of precursor cells situated in the anterior neural plate. The eye precursors extend bilaterally to form the optic pits on either side of the developing forebrain. This process starts on day 22 in human gestation, at 8.5 days post coitus (dpc) in the mouse, and at Hamburger Hamilton (HH) stage 8 in the chick embryo (Larsen 2001; Kaufman 1992; Hamburger and Hamilton 1992). The optic pits continue to extend towards the non-neural surface ectoderm, where they initially form vesicle like structures (Fig. 1.1).

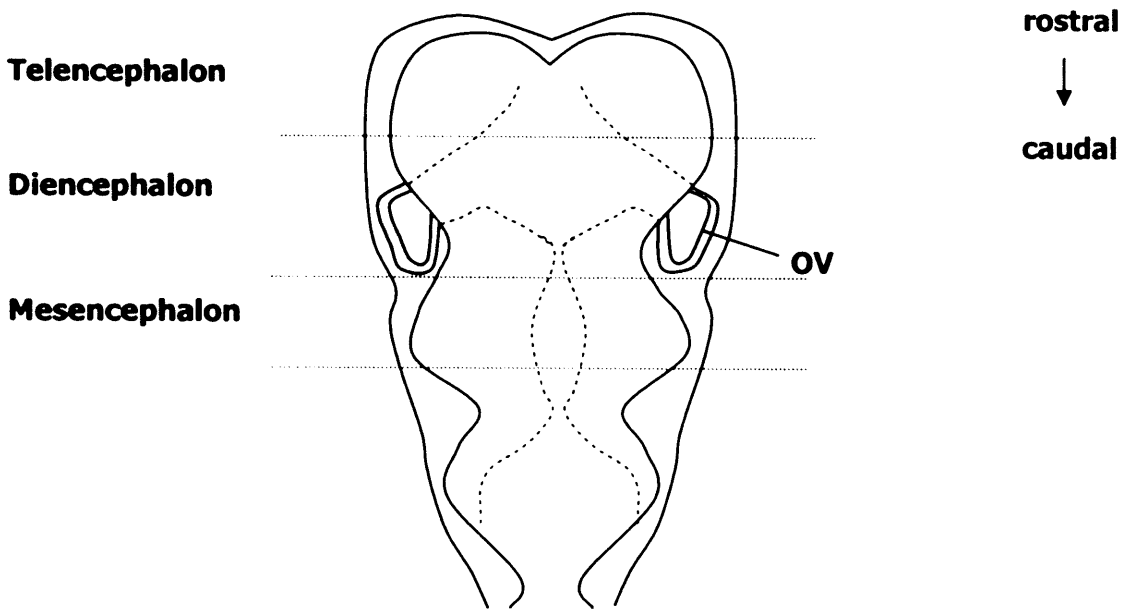

Fig. 1.1 Schematic drawing from a dorsal view of the head of a 9.5 dpc mouse embryo

Schematic shows the optic vesicles (OV) as extensions of the developing forebrain.

Once the optic vesicle has formed (day 24 in human, 9.5 dpc in mouse, HH 10 in chick), invagination into a bilayered optic cup is initiated upon contact with the surface ectoderm (Fig. 1.2). In the rat embryo, a network of collagenous fibrils and cytoplasmic processes have been detected that mediate contact between the surface ectoderm and the neuroepithelium (neural ectoderm) in the optic vesicle (McAvoy 1980). During invagination, the distal region of the optic vesicle, which is in contact with the surface ectoderm, undergoes rapid proliferation, whereby it becomes thicker and forms the neural retina (Fig. 1.2 A,B). The proximal region, which is not in contact with the surface ectoderm, but instead is surrounded by extra-ocular mesenchyme, forms the retinal pigmented epithelium (RPE). The neuroepithelium that connects the invaginating optic vesicle to the ventral developing forebrain, narrows to form the optic stalk (Fig. 1.2 B). Concomitant invagination of the overlying surface ectoderm gives rise to the lens placode (Fig. 1.2 B), a hollow pit, which later separates from the surface ectoderm and fuses to form the lens vesicle (Fig. 1.2 C).

Fig. 1.2 Schematic drawings of mouse eye morphology between 9.5-11.5 dpc

A-C depict sections through the eye along the dorso-ventral axis. D depicts a whole mount view. **(A)** The optic vesicle at 9.5 dpc. The distal layer (Pre.NR) is in touch with the surface ectoderm. **(B)** The invaginating optic cup at 10.5 dpc. The dorsal region is more advanced than the ventral region. The distal layer is thicker than the proximal layer. The lens placode (LP) is undergoing concomitant invagination to give rise to the lens vesicle. **(C)** The optic cup at 11.5 dpc. Both the dorsal and the ventral regions have now invaginated. The lens vesicle is complete, having separated from the surface ectoderm. Dotted line demarcates the distal and the proximal boundaries. **(D)** The optic fissure, a temporary opening in the ventral region of the optic cup, is still present at this stage. The irregular shapes around the developing eye tissues represent mesenchymal cells that surround the eye and invade the vitreous chamber to contribute to the hyaloid vasculature.

Abbreviations: D, dorsal; Di, distal; OS, optic stalk; P, proximal; Pre-NR, presumptive neural retina; Pre-RPE, presumptive RPE; SE, surface ectoderm; V, ventral.

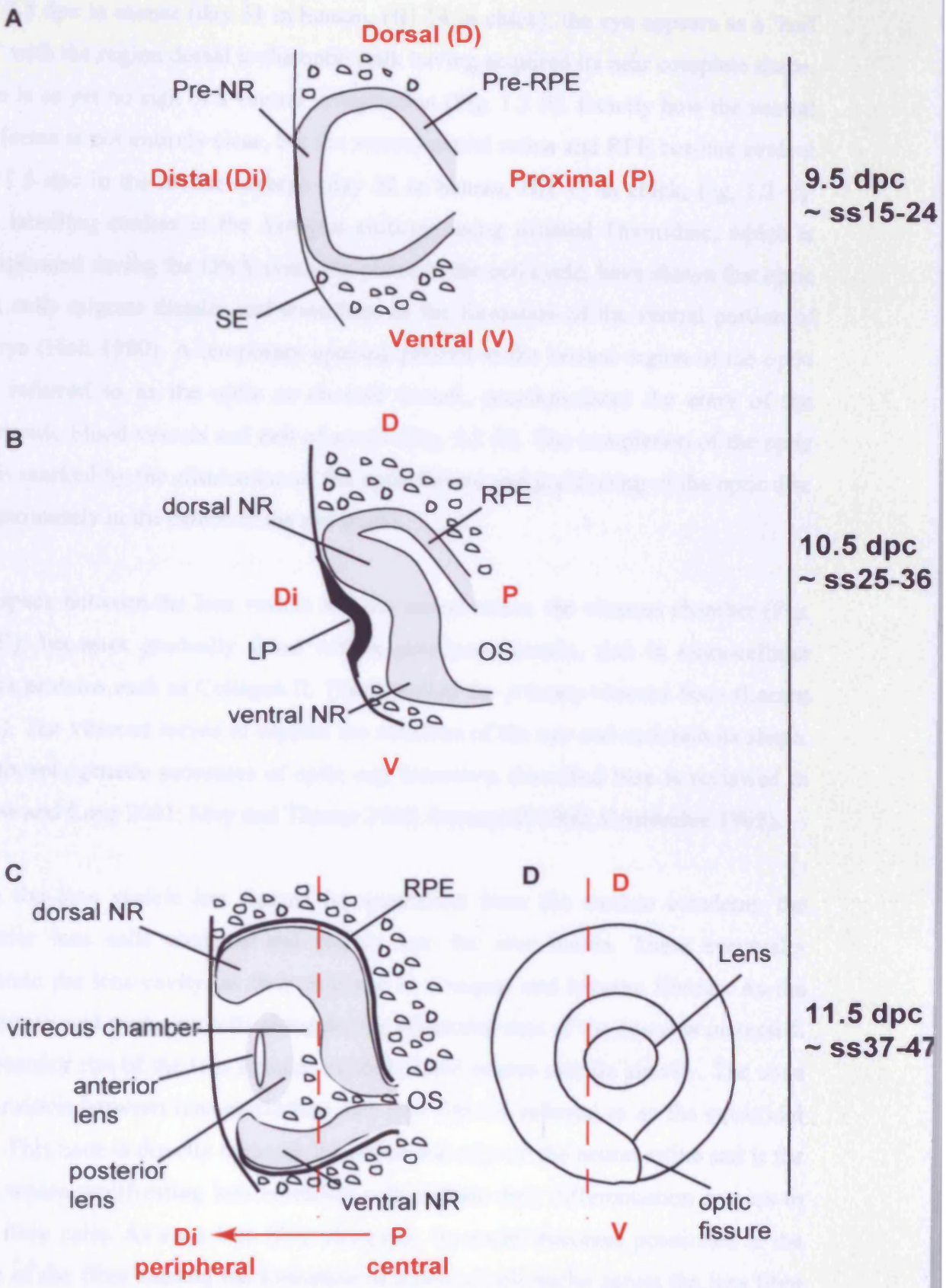
A
Dorsal (D)
Pre-NR
Pre-RPE
Distal (Di)
Proximal (P)
SE
Ventral (V)
9.5 dpc
~ ss15-24
B
D
dorsal NR
RPE
Di
P
LP
OS
ventral NR
V
10.5 dpc
~ ss25-36
C
dorsal NR
RPE
vitreous chamber
anterior
lens
OS
posterior
lens
ventral NR
Di
peripheral
P
central
D
D
Lens
V
optic
fissure
11.5 dpc
~ ss37-47

At 10.5 dpc in mouse (day 31 in human, HH 14 in chick), the eye appears as a 'half cup' with the region dorsal to the optic stalk having acquired its near complete shape; there is as yet no sign of a ventral invagination (Fig. 1.2 B). Exactly how the ventral eye forms is not entirely clear, but the ventral neural retina and RPE become evident by 11.5 dpc in the mouse embryo (day 32 in human, HH 17 in chick; Fig. 1.2 C). Cell labelling studies in the *Xenopus* embryo, using tritiated Thymidine, which is incorporated during the DNA synthesis phase of the cell cycle, have shown that optic stalk cells migrate distally and contribute to the formation of the ventral portion of the eye (Holt 1980). A temporary opening present in the ventral region of the optic cup, referred to as the optic or choroid fissure, accommodates the entry of the embryonic blood vessels and exit of axons (Fig. 1.2 D). The completion of the optic cup is marked by the elimination of the optic fissure and positioning of the optic disc approximately in the centre of the eye globe.

The space between the lens vesicle and the neural retina, the vitreous chamber (Fig. 1.2 C), becomes gradually filled with a gelatinous matrix, rich in extra-cellular matrix proteins such as Collagen II. This is called the primary vitreous body (Larsen 2001). The vitreous serves to support the structure of the eye and maintain its shape. The morphogenetic processes of optic cup formation described here is reviewed in (Chow and Lang 2001; Mey and Thanos 2000; Romanoff 1960; Coulombre 1965).

Once the lens vesicle has formed by separation from the surface ectoderm, the posterior lens cells elongate and project into the lens lumen. These eventually obliterate the lens cavity, as they continue to elongate and become fibrous. As the lens grows and posterior cells elongate, the equatorial axis of the tissue is increased. The anterior rim of the lens remains epithelial and retains mitotic activity. The zone of transition between lens epithelium and lens fibre is referred to as the equatorial zone. This zone is directly opposite the peripheral edge of the neural retina and is the place where proliferating lens epithelial cells initiate their differentiation process to form fibre cells. As each lens fibre elongates, its nuclei becomes positioned at the centre of the fibre causing the formation of a belt of cell nuclei across the lens fibre mass in the posterior lens. As new fibres are added from the equatorial zone, the oldest fibres are found in the centre of the lens. Eventually, the nuclei of these cells

disappear leaving anucleus cells, which is important for the transparency of the developed lens (Coulombre 1965).

Development of the anterior segment of the eye

The anterior segment of the eye which includes the cornea, the iris, the ciliary body, and ciliary muscles, starts to develop after the onset of differentiation of the initial structures of the optic cup. The lens is thought to be important for the development of the anterior segment (Beebe and Coats 2000; Graw 2003). The cornea forms from the surface ectoderm, after lens vesicle formation, and is induced and maintained by the lens and the optic cup (Coulombre 1965), but as the migrating cranial neural crest cells reach the eye, further contributions are made towards the cornea from neural crest derived (and non-neural crest) mesenchymal cells (Gage *et al.* 2005). The iris and the ciliary body serve important functions in facilitating vision. The iris regulates the amount of incoming light into the cup, while the ciliary body is important for supporting the lens and synthesising proteins of the vitreous body, and later in maintaining the intra-ocular pressure. They both form from the peripheral most edges of the neural retina and the RPE, towards the end of gestation, when this region is distinct in terms of gene expression from the rest of the neural retina. The genetic distinction of the peripheral edge of the neural retina has become increasingly well-characterised with the identification of a large number of genes by numerous gene expression studies, most recently using large scale subtractive hybridisation (Kubota *et al.* 2004)

Development of the vasculature that supplies the embryonic eye

During early stages of eye development, at 10.5 dpc in mouse, day 33 of gestation in human, components of the embryonic vascular system of the eye are detected in the optic cup (Schook 1980b). The embryonic vasculature serves to provide the developing eye with nutrients and oxygen during its growth and differentiation before the definitive retinal vasculature has formed in humans and mouse. This vascular network is therefore a transient structure, which regresses postnatally in mouse (Ito and Yoshioka 1999) and around 29 weeks of gestation in humans (Achiron *et al.* 2000), mainly by the process of apoptosis as shown by electron microscopy studies (Mitchell *et al.* 1998; Ito and Yoshioka 1999).

The embryonic vascular system of the eye appears to form by the mechanism of angiogenesis, which involves sprouting and growth of pre-existing vessels (Saint-Geniez and D'Amore 2004). A branch of the ophthalmic artery, which itself is a branch of the internal carotid artery that supplies the head, enters the optic cup through the optic fissure. Here, in the vitreous chamber which is between the lens and the inner layer of the optic cup, the hyaloid artery grows and branches out to form a lattice which fills the vitreous chamber and surrounds the lens. The lattice of vessels that fill the vitreous chamber are called the vasa hyaloidea propria and the capillary network over the lens is referred to as tunica vasculosa lentis (TVL). A fate mapping study in the mouse has shown that both neural crest and mesoderm derived mesenchymal cells that enter the vitreous chamber contribute to the hyaloid vessels by forming pericytes and endothelial cells respectively (Gage *et al.* 2005). A group of congenital defects collectively termed persistent hyperplastic primary vitreous and characterised by the failed regression of the hyaloid vasculature (Reese 1955), have sparked a research interest in the mechanism and molecular control of hyaloid vasculature regression, but less is known about the molecular regulation of the formation of the hyaloid vasculature.

Retinal cell differentiation

Soon after invagination, while some of the anatomical structures of the optic cup are still forming, such as the anterior segment and the hyaloid vasculature, the process of retinal cell differentiation initiates. This is soon after the formation of the optic cup at 11.5 dpc in the mouse embryo (day 47 in human, ~HH 17 in chick; (Graw 2003; McCabe *et al.* 1999; Prada *et al.* 1991). The mature neural retina arises from a population of progenitor cells and is composed of six major types of neurons (retinal ganglion cells, amacrine, horizontal, bipolar, rod, and cone; Fig. 1.3) and one type of glia, Müller glia (Hatakeyama and Kageyama 2004). Each cell type has a specific function and together, they are necessary for the capture of light and transmission of the information to various processing centres in the brain. Upon differentiation of retinal cell types, the retina becomes laminated so that each specific cell type resides within a specific region. The retinal ganglion cells (RGCs) are the projection neurons of the retina which send axons to the brain in a topographic manner.

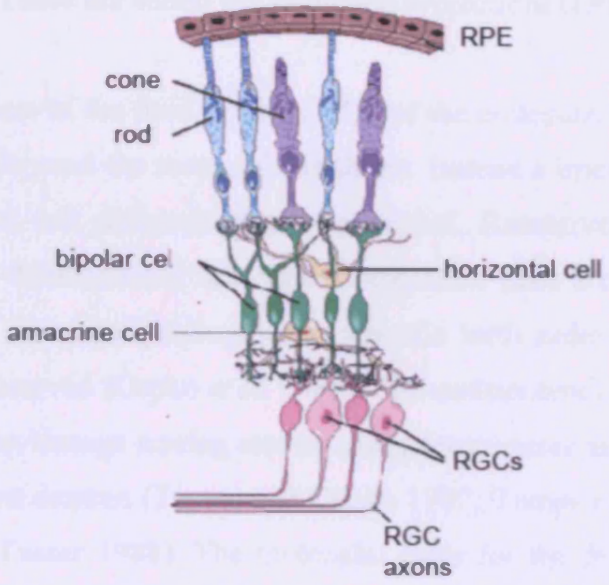

Fig. 1.3 Schematic representation of the six retinal neuronal cell types

The mature neural retina consists of three cellular layers: The rod and cone photoreceptors are in the outer nuclear layer, closest to the RPE on the ventricular side, horizontal, bipolar, amacrine, and Müller glia (not depicted) are in the inner nuclear layer. Retinal ganglion cells (RGC) and displaced amacrine cells (not depicted) reside in the ganglion cell layer on the vitreal side of the neural retina. Abbreviations: RGCs, retinal ganglion cells; RPE, retinal pigmented epithelium. Picture adapted from www.smartdraw.com

In the mouse, the majority of the RGCs from each eye project to the contralateral side of the brain. A small proportion of the projections however, project to the same side of the brain. These are called the ipsilateral projections (Dräger 1985).

An extensive review of the field of knowledge of the molecular control of retinal cell differentiation is beyond the scope of this thesis. Instead a brief overview of the key features of retinal cell differentiation is provided. Extensive research by several laboratories have demonstrated that retinal progenitor cells are multipotent and that the different cell types are produced in a specific birth order which appears to be evolutionarily conserved (Cepko *et al.* 1996). The multipotency of retinal progenitors has been shown by lineage tracing studies using retroviruses and injection of tracers such as fluorescent dextran (Turner and Cepko 1987; Turner *et al.* 1990; Holt *et al.* 1988; Wetts and Fraser 1988). The molecular basis for the genesis of the different cell types within the retina and how the progenitor population of cells in the presumptive neural retina can give rise to such diverse cell types is currently not fully uncovered. However, it is known that a set of basic helix-loop-helix (bHLH) transcriptional repressors maintain progenitors, while bHLH activators promote neuronal differentiation (reviewed by (Hatakeyama and Kageyama 2004). The bHLH factors (e.g. *Math5, NeuroD, Hes1*) regulate neurogenesis in cooperation with various homeobox genes, namely *Pax6*, *Chx10*, *Six3*, *Crx*, *Otx2*, *Prox1*, and *Rax (Rx)*. Many of these genes are expressed by eye precursor cells in the eye field and later by all retinal progenitor cells prior to differentiation. As differentiation proceeds, their expression can be found in distinct laminar layers. Although all these genes appear important for retinal neurogenesis, not one of them is capable of inducing retinal neurons of specific fates by themselves. Rather, a combination of factors are required to generate a specific cell type. Some of them however, can induce ectopic eyes when misexpressed and have collectively been dubbed as the eye specification genes.

The eye specification genes

Genes that belong to this class encode transcription factors, that have several aspects in common. They are expressed in the eye field, at the time when the specification of eye precursors occurs in the anterior neural plate (see Table 1.1 for *Rx, Pax6, Six3, Optx2, Hesx1* and their expression in the mouse). There is evidence for most of them

being able to induce each other's expression when misexpressed, and being able to induce ectopic eyes when misexpressed ectopically in the nervous system in vertebrates, while their homologues in the *Drosophila* fruit fly, do the same when misexpressed in the eye-antennal, as well as other imaginal discs (Chow and Lang 2001; Dominguez and Casares 2005). The imaginal discs in *Drosophila* are the embryonic building blocks which give rise to the different structures of the fly body. The critical role of these genes in eye development is also highlighted by the number of human or mouse mutations that result in severe eye phenotypes, such as the absence or severely reduced eyes (Table 1.1).

1.1.2 Ocular defects that affect the size or the shape of the eye; role of genetics, and known murine and human genes

Focusing of incoming light onto the retina, where it is received requires that all components of the eye are present and have the correct size to collectively function in a synchronous manner (Coulombre 1965).

Congenital eye defects such as microphthalmia (small eye), anophthalmia (no eye), and coloboma (failure of optic fissure closure) arise due to abnormal eye development during embryogenesis, which may include aberrant growth of the ocular primordia (Oyster 1999). The incidences of these defects depend on the population studied (Dolk *et al.* 1998; Gregory-Evans *et al.* 2004), but are relatively low in comparison to other types of visually impairing defects (~1 in 10,000 births). A genetic as well as an environmental basis for these defects have been identified (Graw 2003). They can occur in isolation or in association with other developmental abnormalities, are genetically heterogeneous, and show all three types of inheritance patterns (Gregory-Evans *et al.* 2004).

Several developmentally expressed genes that cause isolated or syndromic cases of microphthalmia, anophthalmia, and coloboma have been identified in humans and mice. Table 1.1 shows some of the genes that cause these defects in humans or in mice when over-expressed or functionally disrupted. These genes are mainly transcription factors or signalling molecules that act at the top of the hierarchy of eye development (Graw 2003). They are all expressed from very early stages of eye

development; some are even expressed as early as the eye field stage. In mouse models that carry mutations of these genes, structural eye abnormalities are evident soon after the onset of the expression of the gene in the majority of cases, suggesting that the defects are due to aberrant development rather than later onset degeneration of a normally developed eye. In addition to the genes listed in Table 1.1, microphthalmia and coloboma can arise due to mutations in genes that are primarily expressed in the lens vesicle (Graw 2003). However, the specific mechanism(s) by which these genes cause eye defects, when mutated, and how they may regulate eye development and growth normally, is currently poorly understood.

Other congenital eye defects with a genetic basis, which are less severe in terms of affecting the structure of the eye, include anterior segment defects (ASDs) such as aniridia (absence or reduced iris), Peter's anomaly (corneal opacity often involving adhesion of the cornea to the lens), cataract (clouding of the lens), as well as conditions affecting the nerve fibre layer such as optic nerve hypoplasia and glaucoma.

Table 1.1: Genes that cause microphthalmia, anophthalmia or coloboma in humans and/or mice

Gene	9.5-11.5 dpc expression in mouse	Human/mouse phenotype	References
PAX6	Eye field, OV, SE, OS, OC, lens	*Heterozygous*: aniridia in human and mouse, macular hypoplasia in human, *small eye* in mouse. *Homozygous*: anophthalmia and failure of nasal tissue formation, onset of lethality soon after birth.	(Walther and Gruss 1991; Inoue *et al.* 2000; Grindley *et al.* 1995; Hill *et al.* 1991; Glaser *et al.* 1992; Jordan *et al.* 1992)
SIX3	Eye field, OV, SE, NR, lens, OS	*Heterozygous*: microphthalmia, and iris coloboma associated with holoprosencephaly in humans. Mice are normal. *Homozygous*: absence of forebrain including eyes in mice.	(Oliver *et al.* 1995; Wallis *et al.* 1999; Lagutin *et al.* 2003)
RX (RAX)	Eye field, OV, NR	*Heterozygous*: no phenotype. *Homozygous*: anophthalmia in humans and mice.	(Furukawa *et al.* 1997; Mathers *et al.* 1997; Voronina *et al.* 2004)
SIX6 (Optx2; Six9)	presumptive ventral forebrain, ventral OV, OS, NR	*Hemizygous:* anophthalmia with optic nerve and chiasm defects in humans. *Heterozygous:* microphthalmia with cataract and nystagmus in humans. *Homozygous:* variable expressivity of retinal hypoplasia, analysed at P35, and absence of optic nerve and chiasm in mice.	(Jean *et al.* 1999; López-Ríos *et al.* 1999; Toy and Sundin 1999; Gallardo *et al.* 1999; Gallardo *et al.* 2004; Li *et al.* 2002)
Hes1 (Hry)	Eye field, OV, SE, OS, NR, RPE, lens	*Heterozygous:* Some indications of a dosage effect, particularly in the early onset of differentiation of retinal neurons has been reported in mice, although specific details of the structure of the eye was not reported. *Homozygous:* microphthalmia with lens and corneal abnormalities in mice. No human mutations identified to date.	(Lee *et al.* 2005; Tomita *et al.* 1996; Lee *et al.* 2005)
SOX2	SE, OV, NR, lens, OS	*Heterozygous:* anophthalmia in humans. No eye phenotype reported in mice. *Homozygous:* pre-implantation lethal in mice.	(Kamachi *et al.* 1998; Furuta and Hogan 1998; Avilion *et al.* 2003; Fantes *et al.* 2003)
HESX1 (Rpx)	Anterior neural plate	*Heterozygous:* mild septo-optic dysplasia in humans, which is characterised by forebrain, midline and pituitary abnormalities. *Homozygous:* septo-optic dysplasia in humans. In mice, microphthalmia and anophthalmia are detected in addition to the human phenotypes.	(Thomas and Beddington 1996; Dattani *et al.* 1998; Thomas *et al.* 2001)
SHH	Prechordal plate, ventral forebrain	*Heterozygous:* holoprosencephaly which can involve anophthalmia, microphthalmia and coloboma, and colobomatous microphthalmia identified in humans. No phenotype in mice. *Homozygous:* cyclopia in mice.	(Echelard *et al.* 1993; Roessler *et al.* 1996; Schimmenti *et al.* 2003; Chiang *et al.* 1996; Furimsky and Wallace 2005)
BMP4	Dorso-distal OV, SE, dorsal NR, extra-ocular mesenchyme, OS	*Heterozygous*: microphthalmia, optic nerve hypoplasia, a range of ASDs and PHPV in mice. No mutations identified in humans. *Homozygous*: embryonic lethal and failure of lens induction in mice.	(Furuta and Hogan 1998; Dudley and Robertson 1997; Dunn *et al.* 1997; Chang *et al.* 2001)
BMP7	Proximal OV, SE, OS, RPE, extra-ocular mesenchyme	*Homozygous*: anophthalmia at birth in mice, though OC forms initially. No mutations identified in humans	(Dudley and Robertson 1997; Godin *et al.* 1998; Dudley *et al.* 1995; Luo *et al.* 1995)

MSX2 (Hox8, Hox8.1)	OV, SE, dorsal NR and lens placode	Transgenic mice that over-express *Msx2* under its own promoter display microphthalmia. Gain and loss of function mutations in humans have been reported in patients with skull malformations and craniosynostosis, but not eye defects.	(Monaghan *et al.* 1991; Wu *et al.* 2003; Wuyts *et al.* 2000; Wilkie *et al.* 2000)
OTX2	OV, RPE	*Heterozygous:* anophthalmia, microphthalmia, and coloboma in humans. Craniofacial malformation in mice. *Homozygous* lack of forebrain/midbrain in mice.	(Simeone *et al.* 1993; Ragge *et al.* 2005; Ang *et al.* 1996; Matsuo *et al.* 1995)
MITF	OV, RPE	*Heterozygous*: Waardenburg syndrome type II associated with hearing loss and pigmentation defects, including that of the eyes, in humans. *Homozygous*: microphthalmia and pigmentation defects in mice.	(Hodgkinson *et al.* 1993; Steingrimsson *et al.* 1994; Nguyen and Arnheiter 2000; Tassabehji *et al.* 1994)
CHX10	OV, NR	*Homozygous*: microphthalmia and cataracts in humans. Microphthalmia and absence of the optic nerve in mice.	(Liu *et al.* 1994; Burmeister *et al.* 1996; Ferda Percin *et al.* 2000; Bar-Yosef *et al.* 2004)
Cx43 (Connexin43; Connexin α; GJA1)	OV, SE, RPE, lens	Heterozygous: oculo-dento-digital syndrome which is associated with microphthalmia, cataracts, and iris abnormalities in humans. *Homozygous*: a 3 bp homozygous duplication reported in a oculo-dento-digital syndrome patient. No eye phenotype in mice.	(Yancey *et al.* 1992; White *et al.* 2001; Paznekas *et al.* 2003; Kjaer *et al.* 2004; Vitiello *et al.* 2005)
Vax1	Ventral OV, ventral NR (briefly) ; OS	*Homozygous*: coloboma and optic nerve dysgenesis as well as variable craniofacial and basal telencephalic defects in mice. No human mutations identified to date.	(Mui *et al.* 2005; Hallonet *et al.* 1999; Bertuzzi *et al.* 1999)
Vax2	Ventral OV, ventral NR	*Homozygous*: coloboma depending on genetic background and abnormal retinocollicular projections in mice. No human mutations identified to date.	(Mui *et al.* 2005; Barbeiri *et al.* 2002; Mui *et al.* 2002)
PAX2	Ventral OV, ventral NR; OS	*Heterozygous:* renal-coloboma syndrome, associated with microphthalmia in some cases in humans. *Homozygous*: coloboma, abnormal optic nerve development and lack of contralateral optic nerve fibre projections in mice.	(Nornes *et al.* 1990; Torres *et al.* 1996; Eccles and Schimmenti 1999)
Gas1	Dorsal OV, SE, NR, RPE, lens	*Homozygous*: microphthalmia with lens and corneal abnormalities in mice. No human mutations reported to date.	(Lee *et al.* 2001a)
Lhx2 (Ap, Lh2, Lh2A)	OV, NR, OS	*Homozygous*: anophthalmia in mice. No human mutations identified to date.	(Porter *et al.* 1997)
Bf1 (Foxg1; Hfh9, Hfhbf1)	Nasal OV,	*Homozygous:* coloboma, reduction or absence of the OS, and small lens in mice. No human mutations identified to date.	(Hatini *et al.* 1994; Huh *et al.* 1999)

The mouse phenotypes are a result of targeted loss of function mutations or naturally occurring mutations in genes.
Abbreviations: ASDs: anterior segment defects; NR, neural retina; OC, optic cup; OS, optic stalk; OV, optic vesicle; P, postnatal day; RGC, retinal ganglion cell; RPE, retinal pigmented epithelium; SE, surface ectoderm.

Apart from the severe structural eye defects described earlier, more subtle alterations in eye size and shape can also have an impact on vision. For optimal perception of visual input, the axial length of the eye and the power of its optics, which include the cornea and the lens, controlled by the ciliary muscles, must correlate well (Coulombre 1965). Abnormal size or shape of the retina, or of the lens or the cornea, will compromise focusing of images onto the retina, resulting in myopia (short-sightedness) or hyperopia (long-sightedness). Myopia occurs when the focused image falls in front of the retina, while hyperopia occurs when the image is focused behind the retina. An elongation of 1 mm without other compensation results in a myopia of -2 to -2.5 diopters (Jacobi *et al.* 2005). This suggests that even slight differences in eye size and shape have a major impact on human visual acuity. A diopter is a unit of measurement of the optical power of the lens that is used to correct for a refractive error.

Various epidemiological studies have provided evidence which suggest a contribution to the development of myopia by visual factors such as intensive reading (Wallman and Winawer 2004). A genetic basis has however also been recognised (Jacobi *et al.* 2005; Wallman and Winawer 2004; Mutti *et al.* 2002). Although several chromosomal loci for pathological or juvenile-onset myopia have been identified by genetic linkage studies, to date, no particular gene has been identified. A genome-wide linkage study in a cohort of dizygotic twins identified strong linkage to the 3' region of the *PAX6* gene (Hammond *et al.* 2004). Another study has reported mutations in *MFRP*, which encodes a protein related to the Wnt receptor frizzled, in patients with extreme hyperopia (Sundin *et al.* 2005). It has been suggested that mutations in genes important for embryonic growth of the eye may also influence growth postnatally (Manson *et al.* 2005). Currently, little is known about the identity of genes that regulate eye shape and if developmentally expressed genes can have an impact on the shape of the adult eye.

Although rare in occurrence, microphthalmia, anophthalmia, and coloboma are the most severe forms of structural eye defects and a cause of childhood blindness. It is therefore of interest to identify the specific genes and mutations that cause these defects and to investigate the mechanisms at the cellular and tissue levels that are

perturbed by such mutations. To do this, it is essential to understand how these genes normally regulate eye development and to characterise the cellular mechanisms that are impaired.

1.1.3 Mechanisms affecting eye size

Eye size is dependent upon several developmental events at the cellular level. It is dependent on the number of neural progenitor cells that are initially specified to form the optic vesicle. Evidence for this is provided by manipulations of eye field transcription factors, which define the progenitor population in the anterior region of the developing forebrain. For example, over-expression of, *XOptx2 (Six6),* one of the genes expressed in the eye field, in *Xenopus* embryos induces the formation of abnormally large eyes by increasing the eye field progenitor population shown by enlarged domains of expression of *Rx1* and *Pax6* on the injected side and by increased proliferation of these cells (Zuber *et al.* 1999). These experiments also demonstrate the role of cell proliferation in the control of the size of the eye. An example where a change in cell fate alone results in an abnormally large eye, is when the *Rx1 or Rx2* genes of zebrafish are misexpressed. Misexpression of either induces eye formation at the expense of forebrain tissue (Chang Chuang and Raymond 2001).

Cell death as well as differentiation are two other mechanisms that if perturbed can cause changes in the size of a tissue. For example, the microphthalmia observed in *Hes1* mutants is at least partly due to premature neuronal cell differentiation at 9.5 dpc when the optic vesicles have not yet invaginated (Lee *et al.* 2005).

The major role of early expressed genes in controlling growth and development of the eye, is highlighted by the type of disease causing genes in Table 1.1. Currently, many genes have been identified that are expressed in the eye, the function of some have been well-characterised, but the overall picture of how the genes fit into the network that controls formation of the eye is far from complete. Interestingly, over the past decade, genes with an asymmetrical expression pattern have been identified in the eye. This suggests that the eye, like the rest of the developing nervous system, is a highly patterned structure and may possess regional developmental programs acting synchronously to drive its development. In other parts of the nervous system

such as the spinal cord, the significance of patterning is more apparent and much more is known about the regulation and outcome of patterning by distinct gene expression domains. In contrast, the structure of the eye, apart from the well-studied requirement of positional information for topographic mapping of RGC axons to the brain, offers little clues as to why distinct gene expression domains are needed, as it does not display profound spatial differences once fully formed. The significance of patterning is addressed in a later section, but first, the genes that display asymmetrical expression in the eye must be introduced. This description is mainly focused on patterning along one of the axes of the eye, the dorso-ventral (D-V) axis, which is the one investigated in this thesis.

1.2 Molecular patterning and regionalisation of the eye

The eye is patterned by localised gene expression along the three main axes of the embryonic body plan. These are the anterio-posterior, the D-V, and the proximo-distal (P-Di) axes. Although initially in line with the main body plan, due to the rotation of the embryo during gastrulation, these axes apply mainly to the developing eye. For example, the anterio-posterior body axis becomes the naso-temporal (N-T) axis of the eye. These are indicated in Fig. 1.2 in schematic drawings of the developing eye as it invaginates.

The first sign of patterning is along the P-Di axis with the specification of the neural retina versus the RPE in the optic vesicle. This event is first obvious in terms of differential gene expression in the proximal versus the distal layer of the optic vesicle, as will be described in more detail in section 1.2.1, and later by the differentiation of the pigmented cells of the RPE and thickening of the neural retina. Transplantation experiments, performed in the chick embryo, have suggested that the N-T and the D-V axes of the eye are also established at optic vesicle stage and during the period of optic vesicle invagination respectively, prior to retinal cell differentiation (Dütting and Thanos 1995; Uemonsa *et al.* 2002). The N-T axis is thought to be determined prior to the D-V axis. When optic vesicles are transplanted in reverse along the D-V axis *in ovo* at ss 8, by the removal of the optic vesicle including the surface ectoderm and surrounding mesenchyme from a donor embryo and placement of it in the reverse orientation along the D-V axis into a cavity created

in a host embryo, the eye develops properly and expresses characteristic markers of the dorsal and ventral neural retina in the correct place with respect to the host axes (Uemonsa *et al.* 2002). Transplantations performed after ss 14 (HH 11) show that the optic cup forms properly but in the reverse orientation to the newly acquired plane with the optic fissure forming in the dorsal region (Uemonsa *et al.* 2002). This suggests that the D-V axis is specified some time between ss 8-14 and prior to optic cup invagination, which occurs at HH 14. Others have shown that the D-V axis can be re-specified according to the host environment up to HH 13 (Goldberg 1976).

Interestingly, although explant cultures are not ideal for examination of eye shape, optic vesicles truncated at ss 10 (HH 10), when the axes may not be established, and cultured for 2-3 days develop round-shaped optic cups, while those explanted at ss 14-17 (HH 11-12) developed oval-shaped optic cups, suggesting that optic cup shape may be linked to the correct establishment of D-V polarity (Uemonsa *et al.* 2002).

The question then arises as to which genes are involved in the molecular regulation of patterning of these axes. Many candidates have been identified based on asymmetrical expression patterns, mostly at RNA level. Some have been experimentally proven to induce profound changes on eye development, by loss of function and/or gain of function studies. For the purpose of this thesis, I will mostly focus on the evidence in the chick and the mouse model systems.

1.2.1 Neural retina versus RPE specification

At optic vesicle stage, the distal and proximal layers of the optic vesicle are equally thin in morphology but by 10.5 dpc in the mouse embryo, when invagination is underway, these layers become morphologically distinct with the distal layer becoming thicker in appearance in comparison to the proximal layer. Pigmentation of the proximal layer becomes apparent shortly after; it is initiated dorsally and spreads ventrally (Robinson 1991). Prior to any morphological manifestations however, the distal region of the optic vesicle becomes specified to form the future neural retina and the proximal region becomes fated towards RPE formation by differential gene expression.

Several signalling molecules and transcription factors have been identified, which are involved in this event. *Microphthalmia associated transcription factor* (*Mitf*) in the mouse, but not in the chick embryo, is initially expressed in the entire optic vesicle and later becomes restricted to the proximal layer (Nguyen and Arnheiter 2000). In the chick embryo, it is detected proximally from the onset of its expression (Mochii *et al.* 1998). The retraction of *Mitf*, in mice, and the induction of neural retinal fate in the distal layer have been attributed to the effect of secreted factors from the surface ectoderm and the extra-ocular mesenchyme. Removal of the surface ectoderm results in a mosaic appearance of intermingled neural retina and RPE cells (Hyer *et al.* 1998). Conversely, signals from the extra-ocular mesenchyme upregulate *Mitf* expression, while repressing neural retina specific genes including *Chx10* (Fuhrmann *et al.* 2000).

Members of the fibroblast growth factor (FGF) family of signalling molecules, which are expressed in the surface ectoderm overlying the optic vesicle, have been shown to possess neural retina inducing abilities. Although *Fgf1* and *Fgf2* compound mutants do not exhibit eye abnormalities (Miller *et al.* 2000), FGF1/2 treatment of the optic vesicle or newly formed RPE, induces the formation of a neural retina instead of the RPE (Zhao *et al.* 1995; Pittack *et al.* 1997; Hyer *et al.* 1998). Furthermore, misexpression of either *Fgf9*, which is normally expressed in the neural retina, in the presumptive RPE region under the regulation of the *Tyrp1* RPE specific promoter, induces the formation of an ectopic neural retina in place of the RPE (Zhao *et al.* 2001).

Members of the Hedgehog (Hh) family of signalling molecules also appear to be involved in RPE formation. Retroviral driven misexpression of *sonic hedgehog* (*Shh*), the vertebrate homologue of the *Drosophila Hh* gene, in the chick induces ectopic *Otx2* expression, a transcription factor normally restricted to the RPE, and pigmentation in the periphery of the inner layer of the optic cup. Downregulation of *Otx2* and neural retina formation is observed in the outer layer of the optic cup in the reverse experiment using a blocking antibody to decrease Shh activity (Zhang and Yang 2001).

The onset of *Chx10* expression at 9.5 dpc in the distal optic vesicle in the mouse embryo is coincident with the retraction of *Mitf* to the proximal region (Liu *et al.* 1994; Nguyen and Arnheiter 2000). Recently it was shown that a dose dependent antagonistic interaction between *Chx10* and *Mitf* exists, which is essential for the maintenance of neural retina and RPE fates (Rowan *et al.* 2004; Horsford *et al.* 2004). In *Chx10* homozygous null mice, the neural retina is progressively pigmented as *Mitf* and its downstream targets are increasingly upregulated with developmental age in the neural retina (Horsford *et al.* 2004; Rowan *et al.* 2004). Mice harbouring various mutated *Mitf* alleles exhibit a progressive RPE to neural retina transformation and show ectopic expression of *Chx10* and other neural retina markers in the transformed RPE (Nguyen and Arnheiter 2000; Bumsted and Barnstable 2000). These observations suggest that *Mitf* and *Chx10* are not required for the induction, but are essential for the maintenance of the two cell fates.

Interestingly, mice carrying several of the mutated *Mitf* alleles display transdifferentiation of the dorsal RPE only (Scholtz and Chan 1987; Nguyen and Arnheiter 2000; Bumsted and Barnstable 2000), suggesting that the specification of the RPE is differentially regulated along the D-V axis of the eye. In further support of this idea, loss of function of *Growth arrest specific gene 1* (*Gas1*), a Glycosyl-Phosphatidyl-Inositol (GPI)-anchored membrane protein, results in the transdifferentiation of the ventral RPE into neural retina (Lee *et al.* 2001a). *Fgf9* homozygous null mutants show a slight expansion of the RPE into the ventral and nasal neural retina only (Zhao *et al.* 2001). Transgenic misexpression of *MITF* in the neural retina on $Chx10^{OrJ\ OrJ}$ background induces a complete transformation of almost the entire neural retina into an RPE except the dorsal periphery (Horsford *et al.* 2004). *Msx2*, a homeobox encoding gene which is expressed in the dorsal region of the developing eye, can suppress the RPE fate when misexpressed in chick RPE cultures (Holme *et al.* 2000), suggesting that it may also do so in the dorsal neural retina during eye development. How or why the regulation of the neural retina and RPE boundaries are separately regulated in the dorsal and ventral regions of the eye is currently not known.

1.2.2 Molecular regulators of dorso-ventral patterning

Signalling molecules, such as members of the Hh, Fgf, Bone morphogenetic protein (Bmp), and Wingless-related (the Wnts) factors, as well as retinoic acid (RA) signalling, are highly conserved in animal development and recur in the development of many distinct tissues of the embryo. Signalling molecules that pattern the limb bud (Tickle 2002), the neural tube (Lee and Jessell 1999; Jessell 2000), or the somites (Hofmann 2003) for example, are also expressed in the developing eye, making it possible to correlate the expression of these factors in relation to each other and compare their interactions within different tissues. The individual role of some of these signalling molecules in the eye is starting to emerge, but their concerted interactions is far less understood. To fully appreciate patterning of a system however, all contributing components and their interactions must ideally be considered. In this section, an overview of asymmetrically expressed genes along the D-V axis and their roles in patterning of the eye is provided. A schematic of the interactions between genes described in this section is given in Fig. 1.4

1.2.2.1 Signalling molecules in D-V patterning of the developing eye

As the optic vesicles are emerging from the developing forebrain, the tissue has already been exposed to various signals in the anterior neural plate, which are likely to affect patterning of the optic vesicles. *Shh* is expressed in the prechordal plate as the optic pits evaginate (Echelard *et al.* 1993). *Shh* is later expressed in the ventral telencephalon and in the *Xenopus* embryo, double-labelling with *Rx* (eye field marker) has indicated that in fact they overlap in expression in the medial region of the eye field at neurula stage (Crossley *et al.* 2001; Zhang and Yang 2001; Furimsky and Wallace 2005; Lupo *et al.* 2005). Shh is a signalling molecule, shown to be acting as a morphogen in the vertebrate neural tube to pattern the ventral neural tube into distinct domains of gene expression and induce ventral cell fates including motor neurons (Briscoe *et al.* 2001). *SHH* mutations have been identified in patients with holoprosencephaly (Roessler *et al.* 1996), which is a heterogeneous condition caused by midline defects in the embryonic forebrain including cyclopia (OMIM #142945). Mice with a targeted disruption of *Shh* also display cyclopia and ventral midline defects (Chiang *et al.* 1996). Analyses of mutants lacking ventral midline

Shh expression in the forebrain, such as the *cyclops* mutant in zebrafish, which encodes a signalling factor related to the mouse Nodal (Feldman *et al.* 1998; Sampath *et al.* 1998; Rebagliati *et al.* 1998), or the *Brain Factor1* (*Bf1*, *Foxg1* – Mouse Genome Informatics) mouse mutant, which specifically loses *Shh* expression in the ventral telencephalon by 10.5 dpc, have revealed that Shh is essential for establishing optic stalk fate, and the boundary between optic stalk and the neural retina. This is evident by the loss of optic stalk at the expense of neural retinal tissue and at the molecular level, it is obvious in the expansion of *Pax6* at the expense of *Pax2* expression (Macdonald *et al.* 1995; Huh *et al.* 1999). In a normal eye, *Pax6* and *Pax2* are reciprocally expressed in the optic cup and the stalk respectively. Injection of *Shh* RNA in zebrafish or misexpression in the chick eye via retroviral gene delivery induces optic stalk tissue at the expense of the ventral neural retina and a distal shift of the *Pax6/Pax2* border into the neural retina (Macdonald *et al.* 1995; Zhang and Yang 2001). Shh signalling also positively regulates the expression of the *ventral anterior homeobox containing* (*Vax*) transcription factors. This has been shown by the expansion of *Vax* upon *Shh* RNA injections in zebrafish, and the reduction of *Vax* gene expression in *smoothened* mutants (Take-uchi *et al.* 2003). Smoothened is a transmembrane protein that mediates the Hh signal (Ingham and McMahon 2001). The same is likely to apply in the chick embryo, where application of a Shh blocking antibody to the optic vesicle at HH 10 abolishes *cVax* expression (Zhang and Yang 2001).

From both zebrafish and chick overexpression studies of Shh, it has been proposed that Shh may have a role in the establishment of the overall D-V axis of the eye and that it does so by repressing *Bmp4*, a member of the Bmp family of signalling molecules. Treatment of the chick optic vesicle by a Shh blocking antibody results in the expansion of *Bmp4* expression ventrally, offering support for a naturally occurring antagonistic relationship between Shh and Bmp4 in the developing chick eye (Zhang and Yang 2001). The idea that Hh signalling is important for D-V patterning of the eye was further strengthened recently with overexpression experiments of Hh related factors in *Xenopus*, in which there was a dorsal shift of several markers namely *Pax2*, *Pax6*, and *Vax* genes, as well as *Aldh1a3* and *ET* (Lupo *et al.* 2005).

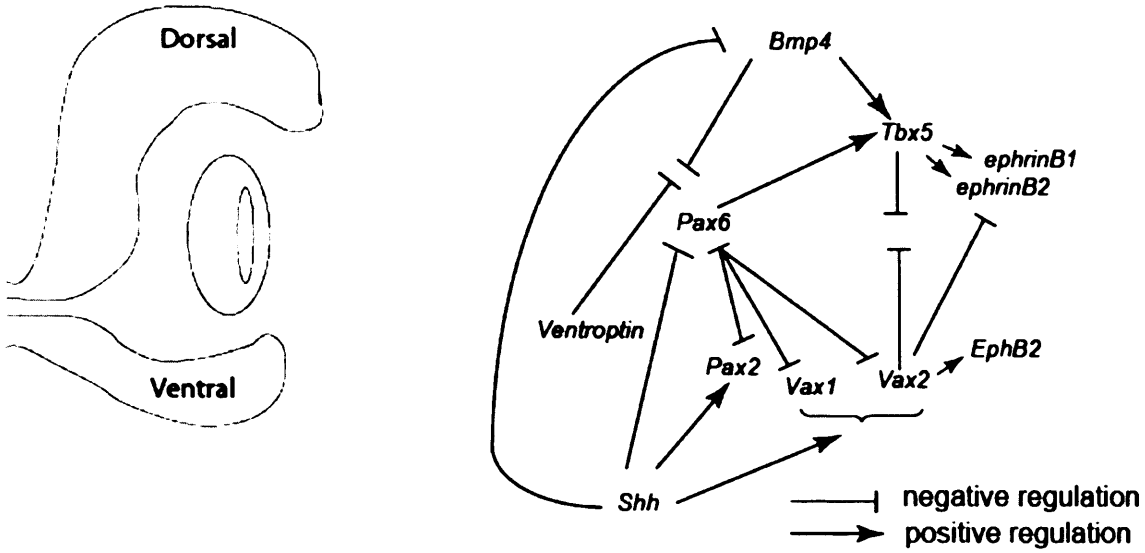

Fig. 1.4 Interactions between genes along the D-V axis of the developing eye as described in text

The information is based on information from mouse mutants and chick misexpression studies. References were described in text. *Bmp4* misexpression induces *Tbx5* expression, which in turn induces the expression of the dorsally expressed ephrinBs and represses the ventrally expressed *EphB2,* which may be indirect via *Vax2.* Lack of *Vax2* induces *EphB2* expression, while *cVax* (chick homologue of *Vax2*) represses dorsal genes when misexpressed. *Bmp4* is antagonised by misexpression of the ventral genes *Ventroptin* and *Shh.* There is also mutual antagonism between *Pax6* and the ventrally expressed *Vax1*, *Vax2*, and *Pax2*, while *Pax6* is thought to positively regulate *Tbx5* expression. This picture highlights the antagonistic relationship between the genes in the dorsal eye and those in the ventral eye. The exact hierarchy in which these interactions occur is currently not fully known.

Shh has also later roles in eye development and appears to be involved in cell differentiation, axon guidance within the retina and also at the chiasm, and has a mitogenic effect in the mammalian retina (Dakubo *et al.* 2003; Ingham and McMahon 2001). In summary, there is evidence that Shh regulates ventral eye fates and may regulate overall D-V patterning by antagonising Bmp4 from the dorsal eye (Fig. 1.4).

Other factors implicated in D-V axial patterning are RA and most recently, there has been evidence of a role for Fgfs. In *Xenopus* neurula stage embryos, RA and Fgfs are thought to influence patterning of the eye already at the eye field stage, when *Fgf8* and RA synthesising enzymes are expressed adjacent to the eye field (Lupo *et al.* 2005). Misexpression studies of Hh-related signalling factors, RA, and an inducible form of Fgf receptor I (FgfrI) in the *Xenopus* eye suggests that these factors probably collaborate in a dose dependent manner to specify the optic stalk and ventral neural fates (Lupo *et al.* 2005).

Although the above described study suggests that Fgf signalling contributes to axial patterning of the developing eye, a similar role in the development of the eye in other species has not been investigated. Moreover, as will be addressed in Chapter 3, the pattern and identity of the Fgfs that are expressed in the eye differ among vertebrate species. As such, data cannot be easily extrapolated between species.

RA, which derives from Vitamin A, is synthesised by the action of retinaldehyde dehydrogenases (RALDH), (Duester 2000). RA activity is asymmetrically distributed along the D-V axis in the neural retina in vertebrate species, including the chick and the mouse. The highest levels of RA activity is detected in the ventral neural retina as compared to the dorsal region. This pattern of activity is established by the action of several RA synthesising and RA degrading enzymes, which are differentially expressed across the neural retina and also possess differing substrate range and enzyme kinetics (McCaffery *et al.* 1991; McCaffery *et al.* 1992; Grün *et al.* 2000).

Using a RA-responsive *lacZ* reporter under the control of the retinoic acid receptor (RAR)ß promoter, the striking pattern of RA responsive regions within the

developing eye has been revealed, which corresponds to the expression patterns of *Aldh1a1* (*Raldh1*, *Ahd2*, *Aldh1*, *E1* – Mouse genome informatics) in a dorsal domain and *Aldh1a3* (*Raldh3*, *Aldh6*, *V1* – Mouse Genome Informatics) in a ventral domain, separated by a sharp middle domain without labelled cells, where members of the CYP26 family degrade RA (Wagner *et al.* 2000). This pattern of RA activity is also evident in the chick eye, with the same spatial expression of RA synthesising enzymes, although temporally they are expressed slightly later in the chick than in the mouse eye (Suzuki *et al.* 2000; Mey *et al.* 2001).

The CYP26 family of enzymes are cytochrome P450-linked oxidases which degrade RA. In the mouse embryo, *Cyp26a1* is the only CYP26 expressed from 9.5 dpc until around 14.5 dpc, when the expression of *Cyp26c1* initiates (Sakai *et al.* 2004). Together they are expressed in a narrow stripe along the N-T meridian of the optic cup, slightly dorsal to the optic disc. This pattern of expression continues until birth after which it starts to decline and disappears by p14 (McCaffery *et al.* 1999; Li *et al.* 2000; Sakai *et al.* 2004).

A role for RA in D-V patterning has been proposed based on its asymmetrical activity along the D-V axis (Marsh-Armstrong *et al.* 1994; McCaffery *et al.* 1999). But investigation of D-V markers in higher vertebrates have until recently not provided any supporting evidence for this hypothesis. Very recently however it was shown that retroviral driven expression of a dominant negative form of RARα in the developing chick eye results in the loss of the ventrally expressed Eph receptors and the dorsally expressed *ephrinB2* (Sen *et al.* 2005). Other asymmetrically expressed genes however are not affected (*Tbx5*, *Vax2*). Neither are they affected when RA signalling is manipulated in mice with targeted disruptions of both *Aldh1a1* and *Aldh1a3*, which are the only RA synthesising enzymes expressed in the optic cup (Matt *et al.* 2005). This is in contrast to experiments in *Xenopus* and zebrafish where addition of RA is reported to expand early ventral markers and abolish dorsal markers (Lupo *et al.* 2005; Hyatt *et al.* 1996).

The role of RA in eye development appears to be dose-dependent and has been best demonstrated in zebrafish; excess RA causes the loss of dorsal markers and duplication of the neural retina due to proliferation of ventral RPE precursor cells

(Hyatt *et al.* 1992; Hyatt *et al.* 1996), while RA deficiency, induced by citral treatment which is a competitive inhibitor of RALDH enzymes, results in failure of ventral neural retinal formation (Marsh-Armstrong *et al.* 1994). Interestingly, application of an RA-soaked bead anywhere around the developing eye induces the formation of an optic fissure (Hyatt *et al.* 1996). RA deficiency during gestation also often causes microphthalmia and anophthalmia (Kalter and Warkany 1959). These studies highlight the importance of D-V patterning for optic cup morphogenesis and growth and suggest that there may be cross-talk between all these signalling pathways or alternatively, that they converge by regulating the same downstream targets. Some of the genes that are affected by manipulations of these factors have already been mentioned. These are mainly transcription factors and other asymmetrically expressed genes, which are introduced more extensively in the following section.

1.2.2.2 Transcription factors and topographic guidance molecules along the D-V axis of the eye

Vax1 and *Vax2* are expressed in a dynamic and overlapping pattern in the ventral optic vesicle and optic stalk from 9.5 dpc in the mouse. By 11.5 dpc, their expression becomes complementary; *Vax2* is expressed in the ventral neural retina while *Vax1* is expressed in the optic stalk (summarised in Mui *et al.* 2005). In the chick embryo, only one *Vax* gene has been identified, *cVax*, which in protein structure is most closely related to the mouse Vax1, but in terms of gene expression encompasses the areas covered by both *Vax1* and *Vax2*. Moreover, its expression appears to be initiated after the onset of optic vesicle invagination, which is slightly later than the onset of *Vax* genes in the mouse, (Schulte *et al.* 1999). Gain of function studies of *Vax* genes in the chick and *Xenopus* embryos, as well as analysis of mice homozygous for a loss of function mutation in *Vax2* or *Vax1* genes, have revealed that they have a vital role in specifying ventral neural retinal cell identity and optic stalk fates and are implicated in topographic mapping. This is based on observations that mice with a targeted deletion of *Vax2* display abnormal axonal projections of ventrally located RGCs (Barbeiri *et al.* 2002; Mui *et al.* 2002), while loss of function of both *Vax* genes simultaneously in the mouse, causes a gradual expansion of neural retinal tissue, so that by 12.5 dpc the neural retina has

replaced the entire optic stalk all the way to the ventral forebrain. By postnatal day (P)7 it has differentiated to possess retinal cell types of a normal retina (Mui *et al.* 2005). This phenotype is suggested to be the result of the absence of the strong direct inhibitory action of the two Vax genes together on the expression of *Pax6,* shown by chromatin immunoprecipitation assays, co-transfection assays, as well as electromobility gel shift assays (Mui *et al.* 2005). In support of a role for Vax genes in repressing *Pax6*, *Vax1* misexpression in *Xenopus* embryos can repress formation of the optic cup by reducing the expression of *Pax6* (Hallonet *et al.* 1999). This interaction seems to be reciprocal as in the absence of Pax6, *Vax1* and *Vax2* are expanded in the entire optic vesicle in the mouse (Bäumer *et al.* 2002). *Pax6* is expressed in the entire optic vesicle and stalk and the overlying surface ectoderm, and later in the optic cup and the lens (Walther and Gruss 1991; Grindley *et al.* 1995).

Targeted deletions of either *Vax1* or *Vax2* result in coloboma with the loss of *Vax1* causing a more severe coloboma than seen in the absence of *Vax2* (Hallonet *et al.* 1999; Barbeiri *et al.* 2002). *Vax2* also plays a role in establishing the pattern of rod photoreceptor differentiation in the ventral neural retina, shown by retroviral misexpression studies in the chick embryo (Schulte *et al.* 2005).

Another ventrally expressed gene that has been well characterised is *Pax2*. *Pax2* is a paired box transcription factor possessing a dynamic expression pattern during optic cup morphogenesis. It is expressed in the ventral optic vesicle and optic stalk, but later retracts to occupy the optic stalk alone (Nornes *et al.* 1990). Mice homozygous for a null allele of *Pax2* exhibit developmental defects affecting several organs in which *Pax2* is expressed, including the eyes (Torres *et al.* 1996). *Pax2* homozygotes have coloboma, due to failure of closure of the optic fissure. They also exhibit abnormal optic nerve development, as the optic stalk differentiates into pigmented cells in the absence of Pax2, which surround the optic nerve fibres. Moreover, the optic nerve is reduced in thickness and all axons project ipsilaterally (Torres *et al.* 1996). Like the Vax genes, *Pax2* and *Pax6* also interact in a mutually antagonistic manner. This has been shown by *in vitro* assays as well as *in vivo*, by the expansion of the expression of one gene at the expense of the other (Schwarz *et al.* 2000). This

interaction is important for the establishment of the optic cup versus the optic stalk boundary along the P-Di axis of the eye.

Pax6 is emerging as an important factor in the regulation of both the dorsal and the ventral neural retina, and may be the gene that coordinates the two regions. In the absence of Pax6, while *Vax* gene expression is expanded, the dorsally expressed T-box gene, *Tbx5* is not present in the optic vesicle (Bäumer *et al.* 2002). A recent report, which studied these interactions using misexpression of *Pax6* in the chick eye by electroporation, glutathione S-transferase (GST)-pull-down assays, and co-transfection assays has suggested that *Pax6* can regulate the expression of the dorsal markers *Tbx5* and *Bmp4* and that Tbx5 in turn can activate the *Pax6* α-enhancer regulatory element as well as bind the full-length Pax6 protein (Leconte *et al.* 2004). Contradictory to the reporting of *Pax6* regulating *Bmp4*, *Bmp4* expression in the homozygous $Pax6^{Sey\text{-}1Neu}$ mouse is normal. *Pax6* expression is also normal in the *Bmp4* loss of function mutant (Furuta and Hogan 1998), suggesting that in the mouse at least, *Bmp4* and *Pax6* do not regulate each other's expression.

The studies described so far highlight that the ventral neural retina is under tight regulation of several signalling molecules and transcription factors and that there is a considerable amount of feed-back in place. When ventral genes are manipulated, conditions such as coloboma, optic nerve defects, and RGC axonal misprojections result. Some information regarding the role of dorsally expressed genes in patterning of the eye has been provided by chick misexpression studies. There is evidence, that manipulations of the dorsally expressed genes *Bmp4* and *Tbx5* in the chick embryo also cause abnormal RGC axonal projections (Koshiba-Takeuchi *et al.* 2000), though milder than those caused by *Vax2*, even though the expression of *Vax2* is disrupted. Misexpression of *Tbx5* and *cVax* in the chick repress each other's expression (Koshiba-Takeuchi *et al.* 2000; Schulte *et al.* 1999), though an antagonistic interaction has not been observed in the loss of function *Vax2* mutant (Barbeiri *et al.* 2002). Both misexpression of *Bmp4*, as well as the Bmp antagonist, *Ventroptin*, in the chick eye have shown that *Tbx5* is downstream of *Bmp4* (Koshiba-Takeuchi *et al.* 2000; Sakuta *et al.* 2001). The role of two other dorsally expressed T-box genes, *Tbx2* and *Tbx3* in amniotes have not been studied and much remains to be learnt about *Bmp4* and *Tbx5* in the regulation of eye development.

The best characterised aspect of D-V patterning of the eye is topographic mapping of RGC axons to the brain. Normally, the medial colliculus in mouse or the medial tectum in chick are invaded by axons from the ventral neural retina, while the lateral colliculus or tectum are invaded by axons from the dorsal neural retina. Several Eph/ephrin molecules are asymmetrically expressed in a graded fashion in the neural retina and in a complementary pattern in the tectum/superior colliculus. As such, they have been subject to much attention as candidates involved in Sperry's long-standing chemoaffinity theory, which proposed that topographic mapping of axonal projections from the neural retina to the brain are facilitated by corresponding graded distribution of molecules on the RGCs and their targets (Sperry 1963). The Eph proteins are transmembrane tyrosine kinase receptors and their ephrin ligands are either transmembrane proteins (ephrinBs) or membrane bound through a GPI linkage (ephrinAs) (Wilkinson 2001). The postulated role of the Eph/ephrin molecules in RGC axon guidance has been substantiated over recent years by *in vitro* and *in vivo* functional studies involving manipulation of the Ephs/ephrins, or other upstream regulators. Progress was first made in identifying and understanding the function of the EphA receptors and ephrinA ligands in the regulation of RGC projections from the nasal and temporal regions of the neural retina to the anterio-posterior axis of the tectum/superior colliculus. The EphA receptors are collectively expressed in a temporal-high nasal-low gradient in the neural retina, while the ephrinA ligands are collectively expressed in a posterior-high, anterior-low pattern in the tectum. A combination of *in vitro* studies of axonal behaviour from different parts of the retina, using the membrane stripe and growth cone collapse assays, and *in vivo* gain of function and loss of function studies have shown that these molecules mediate topographic mapping of axonal projections via repulsive interactions, such that RGCs from the temporal neural retina, which express high levels of EphA receptors, settle in the anterior region of the tectum, which expresses the lowest levels of ephrinA ligands, because further posteriorly, they are repulsed by the increasing ephrinA gradient (O'Leary *et al.* 1999).

The EphB receptors and ephrinB ligands are involved in topographic mapping of the D-V axis of the neural retina along the medio-lateral (M-L) axis of the tectum/superior colliculus. Unlike the repulsive mechanism of topographic mapping

mediated by the EphA/ephrinAs, the EphB/ephrinBs appear to operate on the basis of attraction in the visual system, so that dorsally derived RGCs from the neural retina, where ephrinBs are expressed at high levels, project to the lateral tectum/superior colliculus which expresses high levels of EphB receptors. Along the D-V axis of the neural retina, *ephrinB2* and *ephrinB1* are expressed dorsally, while *EphB2* and *EphB3* are expressed in a ventral-high dorsal-low gradient, with EphB2 shown to be expressed on RGC axons (Holash and Pasquale 1995; Holash *et al.* 1997; Braisted *et al.* 1997; Connor *et al.* 1998; Birgbauer *et al.* 2000; Hindges *et al.* 2002).

In *Xenopus*, *in vivo* experiments that increase or decrease levels of ephrinB2 signalling in the neural retina show that ephrinB2 signalling is important for targeting of axons to the lateral tectum in a concentration dependent manner. For example when wild-type *ephrinB2* is misexpressed in the ventral neural retina, RGC axons originating from this region project incorrectly to more lateral tectal locations, while overexpression of *ephrinB2* in the dorsal neural retina, which already is expressing ephrinB2, causes an even more lateral shift of dorsally derived axons (Mann *et al.* 2002). Furthermore, evidence was provided for attraction of ephrinB expressing dorsal neurites to EphB1 expressing substrate, using a stripe assay.

Analysis of compound mutants with disrupted alleles of *EphB2* and *EphB3* has shown that the EphB receptors are important for correct projections of ventro-temporal RGC axons to the lateral superior colliculus, as these mutants possess ectopic termination zones in more lateral locations (Hindges *et al.* 2002). These mutants also exhibit intra-retinal pathfinding errors to the optic disc, with a higher percentage of dorsal axons missing the optic disc compared to ventrally derived axons (Birgbauer *et al.* 2000).

The role of ephrinB1 in topographic mapping has been studied in the chick tectum. Retroviral mediated targeting of the tectum specifically results in ectopic patches of *ephrinB1* expression, which do not disrupt the primary axonal projection pattern to the tectum. They do however shift the secondary branching of axons more laterally down the endogenous *ephrinB1* expression gradient (McLaughlin *et al.* 2003b). In mice and chick, the final topographic map is fine-tuned by the extension of secondary branches after the primary axons originating from the same location of the

neural retina initially project broadly along the M-L axis of the tectum/superior colliculus. It is these branches rather than the primary axonal projections that get shifted when the endogenous pattern of *ephrinB1* is disrupted (McLaughlin *et al.* 2003b). However, this study does not investigate the role of *ephrinB1* that is expressed in the dorsal neural retina in topographic mapping. Mice with targeted deletions of the dorsally expressed *ephrinB2* have been generated, but not yet analysed for eye or retinocollicular mapping defects (Adams *et al.* 1999).

There are several expression studies in the chick embryo which show that these genes are asymmetrically expressed soon after optic cup formation (HH 17-18), prior to the peak of RGC differentiation (Braisted *et al.* 1997; Peters and Cepko 2002). Expression analysis in the mouse eye has so far been reported for slightly older developmental ages, past 13 dpc and beyond. However, one report has demonstrated the existence of ligands of EphB2 in the dorsal region of the invaginating optic cup of 10.5 dpc mouse embryos using an EphB2-Fc fusion protein, which reveals distribution of proteins but does not distinguish between the different ephrinB ligands (Marcus *et al.* 1996). This suggests that some of these molecules are expressed in the early optic cup, prior to the onset of RGC differentiation, and may therefore have additional roles in the formation of the eye, as has been suggested following the early expression study in the chick (Braisted *et al.* 1997). It is important to determine their expression pattern at the earlier stages, as the expression of these molecules appear to undergo dynamic changes during development. For example, the initial expression of EphB2 at 12-14 dpc is uniform, but later becomes graded (Birgbauer *et al.* 2000). The pattern of expression of *ephrinB2* in the early optic cup of the mouse embryo is examined in Chapter 3 of this thesis. These molecules have been shown to be regulated by *Vax2/cVax* (Schulte *et al.* 1999; Barbeiri *et al.* 2002; Mui *et al.* 2002) and *Tbx5* (Koshiba-Takeuchi *et al.* 2000). It may therefore be a commonality that the Eph/ephrin molecules are downstream of asymmetrically expressed transcription factors.

Functional studies have revealed that the eye is patterned by a complex interaction of the genes mentioned in this section, and undoubtedly other as yet unidentified genes. These interactions not only occur at the RNA level but also at the protein level, and

there appears to be feedback loops which add to the level of complexity that controls overall axial patterning of the eye.

In the next sections, some aspects of eye development which either occur regionally or appear to require positional information, but the underlying mechanisms of which are not understood, are outlined in order to emphasise the importance of studying patterning of the eye.

1.2.3 Significance of regional gene expression in eye development

Despite evidence of polarised gene expression in the neural retina, it does not display a striking distinction, morphologically or qualitatively in terms of differentiated cell types. There is a distinct centre to periphery temporal advancement of cell differentiation, with differentiation initiating centrally and expanding peripherally (Coulombre 1965; Dräger 1985). But the end result is differentiation of the same cell types in all region of the neural retina. A closer examination of the distribution of these cell types however, have revealed more subtle quantitative differences.

It is known that the RGCs form topographic maps in the brain, and require positional information to project correctly to their target sites (McLaughlin *et al.* 2003a). In the mouse, uncrossed or ipsilateral RGC axonal projections originate from the temporal and the ventral neural retina (Dräger 1985). As described earlier, when certain asymmetrically expressed genes are manipulated, RGC axonal misprojections are observed (see section 1.2.2.2). The distribution of certain neuronal cell types can quantitatively differ along the different retinal axes. The density of cones and rods in the human retina is not uniform. For example, the central region of the human fovea, important for high acuity vision, lacks rods and cone density is higher in the nasal than the temporal retina (Curcio *et al.* 1990). The density of S (blue) and M (green) opsins, which are the visual pigments of the cones, is different along the D-V axis of the mouse retina, with M opsins present only dorsally and S opsins most abundant ventrally (Szél *et al.* 1992). In the chick, there is a rod-free zone within the area centralis, which is homologous to the human fovea, and the rod density of the dorsal neural retina is lower in comparison to the ventral region (Bruhn and Cepko 1996). Recently it was shown that the rod pattern in the chick retina is established at the

optic vesicle stage by spatially restricted gene expression, including *cVax* (Schulte *et al.* 2005). These studies together with transplantation and rotation experiments of the optic vesicle, which disrupt early patterning of the eye and the RGC projections, suggest that early patterning, prior to the differentiation of retinal cell types, is important for the correct distribution of cells of the mature retina.

Further evidence that the eye is differentially regulated across its axes comes from discoveries of the occurrence of region-specific defects. When RA signalling is manipulated in the zebrafish, only the ventral eye is affected (see section 1.2.2.1). Patients with superior segmental optic nerve hypoplasia display regionalised defects. This condition is characterised by several abnormalities of the superior (dorsal) region of the eye including a more superior entry of the central retinal artery into the cup, a decrease in the superior optic nerve fibre layer, and loss of inferior visual fields (Unoki *et al.* 2002; Oster *et al.* 2004). In the next section, evidence for regional differences in cell proliferation and cell death during early optic cup formation is discussed.

1.2.4 Regional differences in proliferation and the pattern of cell death in the early optic cup

The morphogenesis of the optic cup and its growth can be divided into two overlapping phases. In the first phase, the optic vesicle invaginates and the distal and proximal layers become distinct in terms of thickness and cellular morphology. There is a dramatic shape change and modest growth. In the second phase, after optic cup formation, there is more profound growth but much less change in the shape of the eye. Analyses in this thesis have been carried out during the first phase and therefore a description of the pattern of cell death and proliferation during the period of optic cup morphogenesis is given here.

Spatio-temporal dynamics of the pattern of cell death during optic cup morphogenesis

During optic cup morphogenesis, the pattern of cell death is highly dynamic and regionalised. In the chick embryo, Tdt-mediated dUTP nick end labelling (TUNEL) of apoptotic cells and Feulgen staining of DNA has revealed that at optic vesicle

stage (HH 13) cell death occurs in the optic stalk and extends to the central region of the optic vesicle. At HH 14, when the optic vesicle has started to invaginate, cell death is still localised to the optic stalk and the central region of the invaginating optic vesicle. By HH 16, cell death is detected in the optic stalk, in the ventral and central regions of the optic cup in both the neural retina and the RPE, and a new area of cell death in the dorsal neural retina is apparent. By HH 18, the heavily labelled patch in the dorsal optic cup can no longer be detected, and labelling is seen in only a few spots within the central neural retina and in the optic stalk (Crossley *et al.* 2001; Trousse *et al.* 2001; Schook 1980a). At HH 17, cell death is also detected in the invaginating lens vesicle which has yet to separate from the surface ectoderm (Schook 1980a).

During optic cup morphogenesis in the mouse embryo, the pattern of cell death is also highly dynamic and regionalised. It appears to be concentrated in the optic stalk region just as invagination starts, but then spreads to the central neural retina by 10.5 dpc. Apoptosis in the invaginating lens vesicle is localised to the tips that are to meet and fuse. Some apoptosis can also be detected in the dorsal neural retina between 10.5 – 11.5 dpc. However, the dorsal cell death in the mouse optic cup is distinctly less abundant than that in the chick embryo (Trousse *et al.* 2001).

Differential rates of proliferation across the D-V axis

The process of optic cup formation is coincident with a proliferative burst of the distal neuroepithelium, the presumptive neural retina, which becomes much thicker in comparison to the proximal neuroepithelium, the presumptive RPE, as the optic vesicle invaginates. Similar to the interkinetic movements of proliferating cells across the laminar axis of the developing chick neural tube, first recognised by Sauer (reviewed in Watterson 1965), proliferating retinal progenitors migrate to the ventricular edge during the M-phase of the cell cycle, when they divide, and migrate away from the ventricular edge during the S- and G-phases of the cell cycle (Sidman 1961). As such dividing cells (in M-phase), which contain phosphorylated histone H3 (pH3), are observed on the ventricular edge of the neural retina when immuno-labelled with a pH3 antibody.

In the literature, the growth of the eye is often described as non-uniform, referring to the centre (proximal) to periphery (distal) gradient of development, which is apparent in terms of neurogenesis during early development, with the first born neurons being detected in the central neural retina, but also later in terms of cell addition, when the central neural retina ceases to proliferate and proliferation becomes localised to the periphery of the optic cup only, resulting in localised cell addition (Robinson 1991). In the mouse, localisation of proliferation to the peripheral optic cup only, occurs one week after birth shown by ^{3}H-Thymidine labelling of proliferating cells (Sidman 1961). Prior to this stage, proliferating cells are detected throughout the neural retina. In the chick embryo, it has been demonstrated that the ventral neural retina possesses a higher proliferative density, measured as the number of mitotic cells per unit area, than the dorsal neural retina at HH 13-14. This is when the optic vesicle has just invaginated. This trend continues also at HH 17-18, although the difference in mitotic activity between the two regions are less marked at this stage (Calvente *et al.* 1988). Differential proliferation has also been reported along the D-V axis in the mouse RPE (Lee *et al.* 2001a).

1.3 The T-box gene family

1.3.1 Discovery of the T-box gene family

The evolutionarily conserved T-box gene family encode transcription factors, which are characterised by a highly conserved DNA binding domain. *Brachyury* (*T*- Mouse Genome Informatics), a mouse mutation that causes a short tail in heterozygous mice, was the first member of this family to be cloned in 1990 (Herrmann *et al.* 1990). Shortly after, the *Drosophila optomotor blind* (*omb*) gene was cloned and found to bear sequence homology to *Brachyury* (Pflugfelder *et al.* 1992a). Subsequently, members of the mouse *Tbx2* subfamily were identified and the existence of a gene family was established (Bollag *et al.* 1994). There are currently 17 members identified in mammals (Naiche *et al.* 2005). The DNA binding domain was named the T-box after *T* which was the first identified member. Various animal mutants of the T-box genes are now emerging and functional studies are providing information about the role of these genes in development. In man, there are six conditions that are known to date to be caused by mutations in various T-box genes

(Naiche *et al.* 2005), two of which occur in T-box genes that are expressed in the eye and will be discussed in the following sections.

1.3.2 DNA binding, transcriptional activity, and binding partners

The protein structure of Brachyury, the prototype and the most studied of all T-box genes, contains an N-terminal DNA binding domain (180-200 amino acids) and a C-terminal domain containing two repression and two activation sites, suggestive of a role as a transcriptional repressor as well as an activator. Like other transcription factors, it also contains nuclear localisation domains (Fig. 1.5).

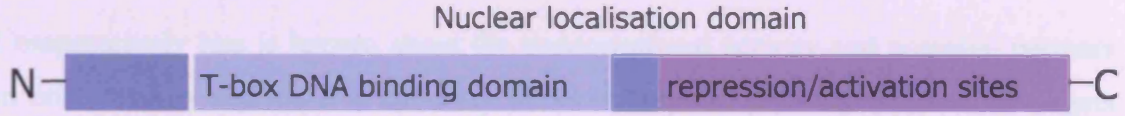

Fig. 1.5 Schematic representation of the Brachyury protein structure

The crystallographic structures of *Xenopus* and human Brachyury, and human TBX3 bound to a palindromic DNA sequence *in vitro* have been determined and although the T-box genes are highly conserved, T binds DNA as a dimer (Papapetrou *et al.* 1997; Muller and Herrmann 1997) but TBX3 binds as two separate monomers to the palindromic sequence, called the T-site (Coll *et al.* 2002). It has also been reported that TBX2, like TBX3, interacts more efficiently with only a T-half site (Sinha *et al.* 2000). Furthermore, different T-box proteins show preference for different combination, orientation, number, and spacing of T-half sites *in vitro* (Conlon *et al.* 2001). Hence regardless of their highly conserved DNA binding domain, T-box proteins have differing DNA binding properties, which may partly account for their ability to regulate different downstream targets.

There is evidence that T-box proteins regulate gene expression in combination with other transcription factors. The investigation and identification of T-box protein partners is most advanced for those acting in the developing heart, where cooperative binding of promoters with several heart specific transcription factors have been

identified *in vitro* (Naiche *et al.* 2005). There is evidence for the T-box proteins in both activating and repressing gene expression. For example Tbx5 has been reported to act as an activator (Hiroi *et al.* 2001), while Tbx3 has been reported to act a repressor (Lingbeek *et al.* 2002). Tbx2 has been reported to act both as an activator and as a repressor depending on promoter context (Carreira *et al.* 1998; Habets *et al.* 2002; Paxton *et al.* 2002; Hiroi *et al.* 2001). Microarray analysis of differentially expressed genes in several different cell lines following transfection of *Tbx2* confirm that a context-dependent upregulation and downregulation of gene expression can be achieved by *Tbx2* (Chen *et al.* 2001). Although this does not differentiate between gene expression changes caused by Tbx2 directly and those caused indirectly.

Comparatively less is known about the transcriptional activity and potential partners in other tissues and there is currently no knowledge of potential partners or targets for T-box genes in the developing eye. Two factors that may be of relevance to the eye are Connexin43 (Cx43) and Mitf. Cx43 is a gap-junctional protein which is expressed in several tissues in which *Tbx2* is expressed, including the chamber myocardium of the developing heart, developing rat coronal sutures, and in the eye of several vertebrate species (Yancey *et al.* 1992; Janssen-Bienhold *et al.* 1998; Borke *et al.* 2003). The *Cx43* promoter contains T-sites and in transfection assays is repressed by Tbx2 (Borke *et al.* 2003; Chen *et al.* 2004). Though not a target, in melanocytes, Mitf has been shown to regulate *Tbx2* expression (Carreira *et al.* 2000).

1.3.3 Functions in development

T-box genes have been isolated from all metazoan species examined so far and are expressed in a variety of tissues during development in spatio-temporally distinct, but also overlapping patterns (Papaioannou 2001). Although they are expressed in structurally and functionally different tissues and undoubtedly are implicated in tissue specific developmental events, there are some similarities that can be drawn regarding the function of T-box genes in development.

As no unicellular organisms express these genes, it has been speculated that they may be important in cell interaction, tissue specification, and differentiation decisions during development (Papaioannou 2001). There is some strong evidence

that supports these hypotheses. For example, *Xbra* (*Xenopus* orthologue of mouse *Brachyury*) is essential for ventral mesoderm induction (Cunliffe and Smith 1992) and heterozygous *Brachyury* mice have a short tail while homozygotes die before birth due to a lack of notochord and posterior mesodermal defects (Tada and Smith 2001). *Tbx6* is expressed in paraxial and presomitic mesoderm in mouse embryos and in *Tbx6* null mice, caudal somites are converted into neural tubes, indicative of a requirement for *Tbx6* in promotion of mesodermal tissues (Chapman and Papaioannou 1998). In *mab-9* mutants (*C.elegans* orthologue of human *TBX20*) two posterior blast cells that are precursors of the hindgut take on the properties of their anterior neighbouring blast cells, causing abnormal male tail development (Woollard and Hodgkin 2000).

Moreover, there is an emerging role for T-box genes in tissue patterning and regional specification within tissues. Mice homozygous for a mutation of *Tbx18* have revealed that *Tbx18*, which is expressed in the anterior region of somites, is required for the maintenance of the separation of anterior and posterior somite compartments. These mutants display rib and vertebrae defects (Bussen *et al.* 2004). In the developing heart, *Tbx2* is thought to spatially define the atrioventricular canal (AVC) region, where it is expressed. In mice with a targeted mutation of *Tbx2* AVC differentiation is lost at the expense of chamber myocardium so that the developing left ventricle becomes connected to the atria and no longer separated by the AVC (Harrelson *et al.* 2004). Conversely, misexpression of *Tbx2* in chamber myocardium blocks chamber differentiation (Christoffels *et al.* 2004).

1.3.4 T-box genes expressed in the developing eye

The vertebrate Tbx2 subfamily contains four members, *Tbx2/3/4/5*, that are also collectively referred to as the *omb*-related genes due to their high resemblance in both DNA and protein structure to the *omb* gene of *Drosophila* than to any other vertebrate T-box gene (Bollag *et al.* 1994). A model has been proposed in which the vertebrate *omb*-related genes have evolved as a result of an unequal crossing event of an ancestral *Tbx2/omb* gene prior to the divergence of the vertebrate and invertebrate lineages. This has given rise to the *Tbx2/3* and *Tbx4/5* primordial genes, which by undergoing a further duplication have resulted in four distinct but highly related T-

box genes (Agulnik *et al.* 1996) (Fig. 1.6). This model does not explain why there are no orthologues of *Tbx4* or *Tbx5* in the nematode or arthropod lineages. But as no new studies addressing this issue have been carried out, the theory of Agulnik et al remains.

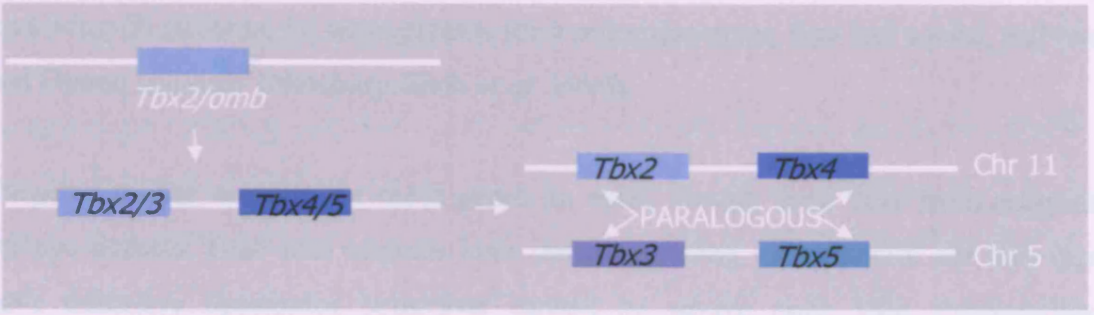

Fig.1.6 The current divergence model of members of the *Tbx2* subfamily in mouse.

An unequal crossing event of an ancestral *Tbx2/omb* gene gave rise to the *Tbx2/3* and *Tbx4/5* primordial genes, which then by undergoing a further duplication followed by a dispersion event have resulted in four distinct but highly related T-box genes (Agulnik et al 1996).

During mouse eye development, *Tbx5*, *Tbx2*, and *Tbx3* are detected in the optic vesicle in an overlapping pattern in the distal layer (Chapman *et al.* 1996; Holt 2003). *Tbx20* has also been detected in the dorsal region of the mouse eye (Kraus *et al.* 2001) and is the only non *omb*-related T-box gene to be expressed during optic cup morphogenesis. No other T-box orthologues were identified in a 15.5 dpc mouse retinal cDNA library screen specifically aimed at detecting T-box genes within the developing mouse eye (Sowden *et al.* 2001).

Currently, very little is known about the function of the T-box genes in eye development. Eye abnormalities in human patients with conditions caused by mutations in the *omb*-related T-box genes are unusual, most probably due to their overlapping expression pattern in the eye. Mutations in *TBX3* and *TBX5* cause the human conditions Ulnar mammary and Holt-Oram syndromes respectively

(Bamshad *et al.* 1997; Basson *et al.* 1997; Li *et al.* 1997). Ulnar-mammary syndrome patients suffer from limb, breast, teeth, and genital abnormalities, which are tissues in which *Tbx3* is expressed during mouse development (Packham and Brook 2003). No ocular abnormalities have so far been reported in these patients. Holt-Oram syndrome is mainly associated with cardiac and skeletal defects, however, in a study involving 66 patients, 16 wore glasses for a refractive error, five had squint, and two had Duane anomaly (Newbury-Ecob *et al.* 1996).

Targeted mouse mutants for these genes do exist, though none have been analysed for eye defects. *Omb* null mutants have defects in wing development but they also have defective optomotor behaviour caused by severe optic lobe abnormalities including the absence of lobula-plate giant nerve fibres leading to visual impairment (Pflugfelder *et al.* 1992b). Misexpression studies have been performed in the developing chick eye for *Tbx5*, and in *Xenopus* for *Tbx2* and *Tbx3*. Although there are some differences in the temporal and the spatial expression of these genes between species, all express *Tbx2*, *Tbx3* and *Tbx5* in the dorsal region of the early optic cup (Takabatake *et al.* 2002; Gibson-Brown *et al.* 1998; Chapman *et al.* 1996; Sowden *et al.* 2001). Ectopic expression of *Tbx5* in the chick eye leads to disruption of D-V patterning and retinotectal projections as described earlier (Koshiba-Takeuchi *et al.* 2000). Misexpression of *Tbx2* and *Tbx3* in the *Xenopus* embryo are reported to cause similar effects to each other, which is not unexpected given the homology of these genes. Misexpressions were performed by injection of capped synthetic RNA into the animal hemisphere of two-cell stage embryos and therefore, defects as a result of non-specific expression of these genes may have resulted. The defects reported include a loss of ventral eye pigmentation, medial displacement of the optic cup (shortened distance between eyes and brain), and fused eyes in the most severe cases (Takabatake *et al.* 2002). These defects are reminiscent of ventral midline defects and hard to reconcile with the dorsal expression of the T-box genes in the eye.

The early onset of T-box gene expression in the optic vesicle prior to the specification of the neural retina versus the RPE, suggests that they may have a role in this specification event. This idea is also supported by the role of several T-box genes in delineating tissue boundaries as discussed earlier. Their asymmetrical

expression pattern in the dorsal eye suggests their early involvement in the specification of the dorsal eye and perhaps overall D-V patterning of the eye. Moreover there is an emerging role for *Tbx2* in cell cycle control and tumourogenesis.

1.3.5 Role of *Tbx2* in cell cycle control and cancer

The cell cycle, which in eukaryotic cells has been divided into two major phases with gaps in between according to the events of DNA replication and partition, is controlled by proteins belonging to the families of cyclins, cyclin-dependent kinases (CDK)s, and cyclin-dependent kinase inhibitors (CDKI)s (Nurse 2000).

Much of the current knowledge of the role of *Tbx2* in cell cycle control comes from *in vitro* studies which were sparked by the discovery that TBX2 can immortalise *Bmi1*$^{-}$ mouse embryo fibroblasts by downregulating $p19^{ARF}$, and that TBX2 is amplified in a subset of primary human breast cancer tumours (Jacobs *et al.* 2000). Since then, more studies have reported the amplification of *TBX2* in human breast tumours and pancreatic cancer cell lines (Bärlund *et al.* 2000; Sinclair *et al.* 2002; Mahlamaki *et al.* 2002) and its overexpression in melanoma cell lines (Vance *et al.* 2005). There is evidence that TBX2, and TBX3, have anti-senescence properties; both can rescue senescence in mouse embryonic fibroblasts (Carlson *et al.* 2001; Jacobs *et al.* 2000) and a dominant negative form of Tbx2 can induce senescence in a melanoma cell line (Vance *et al.* 2005). Furthermore, both can repress the $p14^{ARF}$ promoter *in vitro* (Lingbeek *et al.* 2002). TBX2 can also repress other CDKIs such as p21 (Prince *et al.* 2004).

The mouse $p19^{ARF}$, which is homologous to the human $p14^{ARF}$, together with $p16^{INK4a}$, are transcribed from the Cdk2a (INK4a/ARF) locus and are CDKIs which block cell cycle progression via two different routes (Chin *et al.* 1998). p19ARF traps the oncoprotein MDM2 and thereby stabilises p53. This leads to accumulation of p53, which blocks cell cycle progression or induces apoptosis. $p16^{INK4a}$ on the other hand causes G1 arrest by preventing the inactivation of RB (retinoblastoma protein). Hence both proteins work to prevent cell proliferation.

A similar role for these T-box genes in regulating the expression of cell cycle genes and regulating cell proliferation in developing embryos is currently sparse. Recently, it was shown that Tbx2 represses the expression of *Nmyc*, in mice with a targeted deletion of *Tbx20*, in which *Tbx2* is ectopically expressed (Cai *et al.* 2005).

1.4 BMP4 and patterning in embryogenesis

Previous studies have shown that *Bmp4* is expressed in the dorsal region of the developing eye and is essential for mouse eye development (Furuta and Hogan 1998). Bmps belong to the evolutionarily conserved super family of TGF-β signalling molecules. Members of this family play fundamental roles during development as well as serving roles in adult tissues (Mehler *et al.* 1997; Botchkarev 2003). The basic signal transduction pathway of the TGF-β superfamily involves two receptor serine/threonine kinases, receptor type I and receptor type II, and the Smad family of intracellular receptor substrates as well as the co-mediator Smad. Smad stands for sma/mothers against dpp related, which are the names given to their *c.elegans* and *Drosophila* homologues. Each ligand assembles a certain complex of transmembrane type I and type II receptors, which phosphorylate different Smad proteins in the cytoplasm. These activated Smads form multisubunit complexes and are translocated into the nucleus where they either activate or repress gene expression (Massague and Chen 2000).

Phosphorylation of Smads occurs upon binding to a homo or hetero dimeric unit of Bmps to a Bmp receptor type I (BmprI)/Bmp receptor type II (BmprII) complex. Smad4, the co-Smad, is a crucial partner of phosphorylated Smads in inducing gene regulation once translocated into the nucleus. A complex of receptor activated Smads and Smad4 alter gene expression by binding to Smad binding sites upstream of promoter elements (Fig. 1.7). The interaction of the Smad complex with DNA is of low affinity and is strengthened by additional cofactors. It is thought that these cofactors also confer the mode of regulation of gene expression by the pathway. Both coactivators and corepressors have been identified (Massague and Chen 2000).

This signalling pathway is complex and interactions with other signalling pathways have been demonstrated. There is also some evidence that Bmps and TGF-ß1 may

also act via a mitogen-activated protein kinase (MAPK) pathway in which stimulation of TAK1 (TGFß-activated kinase 1) activates the p38 and c-Jun N-terminal kinase (JNK) pathways (Yamaguchi *et al.* 1995; Moriguchi *et al.* 1996; Atfi *et al.* 1997; Botchkarev 2003; Massague and Chen 2000).

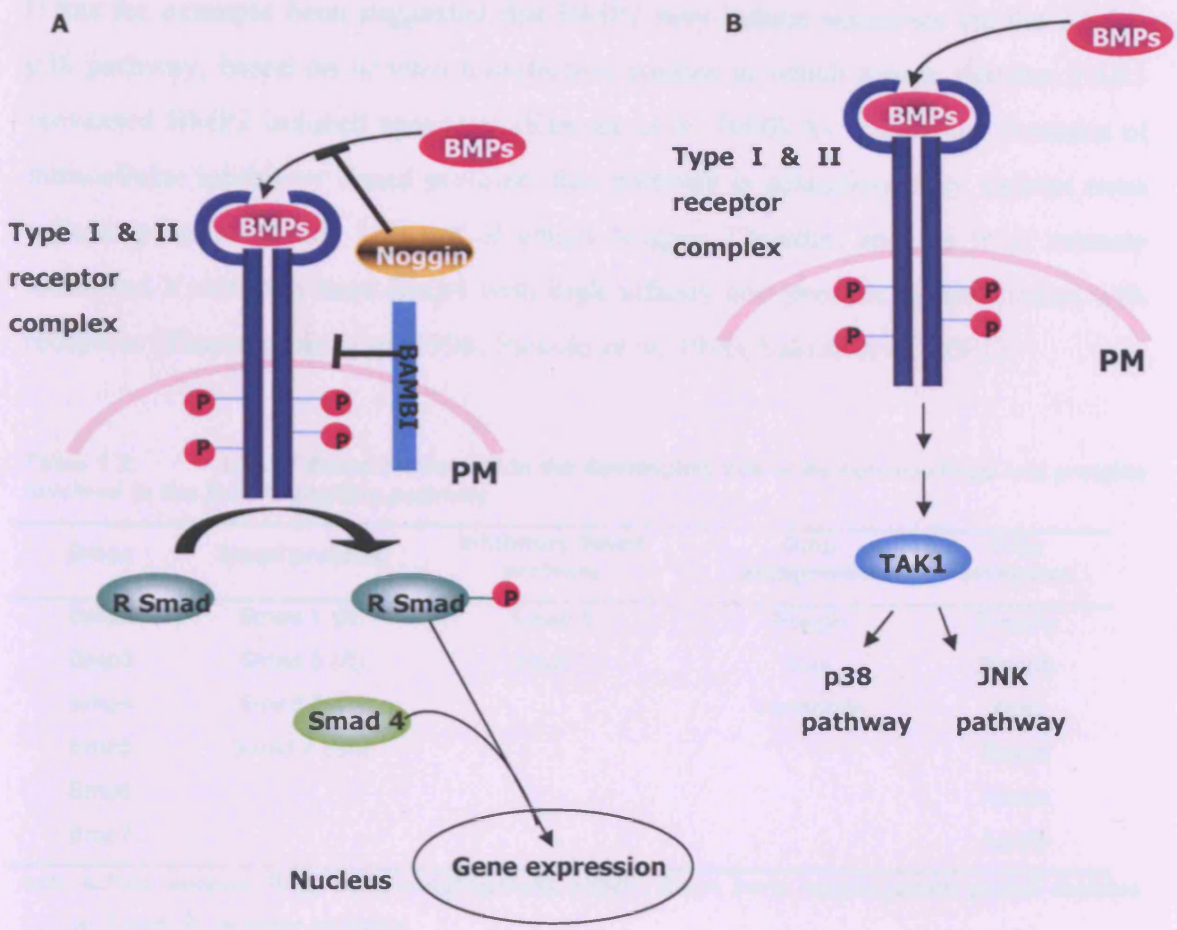

Fig. 1.7 Bmp signal transduction.

A) Homo or hetero dimeric complexes of Bmps bind Type I receptors with high affinity, after which Type II receptors are recruited to form a complex. Type II receptors phosphorylate the Type I receptors, which in turn phosphorylate various intracellular Smad proteins, the receptor activated Smads (R-Smads). R-Smads and Smad4, the co-Smad, undergoes continuous nucleocytoplasmic shuttling. Upon activation, phosphorylated Smads accumulate in the nucleus where they associate with Smad4 and other cofactors to alter gene expression by binding to Smad-binding sites present upstream of gene promoters. Antagonists of this pathway act at multiple levels and include antagonists of the ligands (represented by Noggin in figure), antagonist of the receptors (BAMBI) and antagonists of the Smads within the cytoplasm. **B)** Alternatively, the Bmp signal activates various members of the MAPK family via TAK1 (Shi and Massague 2003). PM, plasma membrane; P, phosphorylation.

It has for example been suggested that BMP2 may induce apoptosis via the TAK1-p38 pathway, based on *in vitro* transfection studies in which kinase inactive TAK1 prevented BMP2 induced apoptosis (Kimura *et al.* 2000).As well as the presence of intracellular inhibitory Smad proteins, this pathway is antagonised by various extra cellular proteins (Table 1.2) out of which Noggin, Chordin, and the most recently identified Ventroptin bind Bmp4 with high affinity and prevent its association with receptors (Zimmerman *et al.* 1996; Piccolo *et al.* 1996; Sakuta *et al.* 2001).

Table 1.2: List of Bmps expressed in the developing eye or its surroundings and proteins involved in the Bmp signalling pathway

Bmps	Smad proteins	Inhibitory Smad proteins	Bmp antagonists	Bmp receptors
Bmp2	Smad 1 (R)	Smad 6	Noggin	Bmprla
Bmp3	Smad 5 (R)	Smad 7	Dan	Bmprlb
Bmp4	Smad 8 (R)		Ventroptin	Actrl
Bmp5	Smad 4 (Co)			Bmprll
Bmp6				Actrlla
Bmp7				Actrllb

Actr, activin receptor; Bmp, bone morphogenetic protein; Bmpr, bone morphogenetic protein receptor; Co, co-Smad; R, receptor activated.

1.4.1 Bmp signalling in the developing eye

Several Bmps are expressed in an overlapping pattern in the dorsal forebrain and surface ectoderm during forebrain development (Furuta *et al.* 1997), including *Bmp2*, *Bmp4* and *Bmp7* that are later also expressed in the eye. Bmps are secreted factors in the extracellular environment that trigger intracellular responses via the signal transduction pathway described earlier. As such, the expression of Bmp receptors and factors that modify this pathway is of relevance towards understanding the spatial distribution of Bmp signalling in a tissue.

Expression of Bmps during early eye development

In the developing mouse eye, *Bmp4* is expressed in the entire distal optic vesicle and the overlying surface ectoderm at around ss 14 – 16 (9.5 dpc) (Furuta and Hogan 1998; Dudley and Robertson 1997; Liu *et al.* 2003). At the time when the lens placode is forming, *Bmp4* becomes restricted to the dorsal region of the distal optic vesicle and continues to be dorsally restricted throughout optic cup formation. The

expression in the surface ectoderm disappears during lens placode formation (Furuta and Hogan 1998). The expression of *Bmp4* in the chick eye is similar to the mouse, with the exception that at optic vesicle stage, *Bmp4* is only detected in the surface ectoderm and not the optic vesicle itself (Trousse *et al.* 2001).

At the optic vesicle stage in the mouse, *Bmp7* is detected in the surface ectoderm and in the optic vesicle, with the strongest expression in the proximal layer, complementary to *Bmp4*. *Bmp7* expression levels in the surface ectoderm decrease gradually and at the optic cup stage, *Bmp7* is still expressed at low levels in the surface ectoderm. At this stage, it becomes restricted to the RPE and the optic stalk (Dudley and Robertson 1997). In the chick embryo, *Bmp7* is only detected in the proximal layer of the optic vesicle and later in the RPE, but not in the surface ectoderm as detected in the mouse embryo (Trousse *et al.* 2001). In the chick optic cup, detection of *Bmp6* and *Bmp5* in the RPE have also been reported (Belecky-Adams and Adler 2001b).

In summary, there are differences detected in Bmp expression between the two species, mainly at the optic vesicle stage when in the mouse *Bmp4* is expressed at high levels in the dorsal optic vesicle and at low levels in the surface ectoderm, while in the chick it is expressed at high levels in the surface ectoderm and only after optic cup formation, it is localised dorsally in the neural retina. *Bmp7* is expressed at high levels in the mouse surface ectoderm at optic vesicle stage, but not in the chick. In both mouse and chick, *Bmp4* and *Bmp7* are expressed in a complementary fashion to each other in the optic vesicle (Dudley and Robertson 1997; Golden *et al.* 1999). These expression data emphasise the existence of some differences which must be taken into account when studying the function of Bmps and their regulation of downstream targets in the two species.

At the optic cup stage, two other Bmps are detected in the eye. *Bmp2* is expressed in the RPE and *Bmp3* is strongly expressed in the mesenchyme surrounding the optic stalk (Dudley and Robertson 1997). In the chick embryo, *Bmp2*, *Bmp4*, *Bmp5*, *Bmp6* have been detected in the extra-ocular mesenchyme at optic cup stage (Belecky-Adams and Adler 2001b).

Targeted disruption of *Bmp4* or *Bmp7* have identified an important role for these genes in lens induction (Furuta and Hogan 1998; Jena *et al.* 1997; Wawersik *et al.* 1999). *Bmp7* null mice are born and show a variable expressivity of the aberrant lens induction phenotype depending on genetic background. They also exhibit microphthalmia and anophthalmia at birth (Dudley *et al.* 1995; Luo *et al.* 1995; Jena *et al.* 1997). Heterozygous *Bmp4* mutants are viable and display variable expressivity of several phenotypes including a low incidence of microphthalmia as well as a range of anterior segment defects detected postnatally (Dunn *et al.* 1997; Chang *et al.* 2001). Misexpression studies in the chick embryo, of the Bmp antagonists Noggin and HtrA1, result in several defects of the eye including microphthalmia, coloboma, pecten agenesis, and expression of optic stalk markers in the ventral neural retina. HtrA1 is a relatively recent addition to proteins that inhibit Bmps, but is not normally expressed in the eye (Adler and Belecky-Adams 2002; Oka *et al.* 2003). The chick misexpression studies indicate that Bmp signalling is important for optic cup morphogenesis and development beyond the period of lens formation, though they cannot differentiate between the roles that each Bmp, that is expressed during early eye development in the chick embryo, is playing in this process and which mechanisms are responsible for these abnormalities.

Bmp receptor expression

A combination of a type I and a type II receptors is vital for Bmps to mediate their signal to the cytosol and eventually to the nucleus. Bmp4 binds with high affinity to Bmprla (also referred to as Alk3), a type I receptor that is ubiquitously expressed in the optic vesicle and cup including the lens vesicle and the surrounding mesenchyme (Furuta and Hogan 1998; Liu *et al.* 2003). It also binds to Bmprlb (also referred to as Alk6), another type I receptor that is expressed in a complementary fashion to *Bmp4* in the proximo-ventral optic vesicle and later in the ventral neural retina and optic stalk (Furuta and Hogan 1998; Liu *et al.* 2003). Bmp7 binds more efficiently to Bmprlb and Activin receptor-I (Actr-I, also referred to as Alk2) (Yamashita *et al.* 1996). Actr-I is expressed in the lens placode and in the overlying surface ectoderm after lens vesicle formation (Yoshikawa *et al.* 2000).

There are currently only two studies reporting the expression of the Bmp type II receptor in the developing mouse eye. Study one utilised immunohistochemistry to show that at optic vesicle stage, the BmprII protein is present in both the proximal and distal layers of the dorsal optic vesicle in a domain wider than Bmp4 as well as in the surface ectoderm. But at the optic cup stage it is confined to the RPE and the anterior rim of the optic cup and in the lens vesicle (Faber *et al.* 2002). The second study utilises *in situ* hybridisation and reports that *BmprII* is barely detectable until the 15 dpc stage where it is expressed in the entire D-V axis of the neural retina, mainly confined to the retinal ganglion cell layer (Liu *et al.* 2003). As Bmp4 has not been shown to bind to any activin type II receptors, the expression reported so far for BmprII suggests that there may be other unidentified type II receptors that have a more closely matched expression pattern to Bmp4 in the eye.

In the chick embryo, *BmprIa* transcripts are ubiquitous in the optic vesicle and the entire optic cup including the lens. *BmprIb* is very weak at optic vesicle stage but is expressed throughout the optic cup, with highest levels in the ventral region (Trousse *et al.* 2001; Hyer *et al.* 2003). Data regarding the expression of *BmprII* is conflicting, with one study reporting expression only in the ventral optic cup by *in situ* hybridisation (Hyer *et al.* 2003), while another reports ubiquitous expression in the optic cup and the lens by both in situ hybridisation and RT-PCR (Trousse *et al.* 2001).

Heterozygous mouse mutants for Bmp and activin type I receptors appear normal, while homozygotes (all except BmprIb) fail to survive past 9.5 dpc (Gu *et al.* 1999; Mishina *et al.* 1995). *BmprIb* homozygous null mutants do not display any major eye phenotype. Except for a ventral retinal ganglion cell axonal guidance defect, there is no change in the expression of D-V markers of the eye or genes involved in retinal proliferation and differentiation such as *Chx10* and *Math5* (Liu *et al.* 2003). This suggests that many of the effects of Bmp signalling can be mediated by other type one receptors such as *BmprIa* which is ubiquitously expressed in the retina. *BmprII* heterozygotes appear normal while homozygotes die before 9.5 dpc (Beppu *et al.* 2000).

Expression of Bmp antagonists

Several inhibitors of the Bmp signalling pathway have been identified. At the optic cup stage, Noggin has been reported to be expressed in a small region of the dorsal neural retina and lens in the chick embryo (Trousse *et al.* 2001; Belecky-Adams and Adler 2001a), but no such pattern has been reported in the mouse (McMahon *et al.* 1998). *Dan*, which is another Bmp antagonist (Hsu *et al.* 1998), is present in the ventral neural retina and the surface ectoderm overlying the lens vesicle in the chick embryo (Ogita *et al.* 2001). No such expression has been reported for its mouse homologue (Stanley *et al.* 1998). *Ventroptin*, the most recently identified Bmp4 antagonist, is expressed in a naso-ventrally high gradient in the neural retina in the chick embryo (Sakuta *et al.* 2001).

A few studies have described the phenotypes of mouse with targeted disruptions of Bmp antagonists, but these phenotypes are related to the early involvement of these antagonists in neural induction and patterning and therefore their effect on eye development specifically cannot be examined. *Noggin* null mice undergo normal gastrulation but have been reported to exhibit skeletal and neural defects later in development (McMahon *et al.* 1998). The neural defects comprise failure of neural tube closure in cranial regions, which contributes to the disruption of eye development, and ventral patterning defects in the posterior neural tube (McMahon *et al.* 1998). *Chordin* null mice undergo normal neural development but display ear, pharyngeal, and cardiovascular abnormalities (Bachiller *et al.* 2000). Double null homozygotes for both *Chordin* and *Noggin* die before birth with severe anterior forebrain truncations and some reveal phenotypes similar to embryos lacking *Shh* including cyclopia (Bachiller *et al.* 2000).

1.4.2 Bmp4 and link to T-box genes

Of particular relevance to the study of the T-box genes in the eye is *Bmp4*, as it is expressed in the dorsal region of the developing eye (see previous section), where T-box gene expression has been detected during early eye development. Moreover, Bmps have been shown to regulate T-box gene expression in various tissues and species.

The *Omb* gene of *Drosophila* is the homologue of *Tbx2* and *Tbx3* in vertebrates (Bollag *et al.* 1994). Besides the high amino acid sequence similarity within the T-box region of these genes, they are expressed in many homologous tissues in the *Drosophila* and the mouse embryos. For example, *Omb* is expressed in the wing disc in the fly embryo, and *Tbx2* and *Tbx3* are expressed in the limb buds in the mouse embryo (Grimm and Pflugfelder 1996; Bollag *et al.* 1994; Chapman *et al.* 1996). *Omb* is expressed in the optic lobe anlagen and in the eye imaginal disc in the fly embryo, and *Tbx2* and *Tbx3* are expressed in the eye primordia of the mouse embryo as described earlier (Poeck *et al.* 1993).

Overexpression of *dpp*, the *Drosophila* homologue of the vertebrate *Bmp2/Bmp4* signalling factors, in the wing disc using an enhancer trap line that drives higher levels of *dpp* expression, induces ectopic *omb* gene expression. Indirect down-regulation of *dpp* by inactivation of *Hh*, which has been shown to regulate *dpp* expression in the wing disc, results in a decrease in *omb* expression (Grimm and Pflugfelder 1996; Nellen *et al.* 1996; Lecuit *et al.* 1996). Studies in vertebrates have also yielded evidence for the regulation of several T-box genes by members of the Bmp family. In the chick embryo, rhBMP2 soaked heparin beads placed lateral to the anterior neural plate of Hamburger Hamilton (HH) stage 5 chick embryos induces strong *Tbx2* and weaker *Tbx3* expression in the close vicinity of the bead (Yamada *et al.* 2000). Beads placed in the wing bud induce ectopic *Tbx3* expression (Tumpel *et al.* 2002) In the chick optic vesicle, forced expression of *Bmp4* by electroporation induces ectopic *Tbx5* expression in the entire optic cup while *cVax* is repressed (Koshiba-Takeuchi *et al.* 2000). *Xbra* expression in *Xenopus* has also been shown to be regulated by *Bmp4* (Jones *et al.* 1996).

These data indicate that Bmp regulation of at least members of the *Tbx2* subfamily, and maybe members of other T-box subfamilies, may be evolutionarily conserved among species and also within species in the formation of different organs. In this thesis, regulation of the T-box genes in the eye by the dorsally expressed *Bmp4* was investigated in mouse eye development.

1.4.3 Evidence of a Bmp4 signalling gradient in development

Patterning is a fundamental process in embryogenesis and allows the distinction and specialisation of groups of cells during development. This is the basis for development of distinct organs from the initial pool of unspecified cells of the embryo (Wolpert and Kerszberg 2003). Early patterning is often established by signalling molecules which induce different patterns of expression of transcription factors or other signalling molecules. The concept of morphogen gradients was introduced in developmental biology as a mechanism by which pattern formation could be achieved. A morphogen is the term given to a signal that fulfils two criteria: 1) it acts directly at a distance, and 2) it induces distinct cellular responses at different concentrations (Vincent and Briscoe 2001). Lewis Wolpert proposed that positional information establishes spatial patterning by the action of morphogens emanating from a localised source which diffuse away to introduce a concentration gradient across a field of cells (Wolpert 1969). These cells acquire a positional value with respect to the morphogen gradient and as such become patterned or distinct from each other. This can translate into unique gene expression, a difference in cell behaviour such as growth, or cell differentiation (Wolpert and Kerszberg 2003). A pattern can therefore be morphologically visible, but in some systems it may also exist even though it is not initially morphologically obvious, such as the topography of the RGCs in the developing eye.

In more recent years, candidate morphogens have been identified based on their concentration-dependent activity, but to prove that they act directly at a distance has been more challenging. Strong evidence has been provided for Dpp acting as a long-range morphogen in the wing imaginal disc on the basis of the following experiments: when a constitutively active form of the type I Dpp receptor *thick veins* (*tkv*) was misexpressed in a patch distinct from the endogenous *dpp* expression domain and that of its downstream targets, *omb* and *spalt,* which are normally expressed in a wider domain than *dpp*, *omb* and *spalt* were autonomously induced within cells that misexpressed *tkv* only. But when *dpp* was misexpressed in a similar manner, *omb* and *spalt* were induced in cells expressing *dpp*, but also in a circle of neighbouring cells of up to at least 20 cell diameters away from the source of *dpp* expression in the case of *omb*. Inactivation of *tkv* in a few cells within the normal

omb expression domain resulted in the absence of *omb* expression in those cells alone, indicating that cells must directly receive the Dpp signal to express *omb* (Nellen *et al.* 1996). The finding that direct Dpp signal transduction is necessary for *omb* and *spalt* gene expression was corroborated by an independent group who however also provided results which suggested that Dpp induction of *omb* expression far away from the *dpp* source may not always occur (Lecuit *et al.* 1996). Findings of a third group have shed some light on this contradiction by showing that Dpp is sufficient to induce ectopic *omb* expression in the hinge region of the wing disc but that in the wing pouch, it requires the presence of Wingless, which is another secreted signalling factor (Grimm and Pflugfelder 1996). Nevertheless, these findings together with the Dpp responsive *spalt* expression nested within the naturally broad expression domain of *omb* in the wing disc, which are both abolished in the absence of *dpp* (Lecuit *et al.* 1996), suggest that direct long-range Dpp signalling induces distinct gene expression in the *Drosophila* wing.

In vertebrates, although there is evidence that Bmps also induce concentration dependent responses, such as specification of distinct cell types in the neural tube (Barth *et al.* 1999; Nguyen *et al.* 2000), evidence for a direct action at a distance *in vivo* has so far not been achieved. Moreover, it has not been possible to directly visualise an endogenous morphogen protein gradient in an *in vivo* system, perhaps due to the inadequate sensitivity provided by current methods of *in situ* protein detection. Though visualisation of secretion of activin from a bead in *Xenopus* animal cap explants showed that exogenous activin, which like Bmp4 belongs to the TGFß super family, can form a concentration gradient in an *in vivo* environment (McDowell *et al.* 1997).

In contrast to the long-range actions of Dpp in *Drosophila* and of activin in *Xenopus*, it has been suggested, though not proven, that Bmp4 is a short-range signalling molecule. However, the experimental data on which this is based are not strong and include mRNA injections of *Bmp4* in one half of *Xenopus* animal cap conjugates (made of two animal cap aggregates) and the detection of *Xbra* in close vicinity of injected cells only (Jones *et al.* 1996). As only *Xbra* expression was analysed, these experiments cannot clarify the diffusion range of *Bmp4*. Detection of phosphorylated Smad proteins in response to Bmp4 signalling in the same type of experiments do

however show that the Bmp4 diffusion range is shorter than that of activin in animal caps (Ohkawara *et al.* 2002).

It has been suggested that the establishment of a concentration gradient of a putative morphogen can be established by other means than just the diffusion of the molecule itself. These include the effect of the distribution of receptors and antagonists, and the affinity of the protein for other extracellular matrix molecules and their availability (Wolpert and Kerszberg 2003). The action range of Bmp2, Bmp4 and Dpp is dependent on a positively charged N-terminal amino acid core which has been shown to restrict the Bmp action range in the mouse neural tube and *Xenopus* animal cap assays in comparison to when a mutation is introduced in this region. It is thought to act by enhancing the affinity of these proteins for extracellular matrix including heparan sulphate proteoglycans (Ohkawara *et al.* 2002; Hu *et al.* 2004). Despite the above described experiments, the actual diffusion range of the Bmp4 protein during *in vivo* development in vertebrate tissues remains unknown.

1.4.4 Conserved regulatory interactions between the Shh, Fgf, and Bmp signalling pathways?

Several groups of signalling molecules involved in the initial patterning of developing tissues have been identified, but the interaction between these molecules are less well understood. In several tissues in vertebrate embryos, antagonistic interactions between Shh and members of the Bmp family of signalling molecules have been demonstrated (see below). Furthermore, the interaction of these signalling factors appear to facilitate an optimal pattern of Fgf expression which drives growth of the tissue. The mRNA expression pattern of these signalling molecules are often detected in juxtaposed or opposite sites in developing tissues. As they are mostly secreted factors, it is thought that they interact to drive tissue growth by creating a pattern across the tissue and either regulate each other's expression or common downstream targets across the range of cells between their sites of expression. These interactions have been best studied during chick limb bud development and in the development of the forebrain, as well as and more caudal regions of the neural tube.

In the chick limb buds, which consist of undifferentiated mesenchymal cells encased in ectoderm, *Shh* is expressed in the polarizing region (posterior region), while several Fgfs are expressed in the apical ectodermal ridge (AER) and members of the Bmp family are detected in the anterior and the posterior mesenchyme as well as in the AER (Fig. 1.8; reviewed in (Tickle 2002). The expression of *Bmp2* and *Bmp4* in the developing limb is dynamic (Francis *et al.* 1994) and although the interaction between Shh and Bmps differ in the anterior region of the limb bud compared to the posterior region (Tickle 2002), it is thought that optimal Fgf expression is achieved in the AER by antagonism of Bmp signalling by Shh in the polarising region (Zúñiga *et al.* 1999; Khokha *et al.* 2003). Shh positively regulates *Fgf4* expression in the AER, which in turn feeds back to maintain *Shh* in the polarising region (Niswander *et al.* 1994; Laufer *et al.* 1994). Bmp signalling on the other hand negatively regulates the expression of Fgfs in the AER (Pizette and Niswander 1999) and it has been shown that the positive effect of Shh on the AER is mediated via inhibition of Bmp signalling. Furthermore, Bmps and Fgfs can antagonise each other's effects on limb growth and chondrogenesis (Niswander and Martin 1993; Buckland *et al.* 1998). Together, interplay between these pathways maintains an optimal level of Fgf expression in the AER which is essential for limb bud growth. The chick limb bud becomes truncated if the AER is removed, while growth can be rescued by implantation of Fgf coated beads (Niswander and Martin 1993; Tickle 2002).

Fig. 1.8 Interaction between the Shh, Bmp, and Fgf pathways in the anterior neural plate and in the limb bud

(A) Bmp, Shh, and Fgf expression in an early limb bud. **(B)** Shh from the polarising region (orange) in the posterior region of the limb bud maintains Fgf expression in the apical ectodermal ridge (AER; green) by indirectly antagonising Bmps in the mesenchyme. Bmps repress Fgf expression in the AER. Fgfs feed-back to maintain Shh expression in the polarising region. **(C)** In the developing anterior neural plate, Shh from the prechordal mesendoderm (orange) and Bmps from the lateral region of the neural plate (arrows) act antagonistically. Shh maintains *Fgf8* expression in the anterior neural ridge (green), while Bmps repress *Fgf8*. **(D)** Summary of the interactions between these pathways.

Abbreviations: ANR, anterior neural ridge; C, caudal; D, distal; P, proximal; Pre, presumptive; R, rostral;

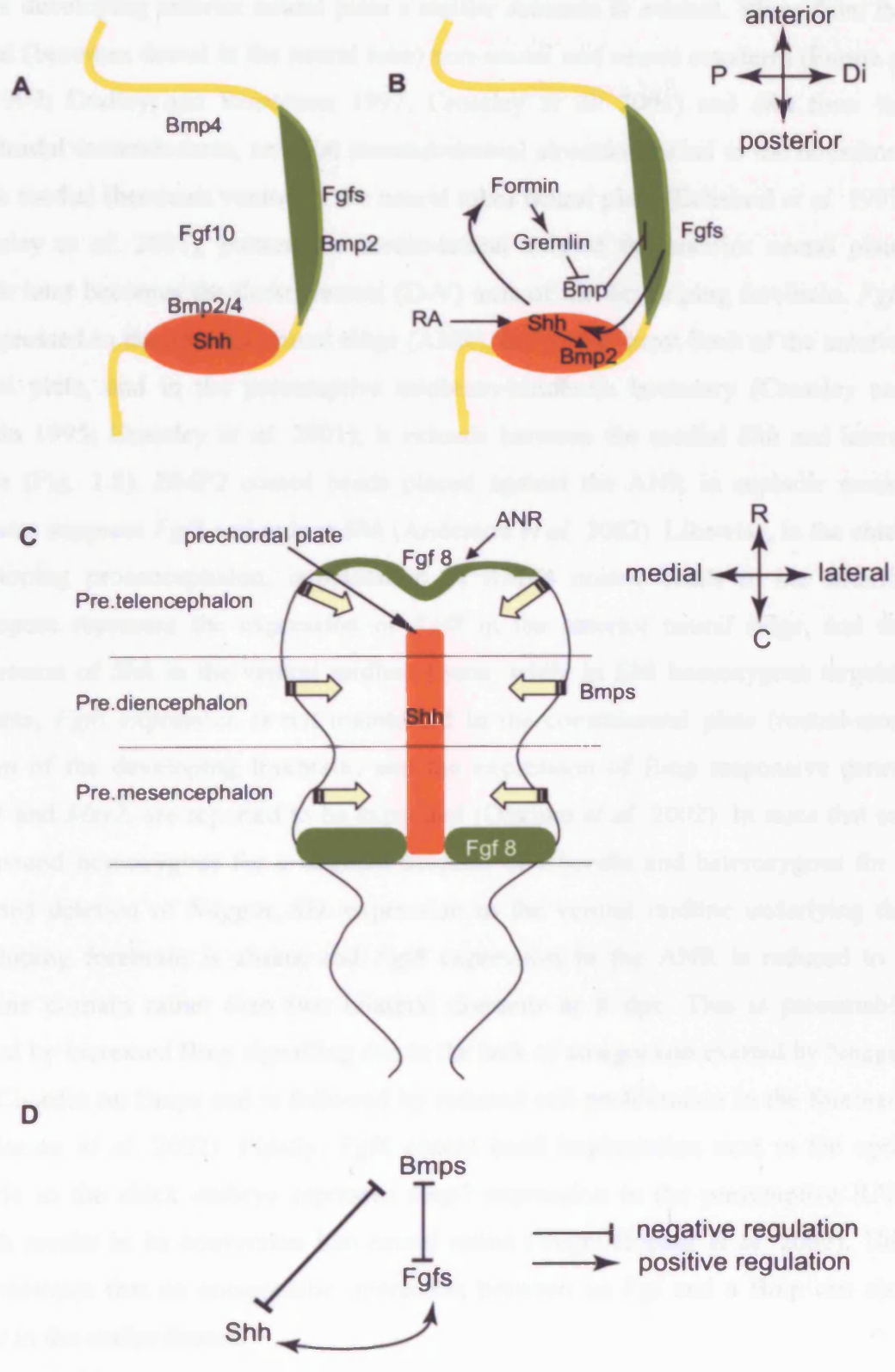
A
Bmp4
Fgfs
Fgf10
Bmp2
Bmp2/4
Shh
B
anterior
P
Di
posterior
Formin
Gremlin
Fgfs
Bmp
RA
Shh
Bmp2
C
prechordal plate
ANR
Fgf 8
R
medial
lateral
C
Pre.telencephalon
Pre.diencephalon
Pre.mesencephalon
Bmps
Shh
Fgf 8
D
Bmps
Fgfs
Shh
negative regulation
positive regulation

In the developing anterior neural plate a similar scenario is evident. Bmps from the lateral (becomes dorsal in the neural tube) non-neural and neural ectoderm (Furuta *et al.* 1997; Dudley and Robertson 1997; Crossley *et al.* 2001) and *Shh* from the prechordal mesendoderm, an axial mesendodermal structure rostral to the notochord in the medial (becomes ventral in the neural tube) neural plate (Echelard *et al.* 1993; Crossley *et al.* 2001), pattern the medio-lateral axis of the anterior neural plate, which later becomes the dorso-ventral (D-V) axis of the developing forebrain. *Fgf8* is expressed in the anterior neural ridge (ANR), the rostral-most limit of the anterior neural plate, and in the presumptive midbrain-hindbrain boundary (Crossley and Martin 1995; Crossley *et al.* 2001); it extends between the medial *Shh* and lateral Bmps (Fig. 1.8). BMP2 coated beads placed against the ANR in cephalic mouse explants suppress *Fgf8* and reduce *Shh* (Anderson *et al.* 2002). Likewise, in the chick developing prosencephalon, implantation of BMP4 coated beads in the anterior neuropore represses the expression of *Fgf8* in the anterior neural ridge, and the expression of *Shh* in the ventral midline tissue, while in *Shh* homozygous targeted mutants, *Fgf8* expression is not maintained in the commissural plate (rostral-most region of the developing forebrain) and the expression of Bmp responsive genes, *Msx1* and *Msx2*, are reported to be expanded (Ohkubo *et al.* 2002). In mice that are compound homozygous for a targeted deletion of *Chordin* and heterozygous for a targeted deletion of *Noggin*, *Shh* expression in the ventral midline underlying the developing forebrain is absent and *Fgf8* expression in the ANR is reduced to a midline domain rather than two bilateral domains at 8 dpc. This is presumably caused by increased Bmp signalling due to the lack of antagonism exerted by Noggin and Chordin on Bmps and is followed by reduced cell proliferation in the forebrain (Anderson *et al.* 2002). Finally, Fgf8 coated bead implantation next to the optic vesicle in the chick embryo represses *Bmp7* expression in the presumptive RPE, which results in its conversion into neural retina (Vogel-Hopker *et al.* 2000). This demonstrates that an antagonistic interaction between an Fgf and a Bmp can also occur in the ocular tissues.

Evidence so far suggests that a pattern in which Shh by antagonising Bmps enables the expression of *Fgf8* resulting in a high proliferation zone that drives forebrain development, reminiscent of limb development (Ohkubo *et al.* 2002). The authors

suggest that the expression of *Bmp4*, *Shh*, and *Fgf8* are interdependent and together create an environment where optimal growth of the forebrain can proceed (Fig. 1.8). Based on the presence of these same factors also in the chick eye, similar interactions have been proposed, although much less is known about them in the eye in comparison to the limb and the forebrain. In the developing mouse eye, the expression pattern of the dorsally expressed Bmp in the eye, *Bmp4*, in relation to *Shh* has not been carefully described, neither has the expression of suitably juxtaposed members of the Fgf family. In Chapter 3 of this thesis, an expression analysis for this purpose is undertaken and a putative interaction between *Bmp4* and a suitably positioned Fgf as well as the effect of the lack of that Fgf on D-V patterning of the eye is investigated.

1.5 Summary

More is currently known about the function of factors that are expressed in the ventral eye than the dorsal eye. It is known for example that disruptions of the ventral genes *Pax2* and *Vax1/2* cause coloboma and optic nerve abnormalities. On the contrary, the importance of genes that are expressed dorsally for optic cup formation is unresolved. With the lack of specialised structures in the dorsal neural retina, such as the optic fissure and the optic disc, a specific role, one that is restricted to the dorsal eye alone, for the dorsal genes in the development of the eye is not easy to envisage. *Bmp4* null mutants display a lack of lens induction, showing that *Bmp4* is essential for eye development (Furuta and Hogan 1998), but the embryonic lethality of this allele, which sets in at mid-gestation (Winnier *et al.* 1995), precludes further analysis of what might be the role of Bmp4 in retinal development. Heterozygous mice are viable and display variable expressivity of several phenotypes including a low incidence of microphthalmia as well as a range of anterior segment defects postnatally (Dunn *et al.* 1997; Chang *et al.* 2001). This suggests that Bmp4 may play several important functions in eye development, one being regulation of the growth of the eye. The anterior segment defects are most likely reflecting a late role of Bmp4 in eye development, when the anterior segment is developing. The incidence of microphthalmia on the other hand could potentially represent an early function of Bmp4 in the eye. Further support for a role in eye growth for Bmp4 comes from chick misexpression studies where *Noggin*, the Bmp

antagonist was misexpressed in the optic vesicle by retroviral delivery, which resulted in microphthalmia (Adler and Belecky-Adams 2002). The mechanisms by which Bmp4 can control the growth of the eye, the downstream genes that could mediate such an effect, and crucially, how a dorsally expressed gene may be implicated in the regulation of eye size and whether it does so by controlling regional growth or exerts an effect globally, remain unanswered. Evidence of T-box gene regulation by Bmps in several tissues and species supports the hypothesis that this may also be the case in the developing eye. In the chick embryo, such regulation has been demonstrated for *Tbx5* by *Bmp4*. In the *Xenopus* embryo, *Tbx2* and *Tbx3* are ectopically induced by *Bmp4*. In this thesis, the mouse model system was used to investigate the regulation of the T-box genes by Bmp4 in the developing mouse eye and the implication of manipulations of Bmp4 as well as the T-box genes for early eye development. The mouse model was used for majority of experiments as it provides a model of mammalian eye development, which is relevant for understanding formation of the human eye. When manipulations were not feasible in the mouse embryo, the chick embryo was utilised, as it offers a more accessible system for somatic cell manipulations.

1.6 Manipulation of gene expression or protein distribution *in vivo*

Manipulation of gene expression during embryogenesis has proved a vital tool in elucidating roles of single or combination of genes at organ or even cellular levels during embryonic development. There are several methods by which the spatial distribution of a gene product can be manipulated in an embryo and the method of choice is often governed by the research question as well as the model organism.

In developmental biology, the chick embryo is a classical model for *in vivo* manipulation studies and widely used for its ease of culture and accessibility in comparison to the mouse embryo for example. There are now several established means to achieve genetic manipulation in the chick embryo including electroporation and retroviral mediated gene delivery. The use of retroviruses for genetic manipulation of the embryo precedes the use of electroporation. The two approaches differ significantly and offer different advantages. For example, retroviral mediated

gene delivery offers integration and inheritance of foreign DNA into the host cell and its progeny (Morgan and Fekete 1996), but takes longer to express the transgene due to the time needed for the virus to integrate into the host genome and express. Moreover, the size of the transgene that can be inserted into the viral backbone is restricted and often it is not possible to express more than one transgene in the same cell. Electroporation on the other hand offers a means to deliver more than one transgene to the same cell and poses no limits on insert size (Momose *et al.* 1999). Moreover, it can be used to deliver viral DNA, in which case the transgene is integrated and inherited (Yasuda *et al.* 2000). The disadvantage of electroporation is the damage it can cause to a tissue as current is applied to make transient openings in cell membranes to allow uptake of foreign DNA.

In the mouse embryo, which is a well characterised mammalian model organism for human development, these types of manipulations are more challenging due to restrictions imposed by development of mouse embryos *in utero*. An *ex utero* culture technique has been developed but is currently restricted to gastrula and early neurula stage embryos, as culture beyond these developmental stages is currently not possible (Cockroft 1990). Delivery of genetic material in combination with the whole mouse embryo culture system is in its infancy and will be addressed in Chapter 6.

With the advent of technological advances such as the creation of mouse chimaeras and targeted mutagenesis by homologous recombination in ES cells, the first mouse 'knockouts' were produced in the 1980's (Papaioannou 1998). This technique has provided a powerful tool for the study of gene function in the mouse. Functional analysis in mice with a germ line mutation benefit from reproducibility of the mutation in future offspring; an advantage lost in approaches involving genetic manipulations in somatic cells of the embryo. Although once germline transmission is achieved, stably inherited genetic manipulations offer the best reproducibility and therefore a more homogenous population for analysis, these approaches are initially more time and cost consuming in comparison to somatic manipulations. Embryonic lethality in knockouts can also be a problem although this can be circumvented by tissue specific gene targeting. Furthermore, spatial regulation of the expression of a gene or dosage control is limited by the availability of tissue specific and dosage specific promoters.

The use of these techniques in understanding the function of a gene and genetic pathways have been demonstrated throughout this introduction. These techniques complement each other and provide necessary tools for genetic studies and ultimately the understanding of genetic pathways in driving tissue development. But the restrictions they each pose highlight the need for further refinements.

1.7 Aims of thesis

The aim of this thesis was to investigate the role of the dorsally expressed genes, *Bmp4*, and the T-box genes in D-V patterning and early development of the eye.

Bmp4 and members of the *Tbx2* subfamily, *Tbx2*, *Tbx3*, and *Tbx5* are expressed in the dorsal region of the developing eye of several vertebrate species. This is suggestive of a highly conserved function for these genes in eye development. Previous functional studies in the chick and analysis of heterozygous *Bmp4* mutants suggest that Bmp4 may be regulating eye growth. Furthermore, *Bmp4* regulates T-box gene expression in several vertebrate as well as invertebrate species. The following hypotheses were therefore tested in this thesis:

1. Bmp4 signalling regulates the expression of the dorsal T-box genes in the developing mouse eye and a Bmp-Tbx genetic pathway is required for the formation and growth of the optic cup.

2. *Tbx2* is required for optic cup morphogenesis and is implicated in the regulation of the expression of molecular and morphological asymmetries during this process;

   a) *Tbx2* regulates the expression of other asymmetrically expressed genes across the D-V axis

   b) *Tbx2* regulates growth of the dorsal optic cup

In **Chapter 3**, RNA *in situ* hybridisation was used to compare the expression pattern of *Tbx2*, *Tbx3*, and *Tbx5* in the mouse optic vesicle and newly formed optic cup. This study also aimed to compare the expression of these genes to the expression of signalling molecules, including *Bmp4*, and other asymmetrically expressed genes in the eye. This analysis served to identify potential interactions between signalling molecules that are expressed during early eye development, their relation to the T-box genes, and putative downstream targets of the T-box genes.

In **Chapter 4**, bead implantation in combination with whole mouse embryo culture was employed to manipulate Bmp4 signalling during optic cup morphogenesis. This approach allowed the investigation of T-box gene regulation by Bmp4. It also allowed the effect of manipulation of Bmp4 signalling to be assessed on eye size and shape. The whole embryo culture system provided excellent preservation of the morphogenetic process of optic cup formation.

In **Chapter 5**, the role of *Tbx2* in early eye development was investigated by analysing mouse embryos with a targeted mutation of *Tbx2* (provided by Professor V.E. Papaioannou, Columbia University, USA). Of the three T-box genes, *Tbx2* was selected for further analysis because of the availability of the *Tbx2* mutants and because *Tbx2* was found to be most responsive to Bmp4 manipulations in Chapter 4. RNA *in situ* hybridisation, immunohistochemistry, and histological analyses were carried out to examine whether loss of expression of *Tbx2* affected optic cup formation, the expression of *Tbx3*, *Tbx5*, and the spatial distribution of other D-V patterning genes.

In **Chapter 6**, retroviral mediated gene delivery was used to misexpress *Tbx2 in ovo* in the developing chick eye. This study investigated the consequence of the loss of the normal dorsal restriction of *Tbx2* expression in eye morphogenesis and growth, as well as early retinal cell differentiation.

This thesis presents novel findings on the role of Bmp4 in regulating D-V patterning and growth of the optic cup and on the function of *Tbx2* in regulating early optic cup growth and morphogenesis.

CHAPTER 2 Materials and Methods

2.1 General solutions, media, and laboratory equipment

2.1.1 General laboratory equipment

Petri dishes, pipettes, eppendorfs and Falcon tubes were supplied by Costar, UK. Pipette tips were supplied by VWR, UK. Pipette tips and eppendorf tubes were autoclaved prior to use. Centrifugations were either performed in a bench-top Sigma 1-15 microfuge (Philip Harris Scientific Ltd., UK) or in a Sorvall SS-34 Rotor (Du Pont Company, USA), as indicated in text. Dissections were carried out under a Stemi SV11 Zeiss microscope (Zeiss, Germany).

2.1.2 General solutions and reagents

Components of solutions made were purchased from Sigma, UK or BDH, UK unless stated otherwise. Basic solutions commonly used in experiments are outlined below. Solutions were autoclaved prior to use.

Diethylpyrocarbonate (DEPC) dH_2O	1% v/v DEPC (Sigma,UK) in dH_2O, shaken vigorously until dissolved, incubated at 37ºC, and autoclaved prior to use
1x Phosphate buffered saline (PBS) pH 7.4	0.15 M NaCl, 8 mM Na_2PO_4, 17 mM NaH_2PO_4
1x PBT (PBS+Tween)	0.1% Tween-20 (Sigma,UK) dissolved in PBS. DEPC treated if required
4% paraformaldehyde (PFA)	4% w/v PFA (Sigma,UK) dissolved in DEPC PBS, heated until ~60ºC while stirring until dissolved. Aliquoted and stored at -20 ºC until used.

2.2 DNA preparation and purification

2.2.1 Culturing of bacteria

All bacterial culture media were autoclaved as soon as prepared. To obtain single colonies, *Escherichia coli* (*E. coli*) bacterial cells were cultured on selective agar plates. All plasmids used in this thesis contained either the Kanamycin or the Ampicillin resistance genes. Therefore, stock solutions of 50 mg/ml of Ampicillin (Sigma, UK) or 30 mg/ml of Kanamycin (Sigma, UK) in dH_2O were added in a 1 in 1000 dilution to the culture media. Agar plates were prepared by pouring 25 ml of freshly prepared and autoclaved LB Agar (1% w/v Peptone 140, 0.5% w/v Yeast Extract, 85 mM NaCl, 1.2% Agar, Invitrogen, UK) plus the appropriate antibiotic into 100 x 20 mm Petri dishes. Once set at room temperature, bacterial cells were plated onto the agar and the dish was cultured upside down at 37°C overnight in a Heraeus Instruments horizontal incubator.

Single colonies were picked from the overnight culture on LB Agar and scaled up by inoculation in a starter volume of 5 ml LB Broth (1% w/v Peptone 140, 0.5% w/v Yeast Extract, 85 mM NaCl, Invitrogen, UK) containing the appropriate antibiotic in a flask that was approximately 5 times larger in volume than the broth volume. The culture was inoculated overnight at 37°C while shaking in an Innova 4300 shaking incubator at 200 revolutions per minute (rpm). If the culture was to be further expanded (large-scale culture), the initial starter culture was diluted 1:500 in fresh LB Broth with antibiotic and cultured for an additional overnight period.

2.2.2 Production of chemically competent bacterial cells

This procedure was performed as described by Inoue *et al.* (Inoue *et al.* 1990). Chemically competent bacteria, DH5α *E. coli* cells were streaked on a non-selective agar plate (no antibiotics) and incubated overnight at 37°C. Twelve colonies were picked and inoculated in 50 ml SOB (2% w/v Bacto peptone, 0.5% w/v Yeast extract, 10 mM NaCl, 2.5 mM KCl, 10 mM $MgCl_2$, 10 mM $MgSO_4$) and cultured while shaking vigorously at room temperature on a bench-top

orbital shaker. Optical density (od) at 600 nm was measured using a Pharmacia Ultraspec III UV/visible spectrophotometer. Once the od reached 0.6, indicative of the exponential growth phase of the culture, the culture was poured into pre-chilled Polypropylene tubes (Becton Dickinson and Co., UK) and incubated on ice for 10 min and then spun at 5000 rpm (1949 *g*) in a Sorvall SS34 rotor centrifuge for 10 min at 4°C. The supernatant was discarded and the pellet was resuspended by careful pipetting in 16 ml of filter sterilised and pre-chilled TB (10 mM Pipes, 15 mM $CaCl_2$, 250 mM KCl, pH adjusted to 6.7 with KOH, 55 mM $MnCl_2$), in which they were incubated on ice for 10 min and then centrifuged at 5000 rpm (1949 *g*) for 10 min at 4°C. After discarding the supernatant, the pellet was again dissolved in 4 ml ice-cold TB by gentle pipetting and incubated for 10 min on ice. Then 0.3 ml (7.5 % v/v) dimethyl sulphoxide (DMSO) was added to the cell suspension and cells were incubated for another 10 min on ice before being aliquoted into cryotubes (VWR International Ltd, UK) and snap frozen in liquid nitrogen. The aliquots were stored at -80°C until used.

To ensure that DH5α cells were not resistant to Ampicillin or Kanamycin, an aliquot of competent cells was plated on Kanamycin and Ampicillin agar plates each, which were incubated at 37°C overnight. No colonies were observed on either plate.

The transformation efficiency of these cells was determined by transforming 50 µl aliquots of competent cells with a 1:1 and a 1:100 dilution of 20 ng of plasmid DNA (see section 2.2.3). Overnight culture at 37°C of transformants on agar plates with the appropriate antibiotic yielded single colonies, which were counted to determine the transformation efficiency expressed as number of colonies per µg of DNA used in transformation. This was found to be ~2 x 10^6 colonies/µg DNA.

2.2.3 Transformation of plasmid DNA in bacteria

DNA transformation was achieved by the heat-shock method. 50-100 ng of DNA was placed in a pre-chilled Polypropylene tube (Becton Dickinson, UK). A 50 µl

aliquot of competent DH5α cells was thawed on ice and gently added to the DNA and mixed by gentle swirling. The mix was incubated on ice for 30 min followed by 45 sec in a 42°C water bath before being put pack on ice for 2 min. 950 μl of LB Broth was then added to the mix which was incubated for 1 hr at 37°C with horizontal shaking. 200 μl of this culture was spread on a selective agar plate, which was cultured at 37°C in order to obtain single colonies.

2.2.4 Purification of plasmid DNA from bacteria

The Qiagen min-prep and midi-prep kits (QIAGEN Ltd., UK) were used for isolation of plasmid DNA from small scale and large scale overnight cultures respectively according to the manufacturer's protocol. For the purpose of making RNA probes for *in situ* hybridisation, templates in plasmids containing cDNA were purified with the QIAGEN mini-prep kit. For *in vivo* transfection in mouse and chick embryos (Chapter 6), plasmid DNA was purified using the QIAGEN midi-prep kit which yields DNA of a higher purity. The basis of these kits is quite similar with the exception of the column-bound membranes used to bind plasmid DNA during the purification procedures. As such the buffers used to allow DNA binding and elution from each column differed. The mini-prep membrane binds DNA in high salt conditions and releases DNA in no or low salt conditions. The midi-prep column is an anion-exchange resin which binds DNA on the basis of the affinity of negatively charged DNA phosphate backbone to positively charged diethylaminoethyl (DEAE) groups on the membrane.

Apart from the initial spin, mini-prep centrifugations were carried out at maximum speed in a bench-top microfuge, while midi-preps were centrifuged in a Sorvall SS-34 rotor at the speeds and durations described in the QIAGEN protocol.

Briefly, for a small-scale preparation, transformed bacteria were cultured overnight in 5 ml of selective LB broth while shaking horizontally at 37°C (see section 2.2.1). The overnight culture was then centrifuged for 15 min at 2800 *g* and 4°C in a Sorvall SS-34 rotor to obtain a pellet of bacterial cells. For large-scale preparations, an initial overnight starter culture of 5 ml was further

expanded by a 1:500 dilution of the overnight inoculation in 25 ml of selective LB broth, which was cultured for an additional overnight period and then centrifuged in the same manner as the small-scale culture to obtain pelleted bacterial cells. Pelleted bacteria were resuspended in Buffer P1 (50 mM Tris-HCl, pH 8.5, 10 mM EDTA, 100 μg/ml RNase A). Cells were then lysed in the alkaline Buffer P2 (200 mM NaOH and 1% w/v sodium dodecyl sulphate [SDS]) by inversion of the tube 4-6 times. Then Buffer N3 was used for mini-preps and Buffer P3 for midi-preps (3 M potassium acetate, pH 5.5) to precipitate cellular debris and denatured proteins and chromosomal DNA while plasmid DNA, which is smaller in size, remained in solution. The lysate was centrifuged to remove the precipitated material and to isolate the supernatant, which was then applied to a QIAprep column containing a silica gel membrane (mini-prep) or a QIAGEN-100 tip containing an anion-exchange resin (midi-prep). All elutions from mini-prep columns were done by centrifugation, while elutions from midi-prep columns occurred by gravity flow.

While membrane-bound, DNA was washed in Buffer PE (mini-prep: contains ethanol) or Buffer QC (midi-prep: 1 M NaCl, 50 mM MOPS, pH 7.0, 15% v/v isopropanol). DNA from the mini-prep column was eluted in 50 μl Buffer EB (10 mM Tris-HCl, pH 8.5) and stored at -20°C. DNA from the midi-prep column was eluted with Buffer QF (1.25 M NaCl, 50 mM Tris-HCl, pH 8.5, 15% v/v isopropanol) and then precipitated with 0.7 volumes of isopropanol followed by centrifugation. The supernatant was discarded and pelleted DNA was washed with 2 ml of 70% ethanol followed by centrifugation. The supernatant was discarded after centrifugation and the DNA pellet allowed to air-dry before being dissolved in 50 μl Buffer EB (10 mM Tris-HCl, pH 8.5) or dH_2O. The concentration of DNA was estimated by agarose gel electrophoresis alongside a known quantity of a molecular weight marker (section 2.2.7). The concentration and purity of DNA was further quantified in a GeneQuant spectrophotometer (Pharmacia Biotech, UK). The absorbance measured at 260nm gave the concentration of DNA while the 260nm/280nm ratio indicated the purity of DNA from proteins. A ratio higher than 1.8 indicated satisfactory purity.

2.2.5 Characterisation and linearisation of plasmids

All restriction enzymes and buffers were purchased from Promega, UK. For characterisation purposes, double digests of plasmid DNA were set up in a final volume of 30 µl. For these digests, two enzymes with compatible buffer conditions were chosen in order to cut out a fragment of known size. For linearisation purposes, single digests were set up in a final volume of 100 µl as follows:

Table 2.1 Composition of characterisation and linearisation digests of plasmid DNA

	Characterisation	Linearisation
dH_2O	to a final volume of 30 µl	to a final volume of 100 µl
10 x Buffer	3 µl	10 µl
DNA	0.6-0.7 µg	10-12 µg
enzyme 1	1 µl	9 µl
enzyme 2	1 µl	n/a

n/a: not applicable.

The digests were mixed by vortexing and then spun for 6 sec in a bench-top microfuge to ensure that the entire volume was at the bottom of the eppendorf tube. Digests were then incubated for 2 hrs (characterisation digests) or 5 hrs (linearisation digests) in a 37°C water bath. 4 µl of the characterisation digests and 2 µl of the linearisation digests were run on an agarose gel next to 0.5 µl of uncut DNA and 5 µl of a molecular weight marker to ensure that all DNA was cut in the linearisation digests and to check that the size of the fragments produced in the double digests corresponded to those expected according to plasmid maps.

2.2.6 Phenol/chloroform extraction of plasmid DNA

Linearised DNA (100 µl) was purified from proteins using the phenol/chloroform method. 100 µl of a mixture of 25:24:1 phenol/chloroform/isoamyl alcohol solution (Sigma, UK) was added to 100 µl of the linearisation digest and mixed by vortexing. The mixture was spun for 5 min at 13,000 rpm in a microfuge, which resulted in the separation of the mix into an aqueous and an organic layer. The aqueous layer (top layer) was removed and

put in a fresh eppendorf tube. To this was added 100 µl of chloroform in order to remove any traces of phenol. The solution was mixed by vortexing and centrifuged for 5 min at 13,000 rpm. The top layer, containing the DNA, was removed and put into a fresh eppendorf tube. DNA was precipitated overnight at -20°C by the addition of 10 µl 3 M sodium acetate (pH 5.3) and 500 µl 100% ethanol to the 100 µl volume of DNA. The next day the solution was centrifuged at 13,000 rpm at 4°C for 30 min. The liquid was decanted and the pellet was washed in 200 µl of 70% ethanol, centrifuged for 10 min at 4°C and 13,000 rpm, and then the DNA pellet was allowed to air-dry before being dissolved in an appropriate volume of DEPC treated dH_2O in order to obtain a concentration of 1 µg/µl. The purified DNA solution was checked by agarose gel electrophoresis.

2.2.7 Agarose gel electrophoresis

This method allows the visualisation and separation of nucleic acid according to size. An appropriate volume of DNA or RNA (as stated under relevant sections) were diluted in dH_2O and 5 x loading buffer (Bioline,UK). The agarose gel was prepared by dissolving agarose powder (Flowgen, UK) in 1xTAE (Tris-acetate EDTA; 0.04 M Tris-acetate, 1 mM EDTA, pH 8.0) and heating the mix in a microwave oven until no powder or bubbles remained. The heating period differed between approximately 2 min for mini-gels of 50 ml and 1% w/v to 12-15 min for maxi-gels of 300 ml and 2% w/v. The concentration of agarose gels depended on the size of the genetic material to be analysed. To check digests of plasmids and linearised probes, a 1% w/v agarose gel was used. For the low molecular weight PCR products obtained from genotyping of *Tbx2*$^{-/-}$ embryos, a 2% w/v gel was used. Ethidium bromide, which intercalates into the DNA backbone was added to the gel at a final concentration of 0.5 µg/ml. The gel was then allowed to set at room temperature in a gel cast with an inserted comb in order to make wells that could hold the loaded volume. Once set, the gel was submerged in 1xTAE in an appropriately sized gel tank (Gibco BRL, UK). The previously prepared dilutions of the DNA or RNA were loaded into the wells. For quantification purposes, 5 µl of a DNA molecular weight marker (ladder) was also loaded onto the gel. The DNA ladder used for quantification purposes during agarose gel electrophoresis were the 2-Log DNA ladder (New England

Biolabs Inc., USA), the Hyperladder I (Bioline, UK), or the GenRuler (Fermentas) all of which contain fragments of plasmid DNA ranging from 100/200 bp to 10,000 bp in size. At 5 μl, the quantity of each fragment in the ladder was known. Current was applied at approximately 60 V for mini-gels and 130 V for maxi-gels in order to allow the migration of DNA fragments across the gel. After completion, the gel was visualised under ultra violet (UV) light and images were captured using a UVitec camera and the AlphaImager Programme.

2.3 Mouse models; obtaining and genotyping embryos

The mouse models used in different Chapters of this thesis include the inbred CBA/Ca wild-type strain in Chapters 3 and 4, the Fgf15 knock-in allele on a mixed genetic background (A. Battersby, University of Wales Cardiff) in Chapter 3, the *Tbx2*^{tm1Pa} allele on a mixed Sv/C57/ICR background (Harrelson *et al.* 2004) in Chapter 4, and the spontaneous *Chx10*^{OrJ} allele (Burmeister *et al.* 1996) on a 129/Sv background in Chapter 4. The CBA/Ca strain used in the embryo culture experiments in Chapter 4 is a widely used strain in research due to good breeding performance and litter size (Mouse Genome Informatics). It is a pigmented strain, suitable for studies of eye development.

2.3.1 Maintenance of adult animals

Mice were maintained in a barrier facility on a daily cycle of 12 hours (hrs) artificial light and 12 hrs darkness. Caging, feeding, breeding, and general maintenance were according to Home Office (UK) regulations

2.3.2 Timed mating

Mice reach breeding age around six weeks after birth (Hetherington *et al.* 2000). Matings were set up between three or four females and a male per cage overnight. In the morning, females were checked for vaginal plugs with a blunt metal probe. The plug, which is a white coagulate, forms in the opening of the vagina after mating has occurred. Upon identification of a plug, the female was

removed from the breeding cage and kept separately. Mice usually mate in the middle of the dark period (Hetherington *et al.* 2000). The age of the litter at midday of the day of the detection of a vaginal plug was therefore designated 0.5 days post coitum (dpc).

2.3.3 Obtaining homozygous embryos

To obtain homozygous embryos for the *Tbx2*^{tm1Pa} and the *Fgf15-Egfp* alleles, timed matings were set up between heterozygous animals as described in Section 2.3.2. *Chx10*$^{OrJ/OrJ}$ homozygous embryos were obtained from timed matings of homozygous breeding pairs of adult mice, as the *Chx10*$^{OrJ/OrJ}$ mice are viable and fertile.

2.3.4 Dissection of embryos from pregnant females, fixation, and storage

Pregnant animals were killed by cervical dislocation and embryos were dissected out of the uterus in PBS if they were to be fixed, and in Dulbecco's modified Eagle's medium (DMEM, Gibco BRL, UK) containing 10% heat inactivated fetal calf serum (FCS, Sigma, UK) if they were to be cultured, using No5 Watchmakers forceps (Interfocus, UK).

The uterus was removed through a horizontal incision across the mouse abdomen and washed in PBS. The decidual swellings were taken out of the uterus individually by carefully teasing open the uterus from one end, at the mesometrial surface until a decidual swelling was visible. Keeping the forceps close together and working with small motions, the tear in the uterine wall was made larger until more of the decidua was visible. The decidual swelling was then freed from the uterine wall by gentle squeezing with the forceps. This was repeated until all decidual swellings were out. The decidua, trophoblast, and Reichert's membrane were carefully trimmed around the ectoplacental cone until the yolk sac and the embryo were completely revealed. Then, a small hole was made in the yolk sac, where it meets the placenta. This hole was made in an avascular region, taking great care not to rupture any of the yolk sac vessels. The

hole was then made bigger by making small tears while going around the placenta with the forceps. The yolk sac, together with the amnion, were pulled over the head of the embryo and positioned under its tail, exposing it for manipulations. This allowed easy access to the eye for bead implantation purposes.

Embryos that were to be fixed immediately after dissection were freed from all extra-embryonic layers. For genotyping purposes of mutant litters, the yolk sac of each embryo was dissected with great care in order to avoid tissue contamination between embryos or between embryo and the placenta; forceps were often wiped clean and flamed between the dissection of each embryo. Isolated yolk sacs were rinsed in PBS and kept for genotyping at -20 °C. Embryos were fixed overnight in 4% w/v PFA in DEPC treated PBS at 4 °C. After fixation, they were rinsed twice in DEPC treated PBT, and dehydrated to 100% methanol through an increasing concentration series of methanol : DEPC PBT (25%, 50%, 75%, 100%) while rocking gently at 4 °C. 9.5-10.5 dpc embryos were washed for 20 min in each solution, while older embryos were washed for 25 min. After the last wash embryos were put in fresh 100% methanol, in which they were stored until further use at -20°C.

2.3.5 Genotyping of embryos by Polymerase Chain Reaction (PCR)

2.3.5.1 Isolation of genomic DNA

To obtain genomic DNA from embryos for genotyping, yolk sacs were digested overnight at 55 °C with 0.1 mg/ml Proteinase K (Sigma, UK) in 200 μl "lysis buffer" (50mM Tris pH 8.0, 100 mM NaCl, 100 mM EDTA, 1% SDS). Lysates were shaken for 5 min on a horizontal shaker, after which 100 μl of saturated (6M) NaCl was added to each tube. Samples were again shaken for 5 min on a horizontal shaker and then spun for 10 min at 13,000 rpm in a microfuge to pellet proteins at the bottom of the eppendorf tube. Supernatants were gently poured into new eppendorf tubes and 250 μl of 2-isopropanol was added to each sample to precipitate DNA. Tubes were inverted 3-5 times to mix all components and were then spun for 10 min at 13,000 rpm to pellet DNA. Supernatants were

carefully poured out and DNA pellets were washed with 250 µl of 70% ethanol followed by centrifugation at 13,000 rpm. The ethanol was poured out and pellets were left to dry with each eppendorf tube tilted upside down on a clean sheet of paper. Once dry (~10 min), pellets were re-suspended in 100 µl TE buffer (10 mM Tris pH 8, 1 mM EDTA) and kept at -20 °C until used.

2.3.5.2 PCR amplification

Embryos from matings of *Tbx2*^{tm1pa} heterozygous mice were genotyped using a three-primer system (Table 2.2) as described in (Harrelson *et al.* 2004). Each 20 µl PCR reaction contained the following: 2 µl genomic DNA as template, 200 ng forward primer one, which was specific for an intronic region between exons two and three and was present in the wild-type allele but absent in the mutant allele, 200 ng of forward primer two, which was specific to a region introduced by the insertion of the *loxP* sites in the mutant allele and remained intact after the *cre*-mediated excision of PGK-*neo*, 200 ng of reverse primer three, which was specific for an intronic region between exons two and three in both alleles. To these components were added 0.2 mM of each deoxyribonucleotide triphosphate (dNTP; Bioline, USA), 1x buffer (10 mM Tris-HCL pH 8.0, 50 mM KCL, 2.5 mM $MgSO_4$, 0.5% v/v DMSO, 0.2 mM spermadine, 0.1% v/v Tween-20), and 1 unit of *Taq* DNA polymerase (Invitrogen, USA). Positive controls for each allele were included in each PCR run using DNA templates of known genotypes. A water control, in which the DNA template was substituted for dH_2O was also included to control for DNA contamination. Each reaction volume was made up to 20 µl with dH_2O and tubes were sealed with caps.

Reactions were incubated in a thermal cycler (Biorad MyCycler) at 94°C for 10 sec for the initial denaturing step of double stranded DNA template, followed by 36 cycles of amplification with 10 sec at 94°C to denature, 30 sec at 61°C to allow annealing of primers, and 30 sec at 72°C for extension. At the end of the 36 cycles, reactions were incubated at 72°C for another 5 min, to ensure complete synthesis of all PCR products, and then held at 4°C. A sample of 10 µl of each PCR reaction was run on a 2% agarose gel as described in Section 2.2.7, to separate the amplified products.

Table 2.2 Details of PCR Primers and the expected amplified products

Primer	Sequence	Tm°
1- T2F1	5'-CCAGCCAGGGAACATAATGAGG-3'	58°C
2- T2m4F	5'-CCTGCAGGAATTCCTCGACC-3'	64°C
3- T2R1	5'-CTGTCCCCTGGCATTTCTGG-3'	~1°C
Product size	wild-type allele: 180 bp	
	mutant allele: 80 bp	
Fgf15 (wt) p11	5'-GACTTGATGCAATTAGGAGG-3'	58°C
Fgf15 (wt) p55	5'-CAGCCGTAGAGAAAGAGTG-3'	58°C
Fgf15 (mt) p50	5'-GTAACCATTATAAGCTGCAAT-3'	56°C
Fgf15 (mt) p5	5'-TGCAAGCTTTCCTTGATGGCAATCGTC-3'	~65°C
Product size	wild-type allele: 388 bp	
	mutant allele: 513 bp	

Each *Fgf15* PCR reaction consisted of: 1 µl genomic DNA, 0.75 µl of each primer (10 pmol/µl solution), 1x NH_4 Reaction Buffer (16 mM $(NH_4)_2SO_4$, 67 mM Tris-HCL pH 8.8, 0.1% v/v Tween-20; Bioline, UK) *either* 1.5 mM $MgCl_2$ solution (for primer pair p11+p55 recognising the wild-type *Fgf15* locus) *or* 2.5 mM $MgCl_2$ solution (for primer pair p50+p5 recognising the excised locus), 3 mM dNTP solution, 1.5 unit of BIOTAQ DNA Polymerase (Bioline, UK) in 25 µl H_20 (Sigma, UK). The PCR reaction consisted of an initial 2 min at 96°C followed by 30 cycles of: 95°C for 30 sec (denaturation), *either* 50°C (primer pair p11+p55) or 55°C (primer pair p50+p5) for 30 sec (annealing), and 72°C for 1 minute (extension). A single 5 min elongation step at 72 °C was added at the end of the 30 cycles.

2.4 Mouse whole embryo culture

2.4.1 Preparation of rat serum

Blood was withdrawn from the abdominal aorta of ether-anesthetised male Sprague-Dawley rats, decanted gently into a 15 ml centrifuge tube and centrifuged immediately at 1000 *g* for 5 min. This separated the plasma from red blood cells. The plasma was allowed to clot at room temperature and serum was squeezed out with forceps and transferred to a fresh tube, taking care not to mix with the blood. The serum was centrifuged again at 1000 *g* for 5 min and

transferred to a fresh tube, to ensure that no remnants of blood remained. It was then heat-inactivated at 56 C° for 30 min and stored at -20 C° until used.

2.4.2 Culture of embryos

The whole mouse embryo culture system has successfully been used to study many aspects of embryogenesis, for example neural tube closure (Greene and Copp 1997). It has been demonstrated that mouse embryos can grow and develop as *in utero*, in culture conditions first established by David Cockroft (Cockroft 1990; Martin and Cockroft 1999).

Plugs were obtained and conceptuses dissected out of the uterus as described in Sections 2.3.2 and 2.3.4. Unless embryos were in exceptional health (strong blood circulation) they were put in 'recovery culture' for approximately one hour before further manipulations took place. Embryos were cultured in 30 ml Universal tubes (Nalgene Nunc, USA) at 37°C in a roller incubator (30-40 rpm) for approximately 15-18 hours (hrs) in 3 ml medium containing 25% rat serum in culture saline (0.12 M NaCl, 4 M KCl, 0.4 mM $MgS0_4.7H_20$, 0.25 mM $MgCl_2.6H_2O$, 0.60 mM $NaH_2PO_4.2H_20$, 1.8 mM $CaCl_2.2H_2O$, 11 mM Glucose, 24 mM $NaHCO_3$). Prior to incubation, embryos were manually gassed for approximately 1 min with 95% O_2/ 5% CO_2 (Cryoservice Ltd, UK). The rim of the tubes were smeared with silicone grease to create a gas-tight seal. Assessment of health and growth of embryos after culture are described in Chapter 4.

2.5 Obtaining chick embryos

Handling of eggs and chick embryos were carried out as described in the 'Essential Developmental Biology' book (Stern 1993). For electroporation experiments in Chapter 6 with the pIRES2-EGFP vector, brown eggs were used. For electroporations with the RCAS-AP or retroviral delivery, pathogen-free white Leghorn eggs were used to avoid viral interference from possible previous infections, which would prevent new infection.

2.5.1 Egg incubation

Fertile eggs were purchased from Henry Stewart & Co Ltd, Lincolnshire, UK. They were stored at 15°C for up to 4 days prior to incubation. To initiate development, eggs were placed horizontally in a humidified (Curfew incubators model 747) incubator at 38°C. Manipulations were carried out on day 1.5 of incubation, when most embryos reached Hamburger and Hamilton stage (HH) 9-10, which is the stage when the optic vesicles form (Hamburger and Hamilton 1992).

2.5.2 Preparation of the egg for manipulation

Eggs were placed horizontally, in the same orientation that they had been incubated in, in an egg tray under a dissecting microscope (Stemi SV11, Zeiss, Germany) with transmitted light. The surface of the egg was wiped with 70% ethanol. With the tip of a pair of sharp scissors, the pointy end of the egg, which does not contain the air sac, was gently tapped to make a small hole. A 19 G needle (Becton Dickinson, UK) attached to 5 ml Luer tip syringe (BD, Biosciences, UK) was inserted through the hole and ~3 ml of albumin was removed to lower the embryo from the upper surface of the egg, in order to avoid damaging the embryo when opening the egg. A large part of the upper surface of the egg was then covered with one piece of cellotape and using a pair of fine scissors, an oval-shaped piece of the shell was cut and removed to reveal the embryo. The cellotape helped to minimise cracks and to prevent egg shells to fall on the yolk and the embryo. If large pieces of the shell fell inside the egg, they were gently removed with forceps.

2.5.3 Staging of chick embryos

Embryos were staged according to the Hamburger and Hamilton descriptions of morphology. For younger embryos, staging was based on assessment of the shape of the optic vesicles and the number of somite pairs. After optic cup formation, staging was based on limb morphology and the appearance of the branchial arches.

2.5.4 Explanting embryos from the egg

Using a pair of sharp scissors, four cuts were made in the vitelline membrane around the embryo. For younger embryos (until HH 20) it was possible to lift out the embryo from the egg by grabbing two opposing corners of the cut membrane using watchmakers' forceps. Older embryos (above HH 20) were lifted out in a spoon as they were too heavy to be lifted out with the membrane.

If embryos were to be processed for RNA *in situ* hybridisation, they were rinsed and cleansed from membranes in DEPC treated PBS, but otherwise non-treated PBS was used. Once the vitelline membrane and the yolk sac were removed, embryos were rinsed in fresh (DEPC) PBS and then fixed overnight at 4 °C in 4 % PFA. If not processed further immediately after fixation, embryos were dehydrated in an ascending concentration of methanol involving 20-25 min washes in 25, 50, 75, and 100 % methanol in (DEPC) PBT, which was performed at 4 °C. Embryos were kept in 100 % methanol at -20 °C until used.

2.6 Manipulation of the embryo

Many of the experiments described in this section required pulled glass capillary needles. Borosilicate glass capillaries (Clark electromedical instruments, UK), were prepared by Katy Gardner (Institute of Child Health) on a P-87 Flaming/Brown micropipette puller (Sutter Instrument Co.).

2.6.1 Protein delivery by bead implantation

Human BMP4 is initially translated as a pro-protein of 408 amino acids, which is post-translationally cleaved into an active 116 amino acid peptide. The rhBMP4 used in this study was produced in a mouse myeloma cell line and is a homodimeric form of two 116 amino acid human peptides crosslinked by a disulfide bond (R&D Systems, UK). The human and mouse homologues share 98% amino acid sequence similarity (Botchkarev 2003).

The application of a concentration range of rhBMP4 coated beads [1-100 μg/ml] in the anterior neuropore in chick embryos was previously reported to cause a range of abnormalities with the degree of severity corresponding to the concentration of rhBMP4 protein (Ohkubo *et al.* 2002). In another study where rhBMP4 coated beads at [1-5 μg/ml] were applied to wild-type mouse optic vesicle explant cultures, no effects were observed on eye development, but the application of the same concentration of rhBMP4 to *Bmp4*$^{-/-}$ optic primordia, which lack the ability to form a lens, was reported to rescue lens formation. (Furuta and Hogan 1998). Therefore, in order to achieve an effect on eye development, a 100 μg/ml rhBMP4 solution containing 0.1 % w/v BSA in PBS was used in experiments described in Chapter 4.

The Noggin protein used is a homodimeric form of a chimeric protein consisting of amino acid residues 20-232 of mouse Noggin fused to the Fc region of human IgG_1 via a polypeptide linker. It was produced in a mouse myeloma cell line (R&D Systems, UK). A stock solution of 1mg/ml was made by dissolving the Noggin powder in PBS containing 0.1% BSA. The concentration of Noggin used are stated in the description of relevant experiments in Chapter 4. As a control for the surgical procedure, implantations were performed with beads soaked in 0.1% w/v BSA in PBS.

Affi-Gel Blue beads made of cross-linked agarose gel with covalently attached Cibacron blue (a blue dye) were used as protein carriers (Biorad, USA). 10 μl beads in sodium azide solution with a diameter of 80-150 μm were first washed with embryo water (Sigma, UK) three times and centrifuged to remove the sodium azide. They were then incubated for a minimum of one hour at 37 C° in 5μl of either rhBMP4 or Noggin protein of concentrations stated.

Bead implantation into the eye was performed with the embryo resting on its side in explanting saline (0.12 M NaCl, 4 M KCl, 0.4 mM $MgS0_4.7H_20$, 0.25 mM $MgCl_2.6H_2O$, 0.60 mM $NaH_2PO_4.2H_20$, 1.8 mM $CaCl_2.2H_2O$, 0.83 mM Glucose, 0.6 mM $NaHCO_3$) in a Petri dish. Prior to bead implantation, the location in which the bead was to be inserted was pierced using a sharpened tungsten wire.

A bead was then placed in the pierced location using a pulled glass needle (see section 2.6.2.3) and a mouth pipette. The specific locations of beads are stated in the description of the results.

In experiments where high concentration rhBMP4 was used, the uptake of protein by beads, rather than the concentration of protein solution was increased (Lee *et al.* 2001b). Beads were incubated in an initial 5 µl volume of 100 µg/ml stock solution and allowed to airdry for 2 hrs. They were then incubated in another 5 µl of the protein stock solution but this was done in cycles of ~2 µl volumes in between which the beads were allowed to dry for 2 hrs. This increases the amount of protein uptake by the beads and therefore, more protein can be delivered.

2.6.2 Gene delivery by electroporation

Electroporation is the method whereby the lipid bilayer of the plasma membrane of cells is briefly permeabilised by the application of a single or multiple electric pulses. *In ovo* electroporation in the chick embryo has been employed to misexpress various genes in the developing eye (Koshiba-Takeuchi *et al.* 2000; Sakuta *et al.* 2001; Kubo *et al.* 2003) as well as in other tissues (Itasaki *et al.* 1999; Swartz *et al.* 2001).

2.6.2.1 Vectors used and preparation of the DNA solution

pIRES2-EGFP

The pIRES2-EGFP vector (BD Biosciences Clontech), which expresses enhanced green fluorescent protein (EGFP) when taken up by cells, and the RCASBP-AP vector (here referred to as RCAS-AP), which expresses the human placental alkaline phosphatase (AP) enzyme were used in electroporation experiments. The expression of EGFP can be directly assessed by fluorescence microscopy and the expression of AP can be histochemically assessed at the end of the experiment to visualise plasmid uptake in the eye. Since the chick embryo offered a system, in which retinal cell differentiation and RGC axonal projections could be studied due to the possibility of longer culturing of embryos after

manipulation, a strategy that allowed long term expression of the transgene was desirable. The pIRES2-EGFP vector was not suitable for this purpose but was extremely useful for visualising the targeted cells in live embryos during the experiment and was therefore used in conjunction with the RCAS-AP plasmid (proviral form), which offers long term expression. In this manner, stable transgene expression and direct visualisation of transfected cells could be achieved.

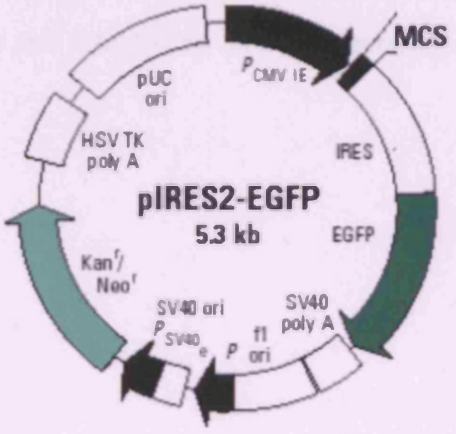

Fig. 2.1 Schematic diagram of the pIRES2-EGFP vector

cDNA inserted into the multiple cloning site (MCS) is driven by the CMV promoter in conjunction with EGFP (BD Biosciences Clontech, UK)

pIRES2-EGFP (Fig. 2.1) contains a multiple cloning site downstream of the constitutively active cytomegalovirus (CMV) promoter, followed by an internal ribosomal entry site (IRES), the EGFP gene, and an SV40 polyadenylation signal. It is constructed so that the cDNA of interest, inserted into the multiple cloning site, is transcribed in conjunction with EGFP as a bicistronic mRNA. But the two proteins are translated separately due to the IRES fragment. The advantage of this vector is that it drives the expression of EGFP and the protein of interest in the same cell, allowing direct detection of the site of plasmid uptake and protein expression. In comparison to other types of vectors, which lack the IRES and tag the protein of interest to a fluorophore or a chromophore, the risk of a conformational change to the protein structure is minimised.

RCAS-AP

The RCASBP (replication-competent, avian leukemia virus long terminal repeat, splice acceptor, Bryan high-titre, polymerase) vectors are derived from the Rous sarcoma virus and encode genes vital for viral replication, production, and integration into the host cell genome but lack the *src* oncogene normally carried by this virus (Fig. 2.2). RCAS-AP encodes a retroviral backbone (RCASBP subtype A) with the *gag, pol*, and *env* viral genes (see Fig. 2.2) as well as the full-length AP cDNA. It produces a replication competent virus, which is capable of infecting avian cells and integrating into their genome.

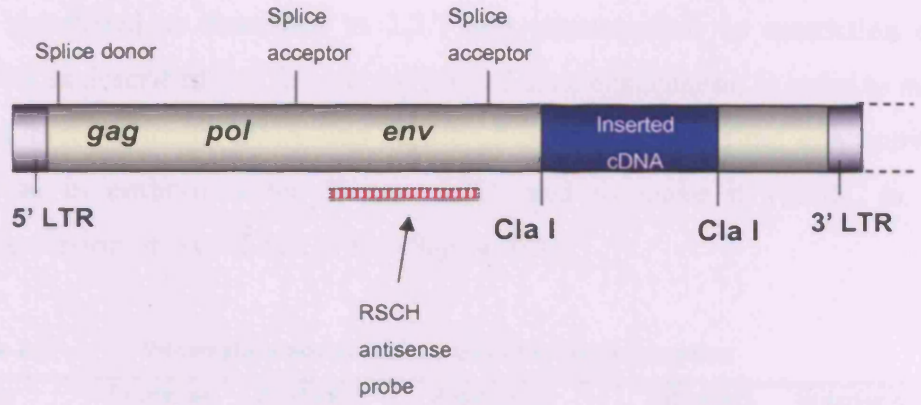

Fig. 2.2 Schematic diagram of the important features of the RCASBP retroviral vector

The provirus (double stranded DNA form) contains two identical untranslated regions called the long terminal repeats (LTR) that contain the viral transcription regulatory regions, which drive transcription of viral genes as well as the inserted gene. The proviral genome also consists of *gag*, which encodes viral protease, nucleocapsid, capsid, and matrix proteins, *pol*, which encodes reverse transcriptase and integrase, and *env*, which encodes viral envelope glycoproteins. The desired cDNA is inserted in the *Cla* I site (blue box). The splice donor and splice acceptor sites enable the production of three different transcripts one of which encodes the inserted cDNA alone. The *RSCH* probe used for detection of the virus in infected tissue is depicted by a stripy pink box.

Plasmids were amplified in DH5α bacterial cells and midi-prepped as described in Sections 2.2.2-2.2.4. DNA was dissolved in buffer EB (10mM Tris, pH 8.2) and quantified as described in 2.2.7 and characterised by restriction enzyme digests as described in 2.2.5. At the start of each experiment, in order to make the DNA more viscous, DNA was dissolved in a 16% w/v final concentration of sucrose in embryo water (Sigma, UK), and to make it visible, in a final concentration of 0.05% fast green (Sigma, UK).

Table 2.3 Information about vectors used for electroporation

Vector (size, bp)	Promoter	Antibiotic resistance	Restriction enzyme used for characterisation	Expected bands (bp)	Supplier of vector
pIRES2-EGFP (5,308)	CMV	Kanamycin	Hind III	5,039 + 269	Dr. C Beesley; (ICH, London, UK; originally purchased from BD Biosciences Clontech)
RCAS-AP (13,842)	LTR	Ampicillin	*Cla* I	11,657 + 2,185	Dr J Chan (ICH, London, UK)

Enzymes and buffers were purchased from Promega, UK

2.6.2.2 Preparation of the injection needle

Glass needles (1 mm) pulled with a micropipette puller to create an injection tip were used as injection needle for all injection and bead implantation experiments described in this thesis. The tip of a pulled glass needle was gently removed by fine forceps under the view of a dissecting microscope. The tip of the injection needle had to be wide enough for fluid to pass through it, but small enough for it to penetrate the embryonic tissue without causing extensive damage. The blunt end of the glass needle was attached to a mouth pipette, which was attached to a pipette tip at the other end for mouth aspiration. A 0.5 µl aliquot of the prepared DNA solution was placed on cling film. The sharp tip of the needle was carefully placed inside the DNA drop at an almost horizontal angle to avoid damage to the

tip of the needle by the surface of the bench. DNA was then sucked up into the needle, avoiding formation of bubbles.

2.6.2.3 Description and preparation of electrodes

Gold electrodes (5 mm thickness) were purchased from Qbiogene,UK. Silver electrodes were prepared from 5 mm thick silver wire, which was insulated by insertion into a glass pasteur pipette (Volac, 230 mm). Tungsten electrodes were prepared from 0.5 mm thick tungsten wire (Agar scientific), also inserted inside pasteur glass pipettes. The tip of the glass pipette was heated in order to melt the glass around the tungsten or silver wire to hold it firmly in place. The tip of the tungsten wire that was to be inserted into the embryo was sharpened in hot sodium nitrite until satisfactory sharpness was obtained. It had to be sharp enough to pierce through the embryonic tissue without causing extensive damage. Gold and Gold/tungsten electrodes were placed ~0.4 mm apart.

2.6.2.4 Mouse electroporation followed by whole embryo culture

Dissection and preparation of embryos for embryo culture were carried out as described in 2.4.2. Embryos at 11.5 dpc were prepared for embryo culture with the yolk sac and the amnion carefully cut open and pushed beneath the embryo to reveal it for ease of access. Prior to electroporation, healthy embryos were cultured for one hour, in order for them to recover from the stress of being explanted from their uterine environment.

Basic setup

The basic electroporation setup consisted of a dissecting microscope (Stemi SV11, Zeiss, Germany) with incident light. Although the earlier preparation of the embryo required transmitted light for clear visibility of the embryo and membranes, incident light from above was sufficient for the purpose of injection of DNA and electroporation of 11.5 dpc embryos. Several agarose gel covered medium sized Petri dishes were prepared by pouring 1.5 % agarose in autoclaved dH_2O into the Petri dish and allowing the gel to set. The agarose gel facilitated

positioning of the embryo and in some experiments also accommodated the electrode. One or both electrodes were held in position by an electrode holder, which was attached to a micromanipulator. Electrodes were connected to an ECM 830 Square Wave Pulse Generator (Qbiogene, UK) via connection cables. The site of DNA injection, the strength of current, and the number and duration of pulses varied and are given for each experiment in Chapter 6. All experiments were carried out with the embryo rested in an agarose covered petridish containing explanting saline (0.12 M NaCl, 4 M KCl, 0.4 mM $MgS0_4.7H_20$, 0.25 mM $MgCl_2.6H_2O$, 0.60 mM $NaH_2PO_4.2H_20$, 1.8 mM $CaCl_2.2H_2O$, 0.83 mM Glucose, 0.6 mM $NaHCO_3$). After current was delivered, the build-up of material on electrodes was cleaned in dH_2O using a brush. In the following subsections, the modified setups and the procedure are described.

Electroporation with gold plated electrodes

Straight gold plated electrodes (Qbiogene,UK), were held in place by the micromanipulator. The embryo was rested on its tail inside a pocket in the agarose bed in explanting saline. The electrodes where positioned on either side of the head of the embryo. The DNA solution was then mouth pipetted into the vitreous chamber of the optic cup with a plasmid DNA filled glass needle (2.6.2.2) and current was delivered immediately.

Electroporation with gold-tungsten combination electrodes

Tungsten electrode insertion into the embryo was first reported in a study where a *lacZ* reporter driven by the CAG promoter was targeted to the chick optic vesicle (Momose *et al.* 1999) and shown to provide a better transfection efficiency than platinum electrodes, which are the predominant type of electrodes used in mouse electroporation studies reported so far. A straight gold plated electrode was fastened to the micromanipulator via a holder. It was connected to the cathode and placed dorsal of the head of the embryo, while the embryo was rested on its side on the agarose bed with one eye facing up. A straight tungsten electrode was then connected to the anode and the sharpened tip was inserted into the extra-ocular mesenchyme directly opposite the cathode. The DNA solution was injected into the eye and current was delivered immediately after injection.

Electroporation with silver electrodes

The tips of the silver wire electrodes were bent into an L-shape. The bent part of the cathode was placed inside a fitting pocket in the agarose cover of the Petri dish in which the embryo was to be rested, so that it was level with the surface of the agarose gel. The embryo was rested on its side with the optic cup positioned directly on top of the cathode. The DNA solution was mouth-pipetted into the optic cup (injection sites varied as described in Chapter 6) facing up, the L-shaped anode was held manually over the injected optic cup in parallel to the cathode and current was delivered. The distance between these electrodes were subject to variability as one was held manually over the optic cup, but approximately, this distance was the same as the width of an 11.5 dpc mouse head.

After electroporation, embryos were returned to culture in the same media as they had been cultured in for one hour prior to electroporation. Embryo culture was described in section 2.4.2.

2.6.2.5 *In ovo* electroporation of the chick embryo

Setup

In contrast to mouse electroporations, all chick electroporations were carried out with the same experimental setup, regardless of electrodes used. The electrodes were fastened in the holder, which was held in place and manoeuvred by a micromanipulator. The current was supplied by an ECM 830 Square Wave Pulse Generator (Qbiogene, UK), to which the electrodes were connected. DNA injection and electroporation were carried out with the egg placed in an egg holder under a dissecting microscope (Stemi SV11) with incident light.

Procedure

Electroporation was performed on HH 9-10 embryos, when the optic vesicle was forming or had just formed. Eggs were prepared and opened as described in section 2.5. Prior to DNA injection, electrodes were put in a suitable position. If a pair of gold plated electrodes were used, they were placed on either side of the

head of the embryo where they covered the optic vesicles. When using the gold/tungsten combination electrodes, the gold plated electrode was connected to the anode and placed lateral to the injected optic vesicle, while the tungsten electrode was connected to the cathode and inserted into the embryonic tissue in close proximity to the injected optic vesicle. DNA was injected into the right optic vesicle lumen with a mouth pipette. The volume injected was variable, but never exceeded 0.5 ul, which was the initial volume of DNA filled into the needle prior to injections. DNA injected into the optic vesicle lumen spread also into the brain vesicles and sometimes poured out through the anterior neuropore, although care was taken to avoid this as much as possible. Preparations of the DNA solution, electrodes, and the injection needle were described in sections 2.6.2.2 – 2.6.2.3. After electroporation, the opening of the egg shell was sealed with cellotape and eggs were returned to the humidified incubator at 38 °C for further culture (as indicated in Chapter 6).

2.6.3 Gene delivery by retroviral vectors

Retroviruses use RNA as their genetic material and the mechanism of retroviral gene delivery to the embryo is based upon the natural ability of the retrovirus to enter a cell via cell surface receptors. Therefore, the host range of each retrovirus is determined by the availability of cell surface receptors on the host cell that can interact with its coat protein. Once inside the host cell, the RNA genome of the retrovirus is converted into double stranded DNA, the provirus, which is then integrated into the host DNA during the S-phase of the cell cycle, when the host DNA is being replicated (Morgan and Fekete 1996). In this manner, the host cell and its future progeny inherit the viral genome. The retrovirus is also capable of infecting neighbouring cells, which together with its heritability by progeny can lead to a widespread infection across a proliferating tissue.

The method used for viral injection into the chick optic vesicle was based on the experimental set-up and procedure reported for targeting of chick limb buds with some adaptations (Logan and Tabin 1998).

The viruses used were produced from an RCAS-AP construct, encoding the human placental alkaline phosphatase, as a control for retroviral delivery, and the type A RCASBP virus containing the full length sequence of chick *Tbx2* (RCASBP-*cTbx2*, here referred to as RCAS-*cTbx2*).

2.6.3.1 Preparation of retroviral stock

The viral stocks were kindly provided by Dr M. Logan (National Institute for Medical Research [NIMR], London, UK) and were prepared by Dr C. Rallis as described in Logan and Tabin (Logan and Tabin 1998). The titre of the viral stocks were estimated to 1 x 10^8 colony forming units (c.f.u)/ml.

2.6.3.2 Injection of virus

Set-up

Pulled borosilicate glass capillary needles were prepared for injection under a dissecting microscope by using forceps to break off the sealed end in order to make an opening with a desired diameter. Several needles were prepared prior to the start of the experiment as they had to be frequently replaced due to clogging. A 0.1 ml Luer tip Hamilton syringe was attached to a 19 gauge needle (1.1 x 40 mm, BD, Biosciences, UK) and both needle and syringe were filled with heavy mineral oil (Sigma, UK), making sure that air-bubbles were excluded. The oil allowed for better control over the volumes injected, while the presence of air-bubbles resulted in build-up of unwanted pressure, which prevented controlled injections. The Hamilton syringe was mounted in a micromanipulator. Then a 2 cm piece of Tygon tubing (Saint Gobain) was used to attach the pulled capillary needle to the 19 G needle on the Hamilton syringe. Under a dissecting microscope, mineral oil was slowly pressed out from the Hamilton syringe so that the Tygon tubing and the capillary needle were also filled with mineral oil to the tip. The viral stock was then thawed on ice and for visualisation purposes, 0.2 % v/v Fast Green (Sigma, UK) was added to the viral stock. A small volume (3 µl) of the viral solution was placed on a piece of cling film. The tip of the capillary needle was inserted just beneath the surface of the bubble of viral solution that formed on the cling film. The capillary needle was then loaded

gently with viral solution by lightly lifting the plunger of the Hamilton needle to generate a slight negative pressure. Before lifting the needle out of the viral solution, it was ensured that the negative pressure was no longer present, as otherwise air-bubbles would be sucked in when the tip of the needle was removed from the solution.

Procedure

White Leghorn eggs were incubated until HH 9-10 and were prepared for injection as described in 2.5.1 and 2.5.2. The tip of the capillary needle was inserted in the embryo so that it touched the neuroepithelium of the left optic vesicle. Viral solution was injected into the lumen of the left optic vesicle, but since this is continuous with the right optic vesicle via the developing telencephalic vesicle, the injected volume appeared to spread equally to both optic vesicles. When possible, virus was also injected into the neuroepithelium itself. Injection was repeated three to four times. Eggs were then sealed with cellotape and returned to the humidified incubator for further incubation. Injected embryos were monitored every day for heart beat and blood circulation. Unhealthy embryos were discarded and at day 5 of incubation (HH 23-25) only healthy embryos with clear presence of heart beat and circulation were analysed further.

2.7 Preparation of tissue sections and histology

For the collection of wax and frozen sections, slides were pre-treated with 3-aminopropyltriethoxysilane (TESPA) in order to increase the adhesion of sections to slides. Slides (BDH, UK) were dipped for 30 seconds in the following solutions in the given order: (1) 10% HCL/ 70% ethanol/ DEPC H_2O, (2) DEPC H_2O, (3) 95% ethanol/ DEPC H_2O. They were then incubated overnight at 65 C° and again dipped for 30 seconds in the following solutions: (1) 2% v/v TESPA (Sigma, UK), (2) acetone (twice), (3) DEPC H_2O. Slides were then allowed to dry at 37 C°.

2.7.1 Vibratome embedding and sectioning

PFA fixed embryos were incubated overnight at 4°C in embedding mix (0.45% w/v gelatin, 28% w/v egg albumin, 18% w/v sucrose in PBS, all from Sigma, UK). They were then positioned in disposable embedding moulds (L.I.P Ltd, UK) containing fresh embedding mix to which was added 25% glutaraldehyde (Sigma, UK) at 1/10 of the volume of the embedding mix. The embryo was orientated quickly under a Stemi SV11 dissecting microscope (Zeiss, Germany). The block was allowed to harden at room temperature for one hour. Vibratome sections of 50 μm thickness were prepared using a 'Vibratome series 1000 sectioning system' (Agar scientific Ltd, UK). Sections were collected in PBS using a fine brush, mounted onto slides and covered with 50% glycerol in PBS. Slides were sealed with a cover-slip (Agar Scientific).

2.7.2 Wax embedding and sectioning

PFA fixed embryos were dehydrated in an increasing series of ethanol in PBS (25%, 50%) until 70% ethanol in water. Embryos were normally stored in this solution until used. The embedding continued with further incubations in 85%, 95%, and twice in 100% ethanol. The ethanol was then gradually replaced first with a ratio of 1:1 Histoclear (Nation Diagnostics, UK): ethanol followed by incubation in 100% Histoclear at 60 C°. The samples were then incubated in 1:1 pre-warmed wax (Raymond Lamb, UK) : Histoclear, followed by two more incubation in wax alone, all at 60 C°. Embryos were placed in disposable embedding moulds and held in the desired orientation in fresh wax until the wax solidified. Wax blocks were trimmed with a razor blade and cut at a thickness of 10 μm using a microtome (Microm HM 330). Strips of adjoined sections were transferred onto pools of distilled water on TESPA coated slides, which were heated on a slide dryer until creases in the wax disappeared. The water was then gently removed and slides were incubate vertically at 25 C° overnight.

2.7.3 Cryo embedding and sectioning

Fixed embryos were first incubated in 20% w/v sucrose in DEPC (if to be used for in situ hybridisation) PBS at 4°C in order to cryoprotect the tissue. The embryo was orientated in OCT compound (BDH, UK) under a dissecting microscope. The block was allowed to freeze on dry ice in a dish containing iso-propanol (Sigma, UK). Sections of 12-20 μm thickness were cut on a cryostat machine (Bright 5040 Model OTF, UK) and the sections were picked up with TESPA coated slides. Slides were allowed to dry at room temperature overnight and stored at -70 C° until used.

2.7.4 Haemotoxylin and Eosin staining

This staining procedure was performed on wax sections. All steps were carried out for five minutes unless stated otherwise. Wax sections were first de-waxed in Histoclear (Nation Diagnostics, UK) twice followed by two 100% ethanol washes. Sections were then rehydrated to water by going through 95% and 70% ethanol washes. Haemotoxylin and Eosin staining was carried out in a series of steps outlined below. However, the length of time given for each step is approximate and had to be adjusted for samples individually.

Haemotoxylin (BDH, UK)	5 min
dH_2O	1 min
Running tap water	5 min
10% HCL in 70% ethanol	10 sec
Running tap water	5 min
Eosin (BDH, UK)	3 min
Running tap water	5 min

Sections were then dehydrated again in an ascending series of ethanol concentrations (70%, 95%, 100%) and washed twice in Histoclear. Slides were finally mounted with DPX .

2.7.5 Methyl green staining

Frozen sections were stained with methyl green solution (0.5% w/v methyl green, BDH UK, 0.1 M NaAc in dH_20) after immunohistochemistry experiments when a DAB colourimetric reaction was used for detection of the antibody signal. Slides were immersed in a coplin jar containing methyl green solution for 5 min, followed by three washes in dH_20 for 10 min each. Sections were then dehydrated in 100% butanol for 5 min followed by Histoclear (Nation Diagnostics, UK) for 5 min. Slides were mounted in DPX (BDH, UK) and cover-slipped.

2.8 Detection of gene and protein expression

2.8.1 Immunohistochemistry

2.8.1.1 Antibody specificity and dilutions

Table 2.4: List of antibodies

1° antibodies					
Antibody [conc.]	**Working dilution**	**Type**	**specificity**	**Supplier**	**References**
Connexin43	1:100	mouse MC	against the cytoplasmic loop of mouse connexin43 at aa 131-142. Recognises a 43 kDa protein by western blotting and sites of connexin43 expression in tissue sections.	Kindly provided by Dr D Becker (UCL)	(Wright *et al.* 2001)
RMO270 [0.5 mg/ml]	1:1500	mouse MC	against the carboxy domain of the 160 kDa intermediate neurofilament. Crossreacts to most vertebrates and invertebrates. In chick, it has been shown to label differentiating RGC bodies during their laminar migration from the ventricular surface to the RGC layer and their processes.	Zymed, USA	(McCabe *et al.* 1999)
VC1.1 [0.6 mg/ml]	1:100	mouse MC	against the HNK-1 antigen which is found in many glycoproteins including NCAM. In the retina, shown to react with differentiated amacrine and horizontal cells as well as a subset of retinal progenitors. Majority of the mitotic progenitors positive for VC1.1 during early development adopt amacrine and horizontal fates.	Sigma, UK	(Naegele and Barnstable 1991; Alexiades and Cepko 1997)
pH3 [1mg/ml]	1:100	Rabbit PC	against aa 7-20 of phosphorylated human histone H3. Recognises phosphorylated histone H3 at serine-10 during the M-phase of the cell cycle.	Upstate, USA	
PECAM1 [0.5mg/ml]	1:150	Rat MC	against 129/Sv mouse-derived endothelial cell line tEND. Recognises endothelial cells of blood vessels.	Pharmingen, USA	(Vecchi *et al.* 1994)
ßIII-tubulin [1mg/ml]	1:1000	Mouse MC	against a peptide at the C-terminus of βIII tubulin. During early retinal development, shown to label RGCs and their processes .	Promega, UK	(Snow and Robson 1995)

Secondary antibodies		
Antibody [conc.]	**Working dilution**	**Supplier**
FITC-conjugated goat anti mouse [1.4 mg/ml]	1:100	Jackson Immunoresearch laboratories, USA
FITC-conjugated goat anti rabbit [1.5 mg/ml]	1:100	Jackson Immunoresearch laboratories, USA
FITC-conjugated goat anti rat [1.5 mg/ml]	1:100	Jackson Immunoresearch laboratories, USA
HRP-conjugated rabbit anti mouse [1.3 mg/ml]	1:100	Dako, Denmark
HRP-conjugated goat anti rat [0.8 mg/ml]	1:1000	Jackson Immunoresearch laboratories, USA

Abbreviations: aa, amino acid; Conc., concentration; FITC, fluorescein isothiocyanate; HRP, horseradish peroxidase; kDa, kilo Daltons; MC, monoclonal; NCAM, neural cell adhesion molecule; PC, polyclonal; PECAM1, platelet endothelial cell adhesion molecule-1; pH3, phospho histone H3; RGC, retinal ganglion cell.

2.8.1.2 Whole mount immunohistochemistry

At the starting point of this procedure, embryos had already been fixed in 4% w/v PFA overnight and dehydrated in a methanol series and stored at -20°C according to descriptions in Section 2.3.4. In a methanol based solution containing methanol: DMSO: H_2O_2 in a 4:1:1 ratio, embryos were washed at room temperature for 5 hrs while gently rocking. Each wash (throughout the procedure) was in a 1.5 ml volume and the solution was changed once an hour. This step was crucial for permeabilisation and bleaching of whole mount tissue. Embryos were then rehydrated while rocking at room temperature through a series of 50% then 25% methanol in PBT washes for 20 min each and finally three PBT washes for 10 min each. This was followed by incubation of embryos in blocking solution.

For PECAM-1 immunohistochemistry of mouse embryos (Chapter 5), the blocking solution consisted of PBSMT (2% w/v non-fat milk, Nestle, USA, 0.5% v/v Triton X-100, 0.2% w/v BSA in PBS). For ßIII-tubulin immunohistochemistry of whole neural retinae (Chapter 6), the blocking solution consisted of PBS with 10% v/v FCS, 1% w/v BSA, and 0.5% v/v Triton X-100. Embryos were blocked while gently rocking at room temperature in washes consisting of two times 5 min, then three times 15 min, and finally two times 1 hr. The primary antibody was appropriately diluted (see Table 2.4) in fresh blocking solution and incubated with embryos overnight while rocking gently at 4°C. From this step onwards, all washes were carried out at 4°C while gently rocking. The next day, embryos were washed in freshly made blocking solution twice for 5 min to eliminate excess unbound antibody. Three more washes for 15 min each and then three to four washes of 1 hour each followed. Embryos were then placed in secondary antibody diluted appropriately in fresh blocking solution and incubated (at 4°C) overnight. The next day, excess secondary antibody was washed off in a series of 5 min (three times), then 15 min (three times), and finally 1 hour (four times) washes in blocking solution. When an FITC-tagged secondary antibody was used (Chapter 6), washes were continued overnight, followed by a few one hour washes in PBS with 0.5% v/v Triton X-100 before retinae were flat mounted on slides and covered in CITIFLUOR

(Citifluor Ltd., UK) and a coverslip. Embryos incubated with a horseradish peroxidase (HRP)-tagged secondary antibody were washed in PBS containing 0.5% v/v Triton-X 100 a few times and then incubated in PBS with 0.5% v/v Triton X-100, 0.08% w/v $NiCl_2$ (Sigma, UK), and 250 μg/ml diaminobenzidine tetrahydrochloride (DAB, Sigma, UK) while gently rocking at room temperature for 10 min. To this solution was added 0.03% v/v H_2O_2. The enzymatic colour reaction was stopped with PBS when satisfactory labelling was detected. Whole mounts were photographed and stored at 4°C in PBS containing 0.018% w/v Thimerosal (Sigma, UK).

2.8.1.3 Section immunohistochemistry

A list of antibodies and dilutions is given in Table 2.4. The detergent used to allow penetration of antibody to access their epitopes was 0.1% v/v Tween-20 (Sigma, UK) for the pH3 antibody and 0.1% TritonX-100 for all other primary antibodies. All section immunohistochemistry described in this thesis were performed on 12 or 15 μm frozen sections prepared from 4% PFA fixed tissue embedded in OCT. Samples were prepared and sectioned as described in Section 2.7.3. Twenty minutes prior to the start of the procedure, sections were removed from -80°C and thawed at room temperature. The OCT medium was washed off with two washes of PBS for 5 min each. After the first wash, each section was encircled with a PAP pen (Sigma, UK), which repulses water and therefore allows the sections to be submerged in a small quantity of liquid. As well as minimising the amount of media needed during the entire experiment, this also enables sections on the same slide to be treated differently. From this step onwards, each section was submerged in no more than 60 μl of liquid.

If the primary antibody was to be detected with an HRP-tagged secondary antibody, endogenous peroxidase activity was quenched with 3% H_2O_2 in PBS containing 0.1% detergent for 10 min at room temperature, otherwise this step was omitted. Sections were then washed three times for 5 min in PBS containing 0.1% detergent and then incubated in a blocking solution (10% v/v heat-inactivated FCS (Sigma, UK), 1% BSA (Sigma, UK) in PBS containing 0.1% detergent). The blocking solution was replaced with the appropriate dilution of

the primary antibody (as given in Table 2.4) in fresh blocking solution. Sections were incubated in primary antibody overnight at 4°C. The next day, sections were washed three times 10 min in PBS containing 0.1% detergent and then incubated in blocking solution containing an appropriate dilution of a secondary antibody (see Table 2.4 for specific details of the secondary antibodies used to detect each primary). This incubation was carried out at room temperature for 1 hour.

Secondary antibody tagged with fluorophore

After incubation with the secondary antibody, sections were washed three times 10 min in PBS with 0.1% detergent. For nuclear counterstaining, sections were incubated in either a 1:1500 dilution of Hoechst 33258 (Molecular Probes, UK) or 1 μg/ml propidium iodide (Sigma, UK) in PBS with 0.1% detergent for 30 min at room temperature. Finally, sections were washed twice for 10 min in PBS with 0.1% detergent and then mounted in CITIFLUOR (50% glycerol in PBS, Citifluor Ltd., UK), and cover-sliped (Marienfeld, Germany). To avoid evaporation of the mounting media, coverslips were sealed with nail varnish.

Secondary antibody tagged to HRP

After incubation with the secondary antibody, sections were washed three times in PBS with 0.1% detergent. The chromogenic colour reaction was developed with PBS containing 250 μg/ml diaminobenzidine tetrahydrochloride (DAB, Sigma, UK) and 0.03% v/v H_2O_2. The reaction was stopped by washing the sections in dH_2O when satisfactory colour was detected. To counterstain, sections were dipped in 0.5% w/v methyl green (BDH, UK) for 5 min followed by three washes in dH_2O for 1 min each. Sections were then dehydrated in 100% butanol for 5 min, before being cleared in Histoclear for 5 min. Sections were mounted with DPX mounting media containing 80% Xylene (BDH, UK) and then cover-slipped. Slides were allowed to dry horizontally in a fume hood.

2.8.2 RNA *in situ* hybridisation

In situ hybridisation was carried out essentially as described by D.G. Wilkinson (Wilkinson 1992). Chick and mouse embryos were treated similarly. RNA is

highly susceptible to degradation by ribonucleases. Therefore, most solutions were DEPC treated, which inactivates ribonucleases, prior to autoclaving. Solutions that could not be autoclaved, such as sodium dodecyl sulphate (SDS), were made with DEPC treated H_2O instead. RNAse-free pipette tips and sterile tubes were used until at least after the hybridisation step.

2.8.2.1 Probe templates

Table 2.5: Details of templates used for probe synthesis

Gene	Antibiotic	Vector	sense (enzyme/ RNA Pol)	α-sense (enzyme/ RNA Pol)	Insert size (bp)	References/supplier
Jagged1	Ampicillin		HindIII/T7	EcoRI/T3	1800	(Mitsiadis *et al.* 1997)
ephrinB2	Ampicillin	pBS SK		HindIII/T3	3800	Kindly provided by Dr D. Wilkinson (NIMR, London)
Fgf15	Ampicillin	pGEMT	NcoI/Sp6	NotI/T7	806	(McWhirter *et al.* 1997)
Tbx2 (m)	Kanamycin	pBK CMV	XhoI/T3	EcoRI/T7	2200	Sowden lab
Shh	Ampicillin	pB(II)KS	PstI/T7	HindIII/T3	640	(Echelard *et al.* 1993)
Tbx3	Ampicillin	pB(II)KS	EcoRV/T7	PstI/T3	1000	(Chapman *et al.* 1996)
Tbx5	Ampicillin	pB(II)KS	BamHI/T3	EcoRV/T7	1000	(Chapman *et al.* 1996)
Tbx2 (c)	Ampicillin	pBS SK	NotI/T3	SalI/T7	2500	Kindly provided by Dr Logan (NIMR,London)
Msx2	Ampicillin Kanamycin	pCR2.1	NotI/Sp6	BamHI/T7	1000	Kindly provided by Prof. P Sharpe (King's College, London)
Bmp4	Ampicillin	pSP72	SmaI/T7	EcoRI/Sp6	1000	(Furuta *et al.* 1997)
Vax2	Ampicillin	pBS SK	KpnI/T7	EcoRI/T3	700	(Schulte *et al.* 1999)
RSCH	Ampicillin	pBS SK	ClaI/T7	SalI/T3	900	Kindley provided by Dr Logan (NIMR, London)
Silver	Ampicillin	modified pBS (3)		KpnI/T3		(Baxter and Pavan 2003)
Fgf8	Ampicillin	pBS SK		BamH1//T7	875; full coding sequence plus 16 bp of 5'UTR	(Crossley and Martin 1995)

2.8.2.2 Probe synthesis

In order to obtain single stranded RNA probes, *in vitro* transcription was performed using cDNA templates in plasmid vectors (see Table 2.5). To obtain DNA template, plasmids were purified using the miniprep method 2.2.4. Then 10-12 µg of the template was linearised as described in 2.2.5 and the linearised template was purified by phenol-chloroform extraction. The *in vitro* transcription reaction contained the following: 1 µg/µl linearised template, 4 ul 10 x dNTP mix (10 mM each of ATP, CTP, and GTP; 6.5 mM UTP; 3.5 mM digoxigenin or fluorescein-UTP; Roche, Germany), 2 ul 10x buffer (Roche, Germany), 1ul RNasin ribonuclease inhibitor (Promega, UK), 2 µl T3, T7, or SP6 RNA polymerase (Roche, Germany) in a final volume of 20µl DEPC dH_20. The reaction was incubated for 2hrs in a 37°C water bath. Labelled probe was precipitated with 100 µl 2.5 M ammonium acetate in DEPC dH_20 and 300 µl 100% ethanol overnight at -20°C. The next day, this was spun for 30 min at 4°C, 13000 rpm, in a bench-top microfuge. The supernatant was gently poured out and the pellet washed with 100 µl 100% ethanol. The pellet normally dislodged at this step and the eppendorf tube was carefully flicked to wash the pellet, which was spun again for 10 min at 4°C, 13000 rpm. The supernatant was discarded and the pellet air-dried before being dissolved in 20 µl DEPC dH_20. One µl was taken out to run on an agarose gel, as described in 2.2.7, then 20 µl formamide and 1µl RNasin were added. The solution was vortexed, spun and stored at -20°C.

If examination of the probe on an agarose gel showed a thick band, approximately 10 x brighter than the DNA template, which was still present, the probe was sufficiently good to proceed with *in situ* hybridisation.

2.8.2.3 Single and double whole mount *in situ* hybridisation

Samples were prepared in advance by fixation overnight in 4% PFA and dehydrated in an increasing series of methanol in PBS (25%, 50%, 75%, 100%)

on ice. All steps of this procedure were carried out in 5 ml polystyrene round-bottom tubes (Beckton Dickinson, UK). Samples were stored in 100% methanol until the day of the procedure. Each dehydration step was performed for 15-30 min on ice depending on the size of the sample. Mouse embryos at 9.5-10.5 dpc were washed for 15 min, while older embryos and chick embryos were washed for 25-20 min. Washes throughout this procedure were performed in a 5 ml volume of solution.

Rehydration and H_2O_2 treatment

All steps were carried out on ice. Embryos were rehydrated through a decreasing series of methanol in PBT (75%, 50%, 25%), each step being performed for 15-30 min on ice depending on the size of the sample as indicated in the previous section. After the last rehydration step, samples were washed twice in PBT, for 5 min each, and treated then with 6% H_2O_2 (Sigma, UK) for 1 hr.

Permeabilisation

The concentration and length of proteinase K (Sigma, UK) treatment was adjusted according to the size and age of the tissue. Table 2.6 gives the approximate times used for different samples. Embryos were treated with proteinase K in order to permeabilise cells and degrade proteins surrounding the mRNA, hence maximising probe penetration.

Table 2.6: Approximate length of time of proteinase K treatment of tissue according to stage and size

Stage of embryo/tissue	[Proteinase K]	Length of treatment
HH 23-25 chick embryos	20 µg/µl	15 min
HH 9-16 chick embryos	10 µg/µl	12 min
HH 23-25 optic cups	10 µg/µl	15 min
11.5 dpc (post-culture mouse embryos, 45-53 s)	10 µg/µl	15 min
11.5 dpc (pre-culture mouse embryos, 40-45 s)	10 µg/µl	12 min
10.5 dpc mouse embryos (34-40 s)	10 µg/µl	7 min
10.5 dpc mouse embryos (26-34 s)	5 µg/µl	5 min
10.5 dpc mouse embryos (20-26 s)	3 µg/µl	3 min

Dpc, days post coitum; S, somite pairs.

Proteinase K digestion was stopped with 2mg/ml glycine in PBT, followed by two 5 min PBT washes. Embryos were refixed in 0.2% glutaraldehyde/4% PFA in PBS for 20 min at 4°C. The fixative was washed away with two 5 min washes in PBT.

Hybridisation

Embryos were incubated in pre-warmed (70°C) pre-hybridisation mix (hybridisation mix without probe: 50% formamide; 5X sodium chloride/sodium citrate buffer (SSC) pH 4.5: 0.75 M NaCl, 0.075 M NaCi; 50 µg/ml yeast t-RNA; 1% SDS, 50 µg/ml Heparin). Incubation in this solution was performed at 70°C for 2 hrs in a water bath to equilibrate embryos and block non-specific hybridisation. This solution was then replaced with 1 ml hybridisation buffer containing a 1:100 or 1:200 dilution of labelled sense or anti-sense probes (~0.5-1 µg/ml), depending on the strength of the probe. For probe details please see Table 2.5. For double *in situ* hybridisation experiments, both probes, one conjugated with Fluorescein (fl) and the other with Digoxigenin (DIG), were added at the same time. For single *in situ* hybridisations, DIG-conjugated probes were used as these give a cleaner result. Samples were hybridised overnight at 70°C.

Washing

After the overnight hybridisation step, embryos were washed twice with solution I (50% formamide; 5X SSC pH 4.5: 0.75 M NaCl, 0.075 M NaCi; 1% SDS) at 70°C and twice with solution II (50% formamide; 2X SSC pH 4.5: 0.3 M NaCl, 0.03 M NaCi) at 65°C, each wash lasting 30 min. These formamide based washes, which have a less concentrated salt composition than the hybridisation mix, helped to reduce non-specific hybridisation.

Blocking

After post-hybridisation hot washes, embryos were washed in TBST (137 mM NaCl, 2.7 mM KCl, 0.25 M Tris.HCl pH 7.5, 1% Tween-20, 2 mM Levamisol) three times for 5 min at room temperature and then incubated in 10% v/v heat inactivated sheep serum (Sigma, UK) in TBST for 90 minutes, while rocking.

Antibody solution

Alkaline phosphatase tagged antibodies (sheep polyclonal Fab fragments) were used to detect probes by a colourimetric reaction. To minimise non-specific binding by the anti-DIG (0.75 Units of enzyme activity/µl, Roche, Germany) or anti-fl (0.75 Units of enzyme activity/µl, Roche, Germany) antibodies, they were pre-blocked with embryo powder. Embryo powder was produced by homogenising embryos (9.5-11.5 dpc) in a small volume of PBS, mixing with 4 volumes of ice-cold acetone and incubating the homogenate on ice for 30 min. It was then spun at 10 000 g for 2 hours. Some acetone was added to the pellet which was pulse spun and then grinded on a sheet of filter paper, allowed to air-dry, and stored at -20°C until used. For the preparation of every 5ml of final antibody solution, 7.5 mg embryo powder was first incubated with 1.2 ml TBST in an eppendorf tube at 70°C for 30 minutes. This mix was then vortexed and spun at 3000 rpm for 1 min in a bench-top microfuge. The supernatant containing embryo-derived lipids was discarded and the pellet was mixed in 1.2 ml of fresh TBST. To this was added 125 µl heat inactivated sheep serum (Sigma, UK) together with 2.5 µl antibody. The mixture was incubated for approximately 3 hrs rocking at 4°C, then centrifuged at 3000 rpm in a bench-top microfuge for 10 min and the supernatant was removed and diluted to 5ml with 10% v/v heat inactivated sheep serum in TBST.

Antibody incubation

For detection of bound probe in single *in situ* hybridisation experiments, samples were incubated in 2 ml of pre-blocked anti-DIG solution while rocking at 4°C overnight. For double *in situ* hybridisations, the fl-conjugated probe was detected first with 2 ml of pre-blocked anti-fl. This is because the fl tag is less stable than the DIG tag.

Washing

Samples were first washed three times for 5 min and then five times for 1 hr in TBST, rocking at room temperature to wash away unbound antibody.

Development of the colour reaction

Before being developed, embryos were equilibrated with NTMT (0.1 M NaCl, 0.1 M Tris-buffer pH 9.5, 0.05 M $MgCl_2$, 1% Tween-20, 2 mM Levamisol) three times for 10 min at room temperature. Then 0.2 mM Nitro blue tetrazolium chloride, 0.2 mM 5-bromo-4-chloro-3-inodyl-phosphate, toluidine salt stock solution (NBT/BCIP, Roche, Germany) was added to the NTMT and the colour reaction was allowed to develop until satisfactory colour was observed. BCIP is the substrate of alkaline phosphatase, which becomes de-phosphorylated and then reacts with NBT in a redox reaction step to give a dark blue colour.

Detection of the second probe in double in situ hybridisation

After development of the first colour reaction, of the fl-tagged probe with NBT/BCIP, embryos were washed five times in TBST for 10 min while rocking at room temperature. The alkaline phosphatase of the anti-fl antibody was heat-inactivated in TBST by incubation at 65°C in a water bath for 30 min. Samples were washed again in TBST, twice for 5 min at room temperature, and blocked in TBST containing 10% heat inactivated sheep serum for 1 hr, while rocking at room temperature. 2 ml of pre-blocked anti-DIG was added per tube and samples were incubated at 4°C overnight while rocking. The next day, unbound antibody was washed off with three times 5 min, followed by five times 1 hr washes at room temperature. Samples were then equilibrated in NTMT with three times 10 min washes before being incubated in NTMT containing 0.2 mM 2-[4-iodophenyl]-3-[4-nitrophenyl]-5-phenyl-tetrazolium chloride and 0.2 mM 5-bromo-4-chloro-3-inodyl phosphate, toluidine salt (INT/BCIP). The colour reaction was developed at room temperature until satisfactory colour was observed. This substrate produces a red colour via a redox reaction of the dephosphorylated BCIP by alkaline phosphatase.

Usually, the strongest probe was the one developed with INT/BCIP as the product of this solution is weaker than that produced by NBT/BCIP. When both colour reactions were complete, embryos were stored at 4 °C in PBT containing 0.018 % w/v Thimerosal (Sigma, UK)

2.8.2.4 Section *in situ* hybridisation

Glassware used for this procedure were baked at 280°C for 5 hrs. Frozen sections were cut at 20 µm, as described in 2.7.3, and allowed to dry at room temperature for 2 hrs. Alternatively, previously prepared sections stored at -80°C were taken out to dry at room temperature for 30 min.

Hybridisation

An aliquot of hybridisation buffer (50% formamide; 1x 'salts': 0.2 M NaCl, 5 mM $NaH_2PO_4.H_2O$, 5 mM Na_2HPO_4, 5 mM EDTA, 10 mM Tris pH 7.5; 0.1 mg/ml yeast t-RNA; 10% w/v dextran sulphate, Sigma UK; 1x Denhardt's solution, Sigma UK) was warmed at 70°C. Probe was added to the pre-warmed hybridisation buffer (~0.5-1 µg/ml), heated at 65°C for 5 min to denature probes, and 200 µl was added per slide. Slides were covered with cover-slips and incubated at 65°C in a humidified incubation chamber (Grant Boekel SM30, Grant Instruments Ltd., England) overnight.

Posthybridisation washes

The next day, slides were washed in 35 ml of pre-warmed wash solution (50% formamide, 1x SSC pH7.5, 0.1% Tween-20) in a glass coplin jar in a 65°C water bath for 30 min. Usually cover-slips separated from slides during this wash and could easily be removed without causing damage to sections. Slides were then washed twice more in fresh wash solution for 30 min each at 65°C. This was followed by three times 30 min washes in MABT (0.1 M Maleic acid, 0.15 M NaCl, pH 7.5, 0.1% Tween-20) at room temperature.

Blocking and antibody incubation

Slides were removed from coplin jars, sections were circled with a PAP pen (Sigma, UK) to reduce the amount of solution needed, and incubated in 50 µl per section of blocking solution (2% blocking reagent, Roche UK; 10% heat inactivated sheep serum; 0.1 M Maleic acid, 0.15 M NaCl, pH 7.5, 0.1% Tween-20) at room temperature for 1 hr. This was replaced by blocking solution containing 1:500 anti-DIG (Roche, Germany) and section were incubated overnight at 4°C in a slide chamber.

Washes and colourimetric reaction

Unbound antibody was washed away in three times 10 min MABT washes, followed by three times 10 min NTMT (same as used for whole mount *in situ* hybridisation but with 0.1% Tween-20) washes at room temperature. The alkaline phosphatase reaction was developed with 0.2 mM NBT/ 0.2 mM BCIP (Roche, Germany) at room temperature until satisfactory colour was observed. Slides were washed in dH_20 for 30 min and the dehydrated in 100% butanol for 5 min, followed by Histoclear (Nation Diagnostics, UK) for 5 min, and then mounted with DPX (BDH, UK) and covered with a cover-slip.

2.8.3 Whole mount *in situ* hybridisation followed by immunohistochemistry

This procedure was performed on isolated chick optic cups in Chapter 6. After fixation overnight at 4 °C in 4% w/v PFA in PBS, embryos were rested on their side in a Petri dish containing PBS. Using No. 5 Watchmakers forceps (Raymond Lamb, UK), the lens was carefully dissected out making sure not to tear away any part of the retina. In removing the lens, the surface ectoderm was ruptured, which facilitated the peeling of the rest of the surface ectoderm and the underlying extra-ocular mesenchyme in the distal portion of the eye. When the distal region of the eye was cleaned, the forceps were pierced through the extra-ocular mesenchyme nasal or temporal to the eye, and the eye globe was separated from the head mesenchyme by gentle squeezing of forceps around the globe. Once separated, the globe together with the optic nerve were pulled away from the head. The eye was then further cleaned from all surrounding mesenchyme and when possible, which was in the majority of eyes, the RPE layer was also removed.

Combined whole mount *in situ* hybridisation with immunohistochemistry was performed according to a protocol by Sterit and Stern 2001 with some modifications (Streit and Stern 2001). Whole mount *in situ* hybridisation was carried out as described in 2.8.2.3. Samples were then washed extensively in PBT, 5ml solution, three to five 1hr washes at room temperature, to adjust the

basic pH of the NTMT solution used to develop the colour reaction of *in situ* hybridisation. Samples were fixed in 4% w/v PFA for 1 hr at 4°C, washed in PBT twice for 5 min. The rest of the procedure, which was immunohistochemistry, was carried out as described in 2.8.1.2 (from second paragraph).

After completion of both *in situ* hybridisation and immunohistochemistry, the retina was flat mounted by making 4-6 cuts from the periphery of the retina to its centre. It was then transferred onto a glass microscope slide using a plastic pipette, which had previously been cut at the tip in order to minimise contact between the retina and the pipette tip and hence damage to the retina. The fluid that followed onto the microscope slide was dried using clean tissue and the peripheries of the retina were gently straightened with forceps so that the retina rested flat on the slide. One drop of Citifluour was put on the retina and finally a cover-slip was positioned on top of the retina.

2.8.4 Detection of exogenous alkaline phosphatase activity in whole embryos

Human placental alkaline phosphatase (AP) is heat stable. Therefore, to detect its activity in transfected embryos (Chapter 6) and to differentiate it from endogenous AP, which is heat labile, PFA (4%) fixed embryos in PBT were incubated in a 65 °C water bath for 45 min to inactivate endogenous AP. Embryos were then equilibrated in NTMT (0.1 M NaCl, 0.1 M Tris-Base pH 9.5, 0.05 M $MgCl_2$, 1% v/v Tween-20, 0.05% w/v Levamisol) for 30 min at room temperature, during which time, the NTMT solution was replaced three times. The colour reaction was developed by 2 ml of NTMT containing 0.2 mM NBT 0.2 mM BCIP solution (Roche, Germany) The colour reaction was developed by rocking at room temperature until satisfactory colour was evident. During and after development of the colour reaction, embryos were kept in dark. The colour reaction was stopped by several washes in PBT, in which embryos were kept until photographed. Embryos were stored at 4 °C in PBT containing 0.018 % w/v Thimerosal (Sigma, UK).

2.9 Detection of cell death by apoptosis

Apoptosis was detected using the method of *in situ* labelling of single strand DNA breaks, which occurs during cell death by apoptosis. A deoxynucleotidyl transferase-mediated dUTP nick end labelling (TUNEL) kit (Roche, UK) was used for this purpose according to the manufacturer's protocol. Briefly, frozen sections of 12-20 μm thickness were allowed to thaw at room temperature and were washed twice in PBS. The tissue was permeabilised with 0.1% Triton X-100 in PBS for two min and then incubated at 37°C for one hour with a mixture of enzyme (deoxynucleotidyl transferase) and labelling solution (containing fluorescein dUTP) as described in the manual. Afterwards, sections were washed twice in PBS (5 min) and the cell nuclei were counterstained by adding 200 μl per section of Propidium Iodide (Sigma, UK) at 1 μg/ml in PBS for 20 min. Finally, sections were washed three times ten min in PBS, mounted with CITIFLUOR (50% glycerol in PBS, Citifluor Ltd., UK) and covered with a cover-glass (Marienfeld, Germany). Sections were photographed as described in section 2.10.

2.10. Microscopy

Whole mounts

Images of whole embryos following *in situ* hybridisation were captured with a Leica MZ FLIII microscope (Leica, Germany) fitted with a Leica DC500 camera (Leica, Germany). The Leica IM1000 Image manager V1.20 software was used to operate the camera and import images, which were saved as Tiff files. Some pictures were captured with a 35 mm film camera (MC 100, Zeiss, Germany) attached to a Stemi SV 11 dissecting microscope (Zeiss, Germany). Photos were digitised using a scanner (FilmScan 200, Epson Ltd., UK) and imported into Adobe Photoshop (6.0) as JPEG files. For comparison purposes, the objects were always photographed using the same set-up.

Sections

Images of fluorescently labelled tissue sections were captured using an Axioplan 2 microscope (Zeiss, Germany) attached to a ProgRes Cl4 camera (Jenoptik Jena,

Germany) operated with the Openlab 4.0.4 software (Improvision Ltd., UK). Images were saved in Openlab Liff format for measurement purposes or in Photoshop Tiff format for presentation purposes.

Images of vibratome or frozen sections following *in situ* hybridisation were captured using an Axiophot 2 microscope (Zeiss, Germany) fitted with Differential Interference Contrast (DIC) objectives and a Leica DC500 camera (Leica, Germany). Captured images were imported into Photoshop and saved in Tiff format.

In Chapter 5, some images were taken using a Leica TCS SP Confocal Laser Scanning microscope (Leica, Germany).

Retinal flat mounts

Images of retinal flat mounts (Chapter 6) were captured with the set-up described for whole mounts.

2.11 Analysis of eye size and shape

2.11.1 Estimation of retinal volume

First, 50 µm thick vibratome sections of eyes were prepared as described in Section 2.7.1 and images were digitally captured as described in Section 2.10. Only specimen with a complete set of sections through both rhBMP4 treated and BSA treated eyes (Chapter 4), or with a complete set of sections through a mutant or a wild-type eye (Chapter 5) were included. Moreover, if the thickness of all sections through an eye was not consistent, which was apparent by the colour of the embedding mix, the whole eye (and its contralateral control in Chapter 4) was excluded from analysis. Using the "area tool" in the OpenLab programme, which was pre-calibrated to measure in mm^2 units, the area of the neural retina was measured on each section. The retinal area values were multiplied by the thickness of the section and then summed for each eye to obtain the retinal volume expressed in mm^3. In Chapter 4, data were compared with the

paired t-test, while in Chapter 5, they were compared with the independent samples t-test (see Sections 2.12.3 and 2.12.4)

2.11.2 Estimation of retinal area

This was performed in Chapter 6 as an estimate of the size of the eye in chick embryos. Retinae were flatmounted as described in the first paragraph of section 2.8.3 without disturbing the optic fissure by making incisions in dorsal regions of the retinae after isolation of the optic cup from the head mesenchyme. Digital images were taken of each retinae and stored as a Liff file in the OpenLab programme. Using the 'line measure' tool, calibrated to measure in millimetres, retinal area was measured by following the outline of the tissue.

2.11.3 Estimation of the length of the optic fissure

The optic disc and the optic fissure walls were clearly visible in all flat mounted retinae. Digital images were taken of each retinae and stored as Liff files in the OpenLab programme. Using the 'line measure' tool, calibrated to measure in millimetres, the length of the fissure wall from the optic disc to the peripheral most edge of the ventral neural retina was measured. The line followed exactly the fissure wall and is therefore a measure of the optic fissure length.

2.11.4 Estimation of D-V and N-T axial length of the embryonic eye

Axial length measurements were carried out on high power whole mount images of 11.5 dpc post-culture embryos (Chapter 4), captured with a 35 mm film camera (MC 100, Zeiss, Germany) attached to a Stemi SV 11 dissecting microscope (Zeiss, Germany) and digitally scanned. In Photoshop, the 'measure tool' was used to measure the longest distance of the eye along the D-V and N-T axes as illustrated in Figs. 4.11 and 4.12. Each treated eye was compared to the non-treated control eye of the same embryo. The percent decrease/increase in axial length for each pair of eyes in rhBMP4 treated, BSA treated, and non-treated but cultured embryos were calculated as follows:

$$\frac{C-T}{\frac{1}{2}(C+T)} \times 100$$

C= control eye (or eye two in non-treated control)

T= treated eye (or eye one in non-treated control)

Data was analysed with the paired t-test (see Section 2.12.3).

2.11.5 Estimation of the P-Di axis of the embryonic eye

Serial 50 μm thick transverse vibratome sections of eyes were prepared as described in Section 2.7.1 and images were digitally captured as described in Section 2.10. Only specimens with a complete set of sections through both rhBMP4 treated and BSA treated eyes (Chapter 4) were included in analysis. Moreover, if the thickness of all sections through an eye was not consistent, which was apparent in the colour of the embedding mix, the whole eye (and its contralateral control) was excluded from analysis. Using the "area tool" in the OpenLab programme, which was pre-calibrated to measure in mm units, the longest distance from the ventricular edge of the neural retina (proximal) to the surface ectoderm (distal) was measured on sections. Measurements were carried out in four embryos and values from equivalent sections were plotted as mean ± 1 s.d. according to the position of the section from each eye with section one in each eye being the dorsal-most and section five or six being the ventral-most. The graph revealed the average shape of the eyes in each treatment group.

2.12 Statistical analysis

Analysis of data and production of graphs were facilitated by the use of SPSS 12.0.1 for Windows statistical programme.

2.12.1 Tests of normality of data

Prior to performing a statistical test, the distribution of data was analysed with the construction of a normal plot to determine whether normal distribution could be assumed. The normal plot is constructed by arranging the data set in an ascending order and plotting the values on the x-axis against the corresponding normal score on the y-axis, which is the number of standard deviations away from the mean that each value is expected to fall within. Data were assumed to be adequately normal if the points were close to linear. Normality of data was also assessed by Shapiro-Wilk's test of normality. Data with a P-value > 0.05 were considered to be normally distributed and were analysed with parametric tests.

2.12.2 Logarithmic transformation of data

Non-normal data sets were transformed logarithmically by Log_e (Ln), which helped to bring values closer together. Ln transformed data were checked for normality after transformation as described in 2.12.1.

2.12.3 Paired t-test

Data collected from differentially treated left and right eyes in each embryo were considered paired and were analysed with consideration to their paired nature. The paired t-test examines the difference in means between two groups and therefore requires that data is normally distributed and that the variance around the mean is equal between groups. Variability in the paired t-test is estimated from the differences between paired values. This test was used to compare the axial length and retinal volume in treated versus non-treated pairs of eyes in Chapter 4.

2.12.4 Independent samples t-test

Measurements performed on separate embryos were regarded as independent and were analysed accordingly with the independent samples t-test if only the difference between treated and non-treated specimens were of interest. Like the

paired t-test, this test is based on the difference in means of two groups, therefore requiring data to be normally distributed with equal variance around the mean between groups. This test however estimates variability from the within group variability. The analysis of retinal volumes and head length measurements between embryos of different genotypes in Chapter 5, section 5.3 and in the differences in eye size between two groups in Chapter 6 were analysed with this test.

2.12.5 One-Way Analysis of Variance (ANOVA)

For the analysis of differences between more than two groups of specimens, which were differentiated from each other by only one factor, the One-Way ANOVA test was employed. This test is based on the differences in means between various groups and was used in Chapter 6 for the comparison of eye size between embryos of four developmental stages. An example of a One-Way ANOVA table produced by SPSS is illustrated in Table 2.7 and the mathematical formulae explained.

Table 2.7: **Example of a One-Way ANOVA table produced by SPSS**

	Sum of Squares	**df**	**Mean Square**	**F**	**Sig.**
Between Groups	$\sum$ ($\sum$observed values in a treatment group)^2 – ($\sum$observed values)^2 / n. observations	$n._{groups}$ -1	sum of $squares_{between\ groups}$ / $df_{between\ groups}$	mean $square_{between\ groups}$/ mean $square_{within\ groups}$	P-value for difference between groups
Within Groups	$\sum$ (observed value)^2 – $\sum$ ($\sum$observed values in a treatment group)^2)	$n._{observations}$- $n._{groups}$	sum of $squares_{within\ groups}$/ $df_{within\ groups}$		
Total	$\sum$ (observed value)^2 – ($\sum$observed values)^2 / n. observations	$n._{observations}$-1			

Key: n, number of; df, degrees of freedom; Sig, significance.

2.12.6 Two-Way Analysis of Variance (Two-Way ANOVA)

For the analysis of differences between more than two data sets, differentiated by two grouping factors, the Two-Way ANOVA test was employed. This analysis was used in Chapter 4 to test for significant differences in cell division and apoptosis in data sets representing several sections from paired eyes of 4-5 embryos, which had been differentially treated. The Two-Way ANOVA allowed the comparison between treated and non-treated pairs of eyes (treatment) within embryos and across embryos (embryo or section). Embryo and treatment were the two grouping factors. Table 2.8 shows an example of a Two-Way ANOVA table produced by SPSS.

Table 2.8 Example of a Two-Way ANOVA table produced by SPSS and formulae for the calculation of the value in each cell

Source	Type III Sum of Squares	df	Mean Square	F	Sig.
Corrected Model	$\sum$ (observed value)^2 – $\frac{(\sum \text{observed values})^2}{\text{n. observations}}$	$df_{treatment} + df_{embryo}$	sum of $squares_{corrected\ model}$ / $df_{corrected\ model}$	mean $square_{corrected\ model}$ / mean $square_{error}$	P-value for model
Intercept		1	sum of $squares_{intercept}$ / 1	mean $square_{intercept}$ / mean $square_{error}$	
treatment	$\sum$ ($\sum$observed values in a treatment group)^2 - $\frac{(\sum \text{observed values})^2}{\text{n. observations}}$	$n._{treatments}$ -1	sum of $squares_{treatment}$ / $df_{treatment}$	mean $square_{treatment}$ / mean $square_{error}$	P-value for difference between treatments
Embryo	$\sum$ (observed value)^2 – $\sum$ ($\sum$observed values in a treatment group)^2)	$n._{observations}$-1	sum of $squares_{embryo}$ / df_{embryo}	mean $square_{embryo}$ / mean $square_{error}$	P-value for difference between embryos
Error (residual)	$\sum$(observed – predicted)^2	$n._{observations}$ -1	sum of $squares_{error}$ / df_{error}		
Total		$df_{intercept}$+ $df_{treatment}$+ df_{embryo}+ df_{error}			
Corrected Total		n-1			
Key: n, number of; df, degrees of freedom; Sig, significance.					

This test is based on the differences in means of observed values and predicted values. Each predicted value is calculated from the means of the groups into which the observed value falls and the overall mean of all observed values and therefore incorporates the overall variation of values. As the Two-Way anova has two grouping factors, there are two group means that apply to each observed value. Therefore, a **predicted value** is calculated as:

(mean of group 1 + mean of group 2) – overall mean

The difference between the observed value and the predicted value gives the **residual value**. The sum of squares of these residual values are illustrated as 'Error' in Table 2.8.

The 'corrected model' shows the total sum of squares based on observed values and is calculated as:

$$\sum (\text{observed value})^2 - \frac{(\sum \text{all observed values})^2}{\text{n. observations}}$$

The sum of 'sum of squares' of all grouping factors add up to the total sum of squares:

sum of squares of 'corrected model' = sum of squares of embryo + sum of squares of treatment

The degrees of freedom (df) for each grouping factor are derived as illustrated in Table 2.8. The mean squares are the sum of square values divided by the df in each row. Finally, the F-ratio is calculated as the mean square of each grouping factor divided by the residual mean square. The bigger the F-ratio, the more significant the P-value, which is given under 'Sig' in ANOVA tables produced by SPSS.

2.12.7 Analysis of co-variance (ANCOVA)

The ANCOVA test is an ANOVA with the incorporation of the effect of other continuous variables that are known to correlate with the main test variable. The effect of the covariate(s) are incorporated by ANOVA when deriving the predicted values. This test was employed in the analysis of the number of mitotic cell divisions in Chapter 4 and Chapter 5. The programmed cell death was also analysed with this test in Chapter 4. It allowed the examination of the effect of total cell number/surface area on the observed number of dividing/dying cells, otherwise accounted for in many studies by the calculation of the mitotic/apoptotic index ad the comparison of the indices. The ANCOVA table is similar to the ANOVA table with the result of the covariate added as an extra row.

CHAPTER 3 Expression analysis of the T-box genes and their putative upstream regulators and downstream targets along the D-V axis of the developing mouse eye

3.1 Introduction

The first step towards understanding the function of a gene and its position within the genetic cascade in a developing tissue, is to carry out an analysis of its expression pattern within the tissue of interest. Members of the *Tbx2* subfamily have previously been reported to be expressed in the dorsal region of the mouse optic cup (Chapman *et al.* 1996; Sowden *et al.* 2001), but their expression pattern during optic cup morphogenesis has not been reported. This Chapter describes the expression pattern of *Tbx2*, *Tbx3*, and *Tbx5* during early eye development in the mouse embryo, and provides the foundation for the functional experiments presented in subsequent Chapters. Also examined, are the expression patterns of several signalling molecules, and other genes along the D-V axis of the eye, some of which have previously been described during optic cup morphogenesis, others not, in order to place the T-box genes in the context of a molecular network during optic cup formation.

Evidence described in Chapter 1.4.4 regarding the antagonistic interactions between Bmps with the Shh and the Fgf pathways, demonstrated in several developing tissues including the limb bud and the developing forebrain, suggest that the same interactions may also occur in other developing tissues where these signalling molecules are expressed in juxtaposed or close sites. The expression of these factors in close proximity of each other have been described in the developing chick eye (Crossley *et al.* 2001). In literature, several Fgfs are reported to be expressed in the neural retina during eye development. During early stages of eye development in the mouse eye, only *Fgf9* and *Fgf15* have been detected (Colvin *et al.* 1999; McWhirter *et al.* 1997), whereas in the chick neural retina *Fgf3*, *Fgf8*, and *Fgf19* have been detected (Martinez-Morales *et al.* 2005; Vogel-Hopker *et al.* 2000; Crossley *et al.* 2001; Kurose *et al.* 2004). *Fgf8* is expressed juxtaposed to the dorsal *Bmp4* in the developing chick eye (Crossley *et al.* 2001). To find an Fgf that is suitably close to the dorsally expressed *Bmp4* in the early mouse optic cup, the expression patterns of *Bmp4*, *Fgf8*, and *Fgf15* were examined in relation to each other and to *Shh* during mouse eye morphogenesis. Because *Fgf9* is reported to first be expressed at 10.5 dpc (Colvin *et al.* 1999), which is later than when *Bmp4* (Furuta and Hogan 1998) or the T-box genes (Holt 2003) are first detected, it was not included in the analysis. Upon

identification of Fgf15 as a suitable candidate to interact with Bmp4 based on its expression, a putative interaction between *Bmp4*, *Fgf15*, and a role for Fgf15 in D-V patterning in the mammalian eye was explored by examining the expression of *Bmp4*, *Tbx2*, and *Vax2* in mice carrying an enhanced green fluorescent protein (EGFP) expression cassette within the *Fgf15* coding region.

This mouse line has been created by homologous recombination in an embryonic stem (ES) cell line, with *EGFP* targeted to exon 1 of the *Fgf15* allele, which resulted in the deletion of a 100 bp region of exon 1 and the insertion of the *EGFP* coding sequence at the site of the deletion (A. Battersby, University of Wales Cardiff, UK). Mice homozygous for the mutated allele (referred to as $Fgf15^{-/-}$) are viable until at least birth when embryos appear at the expected Mendelian ratio. $Fgf15^{-/-}$ embryos form optic cups and are currently being analysed for eye defects by Dr A. Battersby (University of Wales Cardiff).

This Chapter aims to compare the pattern of expression of the T-box genes in relation to putative upstream effectors and downstream targets along the D-V axis of the mouse eye, and to examine a possible interaction between Bmp4/Fgf signalling in the developing eye. This study is novel because it aims to identify sites of mutually exclusive expression between *Tbx2*, *Tbx3*, and *Tbx5* in the developing mouse eye. It also examines the expression of *Tbx2*, *Vax2*, and *Bmp4* in the absence of a specific FGF.

3.2 Results

Whole mount and section RNA *in situ* hybridisations were performed to detect gene expression patterns using previously published probes as described in Chapter 2.8.2. The described gene expression patterns are based on at least 3 embryos per probe. Sense probes were made for most genes examined here and showed no specific hybridisation signal. Examples are shown in Fig. 3.1 (A-D) of embryos hybridised with sense probes of *Tbx2* and *Tbx5*. Further details of expression are given in the following sections. All genes examined showed expression in tissues as described in previous literature.

Fig. 3.1 Comparisons of *in situ* hybridisation with sense and antisense probes

(A,B) 10.5 dpc embryos hybridised with a *Tbx2* sense probe (A), showing no specific expression. The *Tbx2* antisense probe (B), revealed a specific expression pattern as expected. **(C,D)** 10.5 dpc embryos hybridised with a *Tbx5* sense probe (C), and *Tbx5* antisense probe (D), showing that detection of *Tbx5* expression with the antisense probe is specific and differs from that detected by the *Tbx2* probe.

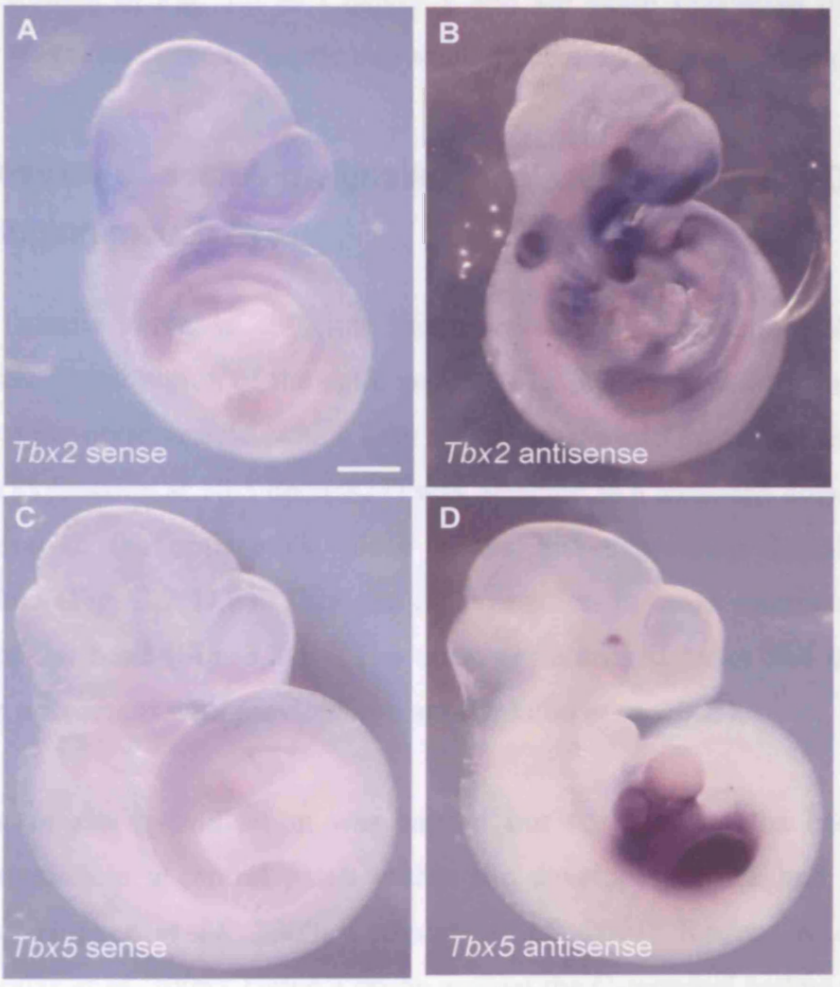
A
Tbx2 sense
B
Tbx2 antisense
C
Tbx5 sense
D
Tbx5 antisense

The nomenclature used for orientations of whole embryo views and section views of eyes were described in Fig. 1.2 of Chapter 1 and are again illustrated in Fig. 3.2 (optic vesicle stage) and Fig. 3.3 (optic cup stage). These apply throughout the thesis

3.2.1 Expression of secreted signalling molecules along the D-V axis of the developing mouse eye

At 10.5 dpc (somite stage, ss, 29), just before optic cup invagination, *Bmp4* was expressed in the dorsal region of the optic vesicle (Fig. 3.2 A). It was confined to the distal region of the optic vesicle, which later differentiates into the neural retina (Fig. 3.2 B,C). *Shh* expression at 10.5 dpc (ss27) was detected in a localised domain in the proximal region of the optic stalk, close to the *Shh* expression domain in the prechordal plate (Fig. 3.2 D,E). This site of expression is more clearly seen in a dorsal view of the head (Fig. 3.2 E). The optic vesicle itself lacks *Shh* transcripts (Fig. 3.2 E) in agreement with previous reports (Dakubo *et al.* 2003).

Whole mount *in situ* hybridisation was carried out for *Fgf8* on the basis of its reported expression in a central patch within the developing chick and zebrafish retinae (Vogel-Hopker *et al.* 2000; Crossley *et al.* 2001; Reifers *et al.* 1998; Martinez-Morales *et al.* 2005). Using a probe against the C-terminal coding sequence shared by all *Fgf8* isoforms, expression was not detected in the optic vesicle (Fig. 3.2 F,G) in agreement with previous reports (Crossley and Martin 1995).

In the limb bud and developing forebrain, members of the Fgf family are expressed in domains in between or in close proximity to Bmps and Shh. The expression of *Fgf15* was analysed in order to examine its spatial distribution to *Bmp4* in the dorsal optic vesicle and *Shh* in the proximal optic stalk. At ss27, *Fgf15* was expressed in two distinct stripes in the central region of the mouse optic vesicle (Fig. 3.2 H-J). Its expression was confined to the distal neuroepithelium (Fig. 3.2 I, arrow) and excluded from the dorsal-most and ventral-most regions of the optic vesicle (arrows in Fig. 3.2 J). It was positioned between the *Bmp4* domain in dorsal and Shh emanating from the optic stalk in the ventral region of the optic vesicle.

Fig. 3.2 Whole mount *in situ* hybridisation analysis of the expression of *Bmp4*, *Shh* and *Fgfs* in the mouse eye at optic vesicle stage (10.5 dpc)

The depicted orientations (D-V; R-C, P-Di) are relative to the optic vesicle and illustrated in the schematic. The plane of coronal sections is illustrated by the dotted line in the schematic. **(A)** Whole mount view of an embryo at ss29, showing the expression of *Bmp4*. Expression in the optic vesicle was confined to the dorsal region (arrow). **(B)** Dorsal view of the head of the embryo in A, showing *Bmp4* transcript localisation to the distal layer (arrow) of the optic vesicle (highlighted in dotted circle). **(C)** Coronal vibratome section through the eye in A-B, confirming *Bmp4* expression in the dorso-distal optic vesicle (arrow). **(D)** *Shh* expression in a whole mount view of an embryo at ss27, expressed in the notochord along the body axis (grey arrow) and in the prechordal plate in the forebrain region (white arrow). **(E)** Dorsal view of the head of the embryo in D, revealing *Shh* expression in two patches in the ventral forebrain at the proximal region (arrows) of the optic stalks (highlighted by the dotted lines). **(F)** Whole mount view of an embryo at ss27 hybridised with the *Fgf8* probe, which was clearly expressed in the isthmus and the apical ectodermal ridge of the forelimb bud, but not the optic vesicle. **(G)** Coronal vibratome section of the embryo in F. *Fgf8* transcripts were present in the surface ectoderm of the presumptive nasal region (arrow) but absent in the optic vesicle. **(H)** Whole mount view of an embryo at ss27 showing *Fgf15* expression in the optic vesicle. **(I)** Dorsal view of the head in H. *Fgf15* was confined to the distal optic vesicle (arrow). **(J)** Enlarged view of the head in H. *Fgf15* transcripts were detected in two stripes within the central region of the optic vesicle (marked by dashed lines). The dorsal-most and ventral-most regions of the optic vesicle are indicated by arrows. Scale bars: 0.5 mm in all except C and G where 0.1 mm.

Abbreviations: AER, apical ectodermal ridge; C, caudal; D, dorsal; Di, distal; FL, forelimb bud; IST, isthmus; OV, optic vesicle; P, proximal; Pre-NR, presumptive neural retina; Pre-RPE, presumptive RPE; R, rostral; V, ventral

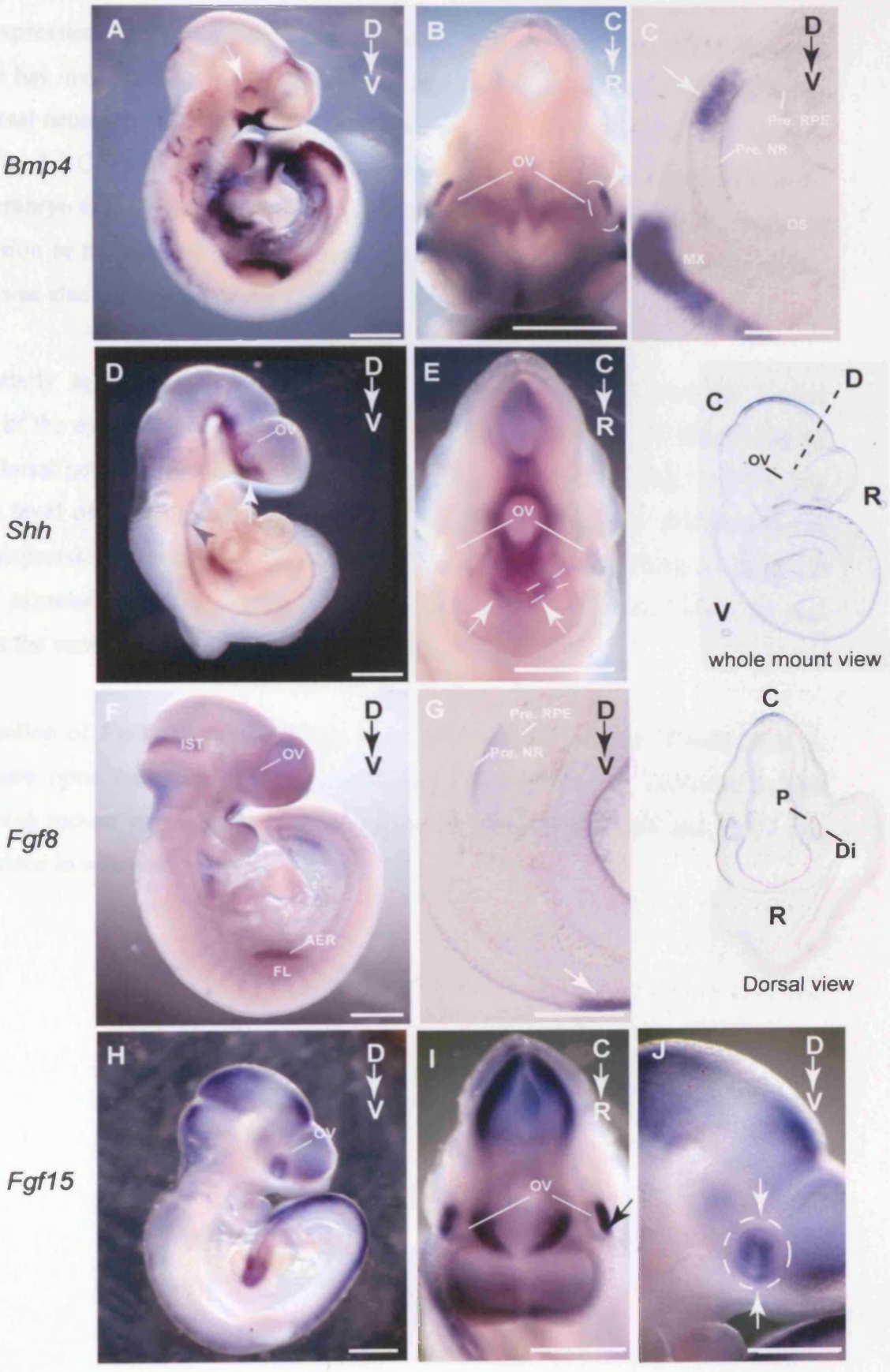
Bmp4
Shh
Fgf8
Fgf15
A
B
C
D
E
F
G
H
I
J
D
V
C
R
OV
Pre. RPE
Pre. NR
OS
MX
IST
AER
FL
P
Di
whole mount view
Dorsal view

The expression of these genes were also compared at 11.5 dpc, when the optic vesicle has invaginated. At ss45, *Bmp4* was expressed in a restricted domain within the dorsal neural retina (Fig. 3.3 A,B). At ss42, *Shh* was not detected within the optic cup (Fig. 3.3 C,D). In the inset in Fig. 3.3 D the floor plate of the neural tube in the same embryo is displayed, confirming positive detection of *Shh* elsewhere. Apparent expression in the optic stalk lumen is trapping; *Shh* is not expressed in this region, which was also confirmed by (Dakubo *et al.* 2003).

In similarly aged embryos (~ss41), *Fgf15* was expressed throughout the central region of the eye in a gradient. Expression was never detected in the distal-most tip of the dorsal neural retina or the ventral region of the neural retina (Fig. 3.3 E,F). The highest level of *Fgf15* signal (arrow in Fig. 3.3 F) appeared to be proximal to the *Bmp4* expression domain in the dorsal neural retina (Fig. 3.3 F). From its strongest site of expression, *Fgf15* expression decreased towards the dorsal distal tip and towards the ventral neural retina in a graded fashion.

Examination of *Fgf8* expression at this stage, showed the absence of transcripts in the mouse optic cup (Fig. 3.3 G), confirming that *Fgf8* is not expressed in the developing mouse eye. The combined expression patterns of *Bmp4* and *Fgf15* are summarised in schematic 3.3 H.

Fig. 3.3 Comparative analysis of the expression of *Bmp4*, *Shh* and *Fgfs* in the mouse embryo detected by whole mount *in situ* hybridisation at optic cup stage (11.5 dpc)

A,C,G,E are whole mount views of the head of embryos. B,D,F are coronal 50 μm thick vibratome sections of eyes. The plane sections is illustrated by the dotted line in the schematic diagram of an 11.5 dpc embryo. The proximo-distal orientation of sections is illustrated in the schematic in H. **(A)** Embryo at ss45, hybridised with the *Bmp4* probe, showing expression in the dorsal optic cup (arrows) and in the maxillary and mandibular processes of the first branchial arch. **(B)** *Bmp4* expression was restricted to the distal region of the dorsal neural retina (arrow). *Bmp4* expression in the roof plate of the same embryo is shown in the inset as a positive control for the signal. **(C)** Embryo at ss42 showing the notochordal *Shh* expression in the tail. Signal in OF is trapping. **(D)** Section of the eye in C, showing lack of *Shh* expression in the optic cup. Signal in OS is trapping. Inset shows the floor plate expression of *Shh* in the neural tube of the same embryo and confirms detection of signal. **(E)** Embryo at ss41 showing *Fgf15* expression. In the optic cup, *Fgf15* expression was strongest in the dorso-temporal region. Signal intensity in the dorso-nasal region was slightly weaker. Its expression was excluded from the dorsal and ventral-most regions of the optic cup. **(F)** *Fgf15* expression was detected in a gradient with the highest signal intensity in the dorsal proximal region of the retina (arrow), decreasing towards the dorsal distal tip of the neural retina (highlighted by the dotted line) and towards the ventral region of the eye. *Fgf15* expression did not extend beyond the optic stalk boundary into the ventral neural retina. **(G)** Embryo at ss42 showing lack of *Fgf8* expression in the optic cup. **(H)** Schematic diagram of a coronal section summarising *Fgf15* and *Bmp4* expression. *Fgf15* is shown in a gradient of blue, with the highest levels of expression in the central neural retina, dorsal to the optic stalk, which decreases towards the dorsal tip of the optic cup and towards the ventral neural retina. *Bmp4* is shown in dotted red, occupying the dorsal distal region of the neural retina. Scale bars: 0.5 mm in A, C, E, G, 0.1 mm in B, D, F. Di, distal; L, lens; MN, mandibular process of the first branchial arch; MX, maxillary process of the first branchial arch; N, nasal; NR, neural retina; P, proximal; OF, optic fissure; OS, optic stalk; RPE, retinal pigmented epithelium; T, temporal.

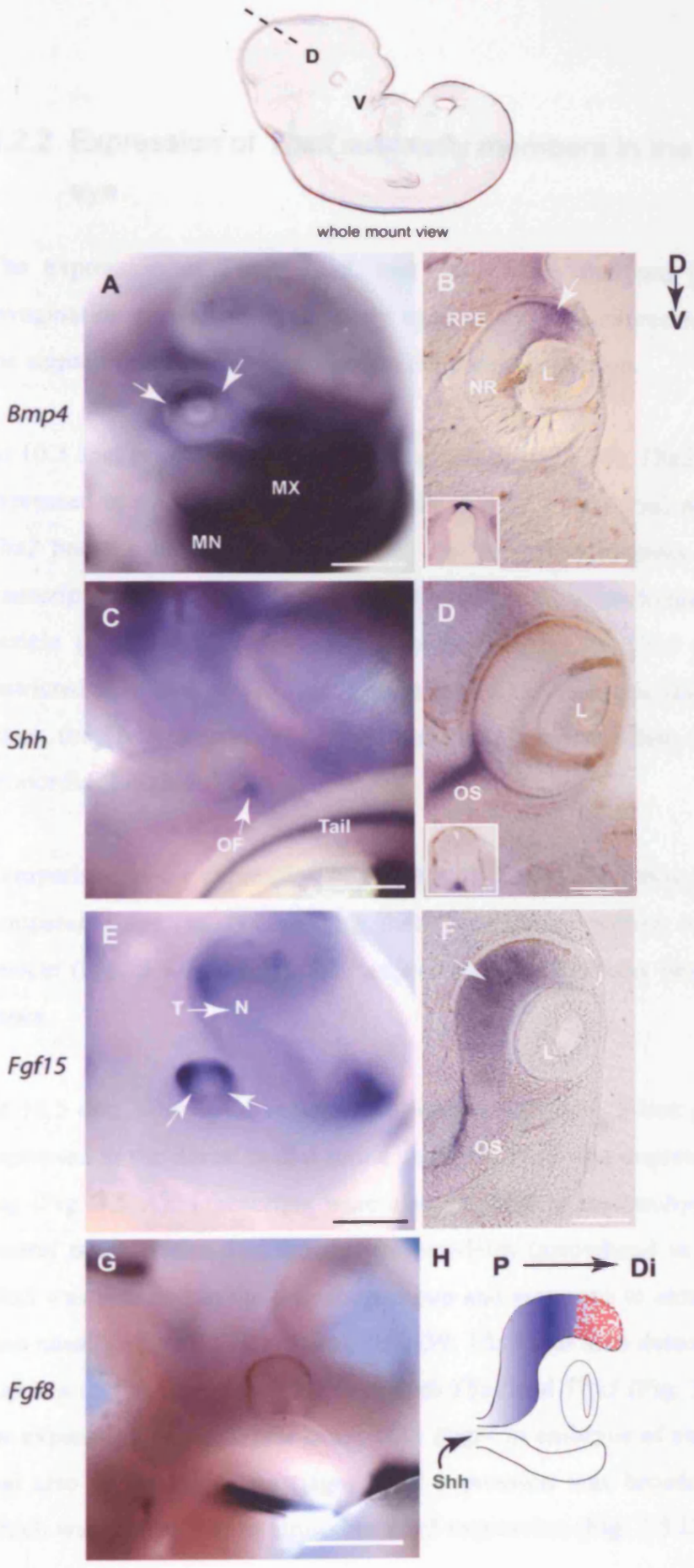
D
V
whole mount view
A
B
RPE
NR
L
D
V
Bmp4
MX
MN
C
D
Shh
L
OS
OF
Tail
E
F
T
N
Fgf15
L
OS
G
H
P
Di
Fgf8
Shh

3.2.2 Expression of *Tbx2* subfamily members in the developing mouse eye

The expression of *Tbx2*, *Tbx3*, and *Tbx5* were analysed prior to optic vesicle invagination as well as in the early optic cup. Their expressions were compared to the signalling molecules described in the previous section.

At 10.5 dpc, prior to optic vesicle invagination (ss25-28), *Tbx2*, *Tbx3*, and *Tbx5* were expressed in overlapping domains in the presumptive dorsal neural retina (Fig. 3.4). *Tbx2* had the broadest expression of the three T-box genes (Fig. 3.4 A,B). *Tbx2* transcripts were also present in the extra-ocular mesenchyme, ventral to the optic vesicle (Fig. 3.4 B, arrowhead). The expressions of *Tbx3* and *Tbx5* were more restricted than that of *Tbx2* within the dorsal optic vesicle (Fig. 3.4 B,D,F). At this stage, the *Tbx3* expression domain was more restricted than *Tbx2* also in the nasal primordia (Fig. 3.4 B,D).

Comparison of the expression of *Bmp4* with that of the T-box genes in an embryo of comparable age (ss24) highlights their overlapping pattern within the dorsal optic vesicle (Fig. 3.4 B,D,F,H). The expression of *Tbx2* was larger than all the other genes.

At 11.5 dpc, after optic vesicle invagination, all three T-box genes continued to be expressed in the dorsal neural retina. At ss44, *Tbx2* was expressed in the dorsal optic cup (Fig. 3.5 A). Transcripts were also detected in mesenchymal cells between the ventral neural retina and the surface ectoderm (arrowhead in Fig. 3.5 A). At ss42, *Tbx3* was detected in the dorsal optic cup and was seen to extend further temporally than nasally (Fig. 3.5 B, arrows). At ss39, *Tbx5* was also detected in the dorsal optic cup in a region more restricted than both *Tbx2* and *Tbx3* (Fig. 3.5 C). Comparison of the expression of the T-box genes with *Bmp4* in embryos of comparable age showed that also at the optic cup stage, *Tbx2* expression was broader than that of *Bmp4*, which was spatially most similar to *Tbx5* expression (Fig. 3.5 D).

Fig. 3.4 T-box gene expression in the mouse embryo at optic vesicle stage (10.5 dpc) detected by whole mount *in situ* hybridisation

(A) Whole mount view of an embryo at ss26 hybridised with a probe for *Tbx2*, showing *Tbx2* expression in the dorsal region of the optic vesicle (arrow). Other sites of expression in the head at this stage included a thin stripe in the nasal region, the maxillary and mandibular processes of the first branchial arch, and the otic vesicle. **(B)** Higher magnification of the head region in A. As well as the dorsal expression domain in the optic vesicle (arrows), *Tbx2* transcripts were detected in the extra-ocular mesenchyme, immediately ventral to the optic vesicle (arrowhead). **(C)** Whole mount view of an embryo at ss25 showing *Tbx3* expression also in the dorsal optic vesicle (arrow). **(D)** Higher magnification of the head in C. *Tbx3* transcripts were found in a smaller region of the dorsal optic vesicle than covered by *Tbx2* expression (arrows). The nasal process expression of *Tbx3* was also narrower than that of *Tbx2*. Unlike *Tbx2*, *Tbx3* was not expressed in the extra-ocular mesenchyme ventral to the optic vesicle. **(E)** *Tbx5* expression in an embryo at ss27. *Tbx5* was expressed in the dorsal optic vesicle (arrow) and was not detected at any other site within the developing head. But more caudally, *Tbx5* transcripts were detected in the sinus venosus/atrium, and in the forelimb bud. The blue colour in the hindbrain region is due to trapping of the colour reaction product. **(F)** Higher magnification of the head region in E. *Tbx5* expression was confined to the dorsal region of the optic vesicle (arrows). **(G)** An embryo at ss24 showing *Bmp4* expression. **(H)** *Bmp4* transcripts within the optic vesicle closely matched that of the T-box genes. Scale bars: 0.5 mm.

Abbreviations: A, atria; D, dorsal; FL, forelimb bud; MN, mandibular process of the first branchial arch; MX, maxillary process of the first branchial arch; NP, nasal process; OT.V, otic vesicle; V, ventral.

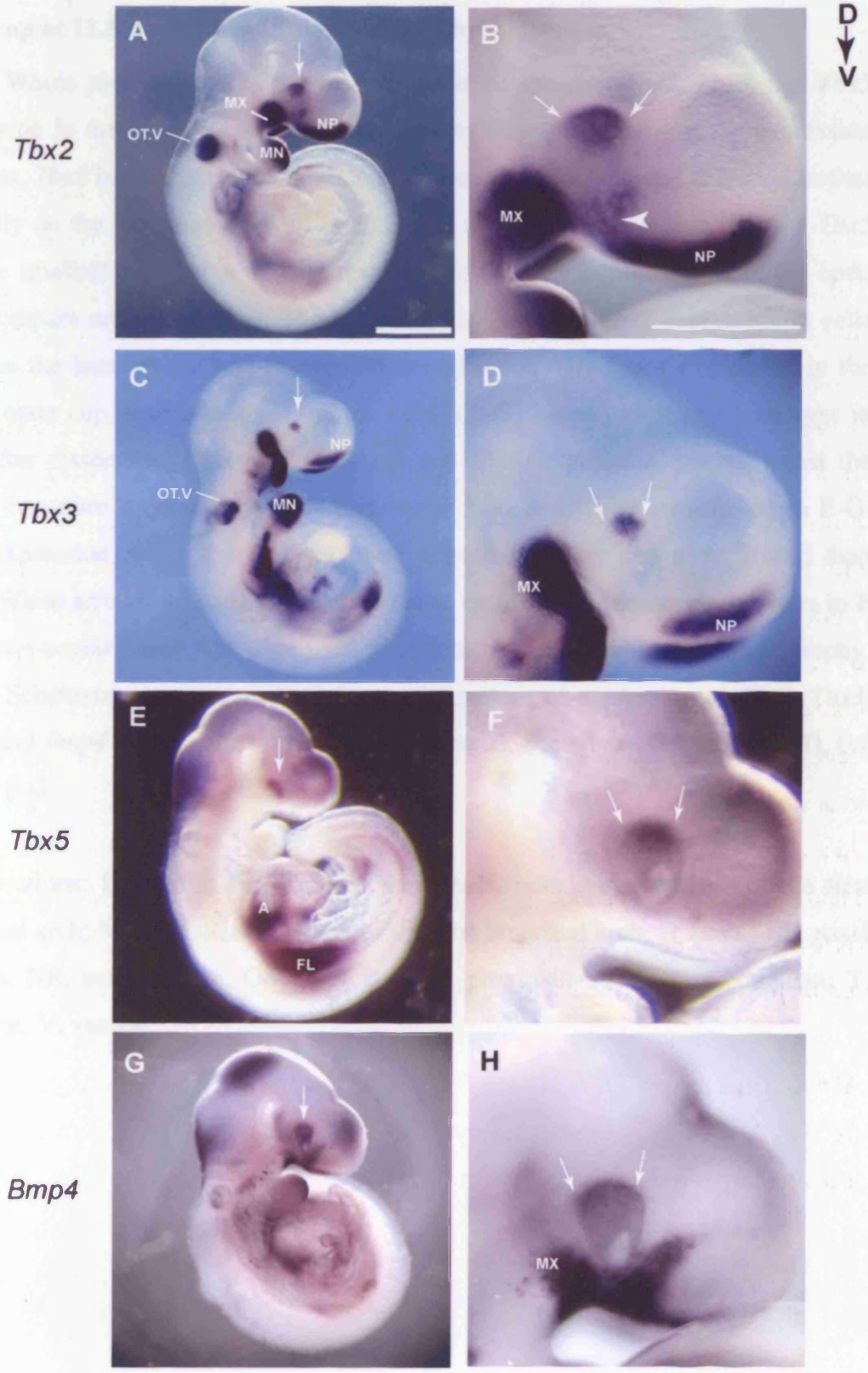
A
B
C
D
E
F
G
H
D
V
Tbx2
Tbx3
Tbx5
Bmp4
MX
NP
OT.V
MN
A
FL

Fig. 3.5 Comparison of the expression of the T-box genes in the mouse optic cup at 11.5 dpc by whole mount *in situ* hybridisation

(A-C) Whole mount views of the head of embryos showing *Tbx2, Tbx3,* and *Tbx5* expression in the optic cup respectively. Arrows show the extent of the expression domains. *Tbx2* had the largest expression domain. The *Tbx3* domain extended further ventrally on the temporal side of the optic cup than on the nasal side (arrow). *Tbx5* had the smallest expression domain restricted to the dorsal-most region of the optic cup (compare arrows in A-C). The arrowhead in A shows *Tbx2* expression in cells between the lens vesicle and the ventral neural retina. **(D)** *Bmp4* expression in the dorsal optic cup most resembles that of *Tbx5*. **(E-G)** Lateral view of whole eyes in A-C after dissection. *Tbx2* and *Tbx3*, but not *Tbx5,* expression extended past the dorsal curvature marked by a grey arrowhead in E and white arrowheads in E-G. *Tbx3* expression past the dorsal curvature appeared weaker and more graded than *Tbx2*. White arrowhead in D shows the ventral extra-ocular mesenchyme. Stars in F show non-ocular tissue that were used to support the optic cup during photography. **(H-K)** Schematic representation of the spatial pattern of expression of *Tbx2*, *Tbx3*, *Tbx5*, and *Bmp4* in the dorsal optic cup as indicated. Scale bars: 0.5 mm in A-D, 0.1 mm in E-G.

Abbreviations: D, dorsal; Di, distal; L, lens; MN, mandibular process of the first branchial arch; MX, maxillary process of the first branchial arch; N, nasal; NP, nasal process; NR, neural retina; OS, optic stalk; P, proximal; SE, surface ectoderm; T, temporal; V, ventral.

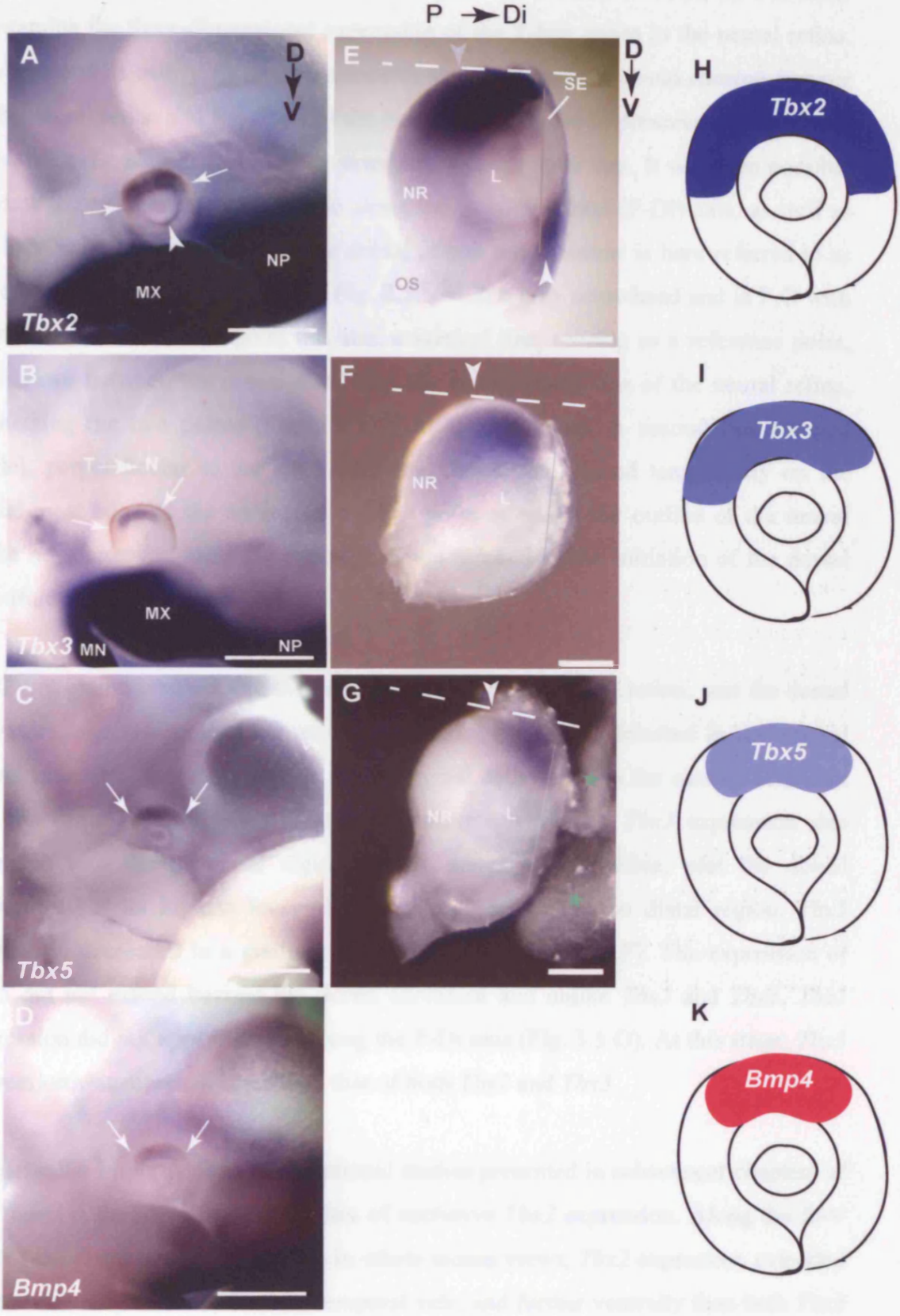
P → Di
A
D
V
NP
MX
Tbx2
B
T → N
MX
Tbx3
MN
NP
C
Tbx5
D
Bmp4
E
SE
NR
L
OS
F
NR
L
G
NR
L
H
Tbx2
I
Tbx3
J
Tbx5
K
Bmp4

Eyes were dissected out of the head mesenchyme and isolated from the RPE in order to examine the three-dimensional expression of the T-box genes in the neural retina. The lens and its overlying surface ectoderm were left intact, to avoid causing damage to the neural retina and the shape of the eye globe, and also to preserve mesenchymal cells that exist between the surface ectoderm and the optic cup. It was then possible to view the expression of each gene along the proximo-distal (P-Di) axis, as well as the D-V axis. The region where the dorsal neural retina curves is here referred to as the dorsal curvature and marked in Fig. 3.5 E with a grey arrowhead and in F,G with white arrowheads. To pinpoint this site, a vertical line, serving as a reference point, was drawn between the dorsal-distal and the ventral-distal tips of the neural retina, connecting the two points (Fig. 3.5 D-F solid grey lines). A second line (dashed white), perpendicular to the solid line, was drawn and placed tangentially on the dorsal-most edge of the neural retina. The point at which the outline of the neural retina no longer followed the dotted line was marked as the initiation of the dorsal curvature.

Tbx2 expression reached into the proximal region of the neural retina, past the dorsal curvature, and was graded across the P-Di axis. It was not detected in the ventral neural retina but was expressed in mesenchymal cells between the surface ectoderm and the ventral neural retina (Fig. 3.5 E, white arrowhead). *Tbx3* expression also extended into the proximal region of the dorsal neural retina, past the dorsal curvature, but its highest level of expression was within the distal region. *Tbx3* expression decreased in a gradient more proximally (Fig. 3.5 F). The expression of *Tbx5* did not extend beyond the dorsal curvature and unlike *Tbx2* and *Tbx3*, *Tbx5* expression did not appear graded along the P-Di axis (Fig. 3.5 G). At this stage, *Tbx5* expression was more confined than that of both *Tbx2* and *Tbx3*.

Of particular importance to the functional studies presented in subsequent chapters of this thesis is the identification of sites of exclusive *Tbx2* expression. Along the D-V axis of the distal neural retina, seen in whole mount views, *Tbx2* expression extended further ventrally than *Tbx5* on the temporal side, and further ventrally than both *Tbx5* and *Tbx3* on the nasal side (Fig. 3.5 A-C). *Tbx2* expression also extended more proximally into the neural retina than either *Tbx3* or *Tbx5* (Fig. 3.5 E-G). Another site of exclusive *Tbx2* expression was in the mesenchymal cells ventral to the optic

cup (Fig. 3.5 E, white arrowhead). The expression of each gene in the dorsal optic cup is depicted schematically in Fig 3.5 H-K.

3.2.3 Expression of other asymmetrically expressed genes along the D-V axis of the developing mouse eye

The expression of several asymmetrically expressed genes, which could be potential T-box gene targets, were examined in order to compare their spatial pattern of expression to those of the T-box genes in the developing eye, in particular to that of *Tbx2* which is the main T-box gene investigated in this thesis. Genes included in this section where chosen on the basis of previous reports that describe their asymmetrical expression pattern along the D-V axis in the developing eye and or reports that have linked them to *Tbx5* or *Bmp4* in the eye (*Vax2*, *ephrinB2*, *Msx2*; see Chapter 1.2.2). The expression of *ephrinB2* has previously been reported to be dorsally confined in the developing mouse eye from 13 dpc onwards (Marcus *et al.* 1996; Birgbauer *et al.* 2000), but its expression in the early optic cup at 10.5 dpc has not been described. *Jagged1* which has not been studied in relation to the T-box genes or Bmp4 previously was also examined. Of all Notch pathway genes reported so far to be expressed during early eye development in the rat embryo (*Notch 1-3,* and their ligands *Delta1-2* and *Jagged1*), the expression of *Jagged1* most closely resembled that of the T-box genes in the dorsal optic vesicle (Lindsell *et al.* 1996; Bao and Cepko 1997), suggesting a possible regulatory interaction between the Notch pathway and the T-box genes. Both dorsal and ventral genes were selected as *Tbx2*, *Tbx3*, and *Tbx5* have been reported to act both as repressors and activators of gene expression *in vitro* and *in vivo* (see Chapter 1.3.2).

At 11.5 dpc (ss45), *Vax2* was expressed in the ventral region of the optic cup (Fig. 3.6 A). Double labelling with the *Tbx2* and the *Vax2* probes revealed a patch of non-expression in between the dorsal *Tbx2* and the ventral *Vax2* domains along the D-V axis of the optic cup (Fig. 3.6 B).

At 10.5 dpc (ss 33-35), *ephrinB2* was expressed in the dorsal optic cup and at this stage, resembled the expression of *Tbx2* in the neural retina (Fig. 3.6 C,D). *EphrinB2* was also detected in the lens vesicle (Fig. 3.6 D).

Fig. 3.6 Expression of a selected group of asymmetrically expressed genes and *Tbx2* in the mouse embryo at optic cup stage by whole mount *in situ* hybridisation

Pictures represent whole mount lateral views of the embryonic head. **(A)** Embryo hybridised with the *Vax2* probe at ss45 (11.5 dpc). *Vax2* was expressed in the ventral optic cup. **(B)** An 11.5 dpc embryo hybridised simultaneously with the *Vax2* and *Tbx2* probes. *Tbx2* transcripts, detected in red, were expressed in all regions described in earlier figures, including the dorsal optic cup (grey arrows) and in the ventral extra-ocular mesenchyme (arrowhead). *Vax2* expression, detected in blue, was separated from *Tbx2* expression by a group of cells (between grey and white arrows) in which neither gene was expressed. The overall blue appearance of the head is due to high levels of non-specific trapping of the reaction product. The *Vax2* signal in the eye however is specific as it is localised ventrally as in A. **(C)** *Tbx2* expression in a 10.5 dpc embryo, just after optic cup invagination. **(D)** A 10.5 dpc embryo hybridised with an *ephrinB2* probe. Transcripts were localised to the dorsal optic cup (arrows) and in the anterior rim of the lens vesicle (L). **(E)** A late 10.5 dpc embryo hybridised with an *Msx2* probe. Transcripts in the eye were confined to the dorsal-most region of the optic cup. **(F)** A 10.5 dpc embryo showing *Jagged1* expression, which was expressed widely in the optic cup except the dorsal most and the ventral most regions (arrows). Scale bars: 0.5 mm

Abbreviations: D, dorsal; L, lens; LE, lens epithelium; MX, maxillary process of the first branchial arch; NP, nasal process; V, ventral.

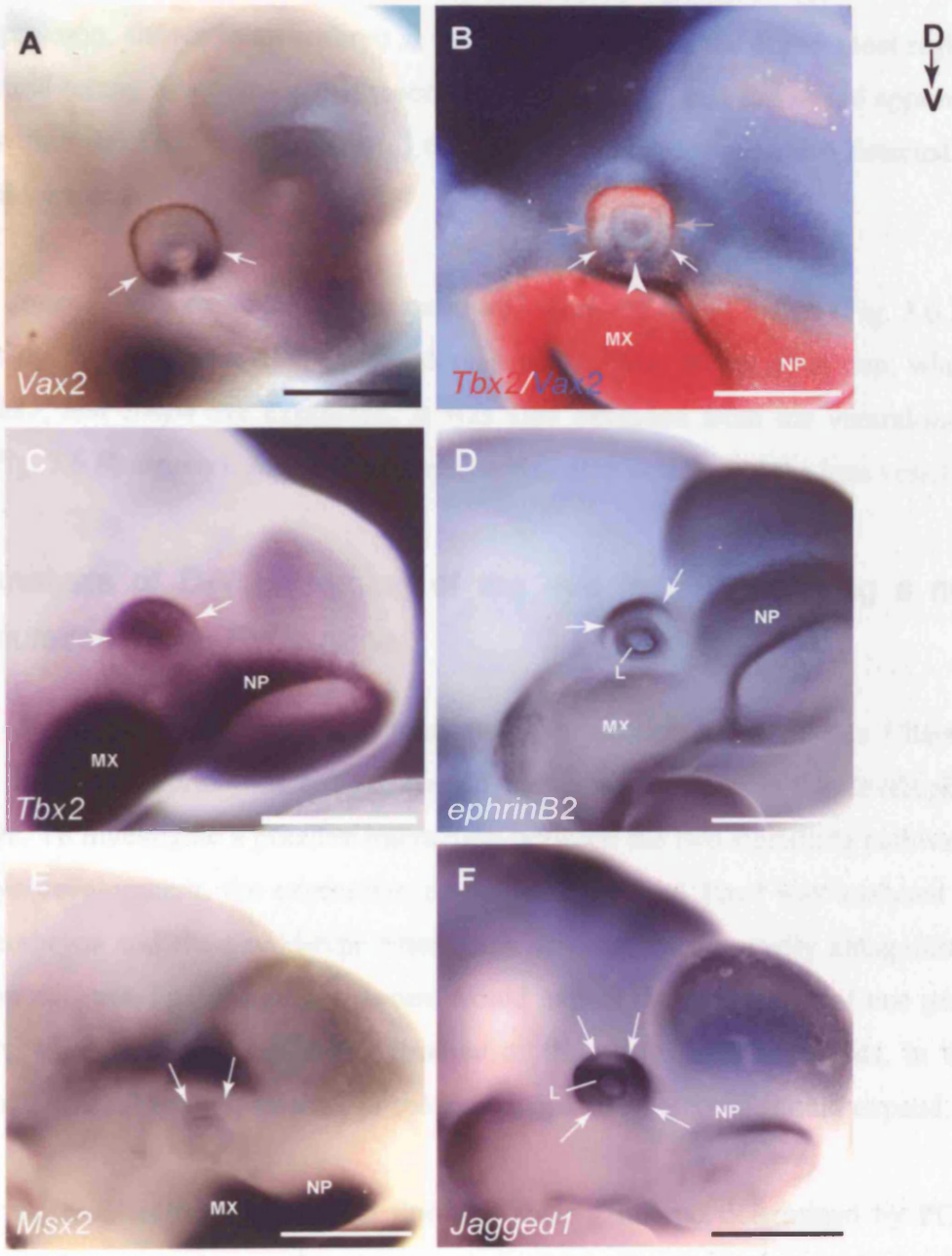
A
Vax2
B
Tbx2/Vax2
MX
NP
D
V
C
NP
MX
Tbx2
D
NP
L
MX
ephrinB2
E
NP
MX
Msx2
F
L
NP
Jagged1

Msx2 expression, shown in an embryo at ss37, was present in the dorsal most region of the neural retina, in a domain that resembled that of *Tbx5*, and *Bmp4* and appeared located within the *Tbx2* domain, (Fig. 3.6 E). *Msx2* expression was also detected in the dorsal lens vesicle.

At ss 35 *Jagged1* was expressed in the nasal and temporal neural retina (Fig. 3.6 F). Interestingly, it was excluded from the dorsal-most region of the optic cup, where *Msx2*, *Tbx5*, and *Bmp4* are expressed. It was also excluded from the ventral-most region (Fig. 3.6 F, arrows). *Jagged1* expression was also detected in the lens vesicle.

3.2.4 Analysis of D-V patterning of the eye in mice carrying a null mutation in the *Fgf15* gene

Analysis of the expression of *Fgf15* and *Bmp4* in section 3.2.1 of this Chapter revealed that their expressions are juxtaposed with some overlap in the developing mouse eye. To investigate a putative interaction between the two signalling pathways during eye development, the expression of *Bmp4*, *Tbx2*, and *Vax2* was analysed in *Fgf15*$^{-/-}$ embryos and their wild-type littermates. If there is a mutually antagonistic interaction between Fgf15 and Bmp4, one would expect the expression of one gene or its target genes to expand in the absence of the other. In other words, in the absence of *Fgf15*, *Bmp4* expression, or the expression of its targets, should expand.

Embryos were collected at 10.5-11.5 dpc and their genotype determined by PCR (Fig. 3.7). In *Fgf15*$^{-/-}$ embryos, *Bmp4* expression was similar to somite matched wild-type littermates at 10.5 dpc (n= 3 per genotype, Fig. 3.8 A,B). The expression patterns of *Tbx2* (Fig. 3.8 C-F) and *Vax2* (Fig. 3.8 G-J) were also indistinguishable between mutant and wild-type somite matched littermates (n= 3 per genotype and probe). This suggests that the lack of *Fgf15* has no effect on *Bmp4* expression and that D-V patterning of the eye is correctly maintained.

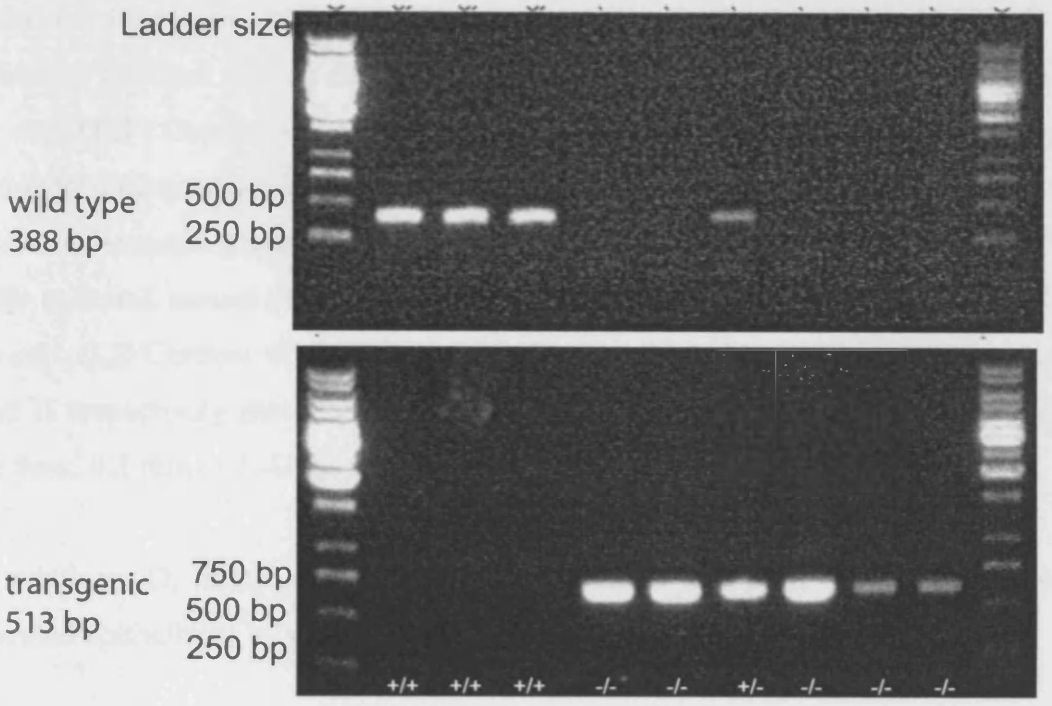

Fig. 3.7 Genotyping PCR products of *Fgf15*$^{-/-}$ and wild-type mouse yolk sac DNA

Examples of 2% agarose gels showing the PCR products obtained from the genotyping reactions of *Fgf15*$^{-/-}$ and wild-type DNA. Genotypes are indicated on the bottom gel. The 388 bp product shows the existence of the wild-type allele, while the 513 bp product indicates the existence of the transgenic allele.

Fig. 3.8 Expression of D-V markers of the optic cup in *Fgf15*$^{-/-}$ mice at 10.5 dpc detected by whole mount *in situ* hybridisation

Pictures represent either whole mount lateral views of the embryonic head or coronal vibratome sections through the eye. **(A)** Wild-type (+/+) embryo hybridised with the *Bmp4* probe. **(B)** Somite matched mutant (-/-) embryo showing normal *Bmp4* expression in the optic cup. **(C)** Wild-type embryo hybridised with the *Tbx2* probe. **(D)** Somite matched mutant embryo showing normal *Tbx2* expression in the dorsal optic cup. **(E,F)** Coronal vibratome sections through the optic cups of the wild-type and mutant embryos shown in C and D respectively, confirming comparable *Tbx2* expression between genotypes. **(G)** *Vax2* expression in a wild-type embryo. **(H)** Somite matched mutant embryo showing normal expression of *Vax2* in the ventral optic cup. **(I,J)** Coronal vibratome sections through the wild-type and mutant eyes in G and H respectively showing normal *Vax2* expression in the ventral neural retina. Scale bars: 0.5 mm in A-D, G, H, 0.1 mm in E, F, I, J.

Abbreviations: D, dorsal; L, lens; NR, neural retina; OS, optic stalk; RPE, retinal pigmented epithelium; V, ventral

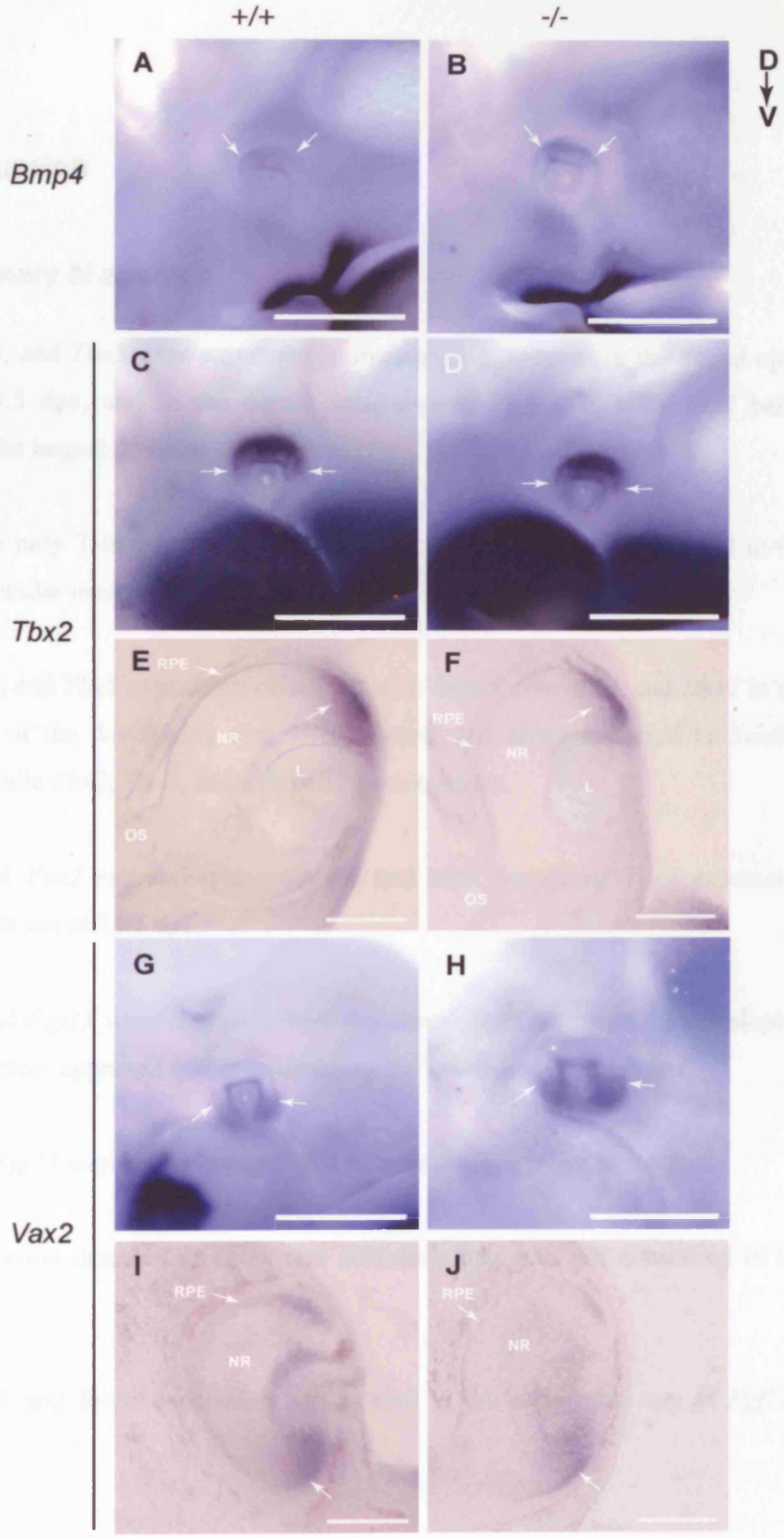
+/+
-/-
A
B
D
V
Bmp4
C
D
Tbx2
E
RPE
NR
L
OS
F
RPE
NR
L
OS
G
H
Vax2
I
RPE
NR
J
RPE
NR

3.3 Discussion

3.3.1 Summary of analysis

1) *Tbx2*, *Tbx3*, and *Tbx5* were expressed in overlapping domains in the dorsal optic vesicle, at 10.5 dpc, and in the dorsal optic cup at 11.5 dpc, with *Tbx2* being expressed in the largest domain.

2) *Tbx2* is the only T-box gene of the three examined, which was expressed in the ventral extra-ocular mesenchyme.

3) *Tbx2*, *Tbx3*, and *Tbx5* expression coincided with *Bmp4*, *ephrinB2*, and *Msx2* in the dorsal region of the developing eye; *Tbx5*, *Bmp4*, and *Msx2* appeared to overlap completely, while *Tbx2*, *Tbx3*, and *ephrinB2* were broader.

4) The ventral *Vax2* expression domain did not meet the dorsal *Tbx2* expression domain, at least not at 11.5 dpc.

5) *Jagged1* and *Fgf15* were excluded from the dorsal-most region of the developing eye; they therefore appeared complementary to the T-box genes and *Bmp4*.

6) *Bmp4* and *Fgf15* were suitably expressed in the developing eye to interact.

7) *Fgf8* expression detected in chick and zebrafish eyes was not conserved in the mouse.

8) *Tbx2*, *Vax2*, and *Bmp4* expression was normal in the early optic cup of *Fgf15*$^{-/-}$ embryos.

3.3.1 The optic cup is divided into distinct domains of gene expression along the D-V axis

Expression analysis of members of the *Tbx2* subfamily, including *Tbx2*, *Tbx3*, and *Tbx5*, during optic cup formation showed that they are expressed in overlapping domains in the dorsal neural retina. Several sites where transcripts of the T-box genes were differentially distributed in the developing mouse eye were identified. Along the D-V axis of the optic cup, *Tbx2* expression extended more ventrally and, along the P-Di axis, it extended more proximally than both *Tbx3* and *Tbx5*. *Tbx5* expression was the most restricted, both along the D-V and the P-Di axes of the optic cup. Along the D-V axis of the optic cup, the expression of the T-box genes was restricted in sharp domains, while along the P-Di axis, the expression of *Tbx2* and *Tbx3* appeared graded.

It has been proposed that the developing chick eye is divided into four compartment-like domains of gene expression based on analysis of the expression of several asymmetrically expressed genes along the D-V axis. These include some of the genes analysed in this Chapter in the mouse embryo, namely *ephrinB2*, *Tbx5*, and *Bmp4* in the dorsal-most region of the chick eye and *Vax2* in the ventral most region (Peters and Cepko 2002). Retroviral driven *lacZ* labelling of cells and their progeny within the described domains in the chick embryo showed that approximately 80% of the cells originating in these domains respect the boundaries of gene expression and do not cross into the next domain, while 57% of cells cross an arbitrary border within a domain. This has led to the suggestion that the eye possesses multiple compartment-like units marked by restricted gene expression along the D-V axis, although these units do not possess the full characteristics of absolute lineage compartments due to the observation that some clonal cells do indeed cross the boundaries. Further support for the eye being composed of units at the cellular level along the D-V axis has come from labelling of a population of cells in the optic stalk region which contribute to the ventral-most domain of the neural retina and form a sharp domain with more dorsally located unlabelled cells in the *Xenopus* embryo during optic cup morphogenesis (Holt 1980).

In addition to the genes analysed by Peters and Cepko in the chick embryo, I have incorporated *Tbx2* and *Tbx3* into the model and confirmed the presence of such distinct gene expression domains also in the mouse eye. The early optic cup of the mouse embryo can be divided into at least four domains of restricted gene expression along the D-V axis (Fig. 3.9). In the dorsal-most domain, dorsal domain 1 (D1), *Tbx5*, *Bmp4*, *Msx2*, were expressed. *Tbx2* was expressed in almost the entire dorsal half of the eye, in dorsal domain 2 (D2) together with *ephrinB2*. *Tbx3* was expressed in D1 and on the temporal side also extended into D2. Double-labelling of *Tbx2* and *Vax2* expression demarcated yet another domain of non-labelled cells, ventral domain 3 (V3), as *Vax2* in the ventral-most domain, ventral domain 4 (V4), was separated from the *Tbx2* domain by a group of non-labelled cells. The expression of *Jagged1* can be described as occupying D2 and V3, but not D1 or V4. It is possible that these domains of gene expression can be further subdivided by the borders of expression of other as yet unidentified genes. Some differences do appear to exists between the developing chick and the developing mouse eyes, notably in the chick eye, the expression of *ephrinB2* was described to be more restricted than *Tbx5* and *Bmp4* (Peters and Cepko 2002), but in the developing mouse eye, *ephrinB2* expression appears similar to *Tbx2* expression.

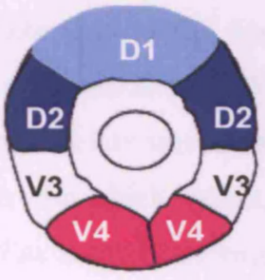

Fig. 3.9 The division of the mouse neural retina into distinct domains of gene expression based on genes examined in Chapter 3

Frontal view of an optic cup. *Tbx5*, *Bmp4*, *Msx2* are expressed in dorsal domain 1 (D1; light blue). *Tbx2* and *ephrinB2* are expressed in D2 (dark blue). *Tbx3* is expressed in D1 and in the temporal neural retina, also extends into D2. *Vax2* is expressed in V4 (pink). V3 demarcates the existence of a domain between *Tbx2* and *Vax2*.

Attempts have been made to identify further genes expressed asymmetrically along the D-V axis. Shintani and colleagues have recently published a large-scale screening of differentially expressed genes in the dorsal, ventral, nasal, and temporal chick retina, based on comparisons of signal intensities of a display of restriction digested cDNA fragments synthesised from RNA that was isolated from the above mentioned regions in a 2-dimensional gel (Shintani *et al.* 2004). Of 47 clones (20 genes) identified to be asymmetrically expressed, none possessed a smaller expression domain than that of *ephrinB2* (D1). In fact all genes identified in the dorsal eye showed expression domains similar to that of *Tbx2* (D2) or to genes confined to D1.

The functional significance of these early divisions is currently not fully understood. However, as described in Chapter 1.2.3-4, there are several manifestations of morphological asymmetries during optic cup morphogenesis. Later, some neuronal cell types display a non-uniform distribution in the mature retina. One aspect of asymmetry in the eye at the cellular level that has been studied extensively is the regulation of the topographic map of RGC axons. Manipulation of the expression of *Vax2/cVax*, *Tbx5*, *Bmp4*, *EphB2* and *EphB3* have all resulted in axonal mis-projections in the brain (Schulte *et al.* 1999; Mui *et al.* 2002; Barbeiri *et al.* 2002; Koshiba-Takeuchi *et al.* 2000; Sakuta *et al.* 2001; Birgbauer *et al.* 2000). Recently, retroviral driven misexpression of *cVax* was shown to result in an increase in the rod density in infected areas in the chick retina, leading to suggestions that the asymmetrical expression of *cVax* at the optic vesicle stage sets the ventral rod-dense, dorsal rod-sparse pattern obvious in late development in the chick eye (Schulte *et al.* 2005). In the same study, misexpression of a retrovirus encoding an *engrailed*-tagged *Tbx5* insert, which acts in a dominant negative manner, also disrupted the rod pattern. Some of the genes described here and in the study of Peters and Cepko (2002) retain their expression pattern seen in the early optic cup as the retina grows, while others are switched off or expanded. How these domains of restricted gene expression are established or maintained in the eye, whether they mark cells that are synchronous in development in terms of proliferation and differentiation, and how the early pattern of these genes in the optic vesicle and during optic vesicle invagination relates to the final topography and shape of the expanded adult retina, the bulk of which is produced after the molecular division of the early optic cup, is

unknown. In Chapter 4 of this thesis, I have attempted to examine the role of Bmp4 in regulating these gene expression domains, specifically those of the T-box genes, along the D-V axis of the mouse optic cup and examined the growth and the formation of the early optic cup after manipulation of Bmp signalling.

3.3.2 Shh, Bmp4, Fgf signalling network in the eye and their function

By analogy to the interaction between *Bmp4*, *Shh*, and *Fgfs* in for example the limb bud, the developing forebrain or the developing chick eye, it has been proposed that this tripartite signalling network may play generalised roles in growth and patterning of embryonic tissues (Crossley *et al.* 2001).

In the chick and zebrafish embryos, *Fgf8* is dynamically expressed in the central region of the neural retina and in the optic stalk (Reifers *et al.* 1998; Crossley *et al.* 2001; Martinez-Morales *et al.* 2005). There are seven *Fgf8* mRNA isoforms expressed during mouse embryogenesis (Crossley and Martin 1995), all of which share the same C-terminal coding region but differ in their N-terminal region. Here, using a probe specific for the C-terminus of *Fgf8*, it was confirmed that unlike in the chick and zebrafish embryos, *Fgf8* is not expressed in the central presumptive neural retina at the optic vesicle stage or in the neural retina at the optic cup stage in the mouse embryo. This is in agreement with the initial expression study of *Fgf8* in the mouse (Crossley and Martin 1995). Comparative analysis, described in this Chapter, of the expression of *Fgf15*, *Bmp4*, and *Shh,* both at the optic vesicle and at the optic cup stages, revealed that *Fgf15* is expressed in between the dorsal *Bmp4* domain and ventral neural retinal tissue that has previously been exposed to Shh emanating from the ventral forebrain. The pattern of expression of these signalling molecules in the developing mouse eye is therefore similar to the relative expression of *Shh*, *Bmp4*, and multiple Fgfs in other tissues described earlier. Therefore, it is possible that similar interactions also occur between these factors during mouse eye development.

The above mentioned idea of a putative interaction between the *Bmp4* and *Fgf15* signalling pathways, was tested by analysing the expression of *Bmp4*, and other asymmetrically expressed genes along the D-V axis of the eye in *Fgf15*$^{-/-}$ mice. These mice form optic cups and are currently being analysed for eye defects by Dr.

A. Battersby (University of Wales Cardiff). The expression of all genes were similar in mutant and wild-type embryos, suggesting that *Fgf15* alone does not regulate *Bmp4* expression or the molecular composition of the eye along the D-V axis. An interaction between the *Bmp4* and the *Fgf15* pathways in the eye is nevertheless still possible, as *Bmp4* could be upstream of *Fgf15*. Evidence for this was recently provided by demonstration of the lack of *Fgf15* expression in the optic vesicle in mice homozygous for a non-functional *Bmp4* allele (Murali *et al.* 2005). Although, this suggests that unlike other developing systems where *Bmp4* antagonises Fgfs, in the developing mouse eye, *Bmp4* is required for *Fgf15* expression in the presumptive neural retina.

The expression analysis carried out here cannot completely exclude a role for Fgf signalling in D-V patterning of the eye. First of all, Fgfs may functionally compensate for each other, hence it is possible that the loss of function of one Fgf does not reveal the true role of Fgf signalling in a tissue. Evidence that corroborates this idea comes from studies in zebrafish, where loss of function of *Fgf8/ace* or *Fgf3/lia* alone has no profound effect on eye development, whereas loss of function of both prevents the onset of retinal cell differentiation (Martinez-Morales *et al.* 2005). Recent evidence that provides support for a role for Fgf signalling in D-V patterning, comes from misexpression of an inducible Fgf receptor I (FgfrI) in the developing *Xenopus* eye, which induces the expansion of ventral retinal and optic stalk markers (Lupo *et al.* 2005). *Noggin* treatment of the chick optic cup, which antagonises Bmp signalling, causes an expansion of the *Fgf8* neural retinal expression domain (Adler and Belecky-Adams 2002). The *Fgf8* expression in the chick central neural retina is juxtaposed to the dorsal *Bmp4* expression domain, in a similar pattern to *Fgf15* in the mouse neural retina. The necessity of *Bmp4* for *Fgf15* induction in the mouse eye compared to the antagonistic effect of Bmp signalling on *Fgf8* in the chick optic cup could be either due to species differences or differences in the experimental approach, including the developmental time points studied; in the mouse, the induction of *Fgf15* was examined in the absence of Bmp4 at optic vesicle stage, while in the chick, *Noggin* was misexpressed only after the induction of *Fgf8* expression in the neural retina at the optic cup stage, and therefore the expansion of the *Fgf8* domain, could reflect an antagonistic relationship that may exist also in the

mouse between *Bmp4* and Fgfs during maintenance rather than the induction of Fgfs in the central neural retina.

Manipulations of *Shh*, *Fgf8*, and *Noggin* in the chick eye are accompanied by morphological abnormalities such as microphthalmia and abnormal optic stalk development (Zhang and Yang 2001; Crossley *et al.* 2001; Adler and Belecky-Adams 2002). The mechanism of these morphological defects or how the three signalling pathways interact are currently not clear. Although the *Shh* expression domain is distant from the optic cup in 10.5-11.5 dpc mouse embryos, it has been shown that *Patched*, the Hh receptor which is a transcriptional target of Shh signalling in all tissues examined and therefore considered to be an indicator of Shh receptive cells (Marigo *et al.* 1996; Ingham and McMahon 2001), is expressed in a graded fashion along the optic stalk (Zhang and Yang 2001; Dakubo *et al.* 2003). Misexpression of *Shh* in the developing chick, zebrafish, and *Xenopus* eyes has a ventralising effect and induces optic stalk and ventral neural retina at the expense of dorsal neural retina at the molecular level. By contrast, antagonism of endogenous Shh, causes suppression of optic stalk and ventral neural retinal fates (Macdonald *et al.* 1995; Zhang and Yang 2001; Take-uchi *et al.* 2003; Lupo *et al.* 2005). This shows that Shh signalling is important for D-V patterning of the eye, even though its site of expression is a distance away in the ventral forebrain.

In conclusion, the peripheral optic cup can be divided into at least four distinct domains of gene expression along the D-V axis. The T-box genes occupy D1 and D2. The signalling molecule that most closely overlaps in expression pattern with the T-box genes is *Bmp4*, which is expressed in D1. *Bmp4*, *Fgf15*, and *Shh* expression along the D-V axis of the mouse eye is reminiscent of the expression pattern of *Shh*, *Bmp4*, and Fgfs in multiple other tissues where they have been shown to interact to regulate tissue growth. However, data presented here has excluded *Fgf15* as a regulator of *Bmp4* expression in the neural retina, and shown that in the absence of *Fgf15*, the molecular composition of the eye along the D-V axis is not disrupted.

In the next Chapter, the effect of manipulation of *Bmp4* signalling is analysed with respect to optic cup formation, growth, and regulation of the four domains of distinct gene expression, with emphasis on the T-box genes, along the D-V axis.

CHAPTER 4 Investigation of the role of Bmp4 signalling in T-box gene regulation, D-V patterning and growth of the mouse eye

4.1 Introduction

Analysis of the expression of *Bmp4* and members of the *Tbx2* subfamily during optic cup morphogenesis (Chapter 3) revealed a high degree of overlap in the dorsal region of the developing eye. Preliminary observations in the Sowden laboratory had indicated that ectopic *Tbx5* and *Tbx2* expression could be induced by BMP4 in the presumptive RPE at optic vesicle stage (J. Holt and J. Sowden, unpublished). In this Chapter, experiments that investigated the regulation of *Tbx2*, *Tbx3*, *Tbx5*, as well as the ventrally expressed *Vax2* gene by Bmp4 in the mouse optic cup are presented and the affect of manipulation of Bmp4 signalling on early optic cup morphology is analysed.

Previous work in the chick embryo has demonstrated that electroporation of *Bmp4* into the ventral optic cup can repress ventral retinal genes including *cVax*, the homologue of mouse *Vax2*, and induce *Tbx5*, *ephrinB1*, and *ephrinB2*, which are normally restricted to the dorsal optic cup (Koshiba-Takeuchi *et al.* 2000), suggesting that Bmp4 induces dorsal characteristics. The Bmp4 homologue in *Drosophila*, Dpp, acts as a long-range morphogen in wing disc development (Chapter 1.4.3) The possibility of Bmp4 setting up a long range signalling gradient along the D-V axis of the newly formed optic cup across which the four domains of restricted gene expression are set up as described in Chapter 3, was explored here by assessing the spatial alteration of the four domains upon manipulation of Bmp4 signalling. This was tested by providing an ectopic source of Bmp4 or Noggin in such a way that the putative natural dorsal-high, ventral-low Bmp4 signalling gradient would be enhanced (by ectopic Bmp4) or decreased (by ectopic Noggin).

Analysis of D-V patterning, or growth and development of the eye in mice that are homozygous for a targeted disruption of *Bmp4* has been precluded by the resulting embryonic lethality around mid-gestation (Winnier *et al.* 1995; Furuta and Hogan 1998). In the heterozygous state on a C57BL/6 genetic background however, embryos are born and manifest microphthalmia at a three-fold higher incidence than observed in wild-type mice (Dunn *et al.* 1997). This is corroborated by the recent finding that *Bmp4* heterozygous mutants crossed to mice homozygous for a disrupted

allele of *twisted gastrulation* (*Tsg*), a Bmp binding protein which in the mouse eye has been suggested to boost Bmp4 signalling, exhibit anophthalmia (Zakin and De Robertis 2004). To gain insight into the mechanism(s) by which Bmp4 regulates eye growth, eye size was measured after manipulation of Bmp signalling in experiments described here. The pattern of cell proliferation and cell death were analysed in relation to the distinct gene expression domains along the D-V axis of the eye, and changes in proliferation and apoptosis in Bmp manipulated eyes were correlated to alterations in the gene expression domains along the D-V axis of the optic cup.

To manipulate Bmp signalling in the mouse optic cup, the mouse whole embryo culture system, described by Martin and Cockroft (Martin and Cockroft 1999) was utilised to allow further development of mouse embryos *ex-utero* after manipulation. Exogenous recombinant human BMP4 (rhBMP4) and Noggin protein were delivered by agarose beads, which have previously been shown to be suitable delivery media for these proteins to embryonic tissues (Furuta *et al.* 1997; Lee *et al.* 2001b). The whole embryo culture system in combination with bead implantation is ideal for local delivery of proteins such as signalling factors. It is more accessible for such surgical manipulations of embryos than *in-utero* manipulations. Furthermore, in comparison to explant cultures of eyes, which is another method often used for the study of eye development, it offers superior preservation of eye morphology and allows the analysis of eye size and shape within the embryonic head.

4.2 Results

4.2.1 Optic cup formation and eye development in whole embryo culture

To assess the suitability of the mouse whole embryo culture system for the study of eye development, embryos were cultured for a period of 15-18 (hours) hrs, here referred to as overnight culture, as described in Chapter 2.4.2. The state of health and growth of embryos were assessed according to the following criteria, which are commonly used to assess developmental stage (Brown 1990) and viability . The heart beat and the rate of circulation in the large cranial vessels were examined as a

measure of viability and were given a score for each embryo before (pre) and after (post) culture (Table 4.1; scoring criteria are described in table). Growth of embryos was assessed by measuring the head length as illustrated in Fig. 4.1. Head length, like crown-rump length, increases with developmental age and is commonly used as a measure of growth, although neither show a simple linear nor logarithmic increase with developmental age (Brown 1990). The post-culture head length was compared to the pre-culture head length for each embryo. The number of somite pairs pre- and post-culture were also counted. Table 4.1 illustrates examples of these records for some of the 263 embryos cultured for the experiments reported in this Chapter.

Table. 4.1: Examples of health check records for cultured embryos before (pre) and after (post) 15-18 hrs in culture

	no.	Heart beat		Circulation		Somite pairs		Head length (mm)	
Age		*Pre*	*Post*	*Pre*	*Post*	*Pre*	*Post*	*Pre*	*Post*
11.5 dpc	1	+++	++	+++	+	42	51	3.0	3.5
	2	+++	+++	+++	+++	46	52	3.1	3.6
	3	+++	+++	+++	+++	42	48	3.0	3.3
	4	+++	+++	+++	++	46	50	3.0	2.8
	5	+++	+++	+++	+++	40	50	2.6	3.5
10.5 dpc	6	++	+++	+++	+++	31	37	1.7	2.2
	7	++	-	++	-	25	30	1.4	1.4
	8	++	+++	+++	+++	25	32	1.4	2.1
	9	++	++	+++	++	20	29	1.2	1.7
	10	++	+++	+++	+++	22	29	0.9	1.7

Heart beat: -, none; +, slow; ++, moderately fast; +++, very fast.
Circulation: -, none; +, few circulating blood cells; ++, many circulating blood cells and moderately fast rate of blood flow, +++, many circulating blood cells with very fast rate of blood flow.

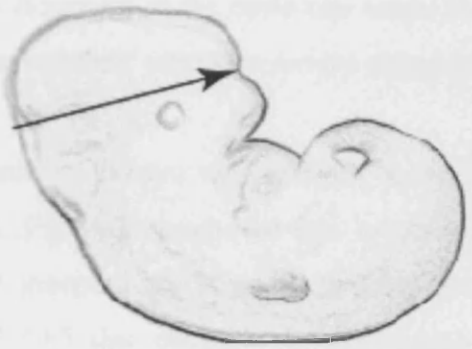

Fig. 4.1 Schematic demonstration of the measurement of head length

Head length was measured from the anterior groove of the forebrain to the posterior most point of the hindbrain, using a 10 mm graticule positioned beneath a petridish containing the embryo rested on its lateral side.

In all experiments presented in this Chapter, post-culture embryos were analysed if they passed the minimum criteria of heart beat = +, circulation = + and showed an increase in the number of somite pairs and an increase in head length compared to their pre-culture state. Embryos lacking circulation after culture but having grown 6 or more somite pairs and showing an increase in head length as well as possessing a more advanced morphology and appearing generally healthy after overnight culture were also included in the analysis. For example, embryos numbered 4 and 7 in Table 4.1 were regarded as unhealthy and therefore excluded from analysis.

Eye development in embryo culture was assessed morphologically and compared to non-cultured embryos. Fig. 4.2 shows examples of eye morphology of cultured embryos in comparison to the eye morphology in embryos equivalent to their pre-culture and post culture states. Overnight cultures of 10.5 dpc embryos in possession of optic vesicles prior to culture (Fig. 4.2 A-C), resulted in the formation of optic cups, in which the neural retina was thick, the RPE layer was thin but still non-pigmented, and the lens vesicle was in most cases completely separated from the overlying surface ectoderm (Fig. 4.2 D-H). Overnight cultures of 11.5 dpc embryos resulted in growth of the optic cup, pigmentation of the RPE, and apposition of the walls of the optic fissure (Fig. 4.2 I-N), which were features also observed in stage

matched non-cultured embryos (Fig. 4.2 O-T). Thus, optic vesicle invagination and further growth and development of the optic cup occur in whole embryo culture with conditions described and closely resemble *in vivo* development.

Eye development in embryo culture was assessed morphologically and compared to non-cultured embryos. Fig. 4.2 shows the eye morphology of cultured embryo in comparison to the eye morphology of an embryo equivalent to its preculture state. Overnight cultures of 10.5 dpc embryos in possession of optic vesicles prior to culture (Fig. 4.2 A-C), resulted in the formation of optic cups, in which the neural retina was thick, the RPE layer was thin but still non-pigmented, and the lens vesicle was in most cases completely separated from the overlying surface ectoderm (Fig. 4.2 D-H). Thus, optic vesicle invagination and growth of the optic cup occurs in whole embryo culture with conditions described

The age of each embryo is described as its age at the time of explantation from the uterus plus information about its culture state. For example, an embryo dissected at 11.5 dpc and cultured overnight is described as 11.5 dpc post-culture.

Fig. 4.2 Development and morphology of the ocular tissues in cultured embryos at 10.5 - 11.5 dpc

Rows show serial transverse vibratome sections through eyes with the dorsal most section displayed at the top and the ventral most section displayed at the bottom of each row. **(A-C)** State of eye development in a non-cultured early 10.5 dpc embryo, still in possession of an optic vesicle. Sections show *Tbx5* expression in the optic vesicle. **(D-H)** State of eye development in an early 10.5 dpc embryo cultured overnight, which prior to culture possessed optic vesicles and was at the same ss as the embryo shown in A-C. Sections show an invaginated optic cup with a tick neural retina and an almost complete lens vesicle. Dorsal sections (D,E) show the expression of *Tbx5* in the dorsal neural retina. **(I-N)** State of eye development in an 11.5 dpc embryo (ss 44) after overnight culture showing further growth of the optic cup, formation of the lens vesicle, pigmentation of the RPE, and alignment of the walls of the optic fissure in close proximity (arrow in N). Prior to culture, this embryo possessed approximately the same number of somite pairs as the embryo shown in D-H. **(O-T)** State of eye development in a non-cultured 11.5 dpc embryo (ss 44), showing similar features as the cultured embryo in I-N. Scale bars: 0.1 mm.

Abbreviations: L, lens; NR, neural retina; OS, optic stalk; OF, optic fissure; P-NR, presumptive neural retina; P-RPE, presumptive retinal pigment epithelium; RPE, retinal pigment epithelium

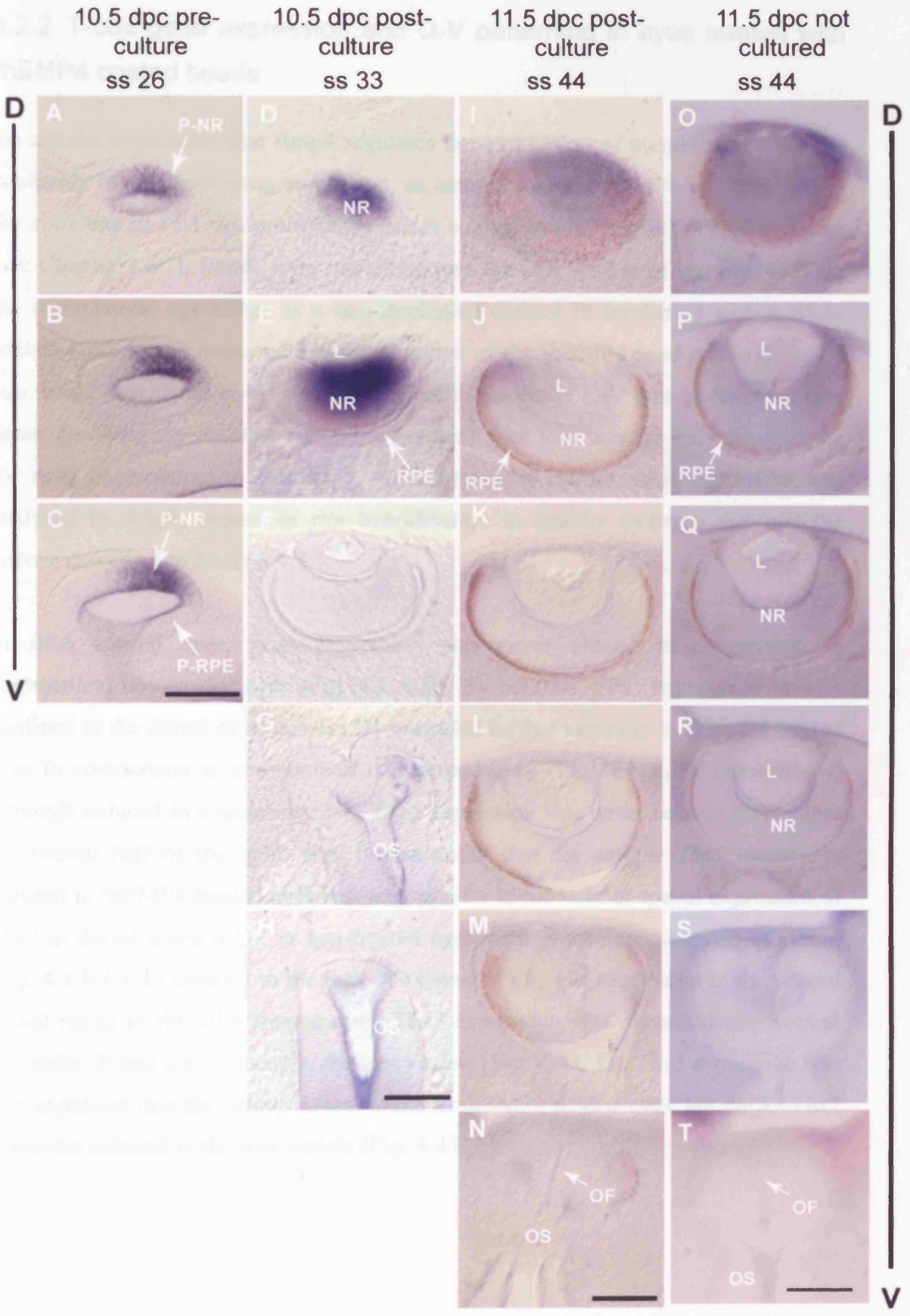
10.5 dpc pre-culture
ss 26
10.5 dpc post-culture
ss 33
11.5 dpc post-culture
ss 44
11.5 dpc not cultured
ss 44
D
V
A
P-NR
B
C
P-NR
P-RPE
D
NR
E
L
NR
RPE
F
G
OS
H
OS
I
J
L
NR
RPE
K
L
M
N
OF
OS
O
P
L
NR
RPE
Q
L
NR
R
L
NR
S
T
OF
OS
D
V

4.2.2 T-box gene expression and D-V patterning in eyes treated with rhBMP4 coated beads

To test the hypothesis that Bmp4 regulates the expression of members of the *Tbx2* subfamily in the developing mouse eye, an ectopic source of BMP4 was provided to the optic cup in 11.5 dpc embryos by beads soaked in [100 μg/ml] rhBMP4 protein (see Chapter 2.6.1). Beads were implanted into the lens vesicle of one eye, keeping the contralateral eye either as a non-implanted control or implanted with a BSA-soaked bead. It was reasoned that implantation of the rhBMP4 bead within the optic cup would provide an equal source of Bmp4 to the entire D-V axis of the optic cup, hence elevating the putative signalling gradient. The lens was the only feasible site for bead implantation at this stage. After overnight culture, gene expression was analysed by whole mount *in situ* hybridisation in healthy embryos that met the criteria described in Section 4.2.1.

In BSA treated eyes, gene expression was never altered in comparison to contralateral non-treated eyes (Fig. 4.3 A,B). By contrast, *Tbx5* expression, usually confined to the dorsal most domain D1 extended further ventrally in rhBMP4 treated eyes in comparison to contralateral non-treated eyes (Fig. 4.4 A,B). Interestingly, although induced in a wider domain, *Tbx5* expression was never seen to extend into the ventral half of the optic cup. It was noted that the ectopic *Tbx5* expression induced in rhBMP4 treated eyes was very similar to the normal spatial expression of *Tbx2* in dorsal domain D2 in non-treated eyes with physiological levels of Bmp4 (Fig. 4.4 B,C). In contrast to the lack of expansion of *Tbx5* expression in the ventral neural retina in rhBMP4 treated eyes, *Tbx2* expression was expanded into ventral territories. It was also induced in the lens vesicle (Fig. 4.4 C,D). *Tbx3* expression was also expanded into the ventral neural retina in rhBMP4 treated eyes, but unlike *Tbx2* it was not induced in the lens vesicle (Fig. 4.4 E,F).

Fig. 4.3 Comparison of gene expression between BSA-treated and non-treated control eyes in an 11.5 dpc post-culture embryo by whole mount *in situ* hybridisation

Pictures depict lateral views of the head of the embryo. **(A)** An 11.5 dpc post culture embryo (overnight culture) showing localisation of *Tbx5* transcripts to the dorsal optic cup (arrows). **(B)** The contralateral eye of the embryo in A implanted with a BSA bead (asterisk), showing similar pattern of *Tbx5* expression (arrows). Scale bars: 0.5 mm.

Abbreviations: BSA, bovine serum albumin; D, dorsal; MN, mandibular process of the first branchial arch; V, ventral.

Tbx5

11.5 dpc post-culture

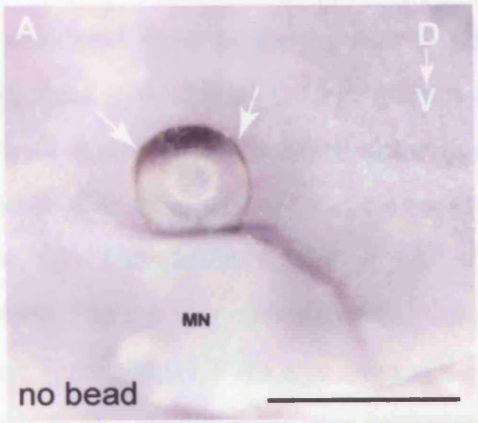

11.5 dpc post-culture

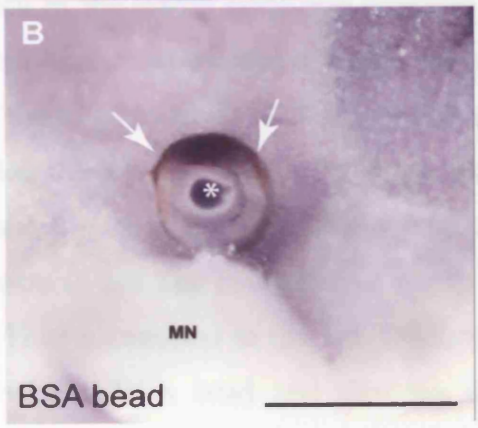

Fig. 4.4 Gene expression along the D-V axis of the optic cup by whole mount *in situ* hybridisation upon rhBMP4 treatment

Somite stages of each embryo are indicated next to their pictures with the post-culture somite count outside of the brackets followed by the pre-culture somite count within brackets. Beads are indicated with asterisks. All pictures show lateral views of the head of the embryos. **(A)** Control eye of a cultured embryo showing *Tbx5* expression in a non-manipulated eye. **(B)** The rhBMP4 treated eye of the embryo shown in A. *Tbx5* expression was detected in a wider domain of the dorsal optic cup, extending beyond the dorsal curvature (arrows). **(C)** An eye implanted with a BSA bead showing normal *Tbx2* expression in the dorsal optic cup (arrows). Arrowhead indicates *Tbx2* expression in the extra-ocular mesenchyme within the ventral optic cup. **(D)** The rhBMP4 treated eye of the embryo in C. *Tbx2* expression was detected in almost the entire optic cup including the lens. Arrows point to the ventral limit of *Tbx2* expression. **(E)** An eye implanted with a BSA bead showing normal *Tbx3* expression in the dorsal optic cup (arrows). **(F)** The contralateral eye to E implanted with an rhBMP4 bead and showing *Tbx3* expression in the entire neural retina. **(G)** Lateral view of an eye implanted with a BSA bead and showing normal *Vax2* expression (arrows). **(H)** Contralateral eye of G implanted with an rhBMP4 bead showing absence of *Vax2* expression was absent in this eye. Arrows are replicas of those in G and indicate the region in which *Vax2* would normally be expressed. **(I)** Schematic representation of the expression of *Tbx2*, *Tbx5*, and *Vax2* relative to each other in a lateral view of a non-treated neural retina in a cultured embryo. **(J)** Schematic representation of the ventral shift of gene expression along the D-V axis in rhBMP4 treated eyes. Scale bars: 0.5 mm.

Abbreviations: D, dorsal; MN, mandibular process of the first branchial arch; MX, maxillary component of the first branchial arch; V, ventral.

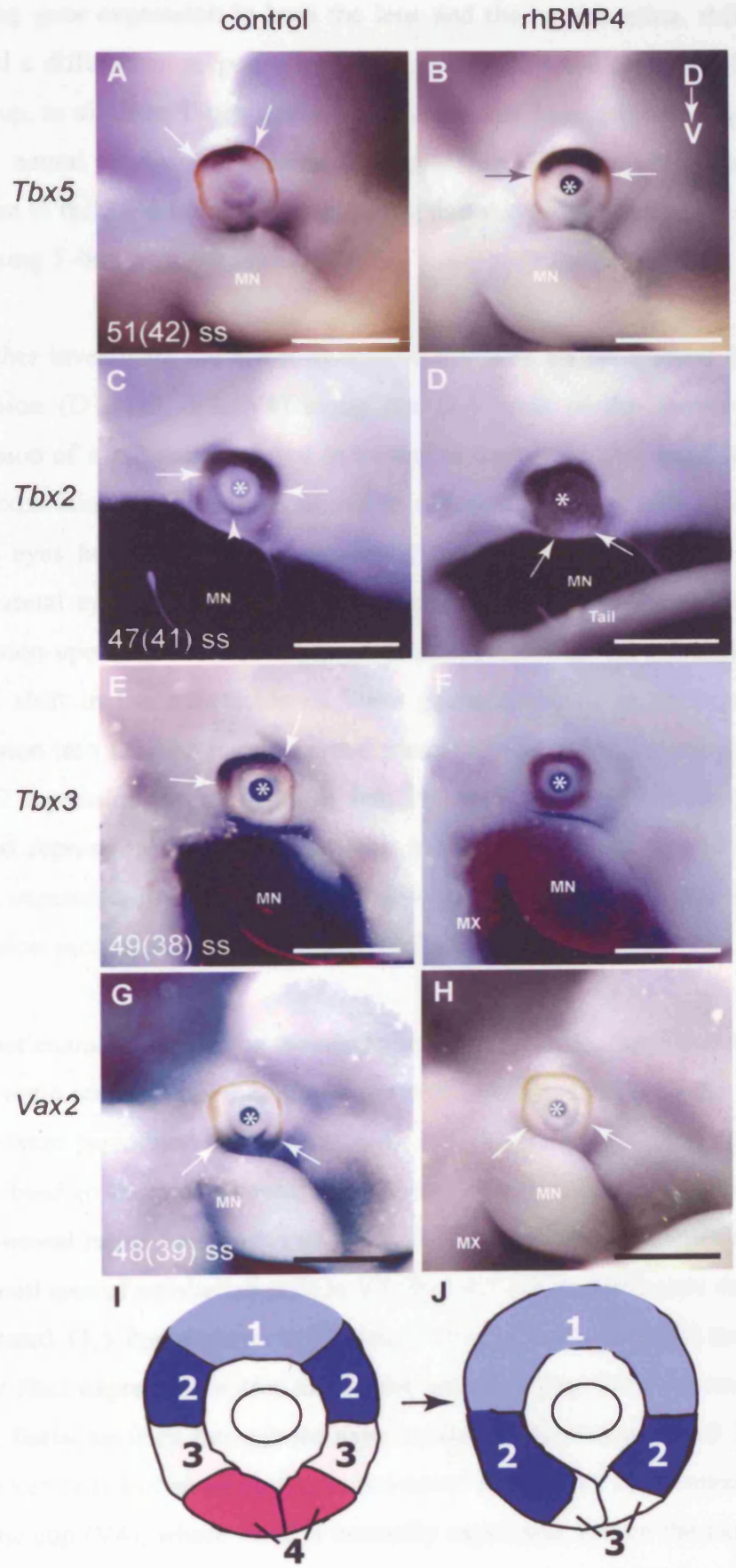
control
rhBMP4
Tbx5
Tbx2
Tbx3
Vax2
A
B
D
V
MN
51(42) ss
C
47(41) ss
D
Tail
E
49(38) ss
F
MX
G
48(39) ss
H
I
J
1
2
3
4

These data show that rhBMP4 bead implantation in the lens vesicle is capable of affecting gene expression in both the lens and the neural retina. rhBMP4 treatment induced a differential response in T-box gene expression along the D-V axis of the optic cup, as all three T-box genes were ectopically induced in a unique manner. The ventral neural retina was capable of expressing *Tbx2* and *Tbx3*, but not *Tbx5* in response to rhBMP4 treatment, suggesting that the ventral neural retina is capable of expressing T-box gene expression.

To further investigate the effect of ectopic rhBMP4 on the distinct domains of gene expression (D1, D2, V3, V4) along the D-V axis of the mouse optic cup, the expression of *Vax2* was analysed in treated embryos. As described in Chapter 3.2.3, *Vax2* expression is normally confined to the ventral neural retina (V4). In rhBMP4 treated eyes however, it was completely absent, but was present in BSA treated contralateral eyes (Fig. 4.4 G,H). The observed change in transcription factor gene expression upon rhBMP4 treatment is illustrated in Fig. 4.4 I-J. rhBMP4 induced a ventral shift in the expression of these genes resulting in an expansion of *Tbx5* expression into D2, the region normally occupied by *Tbx2* transcripts, an expansion of *Tbx2* expression further ventrally into V3 and V4, though not completely covering V4, and repression of *Vax2* expression in the ventral optic cup. *Tbx3* showed the widest expansion in response to rhBMP4 beads within the neural retina, where its expression encompassed the region normally expressing *Vax2* in V4.

To better examine the shift in transcription factor gene expression along the D-V axis of the optic cup at 11.5 dpc, double *in situ* hybridisation with the *Tbx2* and *Vax2* probes were performed on embryos with rhBMP4 coated bead in one eye and BSA coated bead in the contralateral eye. In BSA treated eyes, *Tbx2* expression in the dorsal neural retina was separated from *Vax2* expression in the ventral neural retina by a small area of unlabelled cells in V3 (Fig. 4.5 A), as previously demonstrated in a non-treated 11.5 dpc embryo in Chapter 3 (Fig. 3.6 A). rhBMP4 treatment induced ectopic *Tbx2* expression within this region and abolished *Vax2* expression in V4 (Fig. 4.5 B). Serial sections through the eyes confirmed the expansion of *Tbx2* expression further ventrally but showed that it was never induced in the ventral most region of the optic cup (V4), where *Vax2* is normally expressed. Hence the expansion of *Tbx2* did not encompass the normal *Vax2* expression domain, yet *Vax2* was abolished (Fig.

4.5 C-H). The number of times altered gene expression was observed for each gene are indicated in Table 4.2.

These experiments suggested that elevated Bmp4 signalling induced molecular changes in the optic cup in the form of ectopic T-box gene expression and repression of *Vax2* expression in the ventral eye. A further set of experiments were conducted, which started at the earlier stage of 10.5 dpc prior to optic cup formation, to test whether alterations in Bmp4 signalling disrupted the formation of the optic cup.

In these experiments, rhBMP4 beads were implanted close to the optic vesicle in the extra-ocular mesenchyme as the lens vesicle had not yet formed, and embryos were cultured through the optic vesicle invagination period. Implantations were performed in several locations around the eye in order to enhance the endogenous Bmp4 signalling. To assess the effect on eye morphology, vibratome sections were prepared, and to assess a disruption of D-V patterning by rhBMP4 beads implanted in these new locations, the expression of *Tbx2* and *Tbx5* were analysed in post-culture embryos.

In a total of 12 embryos examined, optic cup formation proceeded normally regardless of bead location; in all 10.5 dpc post-culture embryos the optic cup and a lens vesicle had formed. Examination of gene expression did not show the reproducible changes observed at 11.5 dpc. rhBMP4 bead implantation in the ventral extra-ocular mesenchyme did not induce ectopic *Tbx5* expression and had no apparent effect on the dorsal expression of *Tbx5* (n= 0/2; Fig. 4.6 A,B). Implantation of the bead temporal to the optic vesicle also failed to induce ectopic *Tbx5* expression (n= 0/1; Fig. 4.6 C,D). In eyes where beads were implanted nasal to the optic vesicle, *Tbx5* expression appeared stronger within its normal domain and was slightly extended (n= 2/2; Fig. 4.6 E-G). Sections through the eyes showed that *Tbx5* was also induced in the RPE next to the bead (Fig. 4.6 H,I, arrow). Finally, implantation of beads dorsal to the optic vesicle resulted in an apparently stronger expression of *Tbx5* within the dorsal neural retina in 1/3 treated eyes compared to non treated contralateral eyes in each embryo (data not shown as similar to the set in Fig. 4.6 E-G).

Fig. 4.5 *Tbx2* and *Vax2* expression in the optic cup by whole mount double *in situ* hybridisation upon rhBMP4 treatment

Beads are highlighted by asterisks. **(A)** Lateral view of the eye of a cultured embryo implanted with a BSA bead, showing normal *Tbx2* expression in red and *Vax2* expression in blue. Arrows indicate the limits of the expression of each gene. Arrowhead point to *Tbx2* expression in the extra-ocular mesenchyme in the ventral optic cup. The strong expression of *Tbx2* in the maxillary and mandibular processes of the first branchial arch is also visible in red. **(B)** The contralateral eye of A, implanted with an rhBMP4 bead. *Tbx2* expression was detected in almost the entire optic cup, but *Vax2* expression was absent. **(C-H)** Serial transverse vibratome sections through the BSA treated and the rhBMP4 treated eyes, showing the expansion of *Tbx2* and loss of *Vax2* expressions. Sections start in the dorsal optic cup at the level of the dotted lines indicated in A and B and continue into the ventral optic cup. The red staining indicated by arrowheads in G and H show *Tbx2* expression in the ventral extra-ocular mesenchyme. Arrows indicate the optic fissure walls. Scale bars: 0.5 mm in A,B; 0.1 mm in C-F.

Abbreviations: D, dorsal; L, lens; MN, mandibular process of the first branchial arch; MX, maxillary process of the first branchial arch; NR, neural retina; OF, optic fissure; V, ventral

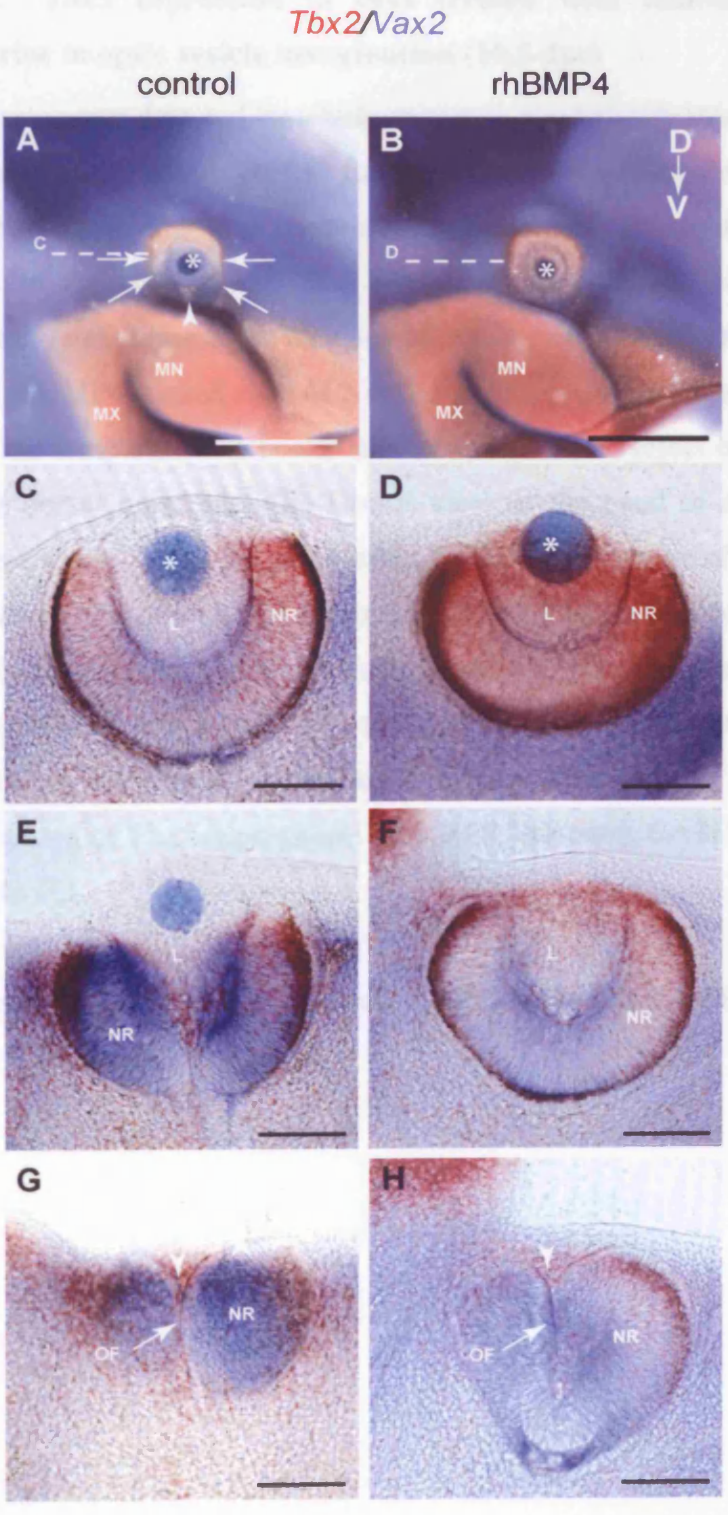
Tbx2/Vax2
control
rhBMP4
A
B
D
V
C
D
MN
MX
MN
MX
C
D
L
NR
L
NR
E
F
L
NR
L
NR
G
H
OF
NR
OF
NR

Fig. 4.6 *Tbx5* expression in eyes treated with rhBMP4 from various locations prior to optic vesicle invagination (10.5 dpc)

Gene expression was detected by whole mount *in situ* hybridisation. The locations of beads are marked by asterisks. **(A)** Lateral view of a non-treated control eye of a cultured embryo showing *Tbx5* expression (arrows). **(B)** The contralateral eye to the eye shown in A with an rhBMP4 bead implanted in the ventral extra-ocular mesenchyme. *Tbx5* expression was not affected (arrows). **(C,D)** Lateral views of control and rhBMP4 treated eyes of a cultured embryo respectively. Implantation of the bead in the temporal extra-ocular mesenchyme had no effect on the expression of *Tbx5* in the dorsal optic cup. **(E)** Dorsal view of the head of an embryo with an rhBMP4 bead implanted in the nasal extra-ocular mesenchyme of one eye (asterisk). *Tbx5* expression was stronger on the treated side. **(F,G)** Lateral views of the control and treated eyes respectively of the embryo shown in E. *Tbx5* expression was also slightly extended on the treated side **(H,I)** Transverse sections through the control and treated eyes respectively at the level of the dotted lines in F,G. Arrow shows ectopic induction of *Tbx5* expression in the RPE. (arrows). Scale bars: 0.5 mm in A-G, 0.1 mm in H,I.

Abbreviations: D, dorsal; L, lens; N, nasal; NR, neural retina; RPE, retinal pigmented epithelium; T, temporal, V, ventral.

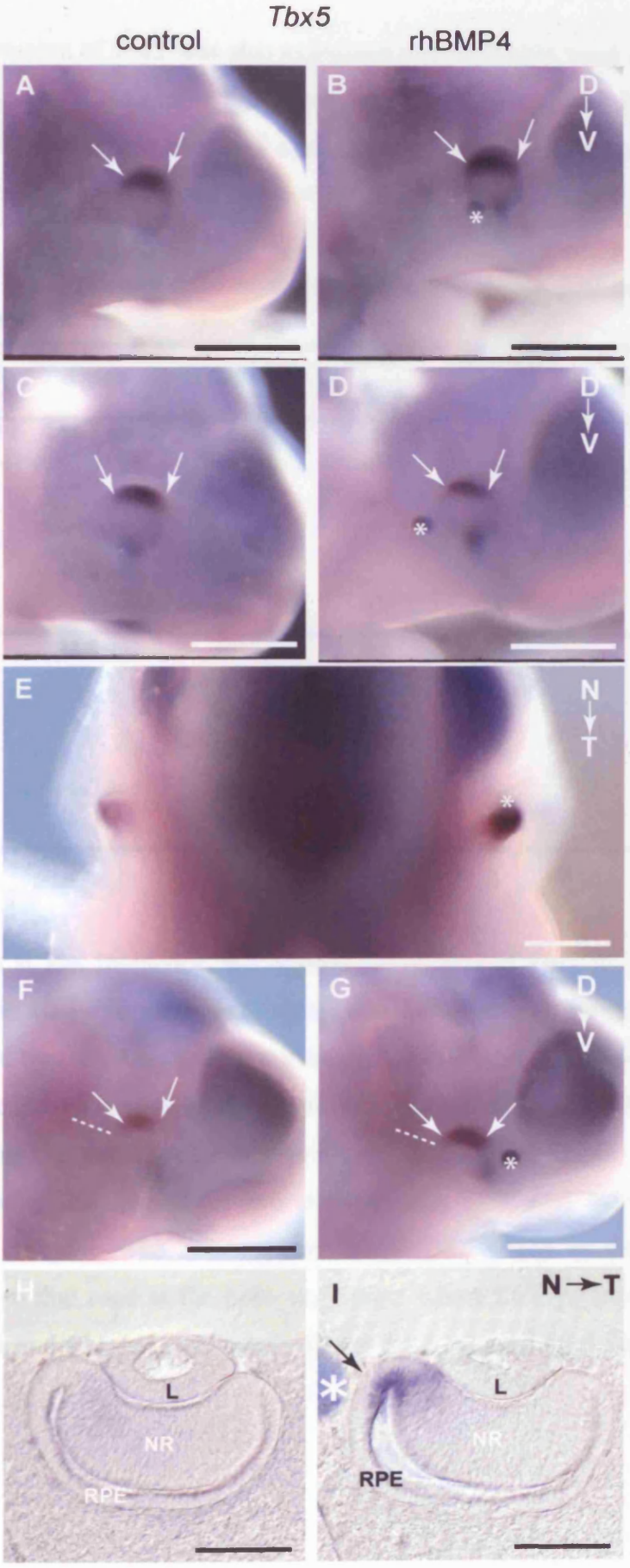
Tbx5
control
rhBMP4
A
B
D
V
C
D
D
V
E
N
T
F
G
D
V
H
L
NR
RPE
I
N→T
L
NR
RPE

The expression of *Tbx2* was also examined after rhBMP4 bead implantation dorsal to the optic vesicle. In one out of three embryos the bead was found proximal to the optic cup after culture and *Tbx2* expression was extended ventrally in comparison to the non-treated contralateral eye (n= 1/3; Fig. 4.7 A-H; Table 4.2).

Table 4.2 Summary of the number of embryos that showed gene expression alterations upon rhBMP4 treatment

Protein	Stage	Gene	Gene expression altered	No change in gene expression	Total	Ratio
rhBMP4	11.5 dpc	*Tbx5*	10	2	12	10/12
		Tbx2	6	0	6	6/6
		Tbx3	3	0	3	3/3
		Vax2	4	0	4	4/4
	10.5 dpc	*Tbx5*	3	5	8	3/8
		Tbx2	1	2	3	1/3
BSA	11.5 dpc	*Tbx5*	0	5	5	0/5
		Tbx2	0	6	6	0/6
		Tbx3	0	1	1	0/1
		Vax2	0	6	6	0/6
	10.5 dpc	*Tbx5*	0	2	2	0/2
		Tbx2	0	2	2	0/2

Although at low incidence, the ectopic expression of *Tbx2* in 1/3 eyes, and *Tbx5* in 3/8 eyes in 10.5 dpc embryos suggests that T-box gene expression is also likely to be controlled by Bmp4 signalling during optic vesicle invagination. The variable effect on gene expression may be due to the reduced ability of rhBMP4 to reach the neural retina from the extra-ocular mesenchyme. The morphogenetic movements that take place during this period in eye development may also have contributed to the variable outcome. The concentration of rhBMP4 used in these experiments was identical to that used at the optic cup stage, where D-V patterning was successfully disrupted, and a higher concentration may have induced more reproducible changes.

Fig. 4.7 *Tbx2* expression upon rhBMP4 bead implantation prior to optic vesicle invagination (early 10.5 dpc)

Gene expression was detected by whole mount *in situ* hybridisation. Location of bead is marked by asterisk. The D-V axis, as indicated, refers to the orientation of A and B, while the indicated N-T axis shows the orientation in C-H **(A)** Lateral view of a non-treated control eye of a cultured embryo showing *Tbx2* expression. **(B)** Lateral view of the contralateral eye of the one in shown in A with an rhBMP4 bead implanted proximal to the optic cup (asterisk). Wider *Tbx2* expression was observed. **(C-H)** Serial transverse vibratome sections of each eye. Sections start from the dorsal region of the eye displayed at the top of each row (C,D) and continue serially to the ventral region of each eye, displayed at the bottom of each row (G,H). *Tbx2* expression was stronger in the dorsal neural retina and reached further ventrally in the rhBMP4 treated eye. Scale bars: 0.5 mm in A,B; 0.1 mm in C-H.

Abbreviations: D, dorsal; L, lens; MN, mandibular process of the first branchial arch; MX, maxillary process of the first branchial arch; N, nasal; NP, nasal process; NR, neural retina; OS, optic stalk; T, temporal; V, ventral

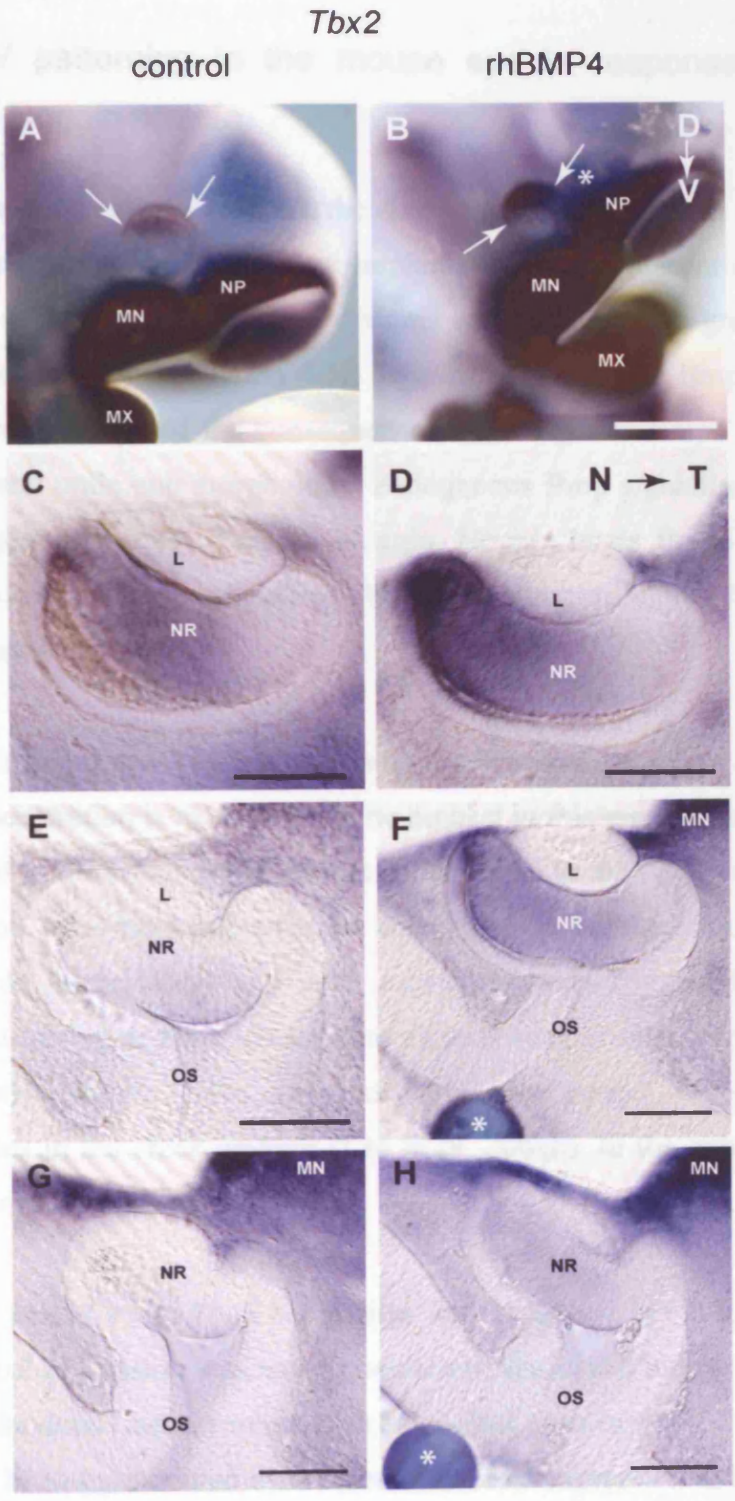
Tbx2
control
rhBMP4
A
NP
MN
MX
B
D
V
NP
MN
MX
C
L
NR
D
N → T
L
NR
E
L
NR
OS
F
MN
L
NR
OS
G
MN
NR
OS
H
MN
NR
OS

4.2.3 D-V patterning in the mouse eye in response to an ectopic source of Noggin protein

As mentioned in previous sections, the change in gene expression along the D-V axis of the optic cup upon rhBMP4 bead implantation is reminiscent of changes in gene expression during manipulations of systems where morphogen gradient models have been proposed (see introduction 4.1). To further investigate Bmp4 regulation of T-box gene expression and the consequences of changes in Bmp4 signalling on D-V patterning and optic cup morphology, endogenous Bmp signalling was manipulated by an exogenous source of mouse Noggin. Noggin binds Bmp4 with high affinity and antagonises Bmp4 signalling by preventing receptor ligand interactions (Zimmerman *et al.* 1996).

As *Bmp4* is expressed in the dorsal neural retina and therefore endogenous Bmp4 protein concentration is most likely to be highest in this region, Noggin soaked beads were placed in the extra-ocular mesenchyme dorsal to the optic vesicle of early 10.5 dpc embryos. After bead implantation, embryos were cultured through the process of optic vesicle invagination and gene expression was compared between Noggin treated, non-treated or BSA treated contralateral eyes in each embryo. Beads soaked in [1mg/ml] Noggin have previously been reported to cause craniofacial abnormalities in the chick embryo (Lee *et al.* 2001b). In the experiments described here, Noggin was used at [1mg/ml].

In Noggin treated eyes, *Tbx5* expression was abolished (n= 6/6; Fig. 4.8 A,B). In contrast *Tbx2* expression was never completely abolished, but restricted to a smaller region of the dorsal neural retina than in control eyes (n= 4/4; Fig. 4.8 C,D). *Tbx2* expression in Noggin treated eyes resembled *Tbx5* expression in D1 in non-cultured embryos of the same age (Fig. 4.8 A,D), much in the same way *Tbx5* expression resembled normal *Tbx2* expression in rhBMP4 treated optic cups (Section 4.2.2, Fig. 4.4 B and C). No changes were observed in the expression of either *Tbx2* or *Tbx5* in BSA treated eyes (n= 0/4; Fig. 4.8 E-H) or non-treated control eyes in cultured embryos (n= 0/14).

Fig. 4.8 T-box gene expression upon Noggin bead implantation prior to optic vesicle invagination (early 10.5 dpc)

Gene expression was detected by whole mount *in situ* hybridisation. Location of bead is marked by asterisk. Pictures show lateral views of the head of embryos. **(A)** A non-treated control eye of a cultured embryo showing the expression of *Tbx5* in the dorsal optic cup (arrows). **(B)** The Noggin treated eye of the embryo in A, showing absence of *Tbx5* expression in the optic cup. Arrows are replicas of those in A, highlighting the area where *Tbx5* would be normally expressed. **(C)** Non-treated control eye of a cultured embryo hybridised with the *Tbx2* probe. *Tbx2* expression in the eye is marked by arrows. **(D)** Noggin treated eye of the embryo in C, showing reduced expression of *Tbx2* within the dorsal optic cup (arrows). **(E,F)** Non-treated and BSA treated eyes respectively of a cultured embryo hybridised with the *Tbx5* probe. **(G-H)** Non-treated and BSA treated eyes respectively of a cultured embryo, showing *Tbx2* expression. **(I)** Schematic representation of normal *Tbx2*, *Tbx5* and *Vax2* expression in a lateral view of the optic cup. **(J)** Schematic representation of the observed dorsal shift of T-box gene expression upon Noggin bead implantation in the dorsal extra-ocular mesenchyme. Scale bars: 0.5 mm.

Abbreviations: D, dorsal; MN, mandibular process of the first branchial arch; MX, maxillary process of the first branchial arch; NP, nasal process; V, ventral

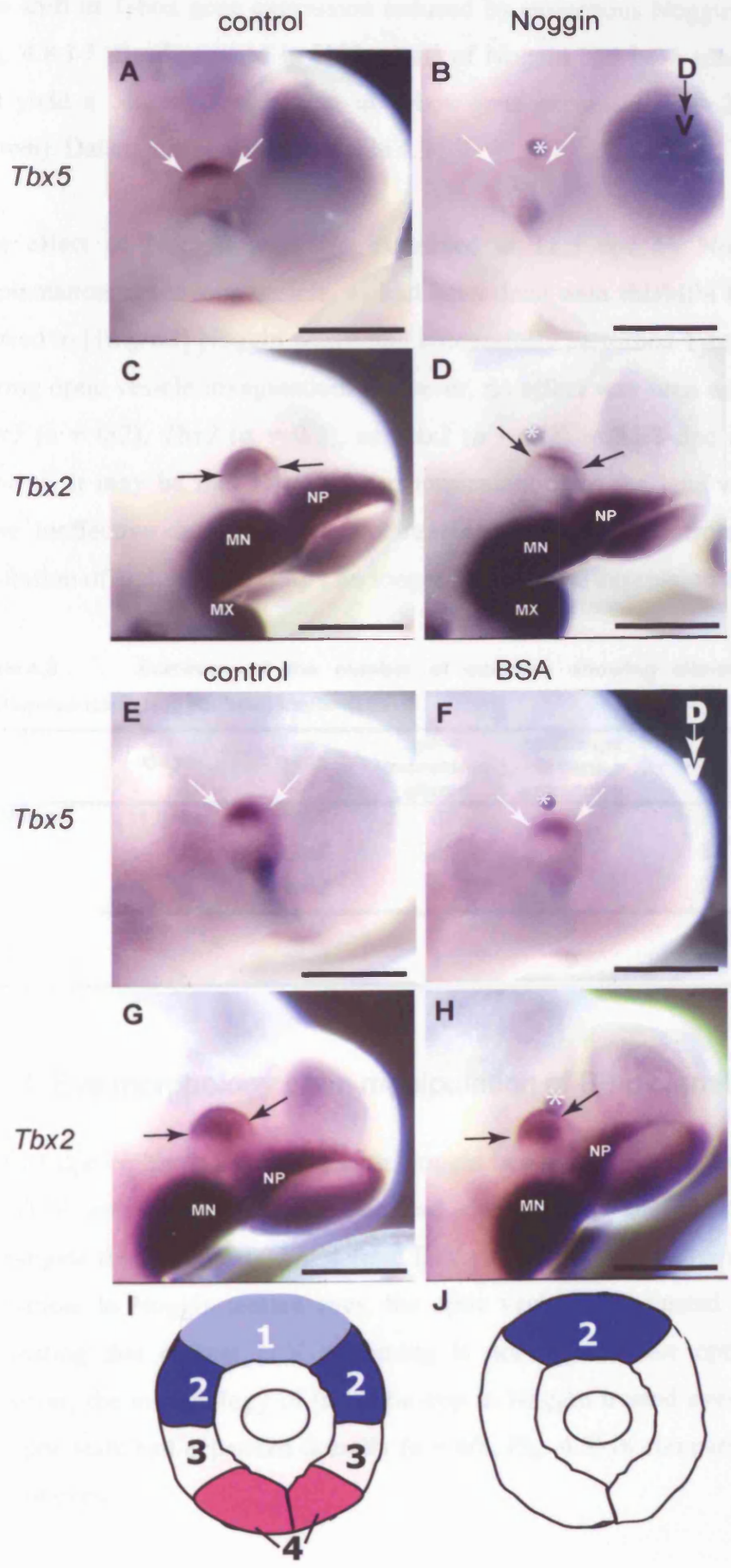
control
Noggin
A
B
D
Tbx5
C
D
Tbx2
NP
MN
MX
control
BSA
E
F
D
Tbx5
G
H
Tbx2
NP
MN
I
J
1
2
2
3
3
4
2

The shift in T-box gene expression induced by exogenous Noggin is summarised in Fig. 4.8 I-J. Beads soaked in [100ug/ml] of Noggin had been tried initially, but did not yield a consistent reduction in T-box gene expression (n= 2/6 *Tbx5*; data not shown). Data is summarised in Table 4.3

The effect of Noggin was also examined at 11.5 dpc by Noggin coated bead implantation in the lens vesicle, as had been done with rhBMP4 beads. Beads were soaked in [1mg/ml] Noggin which had successfully perturbed T-box gene expression during optic vesicle invagination. However, no effect was seen on the expression of *Tbx5* (n = 0/2), *Tbx2* (n = 0/3), or *Vax2* (n = 0/2) in 11.5 dpc embryos (data not shown). It may be that Noggin bead implantations in the lens vesicle at 11.5 dpc were ineffective due to Noggin not reaching the optic cup from the lens, or that inhibition of endogenous Bmp4 no longer affects gene expression at this stage.

Table 4.3 Summary of the number of embryos showing alteration in T-box gene expression upon Noggin bead implantation

	stage	gene	gene expression altered	no change in gene expression	Total	Ratio
Noggin	11.5 dpc	*Tbx5*	0	2	2	0/2
		Tbx2	0	3	3	0/3
		Vax2	0	2	2	0/2
	10.5 dpc	*Tbx5*	6	0	6	6/6
		Tbx2	4	0	4	4/4

4.2.4 Eye morphology upon manipulation of Bmp signalling

In 10.5 dpc embryos implanted with Noggin beads, as T-box gene expression along the D–V axis of the neural retina had clearly been altered, it was possible to investigate the hypothesis that normal D-V patterning may be required for optic cup formation. In Noggin treated eyes, the optic vesicle invaginated into an optic cup, suggesting that correct D-V patterning is not required for optic cup formation. However, the morphology of the optic cup in Noggin treated eyes was abnormal as the optic stalk had expanded dorsally (n = 6/8, Fig. 4.9) in comparison to non-treated control eyes.

Fig. 4.9 Morphology of the ventral optic cup and stalk upon Noggin bead implantation prior to optic vesicle invagination (early 10.5 dpc)

Images in each column show serial vibratome sections through the transverse plane of a Noggin treated eye **(A-D)** and its contralateral control **(E-H)** in an embryo cultured through the optic cup invagination process. The ventral most sections obtained from each eye are at the bottom of the columns and the consecutive sections placed in order towards the top of each column. Each row shows equivalent sections through the treated and the non treated eyes. Pictures were acquired as described previously, but were converted to black and white due to aesthetic reasons as embryo was sectioned after an unsuccessful *in situ* hybridisation experiment. In the Noggin treated eye, optic cup invagination (arrows) and retinal thickening is observed in section **A** but not further ventrally **(B-D)**, while in the control eye, invagination of the cup has advanced further ventrally and is observed in sections **E** and **F** (arrows). Compare eye morphology in B versus F. Scale bars: 0.1 mm.

Abbreviations: D, dorsal; NR, neural retina; OS, optic stalk, V; ventral

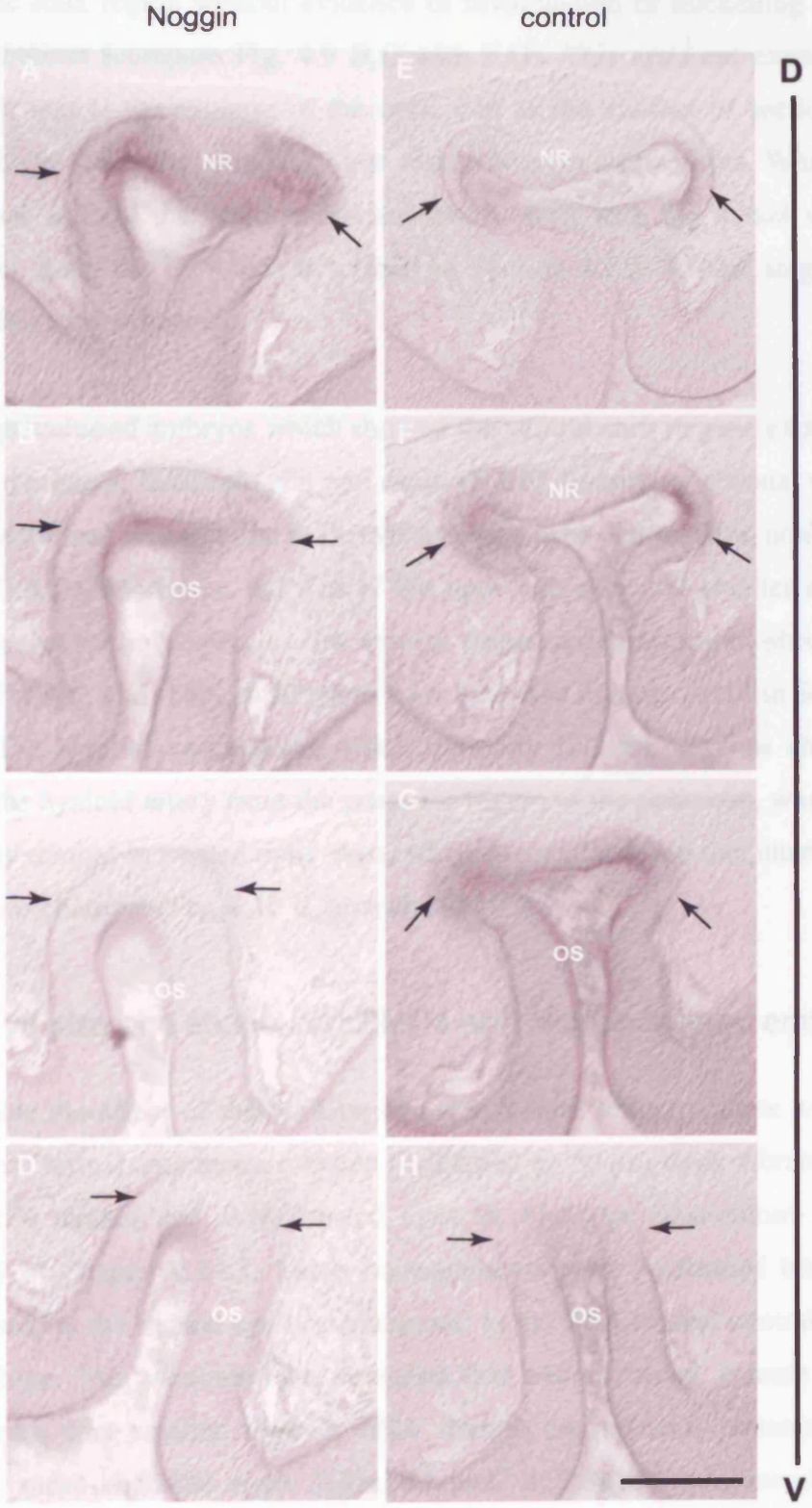
Noggin
control
A
NR
E
NR
D
B
OS
F
NR
C
OS
G
OS
D
OS
H
OS

Based on the thickness of the sections (50 μm), from which eye morphology was analysed in these embryos, the Noggin treated eyes contained between 50-100 μm extra optic stalk region without evidence of invagination or thickening of the distal neuroepithelium (compare Fig. 4.9 B,C with F,G). This apparent expansion of the optic stalk was at the expense of the optic cup as the number of sections obtained from each eye was either similar or one less in Noggin treated eyes. What appears to be a dorsal shift of the optic stalk corresponds well with the dorsal shift of gene expression along the D-V axis described in Section 4.2.3. At this stage no further abnormalities were detected.

In 11.5 dpc cultured embryos which showed the ventral shift in gene expression upon rhBMP4 treatment, haemotoxylin and eosin (H&E) staining of coronal wax sections revealed a thinner neural retina in rhBMP4 treated eyes compared to non-treated eyes (Fig. 4.10 A,B). Moreover, the size of the optic cup appeared smaller and its shape altered in the ventral aspect as the ventral neural retina appeared shorter and less curved. The size and shape differences were analysed in more detail in Sections 4.2.5 - 4.2.6. The hyaloid vasculature, which normally fills the vitreous chamber upon entry of the hyaloid artery from the posterior region of the optic cup, was present and apparently normal in treated optic cups, where it extended into the anterior region of the vitreous chamber (Fig. 4.10 B, arrowheads).

4.2.5 Eye size and shape in rhBMP4 and Noggin treated embryos

To examine the effect of rhBMP4 on eye size, neural retinal volume was estimated from neural retinal area measurements performed on 50 μm thick vibratome sections of rhBMP4 treated and BSA treated eyes in 11.5 dpc post-culture embryos as described in Chapter 2.11.1. These measurements were performed blind and they were paired, as the treated eye was compared to the BSA treated contralateral eye in each embryo. The measurements revealed that neural retinal volume in rhBMP4 treated eyes was smaller than in BSA treated contralateral counterparts (n= 4 embryos; mean rhBMP4 eye= 7.35×10^{-3} mm^3 $\pm$ 2.3×10^{-3} s.d.; mean BSA eye= 10.90×10^{-3} mm^3 $\pm$ 1.95×10^{-3} s.d.; P= 0.033 by paired t-test; Fig. 4.10 C).

Fig. 4.10 Eye morphology and size in rhBMP4 treated optic cups

(A,B) H&E stained coronal wax sections (7μm) of rhBMP4 treated and contralateral non-treated control eyes, as indicated, after overnight culture of 11.5 dpc embryos. rhBMP4 bead implantation in the lens vesicle resulted in a thinner retinal morphology, an overall smaller eye size, and altered the shape of the cup most apparent in the ventral region. The hyaloid vasculature appeared normal in the treated eye as it had extended into anterior regions of the cup (arrowheads). Asterisk marks the bead. **(C)** Bar chart represents estimated mean retinal volume ± s.d. in rhBMP4 treated and BSA treated eyes. The P-value was calculated with the paired t-test. Retinal volumes were measured on 50 μm vibratome sections. Scale bars: 50 μm.

Abbreviations: BSA, bovine serum albumin; D, dorsal; V, ventral.

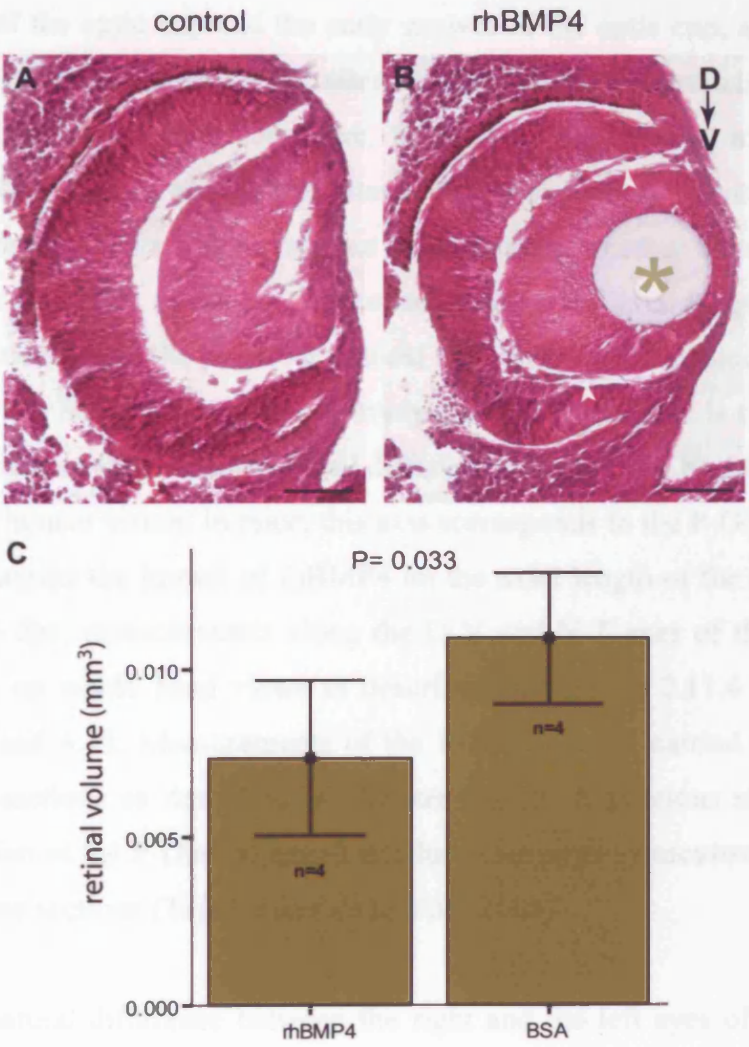
control
rhBMP4
A
B
D
V
C
P= 0.033
retinal volume (mm³)
0.010
0.005
0.000
n=4
n=4
rhBMP4
BSA

The relationship between the shape of the embryonic and the adult eye is not well established. However, the idea that early embryonic events, particularly during the formation of the optic cup and the early growth of the optic cup, affect the shape of the mature eye is plausible. Few studies have attempted a quantitative analysis of the shape and size of the embryonic eye. In view of the changes in gene expression across the D-V axis in response to altered Bmp4 signalling, quantitative analysis of treated embryonic eyes was carried out to investigate whether there was evidence of a change in the shape of the eye. In human patients, the axial length of the adult eye globe, measured from the posterior corneal surface to the inner limiting membrane of retina or to the RPE, is a measure of myopia or hyperopia, and is correlated with the refractive error of the eye. Even small differences in the axial length and shape of the eye impact human vision. In mice, this axis corresponds to the P-D axis of the eye. In order to examine the impact of rhBMP4 on the axial length of the embryonic mouse eye at 11.5 dpc, measurements along the D-V and N-T axes of the optic cup were carried out on whole head views as described in Chapter 2.11.4 and illustrated in Figs. 4.11 and 4.12. Measurements of the P-D axes were carried out on transverse vibratome sections as described in Chapter 2.11.5. A previous study has reported quantification of the P-D axial length in adult mice eyes by measurements performed on transverse sections (Tejedor and de la Villa 2003).

First, the natural difference between the right and the left eyes of cultured, but not treated embryos, was examined to determine the extent of natural variation and to control for any impact of the embryo culture procedure on the difference found between two eyes of an embryo. No significant difference was found in this group, suggesting that there is no significant natural variation in D-V axial length between the left and right eyes in non-treated but cultured 11.5 dpc embryos (Fig. 4.11 A, Table 4.4). In rhBMP4 treated eyes however, the D-V axis was significantly smaller than in contralateral non-treated eyes (Fig. 4.11 B, Table 4.4). In embryos with a BSA coated bead in one eye and no bead in the contralateral eye, the variation in eye size was not found to be significant (Fig. 4.11 C, Table 4.4).

Fig. 4.11 D-V axial length in non-treated and rhBMP4 treated eyes in 11.5 dpc cultured embryos

P-values were calculated with the paired t-test with the raw data set for pairs of eyes. Scatter plots illustrate the percentage difference in D-V axial length between the two eyes in each embryo, calculated as described in Section 4.3.5. **(A)** Difference between left and right eyes in cultured but not treated embryos, representing the natural variation between eyes. **(B)** Difference between rhBMP4 treated and non-treated control eyes in cultured embryos. In all cases, the rhBMP4 eye was smaller than the contralateral non-treated eye. **(C)** Difference between BSA treated and non-treated control eyes in cultured embryos. BSA treated eyes were sometimes smaller and sometimes bigger than their contralateral non-treated counterparts.

Abbreviations: BSA, bovine serum albumin

A
% difference in D-V axial length
-30
-20
-10
0
10
20
30
1
2
3
4
5
6
7
8
9
10
Embryo
non-implanted control
P= 0.108
n= 10
B
% difference in D-V axial length
-30
-20
-10
0
10
20
30
1
4
7
10
13
16
19
22
25
Embryo
rhBMP4
P< 0.0001
n= 25
C
% difference in D-V axial length
-30
-20
-10
0
10
20
30
1
2
3
4
5
6
7
8
Embryo
BSA control
P= 0.07
n= 8

Table 4.4: Percentage difference in eye size between differentially treated pairs of eyes in 11.5 dpc post-culture embryos and P-values by the paired t-test

	Treatment Group	n.	Mean percentage difference ± 1.s.d.	P-value
D-V axial length	none	10	98.1% ± 3.50	0.108
	rhBMP4	25	92.33% ± 3.83	<0.0001
	BSA	8	95.26% ± 7.77	0.07
	Noggin	6	99.97% ± 0.10	0.436
N-T axial length	none	10	99.97% ± 2.92	1
	rhBMP4	25	96.66% ± 4.93	0.001
	BSA	8	97.87% ± 3.50	0.147
	Noggin	6	99.95% ± 0.07	0.133

Although the difference in the D-V axial length in BSA treated embryos was not significant, there appeared to be several embryos that showed similar differences to those detected in rhBMP4 embryos, and because the rhBMP4 treated group was larger than the BSA treated group, it was important to investigate whether a significant difference would be found if the groups were equal in number. Therefore, the rhBMP4 treated group was randomly reduced to eight specimens to match the BSA treated group in the number of observations, and the data was again analysed by the paired t-test and unlike the BSA treated group, was found to be significantly different with n= 8 (P= 0.002).

Comparison of the N-T axial length in a similar manner in cultured embryos revealed no significant naturally occurring differences between left and right eyes of non-treated but cultured embryos (Fig. 4.12 A, Table 4.4). However, significant differences were found along the N-T axis between rhBMP4 treated and non-treated eyes (Fig. 4.12 B, Table 4.4). Eyes implanted with BSA coated beads showed no significant change in the N-T axis compared to non-treated contralateral eyes (Fig. 4.12 C, Table 4.4). In comparison to the difference in D-V axial length, a decrease in N-T axial length in rhBMP4 treated eyes was less frequently observed as not all rhBMP4 treated eyes exhibited a smaller N-T axis, whereas all eyes examined showed a smaller D-V axial length.

Fig. 4.12 N-T axial length of in non-treated and rhBMP4 treated eyes in 11.5 dpc cultured embryos

P-values were calculated with the paired t-test with the raw data set for pairs of eyes. Scatter plots illustrate the percentage difference in N-T axial length between two eyes in each embryo, calculated as described in Section 4.3.5. **(A)** Difference between left and right eyes in cultured but not treated embryos, representing the natural variation between eyes. **(B)** Difference between rhBMP4 treated and non-treated control eyes in cultured embryos. In majority of embryos, the rhBMP4 eye was smaller than the contralateral non-treated eye, with the overall difference being significant between the two groups. **(C)** Difference between BSA treated and non-treated control eyes in cultured embryos. BSA treated eyes showed less variation than rhBMPP4 treated eyes.

Abbreviations: BSA, bovine serum albumin

A
% difference in N-T axial length
-30
-20
-10
0
10
20
30
1
2
3
4
5
6
7
8
9
10
Embryo
non-implanted control
P= 1
n= 10
B
% difference in N-T axial length
-30
-20
-10
0
10
20
30
1
4
7
10
13
16
19
22
25
Embryo
rhBMP4
P= 0.001
n= 25
C
% difference in N-T axial length
-30
-20
-10
0
10
20
30
1
2
3
4
5
6
7
8
Embryo
BSA control
P= 0.147
n= 8

Comparisons were also made between eyes implanted with a Noggin coated bead in the lens vesicle in 11.5 dpc post-culture embryos, in which gene expression changes were not observed (see Table 4.3), and their contralateral non-treated eyes. No significant differences were found between Noggin treated eyes and their contralateral non-treated counterparts in either the D-V or the N-T axes, again supporting the conclusion that changes in axial length were associated with changes in gene expression and not bead implantation alone (Fig. 4.13, Table 4.4).

P-Di axial length measurements were performed on serial vibratome sections through the entire optic cup in four embryos implanted with an rhBMP4 bead in one eye and a BSA bead in the contralateral eye as described in Chapter 2.11.5. When all values were plotted against the position of the section per eye, the plots revealed the relative shape of the eye along the P-Di axis, which in agreement with previous observations on sections, appeared altered in rhBMP4 treated eyes in comparison to BSA treated contralateral eyes (Fig. 4.14 A,B). In particular, this graph demonstrated that the ventral region of the optic cup was especially affected, appearing shorter, hence altering the shape of the optic cup. This was also frequently observed in embryos where one eye was treated with rhBMP4 and the other kept as a non-treated control (Fig. 4.14 C,D).

Together, these data show that addition of exogenous rhBMP4 to the newly formed optic cup reduces eye size (neural retinal volume) and the eye's D-V and N-T axial lengths while altering the P-Di axial length in the ventral region of the eye, thus inducing a change in size and shape of the optic cup.

Fig. 4.13 D-V and N-T axial length in Noggin treated and control eyes in 11.5 dpc cultured embryos

Scatter plots represent the percentage difference in axial length calculated as described in Section 4.3.5. P-values were calculated with the paired t-test with the raw data set for pairs of eyes. **(A)** Difference in D-V axial length in Noggin treated and contralateral non-treated eyes in embryos (n= 6) represented by yellow squares. **(B)** Yellow diagonal squares show the percentage difference in N-T axial length between Noggin treated and contralateral non-treated eyes.

A
% difference in D-V axial length
-0.30
-0.20
-0.10
0.00
0.10
0.20
0.30
1
2
3
4
5
6
Embryo
D-V axis
P= 0.436
B
% difference in N-T axial length
-0.30
-0.20
-0.10
0.00
0.10
0.20
0.30
1
2
3
4
5
6
Embryo
N-T axis
P= 0.133

Fig. 4.14 Representation of P-Di axial measurements in rhBMP4 treated and BSA treated eyes in 11.5 dpc post-culture embryos

(A) Schematic drawing of a coronal section through the eye with orientations as indicated. Dotted lines indicate levels of serial transverse sections corresponding to the x-axis on the graph in B. The P-Di axis (arrow in A) was measured on each transverse vibratome section (50 μm) through the eye. **(B)** Graph shows mean P-Di axial length ± 1 s.d. for four eyes starting from the dorsal most section (x= 1) to the ventral most section obtained from each eye. Note that the number of sections obtained from rhBMP4 treated eyes is less than BSA treated contralateral eyes in all embryos (5 versus 6). **(C-D)** Coronal frozen sections (12 μm) stained with propidium iodide showing the non-treated and the contralateral rhBMP4 treated eyes in a cultured embryo. The ventral region (marked by dotted lines) of the rhBMP4 treated optic cup (D) is shorter and has an altered shape compared to the contralateral non treated eye (C). Scale bars: 0.1 mm

Abbreviations: P-Di, proximo-distal

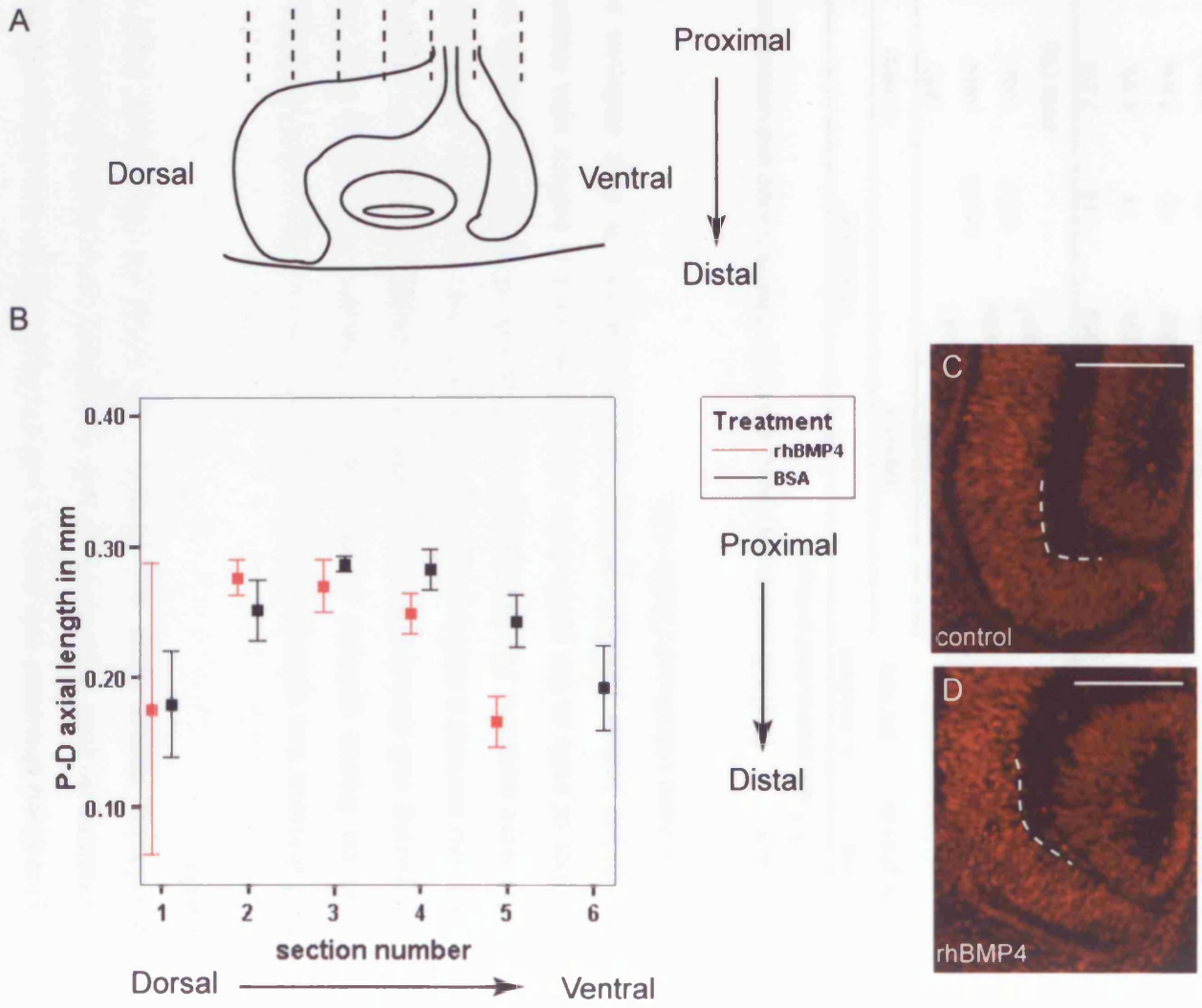
A
Proximal
Dorsal
Ventral
Distal
B
0.40
0.30
0.20
0.10
P-D axial length in mm
1
2
3
4
5
6
section number
Dorsal
Ventral
Treatment
rhBMP4
BSA
Proximal
Distal
C
control
D
rhBMP4

4.2.6 Cell division in rhBMP4 treated eyes

To investigate the mechanisms that may underlie the observed alteration in eye size and shape in rhBMP4 treated optic cups, cell division and apoptotic cell death were examined in rhBMP4 treated and contralateral non-treated neural retinae in 11.5 dpc cultured embryos. Specifically, this study investigated the possibility that regionalised abnormal cell death or cell division may be associated with the observed alterations in gene expression. A role in regional control of cell proliferation in the developing mouse heart was recently discovered for *Tbx20* and *Tbx2* (Cai *et al.* 2005).

Cell division was detected by phospho-Ser10-histone H3 (pH3) labelling of mitotic cells on frozen sections as described in Chapter 2.8.1 (Fig. 4.15 A,B). When comparing cell division between different treatment groups, it is important to also take into account a measure that correlates with the size of the area in which mitotic cells were counted. For this purpose, the number of pH3 positive cells and the total number of cells in the retina were counted and retinal surface area measured in 3-4 propidium iodide labelled midline sections per eye in four embryos and mitotic indices were calculated (Table 4.5).

Table. 4.5: Total cell number and mitotic indices in rhBMP4 treated and contralateral non-treated eyes in 11.5 dpc post-culture embryos

Embryo post(pre) ss	n. sections per eye	Treatment					
		rhBMP4			Control		
		n.pH3 cells	pH3 cells/ total cells (%)	pH3 cells/ mm^2	n.pH3 cells	pH3 cells/ total cells (%)	pH3 cells/ mm^2
1. 48(40) ss	4	70	4.6%	556	118	7.2%	879
2. 52(42) ss	3	36	2.0%	294	74	4.5%	598
3. 50(42) ss	4	37	2.1%	268	45	2.6%	315
4. 48(42) ss	4	34	1.5%	227	42	1.8%	295

ss, somite stage. The somite stage of each embryo, pre-culture is given in brackets, and post-culture outside of the brackets.

All data analysed in this section were Ln transformed to acquire normal distribution and normality was checked as described in Chapters 2.12.1-2. First the difference in the number of pH3 positive cells between rhBMP4 treated and contralateral non-treated eyes were analysed with a Two-Way ANOVA test, which allows the comparison of the paired data within groups (rhBMP4 treated and non-treated contralateral), and also compares the data between embryos and therefore takes into account that data is collected from different embryos, as there was variability in the number of pH3 positive cells between embryos (Fig. 4.15 C; Table 4.5 and 4.6; n= 30 sections in 4 embryos, P= 0.003). The ANOVA table suggested that there is a significant difference between the treatment groups (P= 0.003) and also highlighted the variability between embryos (Table 4.6; P= 0.004). The between embryo variability was also evident in the mitotic indices (Table 4.5) and could be due to a number of potential differences between embryos including differential uptake and release of rhBMP4 protein by implanted beads and differences in somite stages and litters.

In each embryo the number of pH3 cells per total retinal cells or per mm^2 in the rhBMP4 treated eye was lower than in the contralateral non-treated eye (Table 4.5; Fig. 4.15 D) suggesting that there is less cell division in rhBMP4 treated eyes. The total number of cells in each section, or the retinal surface area, was incorporated as a co-variate into the Two-Way ANOVA which analysed the per section data and distinguished between embryos, and the mitotic indices were hence analysed with an ANCOVA to test for the effect of the area counted on the number of pH3 labelled cells. The ANCOVA Table 4.7 suggests that the total number of cells per section had no significant effect on the number of observed mitotic cells (P= 0.966). When the effect of total cell number was adjusted for with the ANCOVA test, the effect of rhBMP4 treatment was still significant (P= 0.005; Table 4.7). The same result was obtained with Ln surface area as a covariate (P= 0.005; data not shown). These analyses show that cell division was reduced in rhBMP4 treated eyes compared to non-treated contralateral eyes. Analysis of the number of pH3 labelled cells was also undertaken in a larger data set consisting of mitotic cell counts from 112 sections in five embryos, and further supported this conclusion (Fig. 4.16; Tables 4.8 and 4.9; Two-Way ANOVA P<0.001). In this analysis, all intact sections obtained from each eye were included and as such the number of sections counted per eye varied

Fig. 4.15 Cell division in rhBMP4 treated and control eyes

(A) Frozen section through the coronal plane of a non-treated control eye in a cultured embryo, showing mitotic cells at the ventricular edge of the neural retina by pH3 immuno-labelling (green) and counterstained with propidium iodide (red). **(B)** Approximately equivalent section of an rhBMP4 treated eye, contralateral to the eye in A counterstained with propidium iodide (red). pH3 labelled cells (green) were detected on the ventricular edge of the neural retina in sparser numbers. **(C)** Scatter plot of Ln transformed number of pH3 labelled cells per section per eye as indicated, in four embryos. P-value is for the between treatment groups comparison and was calculated by the Two-Way ANOVA test. **(D)** Scatter plot of Ln transformed mitotic indices per section per eye. P-value calculated by ANCOVA, with the number of cells per section incorporated as a covariate and the number of pH3 cells as the main variable.

Abbreviations: D, dorsal; L, lens; NR, neural retina; V, ventral

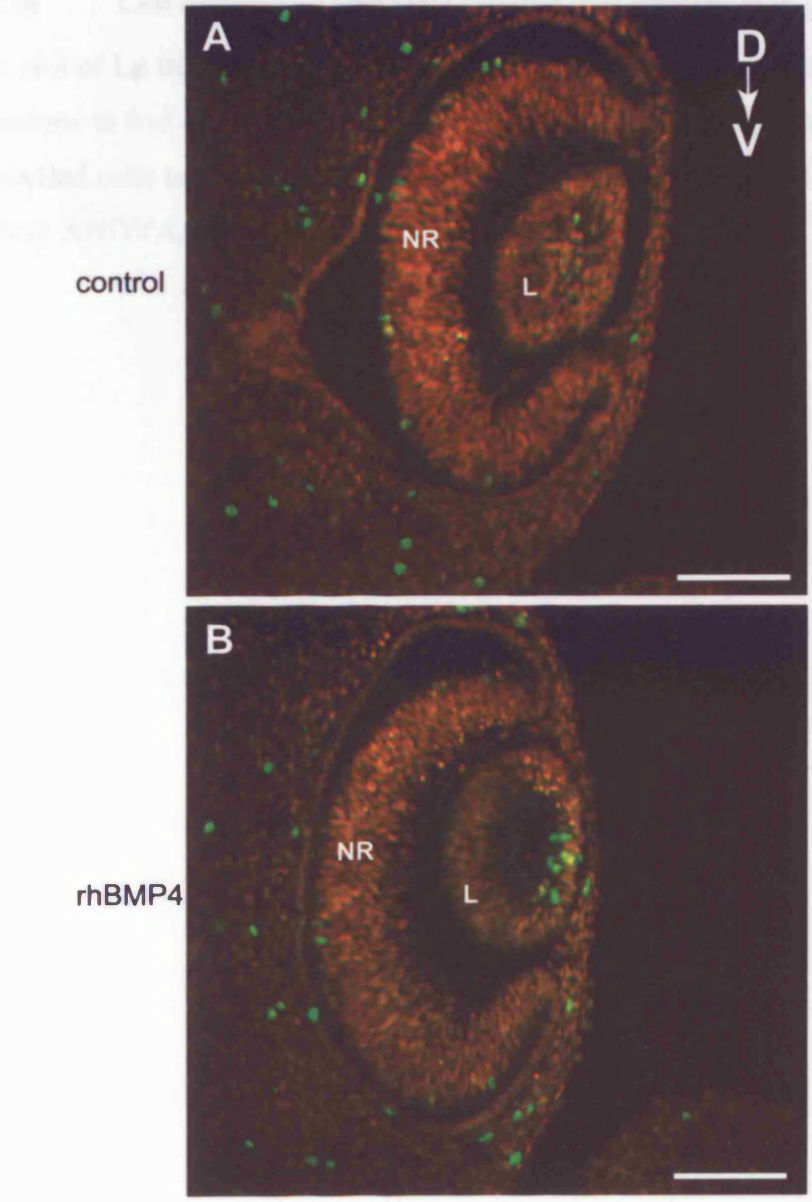
A
D
V
NR
L
control
B
NR
L
rhBMP4

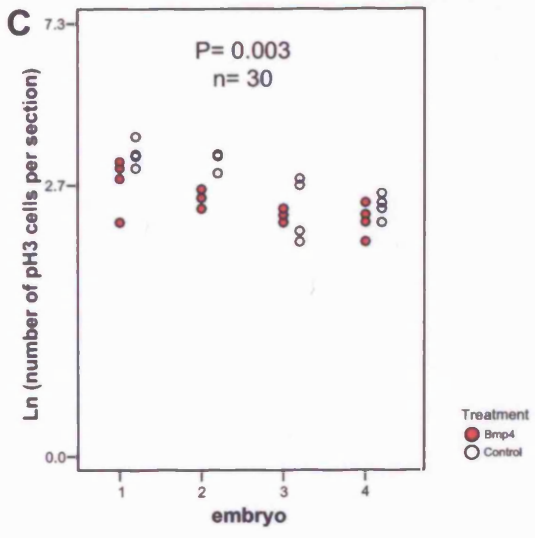
C
P= 0.003
n= 30
Ln (number of pH3 cells per section)
7.3
2.7
0.0
1
2
3
4
embryo
Treatment
Bmp4
Control

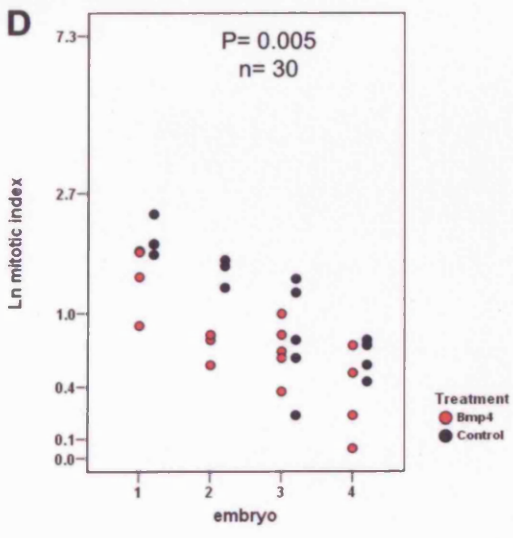
D
P= 0.005
n= 30
Ln mitotic index
7.3
2.7
1.0
0.4
0.1
0.0
1
2
3
4
embryo
Treatment
Bmp4
Control

Fig. 4.16 Cell division in rhBMP4 treated and control eyes (larger data set)

Scatter plot of Ln transformed number of pH3 labelled cells per section in a total of 112 sections in five embryos. rhBMP4 eyes contain significantly smaller number of pH3 labelled cells in comparison to contralateral non-treated control eyes. P-value by Two-Way ANOVA, $P<0.001$

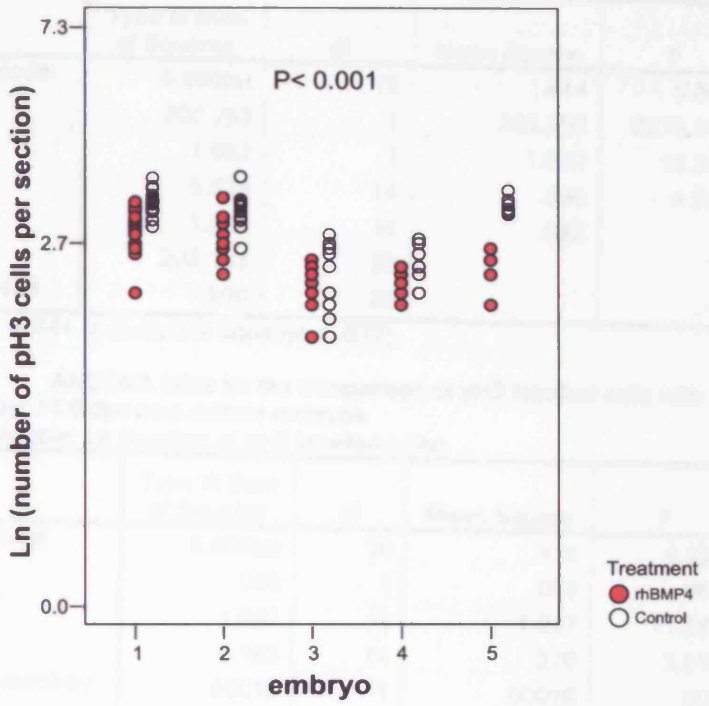
7.3
2.7
0.0
P< 0.001
Ln (number of pH3 cells per section)
1
2
3
4
5
embryo
Treatment
rhBMP4
Control

Table 4.6: Two-way ANOVA table for the comparison of pH3 labelled cells in four 11.5 dpc post-culture embryos

Dependent Variable: Ln (pH3 labelled cells per section)

Source	Type III Sum of Squares	df	Mean Square	F	Sig.
Corrected Model	6.660(a)	15	.444	5.053	.002
Intercept	200.293	1	200.293	2279.534	.000
treatment	1.082	1	1.082	12.311	.003
Sections	5.578	14	.398	4.534	.004
Error	1.230	14	.088		
Total	208.183	30			
Corrected Total	7.890	29			

a R Squared = .844 (Adjusted R Squared = .677)

Table 4.7 ANCOVA table for the comparison of pH3 labelled cells with n.Total cell number as a covariate in four 11.5 dpc post-culture embryos

Dependent Variable: Ln (number of pH3 labelled cells)

Source	Type III Sum of Squares	df	Mean Square	F	Sig.
Corrected Model	6.660(a)	16	.416	4.399	.005
Intercept	.006	1	.006	.063	.806
treatment	1.067	1	1.067	11.281	.005
Sections	5.183	14	.370	3.913	.009
Ln (total cell number)	.00018	1	.00018	.002	.966
Error	1.230	13	.095		
Total	208.183	30			
Corrected Total	7.890	29			

a R Squared = .844 (Adjusted R Squared = .652)

Table 4.8: Total number of pH3 labelled cell counts per eye in rhBMP4 treated and contralateral non-treated eyes in five 11.5 dpc post-culture embryos

Embryo post(pre) ss	n. sections per eye	n. pH3 cells	
		rhBMP4	Control
1. 48(40) ss	18	341	519
2. 52(42) ss	12	199	309
3. 50(42) ss	13	110	133
4. 48(42) ss	7	63	81
5. 48(39) ss	6	64	162
Total	56	777	1,204

ss, somite stage. The somite stage of each embryo, pre-culture is given in brackets, and post-culture outside of the brackets.

Table 4.9: Two-way ANOVA, (larger data set)

Dependent Variable: Ln (pH3 labelled cells per section)

Source	Type III Sum of Squares	df	Mean Square	F	Sig.
Corrected Model	27.093(a)	56	.484	4.577	.000
Intercept	837.917	1	837.917	7926.877	.000
treatment	4.716	1	4.716	44.613	.0001
Sections	22.377	55	.407	3.849	.0001
Error	5.814	55	.106		
Total	870.823	112			
Corrected Total	32.907	111			

a R Squared = .823 (Adjusted R Squared = .643)

The ANCOVA test indicated a significant difference in cell division due to rhBMP4 treatment of eyes, which was corroborated by analysis of pH3 labelled cells in a larger data set. These data were therefore further analysed to investigate whether the reduction in the number of mitotic cells was regional or global along the D-V axis of the neural retina. Sections were divided into dorsal and ventral domains with respect to the boundary of the optic stalk and the normal expression of *Vax2* as illustrated in Fig. 4.17 A. pH3 labelled cells per mm^2 were counted in each region. As division of the neural retina was based upon the morphological boundary of the optic stalk, only sections containing the optic stalk were included in this analysis. The total number of pH3 labelled cells, cells per mm^2, and the number of sections counted per eye for each region are shown in Table 4.10.

Table 4.10 Total number of pH3 labelled cell counts in sections indicated, divided in dorsal and ventral regions per rhBMP4 treated and contralateral non-treated eyes in four 11.5 dpc post-culture embryos

Embryo post(pre) ss	n. sections / eye	Treatment							
		rhBMP4				Control			
		Dorsal		Ventral		Dorsal		Ventral	
		pH3	pH3/mm^2	pH3	pH3/mm^2	pH3	pH3/mm^2	pH3	pH3/mm^2
1. 48(40) ss	6	79	**601**	26	**951**	102	**738**	58	**666**
2. 52(42) ss	3	27	**350**	9	**211**	45	**520**	29	**700**
3. 50(42) ss	9	38	**169**	33	**238**	52	**241**	39	**640**
4. 48(42) ss	4	19	**203**	16	**410**	23	**253**	17	**348**

ss, somite stage. The somite stage of each embryo, pre-culture is given in brackets, and post-culture outside of the brackets.

The number of pH3 labelled cells in dorsal and ventral domains per section were compared separately between embryos by the Two-Way ANOVA test (Fig. 4.17 B-C). The ANOVA tables produced for each region showed that the number of pH3 labelled cells were significantly less in rhBMP4 treated eyes as compared to the non-treated contralateral eyes in both the dorsal and the ventral neural retina (Tables 4.11, 4.12).

Fig. 4.17 Investigation of regional changes in cell division along the D-V axis of the eye in rhBMP4 treated and control eyes

P-values for comparisons between the number of Ln transformed pH3 labelled cells in different treatment groups were calculated by the Two-Way ANOVA test. **(A)** Schematic illustration of the division of the neural retina into dorsal and ventral regions. The dorsal wall of the optic stalk was used as a morphological border. The region of the neural retina above this border was considered as dorsal whereas the region below this border was considered as ventral neural retina. **(B)** Scatter plot of Ln transformed number of pH3 labelled cells in the dorsal neural retina per section per eye in four cultured embryos. The number of pH3 labelled cells in rhBMP4 treated eyes were significantly lower than in contralateral non-treated control eyes. **(C)** Scatter plot of Ln transformed number of pH3 labelled cells in the ventral neural retina of same sections analysed for the dorsal comparison. The number of pH3 labelled cells were also significantly lower in the ventral region of rhBMP4 treated eyes compared to contralateral non-treated eyes.

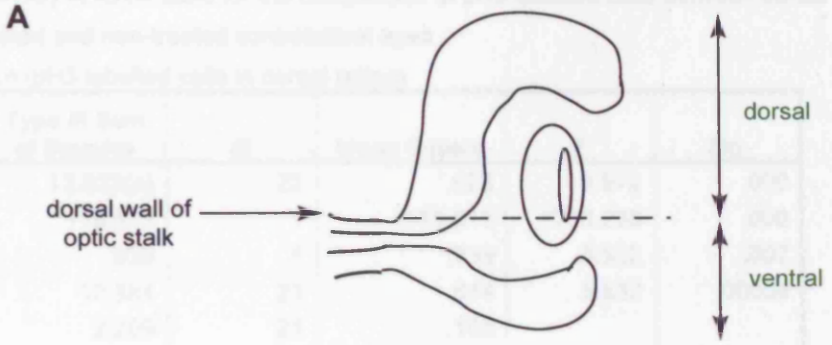
A
dorsal
dorsal wall of
optic stalk
ventral

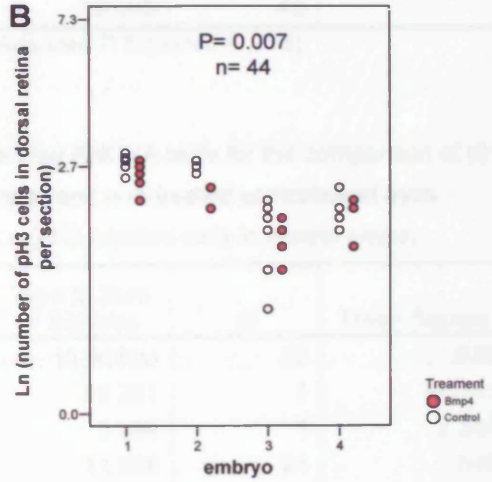
B
P= 0.007
n= 44
Ln (number of pH3 cells in dorsal retina per section)
7.3
2.7
0.0
1
2
3
4
embryo
Treament
Bmp4
Control

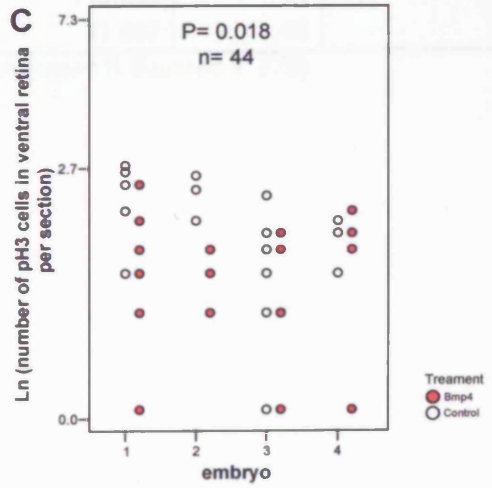
C
P= 0.018
n= 44
Ln (number of pH3 cells in ventral retina per section)
7.3
2.7
0.0
1
2
3
4
embryo
Treament
Bmp4
Control

Table: 4.11 **Two-Way ANOVA table for the comparison of pH3 labelled cells between dorsal regions of rhBMP4 treated and non-treated contralateral eyes**

Dependent Variable: Ln (pH3 labelled cells in dorsal retina)

Source	Type III Sum of Squares	df	Mean Square	F	Sig.
Corrected Model	13.823(a)	22	.628	5.972	.000
Intercept	179.515	1	179.515	1706.238	.000
Treatment	.939	1	.939	8.922	.007
Sections	12.884	21	.614	5.832	.00008
Error	2.209	21	.105		
Total	195.547	44			
Corrected Total	16.033	43			

a R Squared = .862 (Adjusted R Squared = .718)

Table: 4.12 **Two-Way ANOVA table for the comparison of pH3 labelled cells between ventral regions of rhBMP4 treated and non-treated contralateral eyes**

Dependent Variable: Ln (pH3 labelled cells in ventral retina)

Source	Type III Sum of Squares	df	Mean Square	F	Sig.
Corrected Model	13.965(a)	22	.635	1.754	.102
Intercept	86.261	1	86.261	238.300	.000
Treatment	2.384	1	2.384	6.586	.018
Sections	11.528	21	.549	1.516	.174
Error	7.602	21	.362		
Total	110.395	44			
Corrected Total	21.567	43			

a R Squared = .648 (Adjusted R Squared = .278)

These analyses revealed that addition of an exogenous source of BMP4 protein, resulted in a decrease in cell division in the neural retina. This decrease was not regionally restricted but was induced globally along the D-V axis of the neural retina.

4.2.7 Investigation of apoptotic cell death in rhBMP4 treated eyes

As stated in the previous section, apoptosis was analysed in order to investigate factors that may underlie the changes in eye size and shape induced by rhBMP4 treatment, and to investigate whether there are changes in the pattern of apoptosis in these eyes in relation to the changes in gene expression.

During the analysis of cell division, when sections of eyes were counter-stained with propidium iodide, small granular staining, characteristic of apoptotic nuclei were often observed. These granules were mainly seen in the central retina, in the area of the optic disc, in non-treated control eyes, but in rhBMP4 treated eyes, the predominant site of apoptosis appeared to be in the dorsal neural retina (Fig. 4.18 A-D). To verify that these granules were apoptotic cells, the TUNEL assay which labels fragmented DNA by fluorescein tagged dUTP nick-end labelling was used (Chapter 2.9). In non-treated control eyes of 11.5 dpc post-culture embryos, very little TUNEL labelling was detected in the dorsal optic cup, as previously noted with propidium iodide staining (Fig. 4.18 E). In rhBMP4 treated eyes however, increased apoptosis was detected in the dorsal neural retina (Fig. 4.18 F). A high dose of Bmp4 signalling, provided by implantation of beads soaked in a larger amount of rhBMP4 protein than used in experiments described earlier (see Methods 2.6.1), resulted in a more dramatic increase in dorsal apoptosis in rhBMP4 treated eyes in comparison to embryos implanted with the low dose of rhBMP4 (Fig. 4.18 compare F and H). Although increased cell death was also observed in the central and ventral regions of the neural retina, as well as in the anterior region of the lens vesicle, the most dramatic change in cell death was regionally restricted to the dorsal eye, confirming that rhBMP4 treatment can induce a profound regionalised cell death response in the optic cup. Gene expression analysis in previous sections were carried out in embryos treated with the low dose, which triggered a milder apoptotic response.

Fig. 4.18 Pattern of cell death in rhBMP4 treated and control eyes of cultured 11.5 dpc embryos

(A) Propidium iodide stained coronal section (frozen) of a control eye of a cultured embryo showing a few granules of intense staining (arrowheads), characteristic of apoptotic nuclei, in the central neural retina. **(B)** An equivalent section to A through the rhBMP4 treated contralateral eye of the same embryo showing one granule of intense propidium iodide staining in the region where the optic stalk appears in later sections of the eye, but lots of granular staining in the dorsal neural retina (arrowheads). **(C,D)** Higher magnifications of the dorsal neural retina of A and B respectively. Intense propidium iodide stained granules in the rhBMP4 treated eye are marked with arrowheads. **(E)** Coronal section of a control non-treated eye labelled with TUNEL (green). Very few apoptotic cells were detected in this particular section. **(F)** An equivalent section to E, through the coronal plane of the rhBMP4 treated contralateral eye of the same embryo. A large amount of TUNEL labelling was detected in the dorsal neural retina. **(G,H)** Control and contralateral rhBMP4 treated eye with the high dose of rhBMP4. Increased TUNEL positive nuclei detected in the dorsal neural retina of the rhBMP4 treated eye (H, arrow). Labelling was also detected in the ventral neural retina and in the lens vesicle. Scale bars: 0.1 mm.

Abbreviations: D, dorsal; L, lens; NR, neural retina; V, ventral.

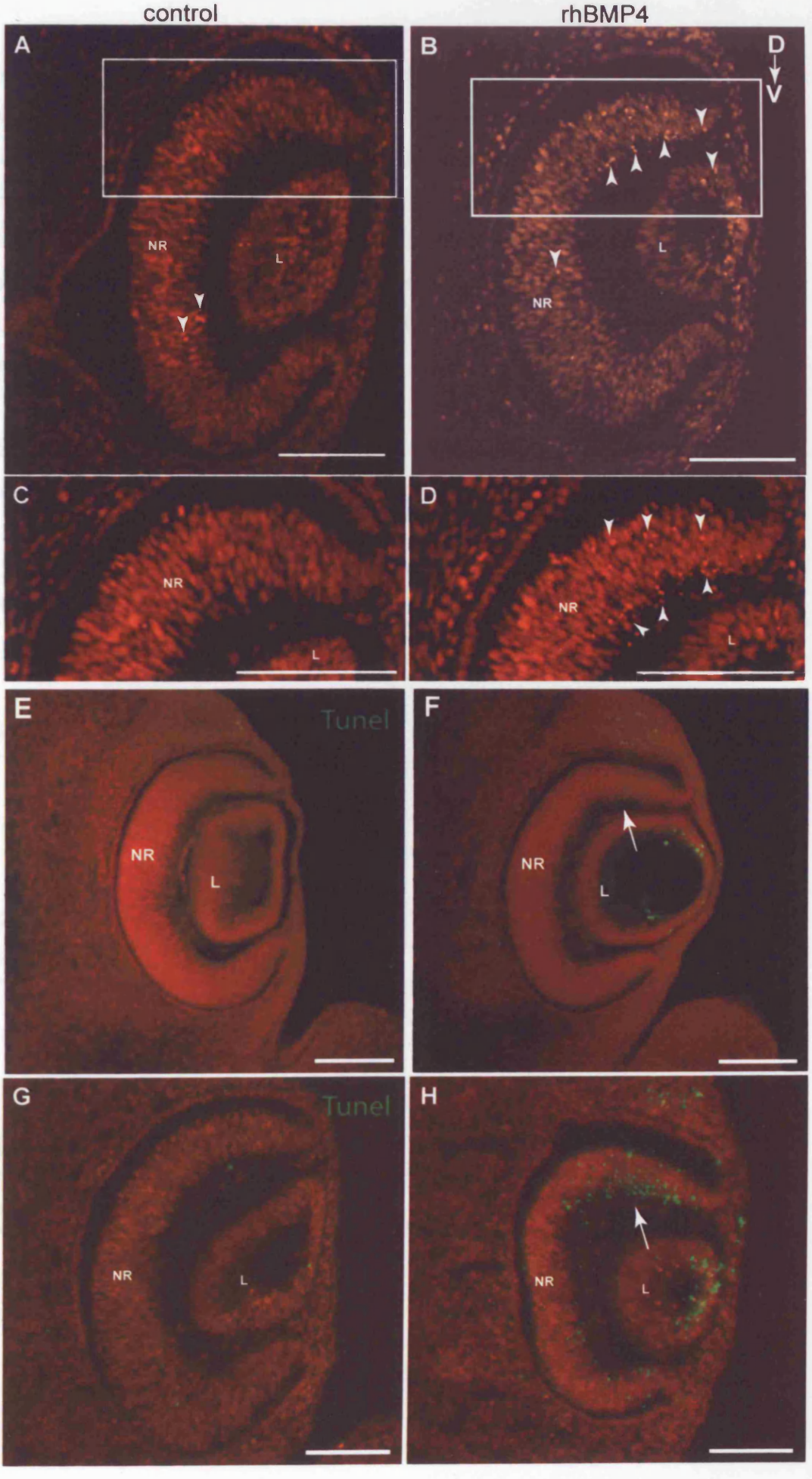
control
rhBMP4
A
B
D
V
NR
L
C
D
E
Tunel
F
G
Tunel
H

For quantification purposes, only embryos treated with the lower dose of rhBMP4 were analysed. Because the pattern of cell death in the early optic cup is normally highly regionalised to separate clusters in the dorsal, and the central neural retina (see Chapter 1.2.4), and the elevated cell death in rhBMP4 treated eyes was regionalised to the dorsal-most neural retina (in D1), the neural retina was divided into dorsal-most, central, and ventral regions as indicated in Fig. 4.19 A and TUNEL labelled nuclei were counted in each region (Table 4.13). In comparison to the divisions used for analysis of mitosis, the dorsal domain used there was further subdivided into the dorsal-most (equivalent to D1) and central domains for the analysis of apoptosis here. The ventral domain still corresponds approximately to the region of normal *Vax2* expression.

Table 4.13 **Total number of apoptotic cells per eye, divided in dorsal, central and ventral regions, in rhBMP4 treated and contralateral non-treated eyes in five embryos**

Embryo post(pre) ss	sections per eye	rhBMP4				Control			
		D	C	V	Total	D	C	V	Total
TUNEL positive cells									
1. 52(42) ss	3	13	1	2	**16**	3	3	1	**7**
2. 48(40) ss	3	5	56	12	**73**	5	6	9	**20**
3. 53(44) ss	2	37	19	13	**69**	4	27	14	**45**
4. 51(41) ss	3	16	10	10	**36**	6	31	11	**48**
5. 52(40) ss	2	8	16	4	**28**	8	6	9	**23**
Total	**13**	**79**	**102**	**41**	**222**	**26**	**73**	**44**	**143**
TUNEL positive cells/mm^2									
1. 52(42) ss	3	289	21	67	**377**	94	45	26	**165**
2. 48(40) ss	3	190	1390	454	**2034**	181	196	344	**721**
3. 53(44) ss	2	2313	471	650	**3434**	222	725	591	**1538**
4. 51(41) ss	3	667	224	367	**1258**	354	1071	306	**1731**
5. 52(40) ss	2	527	510	182	**1219**	500	162	500	**1162**
Total	**13**	**3986**	**2616**	**1720**	**8322**	**1351**	**2199**	**1767**	**5317**

D, dorsal; C, central; V, ventral; ss, somite stage. The somite stage of each embryo, pre-culture is given in brackets, and post-culture outside of the brackets.
Table illustrates the total number of cells counted in 2-3 midline sections (as indicated) per eye.

Fig. 4.19 Investigation of regional occurrence of apoptotic cell death along the D-V axis of the eye in rhBMP4 treated and control eyes

P-values for comparisons between the number of Ln transformed TUNEL labelled cells in different treatment groups were calculated by the Two-Way ANOVA test and with the ANCOVA test with the effect of surface area incorporated. **(A)** Schematic illustration of the criteria for division of the eye used in quantitative analysis. The dorsal region of the neural retina until the dorsal curvature was regarded as the dorsal region. The area below the dorsal curvature, but above the dorsal wall of the optic stalk was regarded as central neural retina. The area below the dorsal wall of the optic stalk was regarded as ventral neural retina. **(B)** Scatter plot of Ln transformed number of TUNEL labelled cells in the dorsal neural retina in 2-3 sections per eye in five embryos. Overall, sections through rhBMP4 treated eyes contained more TUNEL labelled cells in comparison to non-treated control counterparts. **(C)** Scatter plot of Ln transformed number of TUNEL labelled cells in the ventral neural retina of same sections as counted in B. The number of TUNEL labelled cells did not differ significantly in the ventral neural retina of rhBMP4 and non-treated control eyes. **(D)** Scatter plot of Ln transformed number of TUNEL labelled cells in the central neural retina of sections used in B and C. The number of TUNEL labelled cells did not differ significantly in the central neural retina of rhBMP4 and non-treated control eyes. **(E-G)** Scatter plots of apoptotic indices calculated as number of TUNEL positive cells per surface area in the dorsal, ventral, and central neural retina respectively.

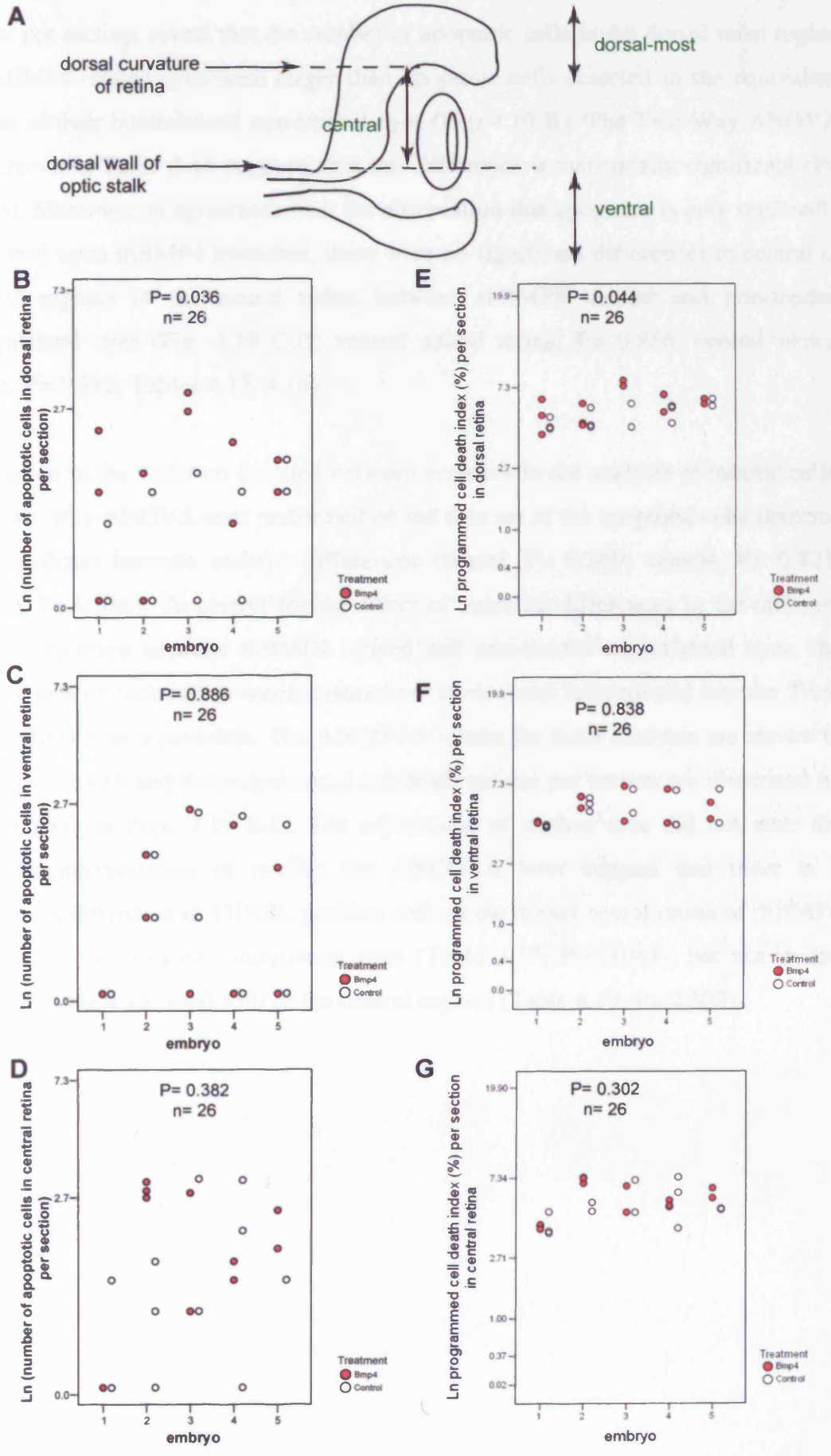
A
dorsal curvature of retina
dorsal wall of optic stalk
central
dorsal-most
ventral
B
P= 0.036
n= 26
Ln (number of apoptotic cells in dorsal retina per section)
embryo
Treatment
Bmp4
Control
E
P= 0.044
n= 26
Ln programmed cell death index (%) per section in dorsal retina
embryo
Treatment
Bmp4
Control
C
P= 0.886
n= 26
Ln (number of apoptotic cells in ventral retina per section)
embryo
Treatment
Bmp4
Control
F
P= 0.838
n= 26
Ln programmed cell death index (%) per section in ventral retina
embryo
Treatment
Bmp4
Control
D
P= 0.382
n= 26
Ln (number of apoptotic cells in central retina per section)
embryo
Treatment
Bmp4
Control
G
P= 0.302
n= 26
Ln programmed cell death index (%) per section in central retina
embryo
Treatment
Bmp4
Control

Both Table 4.13 and the scatter plot illustrating Ln transformed number of apoptotic nuclei per section, reveal that the number of apoptotic cells in the dorsal-most region of rhBMP4 treated eyes were larger than apoptotic cells detected in the equivalent region of their contralateral non-treated eyes (Fig. 4.19 B). The Two-Way ANOVA test shown in Table 4.14 suggests that this difference is statistically significant (P= 0.036). Moreover, in agreement with the observation that apoptosis is only regionally increased upon rhBMP4 treatment, there were no significant differences in central or ventral regions of the neural retina between rhBMP4 treated and non-treated contralateral eyes (Fig. 4.19 C,D; ventral neural retina, P= 0.886; central neural retina, P= 0.382; Tables 4.15, 4.16).

In contrast to the variation detected between embryos in the analysis of mitotic cells, the Two-Way ANOVA tests performed on the data set of the apoptotic cells detected no significant between embryo differences (dorsal, P= 0.369; ventral, P= 0.421; central, P= 0.586). To correct for the effect of potential differences in the different regions analysed between rhBMP4 treated and non-treated contralateral eyes, the surface area of each region was measured per section and incorporated into the Two-Way ANOVA as a covariate. The ANCOVA results for these analyses are shown in Tables 4.17-4.19 and the programmed cell death indices per section are illustrated by scatter plots in Figs. 4.19 E-G. The adjustment of surface area did not alter the previous interpretation of results; the ANCOVA tests suggest that there is a significant difference in TUNEL positive cells in the dorsal neural retina of rhBMP4 treated and non-treated contralateral eyes (Table 4.17; P= 0.044), but not in the ventral (Table 4.18; P= 0.838) or the central regions (Table 4.19; P= 0.302).

Table: 4.14 Two-Way ANOVA table for the comparison of TUNEL labelled nuclei between dorsal regions of rhBMP4 treated and non-treated contralateral eyes

Dependent Variable: Ln (TUNEL labelled nuclei in dorsal neural retina)

Source	Type III Sum of Squares	df	Mean Square	F	Sig.
Corrected Model	13.017(a)	13	1.001	1.552	.227
Intercept	25.667	1	25.667	39.794	.000
sections	9.423	12	.785	1.217	**.369**
treatment	3.594	1	3.594	5.572	**.036**
Error	7.740	12	.645		
Total	46.424	26			
Corrected Total	20.757	25			

a R Squared = .627 (Adjusted R Squared = .223)

Table: 4.15 Two-Way ANOVA table for the comparison of TUNEL labelled nuclei between ventral regions of rhBMP4 treated and non-treated contralateral eyes

Dependent Variable: Ln (TUNEL labelled nuclei in ventral neural retina)

Source	Type III Sum of Squares	df	Mean Square	F	Sig.
Corrected Model	12.229(a)	13	.941	1.040	.476
Intercept	16.687	1	16.687	18.443	.001
treatment	.019	1	.019	.021	**.886**
sections	12.210	12	1.017	1.125	**.421**
Error	10.857	12	.905		
Total	39.774	26			
Corrected Total	23.087	25			

a R Squared = .530 (Adjusted R Squared = .020)

Table: 4.16 Two-Way ANOVA table for the comparison of TUNEL labelled nuclei between central regions of rhBMP4 treated and non-treated contralateral eyes

Dependent Variable: Ln (TUNEL labelled nuclei in central neural retina)

Source	Type III Sum of Squares	df	Mean Square	F	Sig.
Corrected Model	15.725(a)	13	1.210	.876	.594
Intercept	45.150	1	45.150	32.681	.000
treatment	1.138	1	1.138	.824	**.382**
sections	14.587	12	1.216	.880	**.586**
Error	16.578	12	1.382		
Total	77.454	26			
Corrected Total	32.303	25			

a R Squared = .487 (Adjusted R Squared = -.069)

Table 4.17 ANCOVA table for the comparison of TUNEL labelled nuclei between dorsal regions of rhBMP4 treated and non-treated contralateral eyes with Ln surface area as covariate

Dependent Variable: Ln (TUNEL labelled nuclei in dorsal neural retina)

Source	Type III Sum of Squares	df	Mean Square	F	Sig.
Corrected Model	13.062(a)	14	.933	1.334	.320
Intercept	.012	1	.012	.017	.897
treatment	3.637	1	3.637	5.199	**.044**
section	8.384	12	.699	.999	**.504**
Ln Surface Area	.046	1	.046	.065	**.803**
Error	7.694	11	.699		
Total	46.424	26			
Corrected Total	20.757	25			

a R Squared = .629 (Adjusted R Squared = .158)

Table 4.18 ANCOVA table for the comparison of TUNEL labelled nuclei between ventral regions of rhBMP4 treated and non-treated contralateral eyes with Ln surface area as covariate

Dependent Variable: Ln (TUNEL labelled nuclei in ventral neural retina)

Source	Type III Sum of Squares	df	Mean Square	F	Sig.
Corrected Model	12.664(a)	14	.905	.955	.541
Intercept	.557	1	.557	.587	.460
treatment	.042	1	.042	.044	**.838**
section	12.644	12	1.054	1.112	**.434**
Ln Surface Area	.434	1	.434	.458	**.512**
Error	10.423	11	.948		
Total	39.774	26			
Corrected Total	23.087	25			

a R Squared = .549 (Adjusted R Squared = -.026)

Table 4.19 ANCOVA table for the comparison of TUNEL labelled nuclei between central regions of rhBMP4 treated and non-treated contralateral eyes with Ln surface area as covariate

Dependent Variable: Ln (TUNEL labelled nuclei in central neural retina)

Source	Type III Sum of Squares	df	Mean Square	F	Sig.
Corrected Model	19.520(a)	14	1.394	1.270	.358
Intercept	2.805	1	2.805	2.555	.141
treatment	1.303	1	1.303	1.187	**.302**
section	16.218	12	1.352	1.231	**.376**
Ln Surface Area	2.291	1	2.291	2.087	**.179**
Error	10.977	10	1.098		
Total	77.454	25			
Corrected Total	30.497	24			

a R Squared = .640 (Adjusted R Squared = .136)

4.3 Discussion

4.3.1 Summary of findings

The following conclusions can be drawn from this study, which aimed to manipulate Bmp4 signalling during optic cup morphogenesis, using bead implantation as a means of protein delivery, in combination with whole mouse embryo culture.

1. All three T-box genes in the dorsal eye are regulated by Bmp4 signalling.

2. Increased Bmp4 signalling induced a differential pattern of ectopic expression of *Tbx2*, *Tbx3*, and *Tbx5*. Together with the loss of *Vax2* in the ventral eye, the molecular composition along the D-V axis of the eye was shifted ventrally.

3. Decreased levels of Bmp signalling, by the addition of Noggin, shifted T-box gene expression dorsally.

4. Perturbation of Bmp4 signalling and T-box gene expression altered eye size and shape; a reduction in eye size was revealed by measurements of the D-V and N-T axial lengths as well as retinal volume in rhBMP4 treated eyes as compared to BSA treated or non-treated contralateral eyes. Measurements along the P-Di axis provided indications of a shape change in rhBMP4 treated eyes in the form of a reduction of the ventral neural retina.

4.3.2 T-box genes in the eye show differential responsiveness to Bmp4 signalling

In Chapter 3, it was shown that while *Tbx5* was expressed in the same region of the neural retina as *Bmp4*, *Tbx2* and *Tbx3* expression domains were broader than that of *Bmp4* in the optic cup. Data presented in this Chapter show that all three T-box genes are responsive to manipulations of Bmp signalling and in the same way that normal *Tbx2* and *Tbx3* expression domains are broader than *Tbx5*, the ectopic patterns of *Tbx2* and *Tbx3* induced by rhBMP4 were also broader than *Tbx5*. Although there

may be some variability in the amount of protein uptake and release from the beads, the results obtained were extremely consistent in that *Tbx5* was induced in D2 and never in the ventral neural retina, *Tbx3* was induced in the entire neural retina, while *Tbx2* was induced in V3 and also in the lens vesicle.

The question arises as to how these genes are differentially regulated. Data presented here suggest that *Bmp4*, which is transcribed in D1, regulates gene expression outside of its expression domain. The way in which gene expression was altered upon manipulation of Bmp4 signalling is reminiscent of systems where the action of morphogen gradients have been proposed or demonstrated. The similarity lies in several genes being differentially induced or repressed at a distance from the site of expression of a secreted factor (Gurdon *et al.* 1995; Lecuit *et al.* 1996; Nellen *et al.* 1996; Ericson *et al.* 1997; Briscoe *et al.* 2000). Interpretation of results obtained here according to such a model would predict that Bmp4 protein or signalling present in a dorsal-high, ventral-low gradient, with the highest levels of signalling in the dorsal neural retina induces unique domains of expression of the different T-box genes in a concentration dependent manner.

Considering the experimental approach used in this Chapter more closely, in experiments where an rhBMP4 bead was placed in the lens vesicle, a site at an equivalent distance from both the dorsal and the ventral neural retina, it is likely that Bmp4 levels were elevated equally across the D-V axis of the optic cup. Therefore, the dorsal neural retina with high endogenous Bmp4 protein levels would have an even higher concentration of Bmp4, while the ventral neural retina which may or may not be exposed to Bmp4 protein naturally, would have a low level of Bmp4 signalling due to the exogenously provided rhBMP4. The lens which also does not express Bmp4 normally, would also be exposed to Bmp4 signalling due to the rhBMP4 bead. As described in Chapter 1.4.1, the Bmp4 signal transduction machinery are present in both the lens and the ventral neural retina (BmprI, BmprII) in order to mediate the signal.

Fig. 4.20 The envisaged Bmp4 signalling gradient before and after bead implantation

Bmp4 is expressed in the dorsal neural retina. As such, Bmp4 signalling is likely to be highest in this region (red circles). Implantation of the rhBMP4 bead is thought to provide equal amounts of protein to both dorsal and ventral regions, resulting in an enhancement of the putative endogenous Bmp4 signalling gradient, while implantation of a Noggin bead reduces it.

Abbreviations: D, dorsal; V, ventral

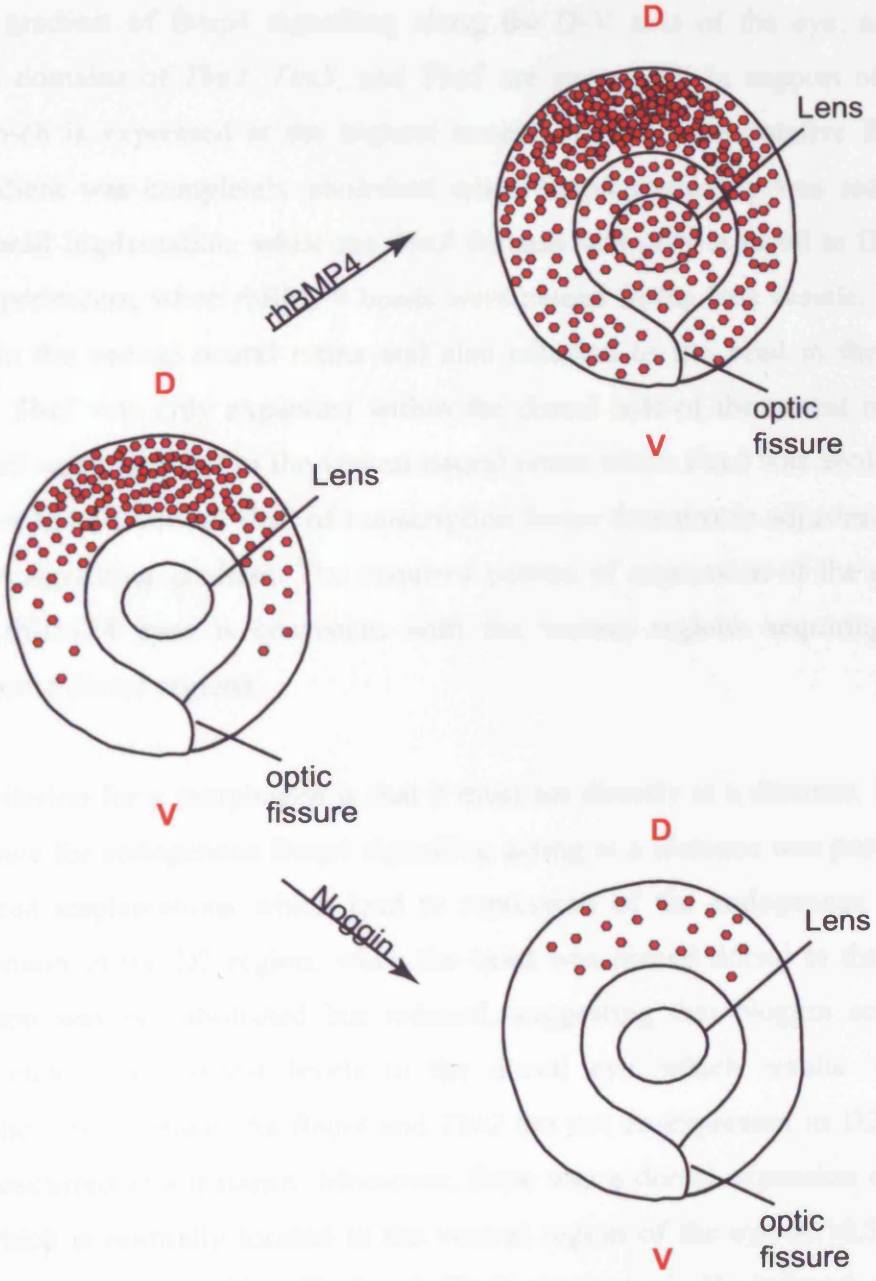
D
Lens
rhBMP4
optic
fissure
V
D
Lens
optic
fissure
V
D
Noggin
Lens
optic
fissure
V

As outlined in Chapter 1.4.3, the first criterion for a morphogen is that it must induce different responses at different concentrations. The results presented here provide indirect evidence in support of the existence of a dorsal-high, ventral-low concentration gradient of Bmp4 signalling along the D-V axis of the eye, across which distinct domains of *Tbx2*, *Tbx3*, and *Tbx5* are expressed. In support of this idea, *Tbx5* which is expressed at the highest concentration of the putative Bmp4 signalling gradient was completely abolished when Bmp4 signalling was reduced with Noggin bead implantation, while the *Tbx2* domain was only reduced to D1. In the reverse experiments, when rhBMP4 beads were placed in the lens vesicle, *Tbx2* was induced in the ventral neural retina and also adjacent to the bead in the lens vesicle, while *Tbx5* was only expanded within the dorsal half of the neural retina. Moreover, *Tbx3* was expanded in the ventral neural retina while *Vax2* was abolished in what appears to be a ventral shift of transcription factor domains in adjustment to the new Bmp4 signalling gradient. The acquired pattern of expression of the genes examined in rhBMP4 eyes is consistent with the ventral regions acquiring the properties of more dorsal regions.

The second criterion for a morphogen is that it must act directly at a distance. Here, indirect evidence for endogenous Bmp4 signalling acting at a distance was provided by Noggin bead implantations which lead to repression of the endogenous *Tbx2* expression domain in the D2 region, when the bead was placed dorsal to the eye. *Tbx2* expression was not abolished but reduced, suggesting that Noggin acts by reducing the endogenous Bmp4 levels in the dorsal eye, which results in the reduction of the *Tbx2* domain. As *Bmp4* and *Tbx2* are not co-expressed in D2, this response has occurred at a distance. Moreover, there was a dorsal expansion of the optic stalk, which is normally located in the ventral region of the eye at 10.5-11.5 dpc, in Noggin treated eyes. That *Tbx5* and *Tbx3* were ectopically induced, while *Vax2* expression in the ventral eye was abolished at a distance away from rhBMP4 beads implanted in the lens, further support that Bmp4 can induce a response at a distance in the developing eye. Whether Bmp4 acts directly or indirectly across a distance to induce these changes cannot be determined based on data presented here. The alternative possibility is that these changes are indirect and instead caused by a relay mechanism in which Bmp4 induces other genes in neighbouring cells and so forth. Examination of gene expression within a shorter period after bead implantation

could help to determine the likelihood of a direct response in gene expression to rhBMP4 treatment; if a relay mechanism is involved, changes in gene expression would be expected to take longer to occur, due to the time needed for the expression and action of intermediaries to take place.

Other mechanisms that could account for the observed changes in the pattern of gene expression, would include changes in cell proliferation/cell death or cell migration. Two aspects of the data directly argue against gene expression domains being altered because of cell proliferation/cell death. Firstly, although cell division was decreased in rhBMP4 treated eyes, expression of the T-box genes were expanded, suggesting that these changes are due to induction of gene expression rather than proliferation of cells that already express the T-box genes. Secondly, in the domain where *Vax2* was abolished, no differences were found in the level of cell death, suggesting that *Vax2* expression rather than *Vax2* expressing cells was abolished. The possibility of cell migration also appears inconsistent with the data, as the loss of *Vax2* expression was not accompanied by displacement of *Vax2* expressing cells elsewhere, and rhBMP4 treated eyes still possessed a ventral optic cup region indicated by the presence of the optic fissure. Conversely, there was no evidence of displaced *Tbx5* expressing cells in Noggin treated eyes where *Tbx5* was abolished.

In *Drosophila*, tethered proteins have been used to experimentally show whether a suspected morphogen acts over a distance (Zecca *et al.* 1996). This approach could potentially be used in the mouse embryo in future experiments. For example a transmembrane domain of a transmembrane protein could be attached to Bmp4 and this hybrid protein expressed in the lens vesicle under the regulation of a lens specific promoter, such as the α-crystallin promoter. If it failed to induce the ventral shift in gene expression, this could demonstrate whether exogenous Bmp4 diffuses and acts directly on neural retinal cells to cause gene expression changes.

Other mechanisms or additional factors, apart from interpretation of a Bmp4 signalling gradient, may also contribute to the observed differential response in gene expression. It is for example possible that additional factors predispose certain regions of the optic cup to express a particular T-box gene in response to Bmp4. It is simplest to consider the lens alone when contemplating this idea. That *Tbx2*, but not

Tbx3 or *Tbx5,* are induced in the lens vesicle suggest that *Tbx2* requires the lowest level of Bmp4 signalling to be switched on. However, *Tbx3* which according to this model needs higher levels of Bmp4 than *Tbx2*, is induced in the ventral neural retina but not in the lens. It is unlikely that the lens, containing an rhBMP4 bead, would have lower levels of Bmp4 than the ventral neural retina which is further away from the source, yet expresses ectopic *Tbx3*. Instead, it is likely that the lens is permissive to *Tbx2* expression only, while the ventral most region of the neural retina (V4) is more permissive to *Tbx3* than to *Tbx2* expression. This points towards the existence of differences in the regulatory elements of the T-box genes, other than those that enable each gene to sense a Bmp4 signalling gradient. These could be the existence of binding sites for cofactors which together with phosphorylated Smad complexes may be needed to induce different T-box genes; the expression of these cofactors would then provide a limiting step in the regulation of each T-box gene in response to the Bmp4 signalling pathway. In support for the idea of other factors also being involved, in the *Drosophila* wing, there is evidence that *omb* is induced by the combined actions of Dpp and Wingless (Grimm and Pflugfelder 1996).

Regardless of other differences in the regulation of the T-box genes, Bmp4 signalling is likely to play a significant role in their regulation in eye development. This finding in the mouse embryo is similar to findings in the *Xenopus* embryo, where all three T-box genes were induced in the ventral optic cup in response to *Bmp4* RNA electroporations into the eye field. Although one difference was that all three were reported to show a similar expansion in the *Xenopus* study, which is likely to be due to the different experimental approach (Sasagawa *et al.* 2002). Moreover, the absence of *Tbx5* expression recently reported in the optic vesicle of *Bmp4* null mice demonstrates the absolute requirement of Bmp4 for the induction of *Tbx5* at least (Murali *et al.* 2005). Data presented here, suggest that this requirement is likely to be concentration dependent.

Ventroptin is a Bmp antagonist with high affinity for Bmp4 and no affinity for Bmp7, that is suitably expressed in a ventral and nasal high gradient in the chick neural retina, in order to counteract Bmp4 signalling and create a dorsal-high, ventral-low Bmp4 signalling gradient. It has also been isolated in the mouse, but its expression has not yet been reported (Sakuta *et al.* 2001). Misexpression of

Ventroptin in the chick optic vesicle by electroporation, abolishes *Bmp4* and *Tbx5* expression and induces a complete expansion of *cVax* expression into the dorsal eye. This study suggests that *cVax* is only expressed when Bmp signalling is antagonised. In further support of this idea, an expansion of *Vax2* is observed in mice with only one functional allele of *BmprIb* and no *BmprIa* in the eye (Murali *et al.* 2005). *Ventroptin* can be downregulated by *Bmp4* as retroviral mediated *Bmp4* infection of eyes show an absence of *Ventroptin* expression (Sakuta *et al.* 2001). It is not clear which transcriptional regulators mediate this reciprocal repression of transcription of *Bmp4* and *Ventroptin*, though it should be noted that this type of interaction between two genes that are not normally coexpressed by misexpression studies could be due to the forced expression of these genes, and may not happen naturally

rhBMP4 bead implantation in the extra-ocular mesenchyme at 10.5 dpc did not induce the same consistent results as observed when beads were placed in the lens vesicle at 11.5 dpc, even though Noggin bead implantations in the same region at 10.5 dpc did alter T-box gene expression. Conversely, Noggin bead implantation in the lens vesicle at 11.5 dpc failed to induce changes in gene expression. These differences could arise due to the dramatic morphogenetic movements that take place at least at 10.5 dpc. Alternatively, at 11.5-12.5 dpc, Bmp4 signalling may no longer be required for maintaining the already induced domains of T-box gene expression and as a result, inhibition of endogenous Bmp4 signalling by Noggin has no effect on T-box gene or *Vax2* expression. In support of this idea, endogenous Bmp4 transcripts appear downregulated in the neural retina at 12 dpc (Liu *et al.* 2003).

4.3.3 Role of Bmp4 signalling in controlling growth and shape of the mouse optic cup

Bmp4 haploinsufficiency has been reported to cause microphthalmia and anophthalmia in mice (Dunn *et al.* 1997), but the mechanism responsible for these severe phenotypes has not been investigated. Here, it was shown that cell division was reduced in rhBMP4 treated eyes compared to non-treated contralateral eyes. Regardless of the between embryo variability in the number of mitotic cells detected, the mitotic index was lower in the treated eye in all embryos examined. While the pattern of cell death detected in control eyes correlated well with previous reports of

cell death in the early optic cup (see Chapter 1.2.4), in rhBMP treated eyes beads soaked in 100 μg/μl, induced elevated cell death in the dorsal eye in particular. However, as the number of apoptotic nuclei detected was small, it is most likely that rhBMP4 treated eyes were smaller than control eyes because of a reduction in cell proliferation rather than elevated cell death. Eyes treated with beads soaked in a larger quantity of rhBMP4, which has been reported as a way of increasing the concentration of protein on beads (Lee *et al.* 2001b), resulted in a dramatic increase in cell death, which interestingly was still primarily localised to the dorsal neural retina. This result also confirms that Bmp4 signalling in the eye can induce a different response depending on concentration. Increased levels of cell death in the eye was also reported in BmprIa/Ib compound mutants which lack Bmp signalling (Murali *et al.* 2005), suggesting that an optimal level of Bmp4 signalling is essential for proper eye development as both increased (shown here) and decreased levels of Bmp4 signalling cause increased cell death and decreased cell proliferation.

Analysis of regional differences in cell division, with the neural retina divided into dorsal and ventral regions with respect to the normal *Vax2* expression domain, revealed a reduction in cell division in both regions of rhBMP4 treated eyes. All three T-box genes are ectopically expressed in the dorsal region of rhBMP4 treated eyes, with *Tbx5* being most restricted, while the ventral eye has ectopic *Tbx3* expression and no *Vax2* expression. All three T-box genes have been implicated in the control of cell proliferation [see Chapter 1.3.5 and (He *et al.* 2002; Liberatore *et al.* 2000)] and without further experiments that investigate each gene specifically in the developing eye, it is not possible to pinpoint which downstream pathway of Bmp4 signalling is responsible for the reduction in cell proliferation.

The regional occurrence of cell death in the dorsal neural retina of rhBMP4 treated eyes seems unlikely to be caused by any of the T-box genes. *Tbx2* and *Tbx3* alone or in combination are excluded on the basis that elevated cell death was not detected in the ventral neural retina where they were ectopically induced. It is however still possible that elevated expression of either or all three T-box genes in the dorsal neural retina triggered apoptosis. *Tbx5* in particular has been shown to induce cell death when misexpressed *in vitro*, while *Tbx3* has been identified as an anti-apoptotic gene, also *in vitro* (He *et al.* 2002; Carlson *et al.* 2002). Taken together with the

observation that the ectopic cell death occurred in the dorsal neural retina in response to rhBMP4 carrying beads, where *Tbx5* was induced, it is possible that the observed apoptosis in treated eyes is mediated by *Tbx5*. However, it is also possible that it is induced by *Msx2*, a known mediator of the apoptotic effect of Bmp4 during neural crest cell depletion in the rhombomeres (Graham *et al.* 1994). As demonstrated in Chapter 3 and previously by Monaghan and colleagues (Monaghan *et al.* 1991), *Msx2* is appropriately expressed in the dorsal neural retina to mediate this effect. The regulatory relationship between *Msx2* and the T-box genes has not been elucidated.

The involvement of the Bmp pathway in the control of cell proliferation and cell death during nervous system development has been demonstrated in numerous *in vitro* and *in vivo* studies (Anderson *et al.* 2002; McMahon *et al.* 1998; Bachiller *et al.* 2000; Furuta *et al.* 1997; Mehler *et al.* 1997). These studies highlight that the response to Bmp signalling is context dependent and therefore cannot be generalised.

In the context of eye development in species other than the mouse, investigators have found that retroviral misexpression of *Noggin* in the chick eye at HH 9-10 (ie reduced Bmp4 signalling), causes microphthalmia (Adler and Belecky-Adams 2002). Application of rhBMP4 [1μg/ml] coated heparin beads to the extra-ocular mesenchyme dorsal to newly formed optic cups in the chick embryo increases dorsal apoptosis, which in the chick eye is the site of relatively high levels of naturally occurring apoptosis (Trousse *et al.* 2001). Application of Noggin coated beads [1mg/ml] abolishes the naturally occurring cell death and also reduces cell proliferation within the dorsal eye, whereas BMP4 treatment [40 ng/ml] of retinal cell cultures from HH 18 chick embryos induces cell proliferation (Trousse *et al.* 2001). In contrast to results presented here, the chick study suggests that addition of rhBMP4 induces both cell proliferation and cell death, while exogenous application of Noggin reduces both cell proliferation and cell death in the developing chick eye. However, with regards to the effect of rhBMP4 treatment, as Trousse *et al.* did not analyse cell proliferation and cell death under similar experimental conditions (cell death was analysed in bead implantation study *in vivo* whereas cell proliferation was analysed in dissociated cells), it is hard to make comparisons of the effects in the chick embryo and those reported in this Chapter for the mouse embryo.

As well as a reduction in overall eye size, the shape of the optic cup appeared altered in rhBMP4 treated eyes. Measurements of the P-Di axial length revealed that this most likely was due to the ventral region of the optic cup being shorter or showing reduced bending than in BSA treated eyes. The P-Di axial length in more dorsal aspects were very similar between treatment groups. As mentioned in the introduction (Chapter 1.1.3), even slight changes in the axial length of the mature eye can result in refractive errors, therefore identification of genes and developmental mechanisms that may cause variation in eye shape is of interest.

Comparative studies of the expression of secreted signalling molecules in closely related species that show variation in organ size and shape have revealed that slight differences in the number of cells that express these factors underlie the observed phenotypic variation between species. Of direct relevance is a study that reported the level and temporal onset of *Bmp4* expression in the craniofacial region of several closely related songbird species, to correlate with variations in upper beak morphology (Abzhanov *et al.* 2004). Misexpression of *Bmp4* in the craniofacial mesenchyme of chick embryos can phenocopy the broad and deep beak morphology of songbird species that show the highest level and extent of *Bmp4* expression in their beak primordia during development and also in the duck, which expresses higher levels of *Bmp4* and has a broader and longer beak than the chick (Abzhanov *et al.* 2004; Wu *et al.* 2004). Further evidence for Bmp signalling being implicated in regulating organ shape comes from misexpression studies of *Bmp2* and *Bmp4* in the developing chick limb, resulting in alteration in cartilage size and shape (Duprez *et al.* 1996), and of *dpp* in the *Drosophila* wing, which results in alterations in wing size and shape (Zecca *et al.* 1995).

The development of the shape of the mature eye occurs during the period of optic vesicle invagination into an optic cup. By 13.5 dpc in the mouse, the shape of the eye globe is complete with the optic disc being positioned in the central region of the cup and the optic fissure closed. Data presented here suggest that Bmp4 signalling during this period is one of the signals that ensures the formation of a correctly sized and shaped eye in the mouse embryo.

The initial pattern of *Bmp4* expression in the eye differs between chick and mouse embryos, as *Bmp4* is expressed dorsally from optic vesicle stage in the mouse, but in the chick embryo, the dorsal expression only comes on after optic vesicle invagination has occurred, prior to which, *Bmp4* is strongly expressed in the surface ectoderm (see Chapter 1.4.1). Given the differences also found in the pattern of dorsally restricted cell death, the observation shown here that in the mouse eye higher levels of rhBMP4 treatment could induce dorsally localised cell death, which resembles that in the chick embryo, it is tempting to speculate that the difference in dorsally occurring cell death between the two species may be due to differences in *Bmp4* expression. This in turn may be one of the reasons why the chick eye differs so dramatically in size and shape from the mouse eye. Notably, the chick optic cup is relatively larger and rounder than the mouse optic cup. The thickness of the neural retina also differs between the two, with the chick neural retina being thinner.

As a result of the study presented here, the next step was to examine which of the effects of Bmp4 on eye development, which include the control of D-V patterning and eye size and shape, were mediated by the T-box genes. The two next chapters are concerned with analysing D-V patterning and growth of the eye when *Tbx2*, which showed a dramatic response to rhBMP4, is manipulated. Moreover, the possibility that *Tbx2* may act by controlling regional cell proliferation or cell death was explored.

CHAPTER 5 Analysis of early eye development in mouse embryos with a mutation in the *Tbx2* gene

5.1 Introduction

The objective of this Chapter was to directly investigate the role of *Tbx2* in eye development, in particular to investigate whether *Tbx2* regulates D-V patterning genes and eye morphogenesis, using mice that carry a targeted mutation in the *Tbx2* gene. Several functions have been identified for *Tbx2* both at organ and cellular levels (see Chapter 1.3.3, 1.3.5). However, its role in mammalian eye development remains uncharacterised.

The starting point for this study was the knowledge that *Tbx2* is expressed from the optic vesicle stage and hence is likely to have an early role in eye development, such as coordination of optic cup formation or neural retina versus RPE specification. Its asymmetrical expression in the dorsal optic cup prompted the thinking that it may regulate molecular D-V patterning in the eye and perhaps be involved in mechanisms such as cell proliferation, which numerous studies have shown *Tbx2* to be involved in as discussed in Chapter 1.3.5. Apart from the expression pattern of *Tbx2* in the eye as a basis for the formulation of these hypotheses, they are supported by the findings in Chapter 4, where rhBMP4 treatment of eyes resulted in the expansion of *Tbx2* expression and alterations in eye size and shape. Here, the role of Tbx2 in mediating the effect of Bmp4 in regulating D-V patterning and growth of the eye was investigated.

The *Tbx2* mutant allele, named $Tbx2^{tm1Pa}$ and here forth referred to as $Tbx2^{-}$, was generated in Professor V.E Papaioannou's laboratory (Columbia University) and has been described (Harrelson *et al.* 2004). Briefly, a *Tbx2* genomic clone isolated from a 129/SvJ phage genomic library was used to generate a targeting construct containing a PGK-*neo* cassette flanked by *LoxP* sites and a 5' 2.9 Kb homologous arm and a 3' 6.6 Kb homologous arm from the *Tbx2* genomic sequence on either side of the two *LoxP* sites. Homologous recombination in an ES cell line resulted in a 2.2 Kb deletion of the *Tbx2* sequence including 207 bp of exon 1 and all of exon 2. The PGK-neo cassette was Cre-excised and correctly targeted ES cells were injected into C57BL/6N Tac host blastocysts, which were implanted into the uterus of pseudo-pregnant females. Progeny showing germ line transmission were eventually

maintained on a mixed Sv/C57/ICR background as it was shown that the genetic background did not affect the phenotype (Harrelson *et al.* 2004).

In the time available for undertaking an analysis of the *Tbx2*$^{-/-}$ eye phenotype, it was not possible to re-derive the *Tbx2* mutation on a single genetic background devoid of the non-pigmented ICR strain. The RPE is the source of Dopa production which is a precursor of melanin. The lack of synthesis of melanin or reduced levels of melanin is thought to underlie the albino eye abnormalities including poorly developed central retinae, reduced ganglion cell density, crossing of some ipsilateral axonal projections, and rod photoreceptor deficit (Jeffery 1997). Therefore the use of albino strains in eye research is not ideal. However, this Chapter aimed to study early aspects of eye development, so the great majority of the analysis was performed at 10.5 dpc, when pigmentation of the RPE has not yet initiated. All analysis beyond 10.5 dpc was performed on pigmented embryos. Therefore, it is unlikely that the possible future lack of pigmentation in some embryos would have contributed to the defects identified.

The initial analysis of the heart phenotype of the *Tbx2*$^{-/-}$ mice did not reveal a gene dosage effect as heterozygous embryos are developmentally normal (Harrelson *et al.* 2004). Although heterozygotes are viable and fertile, homozygous embryos die prenatally. The first abnormalities manifest at 9.5 dpc in the developing heart in a subset of mutants, specifically in the atrioventricular canal (AVC), where the endocardial cushions, which normally form by 10.5 dpc and contribute to the septation of the atrial and ventricular chambers are small or absent. This defect compromises the normal conduction of the heart, which the authors propose is the cause of death in these embryos. The heart phenotype is expressed in only 26-35% of mutants at 9.5-10.5 dpc. At 10.5 dpc, a few of the mutant embryos die and by 11.5 dpc, roughly 50% of the mutant embryos are dead. Occasionally homozygous embryos are recovered live at 12.5 dpc but never beyond 14.5 dpc (Harrelson *et al.* 2004). Apart from the heart, other tissues in which *Tbx2* is expressed were not examined in the initial study of *Tbx2*$^{-/-}$ mice. In this chapter I analyse the eye phenotype in *Tbx2*$^{-/-}$ embryos at early stages of eye development.

In agreement with the hypothesised role for *Tbx2* in the regulation of eye growth, I present data which show an abnormally small eye size in mutants. Several mechanisms which could contribute to the small eye phenotype were therefore investigated.

Firstly, molecular analyses were performed. These included investigating the role of *Tbx2* in controlling D-V patterning genes in the eye, which if abnormal could possibly lead to a small eye size as well as affecting other aspects of eye development. Asymmetrically expressed candidates included genes examined in Chapter 3 and genes with a previously known role in eye size regulation: the gap junction protein Cx43 and the homeobox gene *Msx2*. Downregulation of Cx43 in the chick embryo and gain of function of *Msx2* in the mouse and *Drosophila* embryos respectively cause a small eye size (Becker and Mobbs 1999; Wu *et al.* 2003; Mozer 2001). Heterozygous mutations in humans, which are believed to cause loss of function or a dominant negative form of Cx43 result in oculo-dento-digital dysplasia, which is an autosomal dominant disorder characterised by defects affecting several organs including the limbs (syndactyly), craniofacial skeletal development, and the eye. The eye defects include microphthalmia, cataract, and abnormalities of the iris (Paznekas *et al.* 2003; Kjaer *et al.* 2004; Vitiello *et al.* 2005). Furthermore, *Tbx2* expression was examined in a mouse model for microphthalmia, $Chx10^{orJ/orJ}$. These mice are homozygous for a natural mutation in the *Chx10* transcription factor encoding gene, and are microphthalmic due to reduced proliferation of retinal progenitors and a progressive transdifferentiation of the neural retina into RPE (Burmeister *et al.* 1996; Rowan *et al.* 2004; Horsford *et al.* 2004). This experiment was performed to establish whether *Chx10* is upstream of *Tbx2* in a pathway that regulates eye size. Both genes are detected in the distal layer of the optic vesicle from 9.5 dpc (Liu *et al.* 1994; Holt 2003).

Secondly, cellular mechanisms that could limit the growth of the neural retina were investigated including altered retinal cell proliferation, cell death, RPE specification, and premature differentiation of retinal progenitors. To examine whether initiation of differentiation occurs prematurely in $Tbx2^{-/-}$ embryos, hence contributing to the small eye phenotype, the RMO270 and VC1.1 antibodies were used to label early differentiating neurons in 12.5 dpc mutant and wild-type embryos. RMO270 is an

intermediate neurofilament marker that labels RGCs and their processes, while VC1.1, as well as labelling fully differentiated amacrine cells, labels progenitors that later mainly differentiate into horizontal and amacrine cell fates (see Methods 2.8.1.1). The temporal spread of differentiation from the central to peripheral region of the developing eye (Dräger 1985) allowed the comparison of timing of differentiation between mutant and wild-type eyes to be conducted at 12.5 dpc, when the central but not the peripheral neural retina has normally initiated the differentiation process.

Finally, since abnormalities outside of the *Tbx2* expressing region of the optic cup were identified, the expression of *Fgf15* as a secreted factor that may convey some of the non-cell autonomous abnormalities was examined. In Chapter 3 it was established that *Fgf15* is not upstream of *Tbx2*.

5.2 Results

For examination of early eye development, embryos were dissected between 9.5-12.5 dpc, with the majority of the analysis focused at 10.5 dpc. Forty four pregnant females from heterozygous crosses yielded a total of 351 embryos. Sixty nine live embryos were homozygous for the mutated *Tbx2* allele and used in analyses here. Dying or dead embryos, which displayed pericardiac sac oedema and no heart beat or circulation at the time of dissection were discarded and not included in the analysis. Fig. 5.1 shows representative examples of the results of the genotyping PCR reactions.

Fig. 5.1 Agarose gel electrophoresis of PCR products generated from genotyping reactions of *Tbx2*$^{-/-}$ and wild-type mice

(A) The *Tbx2* wild-type coding region, depicting the seven exons of *Tbx2* (top), and the *Tbx2* mutant allele, showing the complete deletion of exon two (bottom). The primer sites used for genotyping are indicated below each allele. Primer 1 is specific for the wild-type allele, while primer 3 is specific for the mutant allele. (B) Both gels show representative 2% TAE agarose gels of genotyping PCR products. Gels are loaded with 1μg of the 2-Log DNA Ladder and 10μl (50% of the total reaction volume) of PCR reactions set up with DNA of previously known genotypes as controls and yolk sac DNA from various dissected embryos of unknown genotypes. The 180 bp product was detected in the wild-type (+/+) and mutant (+/-) controls only and indicates the existence of the wild-type allele. The 80 bp product was detected in the +/- and -/- controls only and indicates the existence of the mutant allele. In reactions where dH_2O was substituted for the DNA template, only dNTPs and primer dimers were detected (red arrowhead). Genotypes are indicated below each lane. Figure in A adapted from Harrelson *et al.* 2004.

Abbreviations: bp, base pairs; dH_2O, distilled H_2O

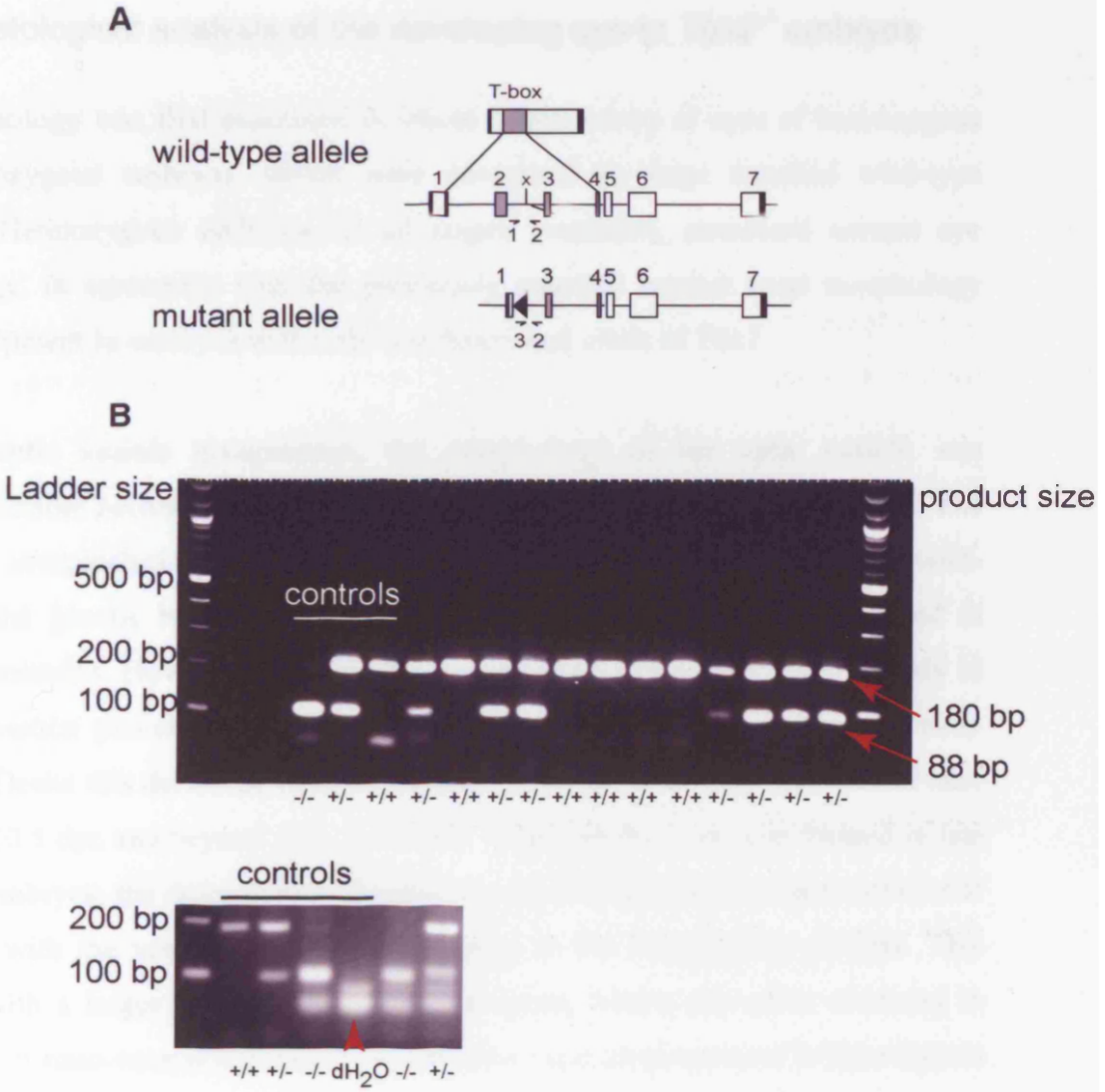
A
T-box
wild-type allele
1
2 x 3
4 5 6
7
1 2
1
3
4 5 6
7
mutant allele
3 2
B
Ladder size
product size
500 bp
controls
200 bp
100 bp
180 bp
88 bp
-/- +/- +/+ +/- +/+ +/- +/- +/+ +/+ +/+ +/+ +/- +/- +/- +/-
controls
200 bp
100 bp
+/+ +/- -/- dH2O -/- +/-

5.2.1 Histological analysis of the developing eye in *Tbx2*$^{-/-}$ embryos

Eye morphology was first examined in whole lateral views of eyes of homozygous and heterozygous embryos, which were compared to stage matched wild-type embryos. Heterozygous embryos, at all stages examined, possessed normal eye morphology, in agreement with the previously reported normal heart morphology and development in embryos with only one functional allele of *Tbx2*.

Prior to optic vesicle invagination, the morphology of the optic vesicle was indistinguishable between homozygotes and wild-type embryos (Fig. 5.2 A,B). The process of invagination was found to initiate at around ss 28-30 (10.5 dpc) in wild-types on the genetic background of the *Tbx2*$^{-/-}$ mice. The same was observed in mutant littermates. However, occasionally some mutant embryos showed a delay in the invagination process compared to somite matched wild-type embryos at early 10.5 dpc. Desite this delay, the optic cup always formed in mutants examined at later stages of 10.5 dpc and beyond (Fig. 5.2 C-H). Although the optic cup formed in late 10.5 dpc embryos, the delay in morphogenesis was also detected in some embryos at 11.5 dpc, with the ventral neural retina lagging in the invagination process. This together with a larger than normal subretinal space, which was often observed in dorsal and or naso-ventral regions of mutant optic cups (demonstrated in later figures and Fig. 5.2 F) resulted in an increased exposure of the optic stalk, which would normally be hidden behind the ventral neural retina in whole lateral views and manifested in a thicker than normal ventral neural retina in some mutants (Fig. 5.2 E,F). At 11.5 dpc, pigmentation of the RPE was also delayed in some mutants (Fig. 5.2 E,F). Other morphological abnormalities apparent after optic cup invagination included smaller eye size (Fig. 5.2 C-H; quantified in Section 5.2.2) and abnormally dense distribution of endothelial cells, which form the hyaloid vasculature, in the optic fissure region (analysed in more detail in Section 5.2.4.5). These abnormalities were never observed in wild-type littermates.

Fig. 5.2 Whole mount views of *Tbx2*$^{-/-}$ and wild type embryos at 9.5-12.5 dpc

Images show lateral views of the head of embryos. **(A)** Wild-type (+/+) embryo at 9.5 dpc, showing the optic vesicle (arrows). **(B)** Mutant (-/-) littermate of embryo depicted in A, showing similar optic vesicle morphology as in A (arrows). Optic vesicles are highlighted in dashed circles. **(C)** Wild-type embryo at 11.5 dpc showing an optic cup. **(D)** Mutant littermate of embryo in C also possessing an optic cup. **(E)** Higher magnification of the optic cup in C showing initiation of pigmentation in the dorsal half of the eye and the presence of the optic fissure in the ventral optic cup. **(F)** Higher magnification of the optic cup in D showing pigmentation in the dorsal optic cup. The ventral region appears thicker than dorsal and a large naso-ventral subretinal space (arrow) is apparent, which exposes the optic stalk that normally would be hidden in a whole mount view of a wild-type eye. Note the smaller lens compared to E. **(G)** Wild-type embryo at 12.5 dpc. **(H)** Mutant littermate of embryo in G. Scale bars: 0.5 mm.

Abbreviations: D, dorsal; dpc, days post coitus; V, ventral

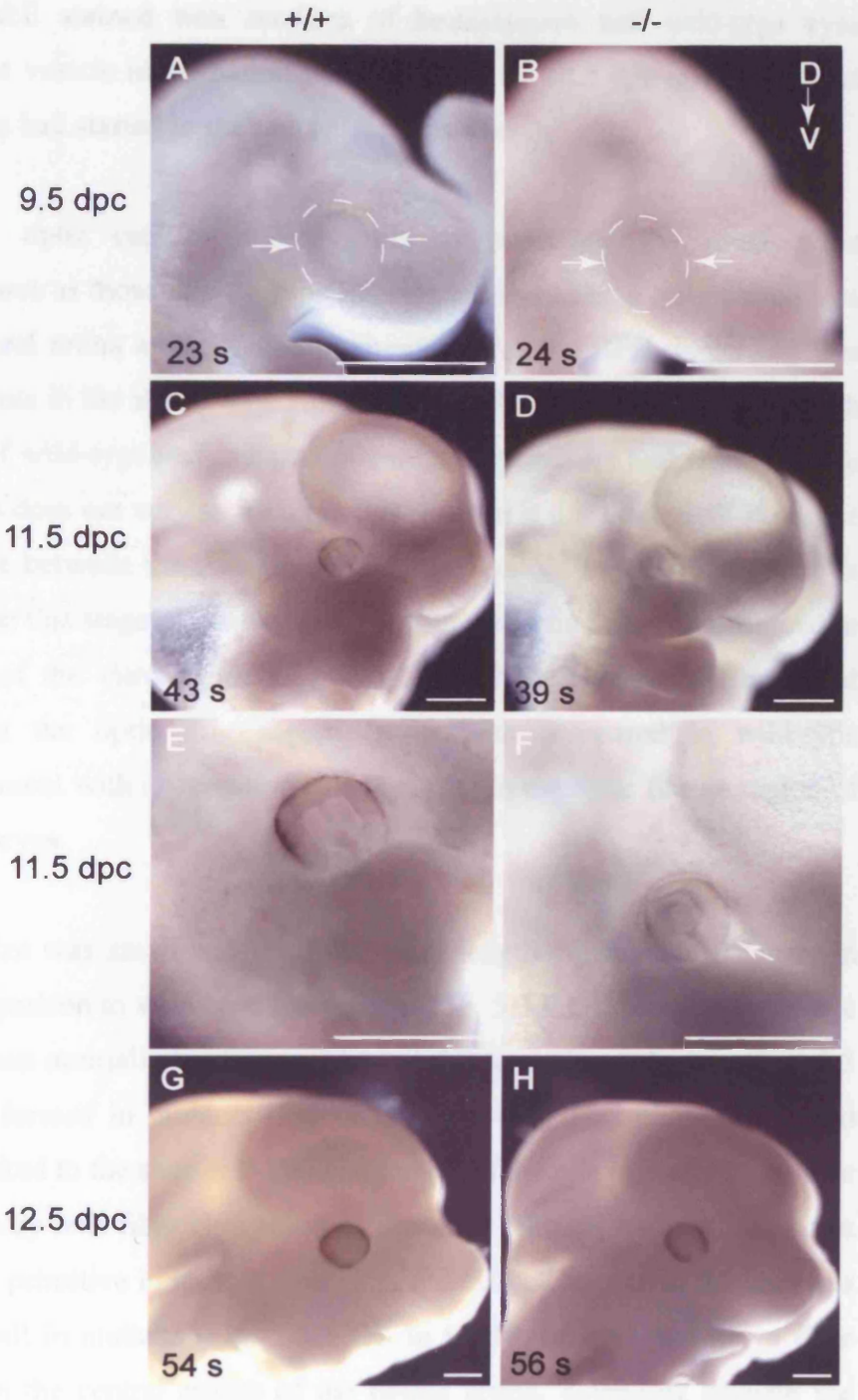
+/+
-/-
9.5 dpc
11.5 dpc
11.5 dpc
12.5 dpc
A
B
D
V
23 s
24 s
C
D
43 s
39 s
E
F
G
H
54 s
56 s

Examination of H&E stained wax sections of homozygous and wild-type eyes confirmed that optic vesicle invagination was underway at 10.5 dpc in mutants and that the neural retina had started to thicken (Fig. 5.3 A-C).

At 11.5 dpc, the optic cup in mutant embryos possessed the same gross morphological features as those of wild-type littermates, including a fully closed lens vesicle, a thick neural retina and initiated pigmentation of the RPE, indicating that the an optic cup forms in the absence of Tbx2. Figs. 5.3 D-E depict sections through the ventral region of wild-type and mutant optic cups respectively and show that the ventral neural retina does not vary so much in thickness as it does in length along the P-Di axis of the eye between the two genotypes. The hyaloid vasculature, which is normally first seen at this stage of development within the optic cup, was observed in the ventral region of the vitreous chamber (Fig. 5.3 D,E). However, it appeared unusually dense in the optic disc region in mutants compared to wild-type littermates, in agreement with observations made earlier in the optic fissure region of 10.5 dpc whole embryos.

At 12.5 dpc, eye size was small and the P-Di axial length considerably shorter in mutant eyes in comparison to wild-type littermates (Fig. 5.3 F,G). Moreover, the eye lid grooves, which can normally be distinguished at this stage in wild-types (Fig. 5.3 I, arrows) had not formed in mutants (Fig. 5.3. J, arrows). This phenotype could either be directly linked to the shorter P-Di axial length of the eye in mutants, or arise independently. Primary lens fibre elongation of posterior lens cells was advanced in wild-types, but very primitive in mutant eyes (Fig. 5.3 F,G). The size of the lens was also abnormally small in mutants (Fig. 5.3 F,G). In wild-type eyes, the nerve fibre layer was evident in the central region of the neural retina, extending through the optic disc (Fig. 5.3 F). In mutant littermates a nerve fibre layer could not be easily distinguished and there were no indications of nerve fibres extending through the optic disc (Fig. 5.3 G).

Fig. 5.3 H&E stained sections of eyes of *Tbx2*$^{-/-}$ and wild-type embryos at 10.5-12.5 dpc

All images show paraffin midline sections of 7 μm thickness cut in the transverse orientation and stained with H&E. **(A)** Initiation of optic vesicle invagination at ss 24 in a wild-type embryo (+/+), evident by the presence of a lens placode (LP) and the thickening and invagination of the distal layer of the neuroepithelium (NE). **(B,C)** Two examples of histology of the developing eye in a *Tbx2* mutant embryo (-/-) at ss 26, showing initiation of invagination and thickening of the neuroepithelium. **(D)** Optic cup at 11.5 dpc in a wild-type embryo, revealing a fully formed lens vesicle (L) and the hyaloid vasculature extending into the vitreal chamber through the optic disc (arrows). **(E)** The optic cup in a mutant embryo at 11.5 dpc, with all expected structures present including the lens, but with the shape of the optic cup being stunted along the P-Di axis (dotted line) and the hyaloid vasculature being dense in the optic disc region (arrow). **(F)** Optic cup of a 12.5 dpc wild-type embryo. The dotted line along the P-Di axis highlights the protrusion of the cup distally (see also I). Arrowhead points to elongating posterior lens cells. Presence of a nerve fibre layer (NFL) indicates differentiation in the neural retina. The hyaloid vasculature is seen in the entire vitreal chamber. **(G)** An example of an abnormal optic cup in a 12.5 dpc mutant embryo. The growth along the P-Di axis is highlighted by the dotted line (see also J). The abnormal posterior lens cells in mutant are indicated by arrowhead and the extent of the spread of the hyaloid vasculature is shown by the arrows. The nerve fibre layer was absent. **(H)** An example of the histology of an eye of a 12.5 dpc mutant embryo with a mild phenotype. The reduced growth of the eye along the P-Di axis is highlighted by the dotted line (see also K). The nerve fibre layer (arrow) and the hyaloid vasculature appeared normal. **(I-K)** Show F-H at a lower magnification. The difference in the P-Di axial length between eyes is highlighted by the black stretch of the dotted lines. Protrusion of eyes are shown by perpendicular solid lines which were drawn in relation to the protrusion of the wild-type eye. Eye lid grooves are indicated by arrows.

Abbreviations: dpc, days post coitus; Di, distal; L, lens; LP, lens placode; N, nasal; NE, neuroepithelium; NFL, nerve fibre layer; NR, neural retina; P, proximal; T, temporal; Scale bars: 0.1 mm.

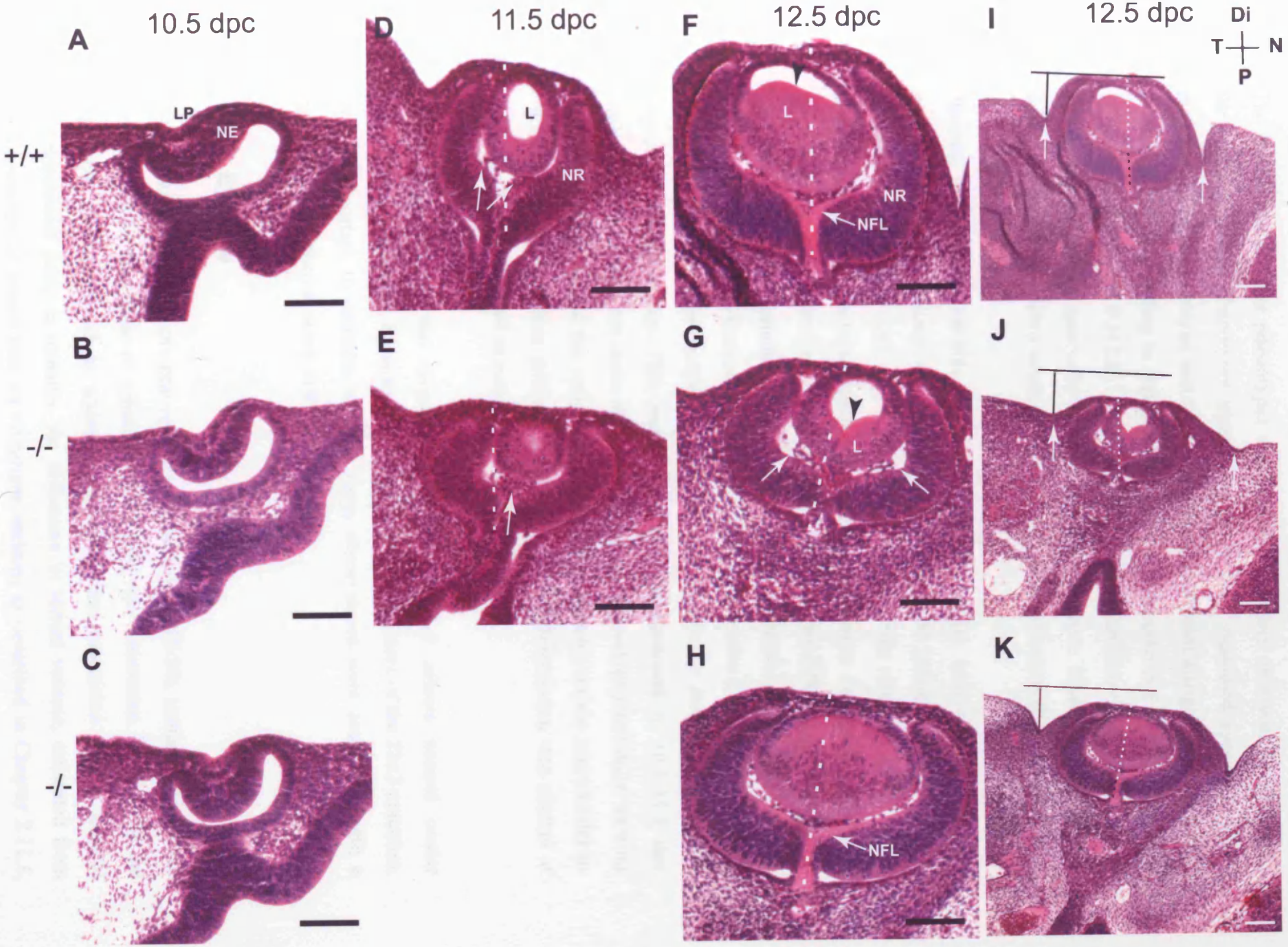
A
10.5 dpc
D
11.5 dpc
F
12.5 dpc
I
12.5 dpc
Di
T
N
P
LP
NE
+/+
L
NR
L
NR
NFL
B
E
G
J
-/-
L
C
H
K
-/-
NFL

The occurrence of these phenotypes was variable in mutant embryos. At 12.5 dpc, the above described phenotypes were observed in 8/12 examined eyes. 4/12 eyes manifested a mild phenotype and appeared normal apart from a slight decrease in the P-Di axial length resulting in less protrusion of the eye compared to wild-type eyes of littermates (Fig. 5.3 F,H,I,K; compare solid lines). Protrusion refers to the extent to which eyes jut out externally beyond other facial tissue. Mutant eyes with the severe phenotype protruded much less than wild-type counterparts (Fig. 5.3 I,J).

Bearing in mind the variable expressivity of phenotype, examination of whole embryos and H&E stained sections of eyes through the period of optic vesicle invagination and early optic cup development revealed that although *Tbx2*$^{-/-}$ optic cups possessed all structural features expected at all stages examined, they were smaller in size than wild-type optic cups. As well as a size difference, the shape of the optic cup was abnormal with a shorter P-Di axial length, which made mutant optic cups protrude less than wild-type optic cups in littermates (Fig. 5.3 D,F,I versus E,G,J). Furthermore, the hyaloid vasculature was abnormally dense in the ventral aspect of the optic cup. This phenotype was most profound in 10.5-11.5 dpc embryos. At 12.5 dpc, the nerve fibre layer was poorly developed and there were no fibres extending beyond the optic disc in mutants. The lens vesicle was smaller in mutants and appeared less differentiated, while RPE differentiation was normal at 12.5 dc, although delayed in some embryos at 11.5 dpc.

These data indicate that targeted disruption of *Tbx2* affects normal ocular development. However, because of the embryonic lethal nature of the *Tbx2* mutation, it was important to establish whether these observations were associated with a general developmental delay in mutant embryos.

5.2.2 Eye size

Soon after the initiation of optic vesicle invagination (ss 28-30), mutant retinae were smaller in size than those of somite matched wild-type littermates. To quantify the eye size phenotype and to address whether it was associated with a general developmental delay in mutants, the difference in retinal volume, estimated from measurements of retinal area on vibratome sections as described in Chapter 2.11.1,

was compared to the difference in head length between mutant and wild-type embryos at ss 33-35 (10.5 dpc). Head length was measured as an indicator of general growth retardation. Although like crown-rump length, head length does not show an exact linear trend with embryonic age, it is commonly used as a measure of growth during embryogenesis and does show an increase with embryonic age (Brown 1990).

Head length measurements did not differ significantly between mutant and wild-type embryos (P= 0.352 by independent samples t-test, unequal variance; Fig. 5.4 A). However, measurements of retinal volume showed that mutant retinae had a significantly smaller volume than wild-type retinae (P= 0.007 by independent samples t-test; Fig. 5.4 B; Table 5.1).

Table 5.1 Head length and retinal volume mean values ± 1.s.d. in ss 33-35 *Tbx2*$^{-/-}$ mutant and wild-type embryos

		n.	Mean	± 1 s.d.
Head length	wild-type	10	2.10 mm	0.07
	Mutant	14	2.14 mm	0.15
Retinal volume	wild-type	7	6.14×10^{-3} mm^3	0.48×10^{-3}
	Mutant	10	5.06×10^{-3} mm^3	0.82×10^{-3}

These data suggest that the small retinal volume in *Tbx2*$^{-/-}$ embryos is not associated with a general developmental delay and is likely to be occurring as a direct effect of the loss of Tbx2 in the developing eye.

Fig. 5.4 Quantification of eye size and head size in mutant and wild-type embryos

(A) Bars represent the mean head length ± 1 s.d. in 10.5 dpc mutant and wild-type embryos (ss33-35). No significant difference was detected between the two genotypes analysed by the independent samples t-test, unequal variances (n= number of embryos). **(B)** Bars represent mean retinal volume ± 1 s.d. in 10.5 dpc mutant and wild-type embryos (ss33-35). Retinal volume was significantly smaller in mutant eyes compared to stage matched wild-types (independent samples t-test, n= number of eyes).

Abbreviations: ss, somite stage

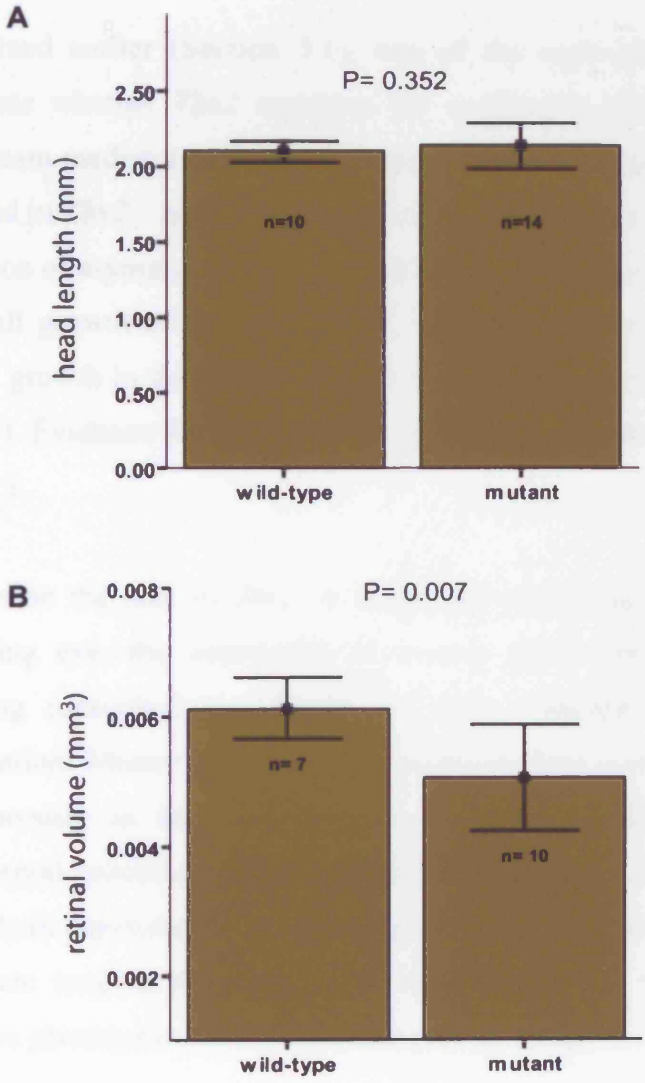
A
P= 0.352
head length (mm)
2.50
2.00
1.50
1.00
0.50
0.00
n=10
n=14
wild-type
mutant
B
P= 0.007
retinal volume (mm3)
0.008
0.006
0.004
0.002
n= 7
n= 10
wild-type
mutant

5.2.3 Molecular patterning along the D-V axis of the optic cup

As outlined earlier (Section 5.1), one of the main aims of this Chapter was to investigate whether *Tbx2* regulates the expression of D-V patterning genes as a downstream mediator of Bmp4 signalling. Moreover, given the small eye phenotype identified in *Tbx2*$^{-/-}$ mice, disruption of D-V patterning was investigated as abnormal expression of asymmetrically expressed genes may cause a defect in the coordination of overall growth of the optic cup. This hypothesis is supported by evidence that regional growth in the developing heart is linked to regional gene expression (Cai *et al.* 2005). Evidence for the existence of regional growth in the eye was discussed in Chapter 1.

To examine the role of *Tbx2* in molecular patterning along the D-V axis of the developing eye, the expression of several genes previously implicated in D-V patterning (described in Chapter 3) were examined by whole mount *in situ* hybridisation. Mutant and wild-type embryos were somite matched and processed simultaneously in the same tube to minimise variability of signal due to the experimental procedure. When possible and indicated in the text, littermates were used in both experimental groups. Control embryos possessing two normal copies of *Tbx2* were used in the majority of experiments, but where stated, heterozygotes which are phenotypically normal were used as controls.

Apart from serving as dorsal or ventral retinal markers, other reasons also lay behind the choice of the panel of genes selected for the analysis presented in this section. The panel includes *Bmp4*, investigated for the possibility of a feed-back loop, in which *Tbx2* exerts regulation on *Bmp4* expression in the dorsal eye. *Msx2* was also of interest as its overexpression in the mouse eye and likewise the misexpression of its homologue *Msh* in the *Drosophila* eye cause microphthalmia in mice and a small eye phenotype in *Drosophila* (Wu *et al.* 2003; Mozer 2001). *EphrinB2* was also analysed due to its role in the regulation of RGC axonal projections from the dorsal eye in *Xenopus* and its regulation by Tbx5 in the developing chick eye (see Chapter 1.4.2). Analysis of *Tbx3* and *Tbx5* expression served to investigate whether the T-box genes of the eye regulate each other, while *Vax2* was selected as a ventral neural retinal

marker. Finally, *Tbx2* mRNA expression was examined to trace cells that would have expressed Tbx2 in order to investigate their fate.

Bmp4

Expression of *Bmp4* in the dorsal neural retina was similar in mutant and wild-type eyes at 10.5 dpc (n= 6 eyes per genotype) and 11.5 dpc (n= 2 -/- eyes, 6 +/+ eyes; Fig. 5.5 A-D). However, *Bmp4* expression in the maxillary process of the first branchial arch and in the nasal process was much reduced in mutants at 10.5 dpc, and remained more restricted also at 11.5 dpc compared to wild-types (Fig. 5.5 A-D).

Msx2

No difference was observed in *Msx2* expression between wild-type and mutant optic cups at 10.5 dpc (n= 4; Fig. 5.5 E,F), suggesting that *Tbx2* is not upstream of *Msx2* expression during mouse eye development and that Bmp4 regulation of *Msx2* is normal in $Tbx2^{-/-}$ eyes.

ephrinB2

The colourimetric reaction of the *ephrinB2* whole mount *in situ* hybridisation experiment was stopped after two hours, at which point all embryos were photographed, and the reaction was re-started and allowed to proceed for a further three hours with half of the embryos, to ensure full detection of *ephrinB2* expression. In this experiment embryos with normal and heterozygous genotypes were used as controls.

After two hours, *ephrinB2* expression in wild-type eyes was restricted to the anterior edges of the invaginating lens epithelium and to the dorsal neural retina and RPE (Fig. 5.6 A,C). In mutants, *ephrinB2* was still localised to the dorsal neural retina and RPE, but in comparison to wild-types, appeared broader. Moreover, it was detected in the entire invaginating lens epithelium (Fig. 5.6 B,D; n= 5/6). After longer development of the colour reaction, the signal detected in the invaginating lens epithelium appeared spatially similar in whole mount and section views of both genotypes (Fig. 5.6 E,F). The signal intensity in the neural retina of overdeveloped embryos was still higher and expression was broader in mutant retinae compared to wild-types (Fig. 5.6 E,F see arrowheads).

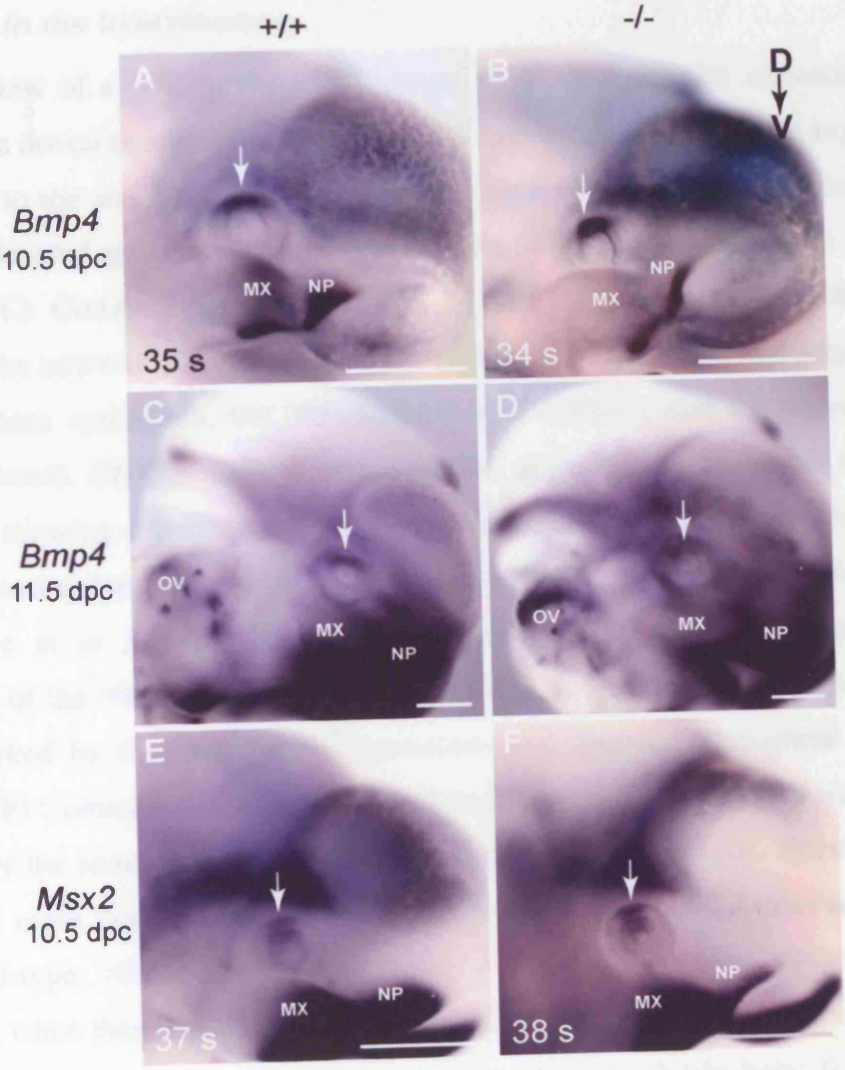
+/+
-/-
A
B
D
V
Bmp4
10.5 dpc
MX
NP
35 s
34 s
C
D
Bmp4
11.5 dpc
OV
MX
NP
E
F
Msx2
10.5 dpc
37 s
38 s

Fig. 5.5 *Bmp4* and *Msx2* expression in *Tbx2*$^{-/-}$ and wild-type eyes by whole mount *in situ* hybridisation

All images depict lateral views of the head of embryos. **(A)** 10.5 dpc wild-type (+/+) embryo at ss 35 showing the normal pattern of expression of *Bmp4*, including the dorsal optic cup expression (arrow). Other sites of expression in picture include the maxillary (MX) and nasal (NP) processes. **(B)** 10.5 dpc mutant (-/-) embryo at ss 34, showing similar *Bmp4* expression to wild-type in the dorsal neural retina (arrow). In the maxillary and nasal processes, its expression was more restricted than normal. **(C)** *Bmp4* expression in an 11.5 dpc wild-type embryo. Expression was detected in the dorsal neural retina (arrow), the maxillary and nasal processes. **(D)** 11.5 dpc mutant embryo showing spatially normal *Bmp4* expression in the dorsal neural retina (arrow). **(E)** 10.5 dpc wild-type embryo at ss 37 hybridised with the *Msx2* probe. *Msx2* expression was detected in the dorsal neural retina (arrow) and dorsal anterior lens epithelium. **(F)** Mutant embryo at ss 38 showing normal *Msx2* expression. Scale bars: 0.5 mm

Abbreviations: D, dorsal; MX, maxillary process of the first pharyngeal arch; NP, nasal process; OV, otic vesicle; ss, somite stage; V, ventral

.

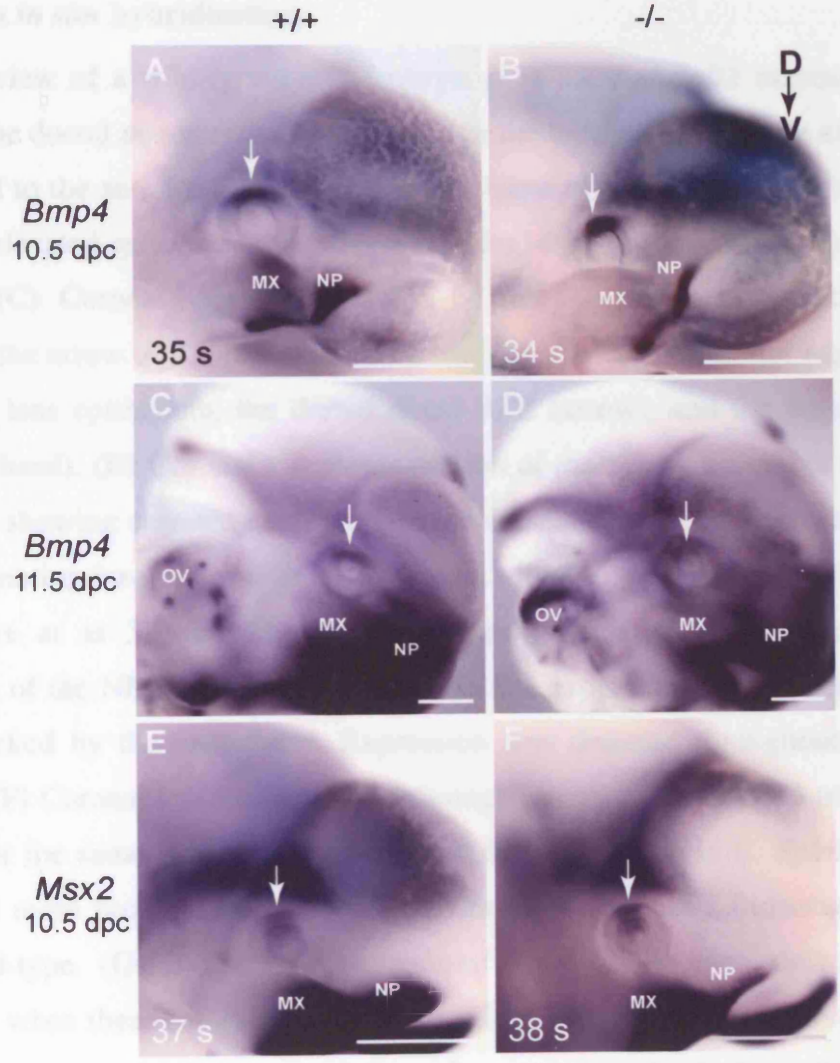
+/+
-/-
Bmp4
10.5 dpc
Bmp4
11.5 dpc
Msx2
10.5 dpc
A
B
C
D
E
F
D
V
MX
NP
OV
35 s
34 s
37 s
38 s

Fig. 5.6 *ephrinB2* expression in *Tbx2*$^{-/-}$ and wild-type eyes at 10.5 dpc by whole mount *in situ* hybridisation

(A) Lateral view of a wild-type (+/+) embryo at ss 33. *EphrinB2* expression was detected in the dorsal neural retina (arrow) and in the lens placode, where expression was confined to the anterior portion. **(B)** Lateral view of a mutant (-/-) embryo at ss 33 showing elevated *ephrinB2* expression in the dorsal neural retina (arrow) and lens epithelium. **(C)** Coronal vibratome section of the eye in A through the plane indicated by the arrow. *EphrinB2* expression was detected in the anterior edges of the invaginating lens epithelium, the dorsal distal RPE (arrow), and the dorsal neural retina (arrowhead). **(D)** Coronal vibratome section of the eye in B through the plane of the arrow, showing elevated expression in the dorsal neural retina (arrowhead) and in the invaginating lens epithelium. **(E)** Coronal vibratome section through another wild-type eye at ss 33 showing *ephrinB2* expression after a longer period of development of the NBT/BCIP colour reaction. The expression in the dorsal neural retina is marked by the arrowhead. Expression was detected throughout the lens epithelium. **(F)** Coronal vibratome section through a mutant eye at ss 33 treated and developed for the same length of time as the wild-type section in E. *EphrinB2* was strongly and more broadly expressed in the dorsal neural retina (arrowhead) than seen in wild-type. **(G-H)** Show whole mount views of the eyes shown in E-F respectively, when these embryos had been developed for as long as embryos shown in A-B, prior to overdevelopment of the colour reaction. Scale bars: 0.5 mm in A,B,G,H and 0.1 mm in C-F

Abbreviations: D, dorsal; LE, lens epithelium; MN, mandibular process of the first pharyngeal arch; MX, maxillary process of the first pharyngeal arch; NP, nasal process; NR, neural retina; RPE, retinal pigment epithelium; ss, somite stage; V, ventral.

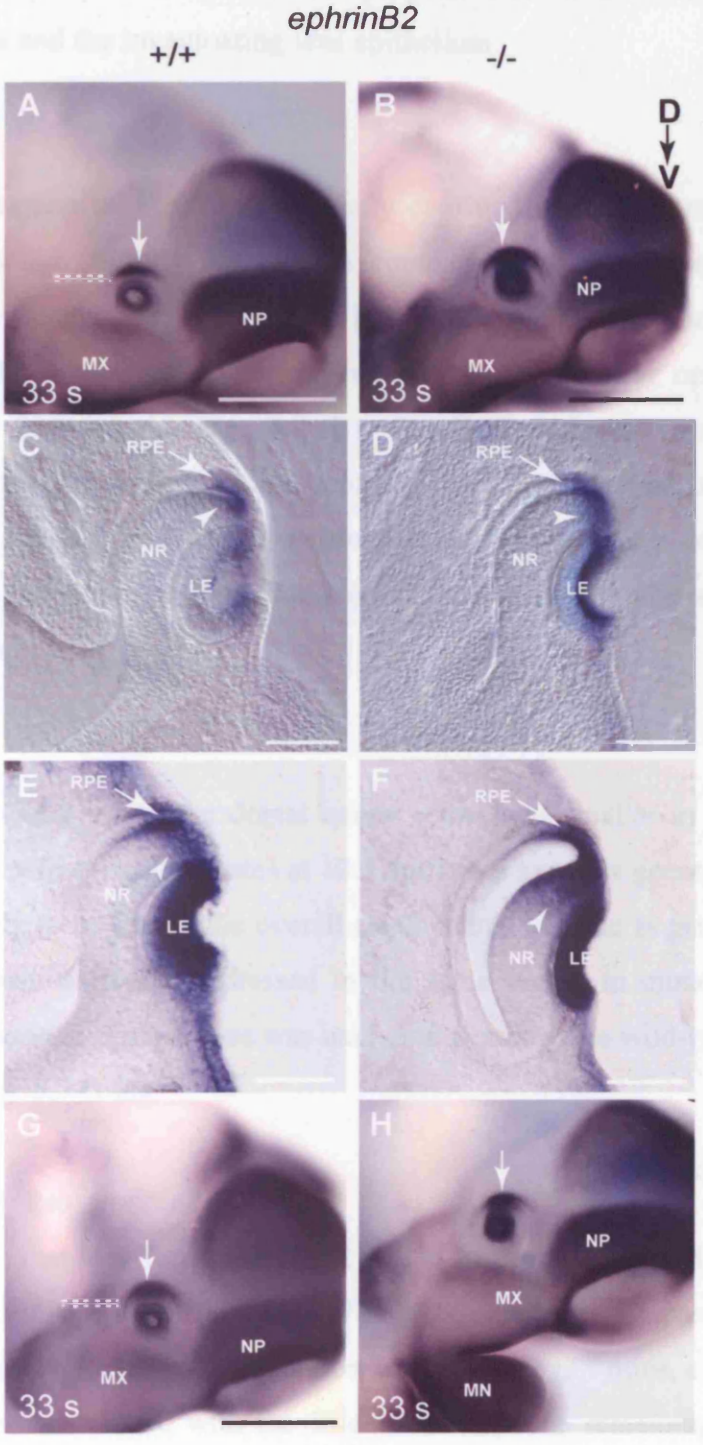
ephrinB2
+/+
-/-
A
B
D
V
NP
MX
33 s
C
RPE
NR
LE
D
E
F
G
H
MN

These data suggest that *ephrinB2* levels may be upregulated in the absence of Tbx2 in both the neural retina and the invaginating lens epithelium.

Vax2

At 10.5 dpc, the expression of *Vax2* was correctly confined to the ventral neural retina in mutants although slightly reduced in comparison to wild-type somite matched littermates (n= 6 eyes per genotype; Fig 5.7 A-D). Note the abnormally large space between the inner and outer layers of the naso-ventral optic cup, mentioned previously (asterisk in Fig. 5.7 B). As *Vax2* induces ventral eye properties, this shows that the ventral neural retina is correctly specified in $Tbx2^{-/-}$ embryos but may gradually lose *Vax2* expression in the absence of Tbx2. Alternatively, the smaller *Vax2* expression domain may be due to the reduced size of the ventral neural retina.

Tbx5 and *Tbx3*

The expression domain of *Tbx5* in the dorsal neural retina was smaller in mutants than in somite matched wild-type littermates at 10.5 dpc (n= 6 eyes per genotype Fig. 5.7 E-F). This is unlikely to be due to the overall small retinal volume as genes such as *Msx2*, and *Bmp4* were normally expressed in the same region in mutant eyes. Moreover, *Tbx3* expression in mutant eyes was unaltered compared to wild-types (n= 4 eyes per genotype; Fig. 5.7 G-H).

Detection of cells destined to express Tbx2

Tracing of mutant cells, that lack functional Tbx2 due to incomplete transcription of *Tbx2* mRNA, was performed using a full length *Tbx2* RNA probe encompassing the entire cDNA, including the 5' end. In the mutation carried by $Tbx2^{-/-}$ mice, exon two and part of exon one were deleted, with the 5' end of exon one remaining intact, which made detection of transcripts with the full length probe possible. This experiment revealed that the population of cells in the dorsal neural retina that would normally be expressing *Tbx2* were present in their normal location and in an apparently normal quantity in 35-36 ss (10.5 dpc) embryos (n= 4; Fig. 5.7 I,J).

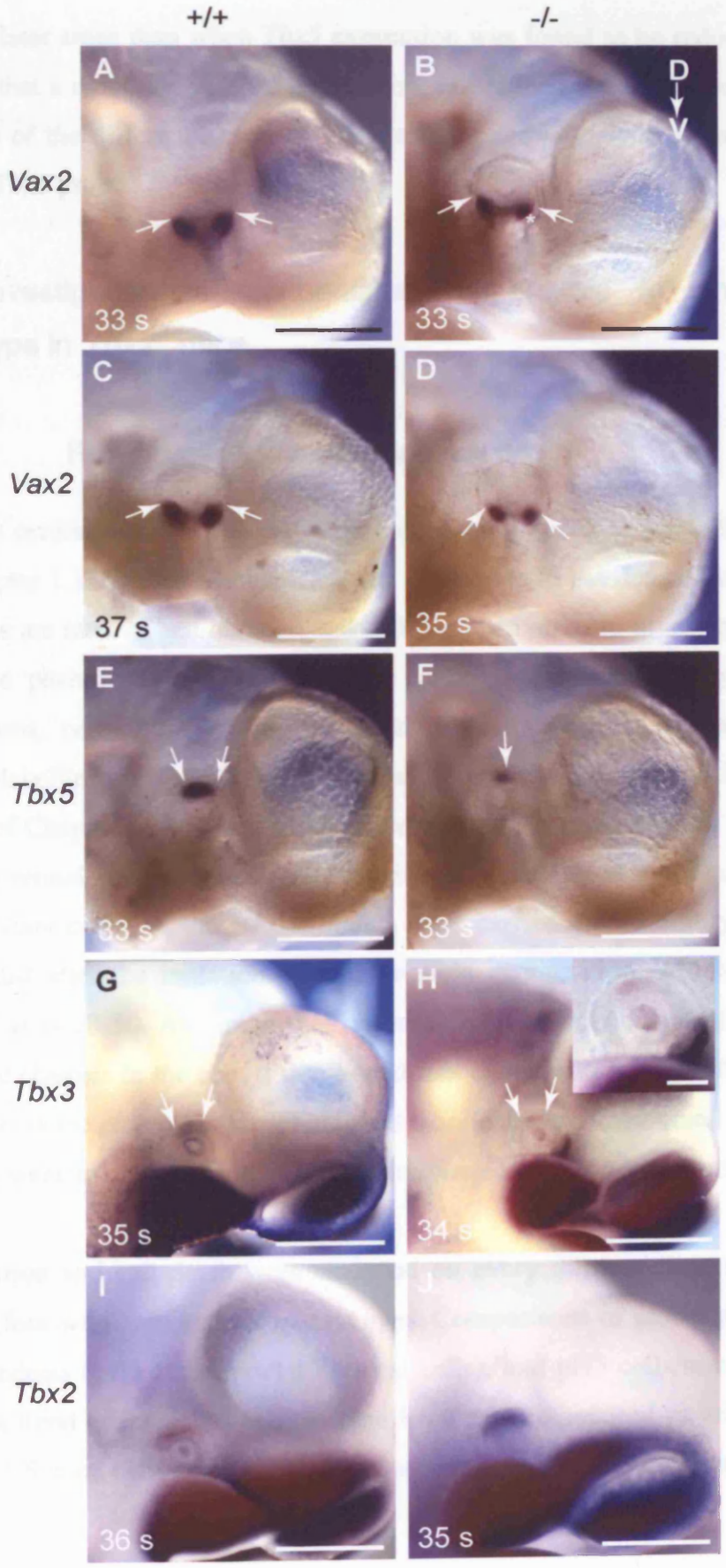
+/+
-/-
Vax2
Vax2
Tbx5
Tbx3
Tbx2
A
B
D
C
D
E
F
G
H
I
J
33 s
33 s
37 s
35 s
33 s
33 s
35 s
34 s
36 s
35 s

This is a later stage than when *Tbx5* expression was found to be reduced and further supports that a reduction in *Tbx5* expression, rather than diminished cell numbers, is the cause of the difference seen between mutant and wild-type embryos hybridised with the *Tbx5* probe.

5.2.4 Investigation of mechanisms responsible for the eye size phenotype in *Tbx2*$^{-/-}$ mice

5.2.4.1 Retinal cell proliferation and cell death

There are several mechanisms that if perturbed could result in a small eye phenotype (see Chapter 1.1.3). Two mechanisms that contribute to the determination of growth of a tissue are rates of cell division and cell death. In order to investigate whether the small eye phenotype in *Tbx2*$^{-/-}$ mice is caused by defects in any of these two mechanisms, cell division and cell death by apoptosis were analysed by pH3 immuno-labelling and the TUNEL assay respectively as described in Sections 2.8.1.3 and 2.9 of Chapter 2. As eye size and morphology appeared normal at optic vesicle stage but retinal volume was already significantly smaller at optic cup stage (ss 33-35) in mutant embryos, these experiments were carried out on embryos at ss 30-31. This is just after the initiation of optic vesicle invagination, which in these mice occurred at ss 28-30. Assuming that observable changes in morphology lag behind molecular changes in the cell, it was hoped that changes in cell proliferation and cell death were detected prior to morphological manifestation of the small eye phenotype. Embryos were somite matched in order to minimise between embryo variability.

Cell division and cell death were analysed on every third midline section (12 μm thick) in four wild-type and six mutant eyes. Comparisons of global pH3 cell counts, mitotic indices (pH3 cells divided by total cells), and pH3 cells/mm^2 of the retinae showed a trend of increased cell division in mutants compared to wild-types (Table 5.2; Fig. 5.8; total cells counted= 2189 in wild-types and 2990 in mutants).

Fig. 5.8 Cell proliferation detected by immunohistochemistry with an M-phase marker of the cell cycle

Pictures depict midline frozen sections cut in the coronal plane. **(A,B)** Wild-type eye labelled with anti phospho-histone H3 (pH3, green), showing dividing cells of the ventricular surface of the neural retina and counterstained with propidium iodide (PI, red). **(C,D)** Mutant eye labelled with anti-pH3 (green) and stained with PI (red) showing dividing cells at the ventricular surface also in the mutant retina. Dotted lines outline the ventral neural retina. Arrowheads highlight dividing cells (in mutant eye) in the ventral mesenchyme in which *Tbx2* is normally expressed. The displaced RPE in pictures of the mutant eye is due to a sectioning artefact. **(E)** Scatter plot of the number of pH3 positive cells per section in mutant (n= 14) and wild-type (n= 8) eyes from 4 and 6 eyes respectively. **(F)** Scatter plot of the mitotic indices per section. Data was analysed with a One-Way ANOVA in E (P= 0.15) and with an ANCOVA in F (P= 0.1) with the total number of cells per section included as a covariate. Scale bars: 50 μm.

Abbreviations: D, dorsal; LE, lens epithelium; NR, neural retina; s, somite pairs; V, ventral

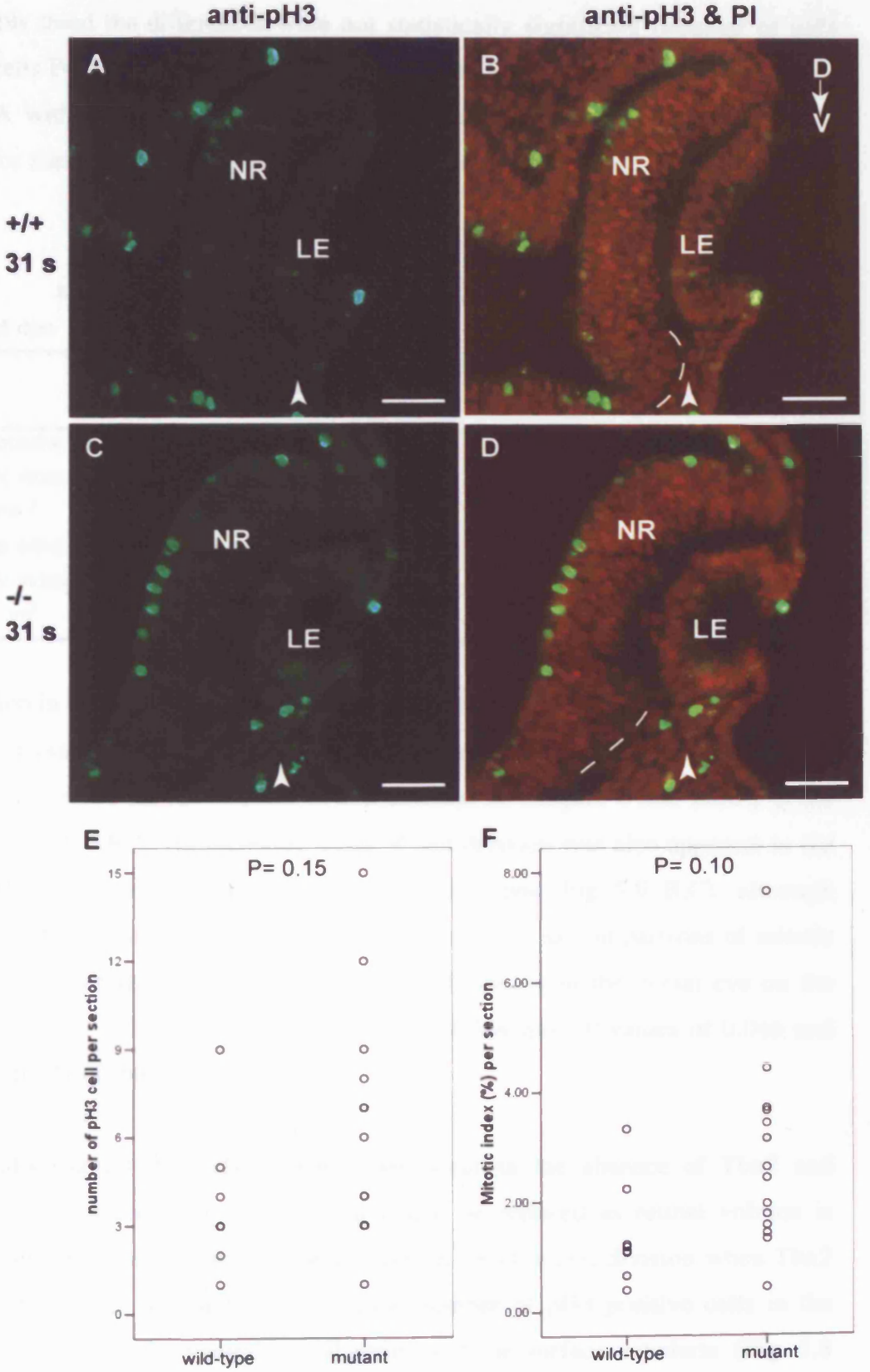
anti-pH3
anti-pH3 & PI
A
B
C
D
NR
LE
+/+
31 s
-/-
31 s
D
V
E
F
P= 0.15
P= 0.10
number of pH3 cell per section
Mitotic index (%) per section
wild-type
mutant
0
3
6
9
12
15
0.00
2.00
4.00
6.00
8.00

Despite this trend the differences were not statistically significant (number of pH3 positive cells P= 0.15, by One-Way ANOVA, Table 5.3; mitotic indices P= 0.10 by ANCOVA with the total cell number per section incorporated as a covariate to account for the effect of cell number on the number of mitotic cells, Table 5.4; P= 0.12).

Table 5.2 Mean counts of mitotic cells and indices in *Tbx2*$^{-/-}$ mutant and wild-type retinae at early 10.5 dpc.

	Mean ± 1 s.d.	
	wild-type (8 sections)	mutant (14 sections)
global pH3 positive cells	3.8 ± 2.4	6.1 ± 3.9
global mitotic index	1.4 ± 0.9	2.8 ± 1.8
global pH3/mm^2	197 ± 131	302 ± 179
dorsal pH3 positive cells	2 ± 1.4	4 ± 2.4
dorsal mitotic index	1.5 ± 1.2	2.9 ± 1.8
dorsal pH3/mm^2	181 ± 139	322 ± 179

Cell division in the dorsal eye only was also compared between genotypes, as *Tbx2* is expressed dorsally (Table 5.2; Fig. 5.9). For this purpose, the eye was divided as previously described for the analysis of cell division in Chapter 4 and shown in the schematic in Fig. 5.9 A. An increased trend of cell division was also apparent in the dorsal neural retina in mutants compared to wild-types (Fig 5.9 B,C), although comparisons of cell counts by One-Way ANOVA as well as comparisons of mitotic indices by incorporation of the effect of total cell number in the dorsal eye on the number of mitotic cells in the dorsal eye by ANCOVA gave P-values of 0.046 and 0.05 respectively (Table 5.5 and 5.6).

These results suggest that cell division does occur in the absence of Tbx2 and contrary to expectations that cell division would be reduced as retinal volume is reduced in mutants, there appears to be an upward trend in cell division when Tbx2 is lacking in the eye. Also note the increased number of pH3 positive cells in the mesenchyme between the ventral neural retina and the surface ectoderm (Fig. 5.8 B,D arrowheads), where *Tbx2* is normally expressed as shown in Chapter 3 (Fig. 3.5 E).

Fig. 5.9 Cell proliferation in the dorsal neural retina of *Tbx2*$^{-/-}$ and wild-type eyes

(A) Schematic diagram of the developing eye at 10.5 dpc. The dorsal region of the neural retina was demarcated as depicted by dotted lines. **(B,C)** Scatter plots of the number of pH3 positive cells counted per section in the dorsal region of mutant (n= 14) and wild-type (n= 8) retinae from 4 and 6 eyes respectively. Data was analysed with a One-Way ANOVA in B (P= 0.046) and with an ANCOVA in C (P= 0.05) with the total number of cells in the dorsal neural retina per section included as a covariate

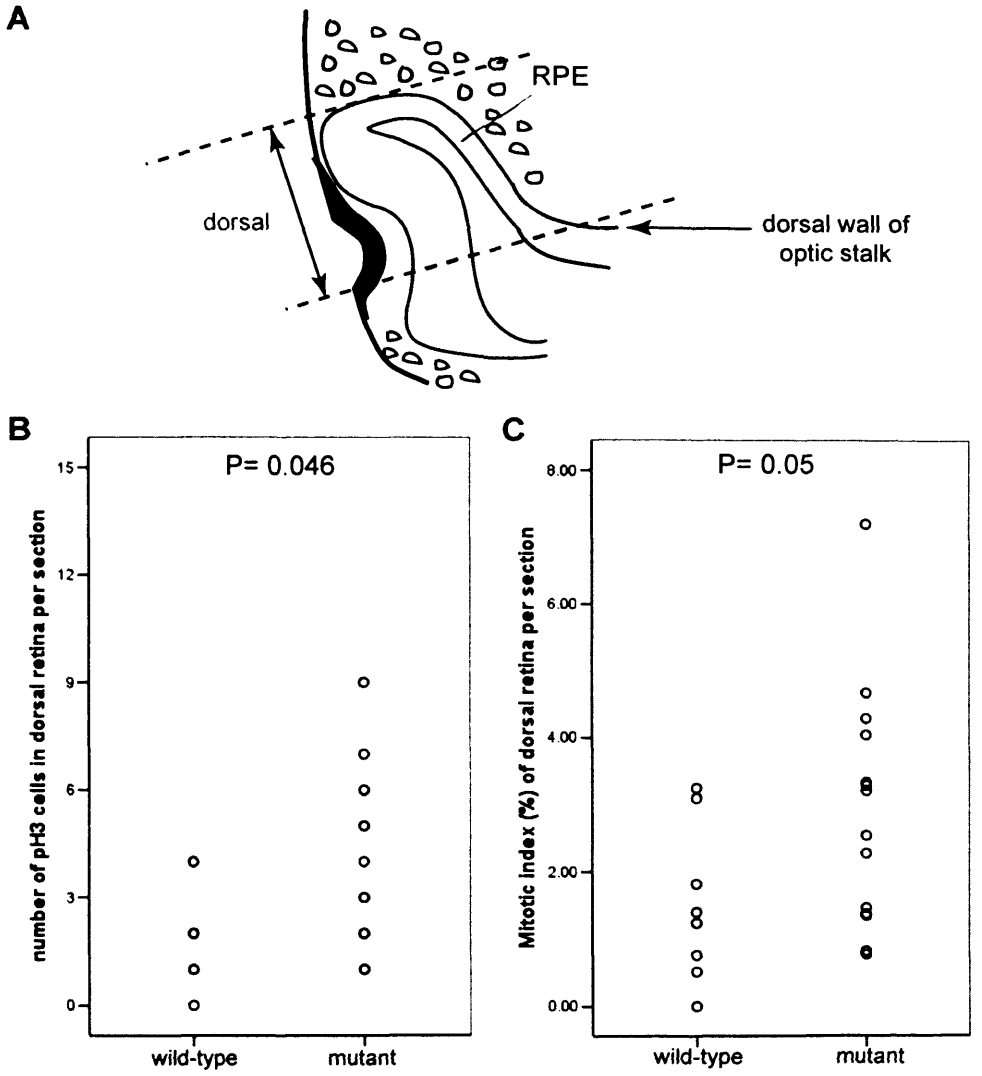
A
RPE
dorsal
dorsal wall of
optic stalk
B
P= 0.046
number of pH3 cells in dorsal retina per section
15
12
9
6
3
0
wild-type
mutant
C
P= 0.05
Mitotic index (%) of dorsal retina per section
8.00
6.00
4.00
2.00
0.00
wild-type
mutant

Table 5.3: One-Way ANOVA for the comparison of global pH3 labelled cells in *Tbx2*$^{-/-}$ mutant and wild-type retinae

Dependent Variable: n. pH3 labelled cells per section

Source	Type III Sum of Squares	df	Mean Square	F	Sig.
Corrected Model	27.435(a)	1	27.435	2.263	.148
Intercept	491.071	1	491.071	40.513	.000
genotype	27.435	1	27.435	2.263	**.148**
Error	242.429	20	12.121		
Total	871.000	22			
Corrected Total	269.864	21			

a R Squared = .102 (Adjusted R Squared = .057)

Table 5.4 ANCOVA table for the comparison of global pH3 labelled cells in *Tbx2*$^{-/-}$ mutant and wild-type retinae, with Total cell number incorporated as a covariate

Dependent Variable: n. pH3 labelled cells per section

Source	Type III Sum of Squares	df	Mean Square	F	Sig.
Corrected Model	38.750(a)	2	19.375	1.593	.229
Intercept	.330	1	.330	.027	.871
Total cell number	11.315	1	11.315	.930	**.347**
genotype	37.146	1	37.146	3.054	**.097**
Error	231.114	19	12.164		
Total	871.000	22			
Corrected Total	269.864	21			

a R Squared = .144 (Adjusted R Squared = .053)

Table 5.5: One-Way ANOVA for the comparison of dorsal pH3 labelled cells in *Tbx2*$^{-/-}$ mutant and wild-type retinae

Dependent Variable: n. pH3 labelled cells in dorsal retina per section

Source	Type III Sum of Squares	df	Mean Square	F	Sig.
Corrected Model	20.364(a)	1	20.364	4.525	.046
Intercept	183.273	1	183.273	40.727	.000
genotype	20.364	1	20.364	4.525	**.046**
Error	90.000	20	4.500		
Total	346.000	22			
Corrected Total	110.364	21			

a R Squared = .185 (Adjusted R Squared = .144)

Table 5.6 ANCOVA table for the comparison of dorsal pH3 labelled cells in *Tbx2*$^{-/-}$ mutant and wild-type retinae, with n.dorsal cell number incorporated as a covariate

Dependent Variable: n. pH3 labelled cells in dorsal retina per section

Source	Type III Sum of Squares	df	Mean Square	F	Sig.
Corrected Model	20.674(a)	2	10.337	2.190	.139
Intercept	2.605	1	2.605	.552	.467
Dorsal cell number	.310	1	.310	.066	**.800**
genotype	20.608	1	20.608	4.366	**.050**
Error	89.690	19	4.721		
Total	346.000	22			
Corrected Total	110.364	21			

a R Squared = .187 (Adjusted R Squared = .102)

Fig. 5.10 Analysis of cell death in *Tbx2*$^{-/-}$ and wild-type eyes, using the TUNEL assay

Pictures depict midline frozen sections cut in the coronal plane. **(A,B)** Wild-type eye labelled with the TUNEL assay (green), showing the pattern of apoptosis in the eye. **(C,D)** Mutant eye labelled with the TUNEL assay (green) showing a similar pattern of apoptosis. Sections were counterstained with PI (red). Scale bars: 50 μm.

Abbreviations: D, dorsal; LE, lens epithelium; NR, neural retina; RPE, retinal pigmented epithelium; s, somite pairs; V, ventral.

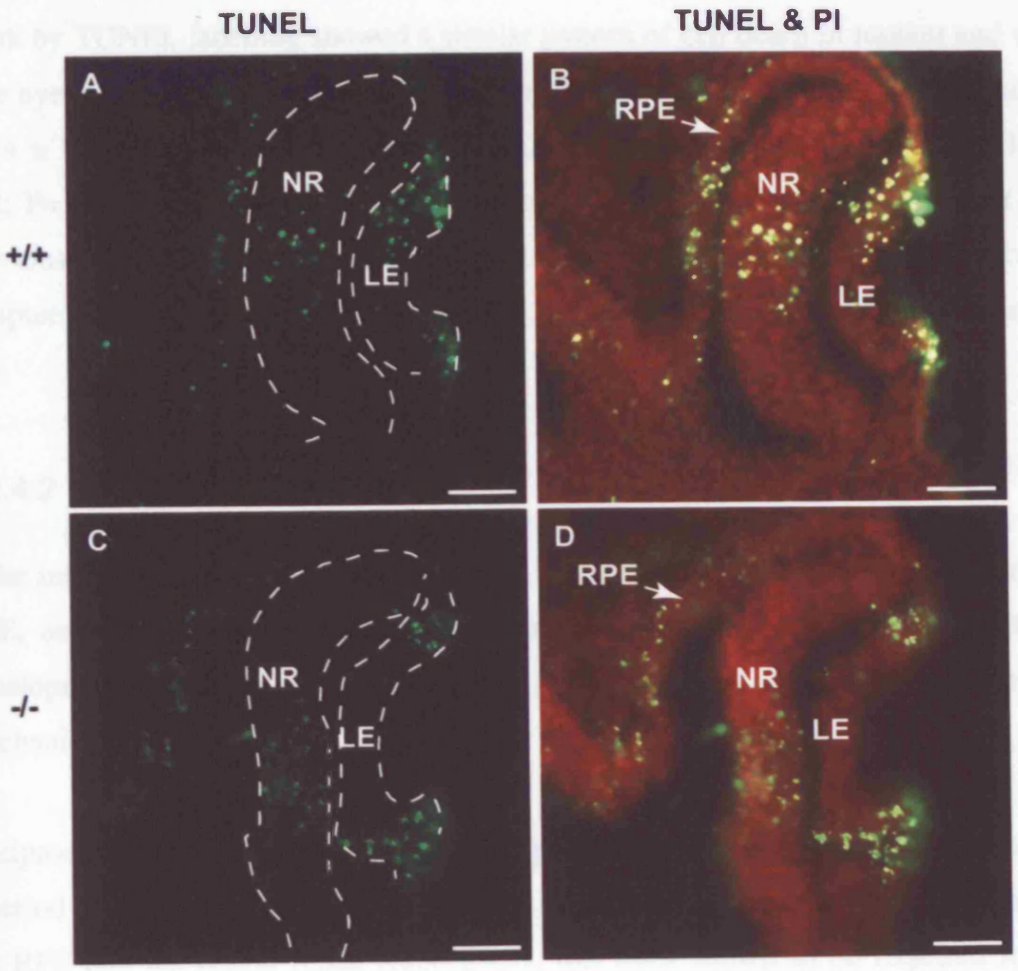
TUNEL
TUNEL & PI
A
B
C
D
+/+
-/-
NR
LE
RPE
NR
LE
RPE
NR
LE
NR
LE

In the ventral extra-ocular mesenchyme however, where *Tbx2*, but none of the other T-box genes is expressed (Chapter 3, Fig. 3.4), dividing cells were more abundant in mutants compared to wild-types (Fig. 5.8 B,D, arrowheads). Examination of cell death by TUNEL labelling showed a similar pattern of cell death in mutant and wild-type eyes (Fig. 5.10; wild-type n= 18, mean TUNEL= 24 ± 22, mean TUNEL/mm^2= 1214 ± 1029; mutant: n= 11, mean TUNEL= 17 ± 15, mean TUNEL/mm^2= 1126 ± 912; P= 0.358 by independent samples t-test). This pattern was in agreement with previous descriptions of the pattern of cell death in the optic cup at 10.5 dpc (see Chapter 1.2.4), suggesting that, at this stage, apoptosis occurs normally in the mutant eye.

5.2.4.2 RPE specification

If the initial pool of retinal progenitor cells is smaller due to mis-specification of the RPE, one could expect this to result in an overall smaller retinal volume later in development even if there is normal progression of other growth limiting mechanisms.

Reciprocal antagonism between the transcription factors *Mitf* and *Chx10*, which after a period of co-expression in the distal optic vesicle, become exclusively expressed in the RPE and the neural retina respectively, has been shown to be required for the maintenance of neural retina versus RPE fates (Horsford *et al.* 2004; Rowan *et al.* 2004). The pigment-cell specific gene *Silver* (*Pmel17*, *gp87*- Mouse Genome Informatics) encodes a transmembrane protein, which is detected in the presumptive RPE already at 9.5 dpc and is not expressed in *Mitf*$^{mi/mi}$ mutants (Baxter and Pavan 2003). It is therefore thought to be an early marker of the RPE under the regulation of *Mitf*. To investigate a possible role for *Tbx2* in the formation of the dorsal boundary between the RPE and the neural retina, and to examine whether the RPE domain is expanded at the expense of the neural retina, thereby diminishing the neural retinal progenitor pool, expression of *Silver* was examined in *Tbx2*$^{-/-}$ eyes. Furthermore, the expression of *Tbx2* was examined in the *Chx10*$^{OrJ/OrJ}$ mice that first display a small eye phenotype at 10.5 dpc, around the same developmental period as the observed eye size phenotype in *Tbx2*$^{-/-}$ mice. The underlying cause of the small eye phenotype in *Chx10*$^{OrJ/OrJ}$ mice has been assigned to a lower rate of retinal cell

proliferation and a progressive transdifferentiation of the neural retina into RPE, which is apparent at 10.5 dpc with the ectopic expression of *Mitf* in the *Chx10*$^{OrJ/OrJ}$ neural retina (Burmeister *et al.* 1996; Rowan *et al.* 2004; Horsford *et al.* 2004). Examination of *Tbx2* expression in these mice served to clarify whether *Tbx2* is downstream of *Chx10* in the regulation of eye size and whether the phenotypes of these mice are caused by the same aberrant mechanisms.

Silver

Section *in situ* hybridisation with the *Silver* probe revealed expression in the RPE of wild-type embryos at 10.5 dpc in accordance with previous reports (Fig. 5.11 A). In 6/6 mutant eyes, *Silver* expression was detected in the RPE (Fig. 5.11 B). This experiment showed that the RPE was correctly specified at 10.5 dpc as the expression of the *Mitf*-dependent gene *Silver* was spatially normal and did not extend into the neural retina in *Tbx2*$^{-/-}$ embryos.

Tbx2 expression in Chx10$^{OrJ/OrJ}$ *embryos*

Chx10$^{OrJ\ OrJ}$ embryos were obtained from homozygous *Chx10*^{OrJ} crosses on the Sv129 genetic background. Wild-type embryos, serving as controls, were collected from timed matings of Sv129 mice. Embryos were harvested at 10.5 dpc and somite matched between genotypes.

Tbx2 expression detected by whole mount *in situ* hybridisation at 10.5 dpc was restricted to the dorsal neural retina in mutant embryos and did not differ from the expression in wild-type somite matched controls (n= 6 eyes per genotype; Fig. 5.11 C,D). These data therefore suggest that *Tbx2* is not downstream of *Chx10* and that *Tbx2* expression is not dependent upon *Mitf*, which in 10.5 dpc *Chx10*$^{OrJ/OrJ}$ embryos is ectopically expressed in the neural retina (Horsford *et al.* 2004). Together, these experiments provide evidence that the RPE is correctly specified in the absence of Tbx2.

Fig. 5.11 Examination of RPE specification in *Tbx2*$^{-/-}$ mice and *Tbx2* expression in *Chx10*$^{orJ/orJ}$ mice

(A,B) Coronally cut frozen sections (15 μm thick) showing *Silver* expression in the RPE of wild type (+/+) and mutant embryos at ss 34 respectively, detected by section *in situ* hybridisation. Note the distinct accumulation of cells in the ventral region of the mutant optic cup (arrowhead) and the lack of ventral optic cup invagination. **(C)** Lateral view of a 10.5 dpc wild-type embryo at ss 31 hybridised with the *Tbx2* probe. **(D)** *Tbx2* expression in a *Chx10*$^{orJ/orJ}$ (-/-) embryo at ss 31. Expression was normal and is marked by arrows in C-D. Scale bars: 50 μm in A,B and 0.5 mm in C,D.

Abbreviations: D, dorsal; LP, lens placode; MN, mandibular process of the first pharyngeal arch; MX, maxillary process of the first pharyngeal arch; NP, nasal process; NR, neural retina; RPE, retinal pigmented epithelium; ss, somite stage; V, ventral

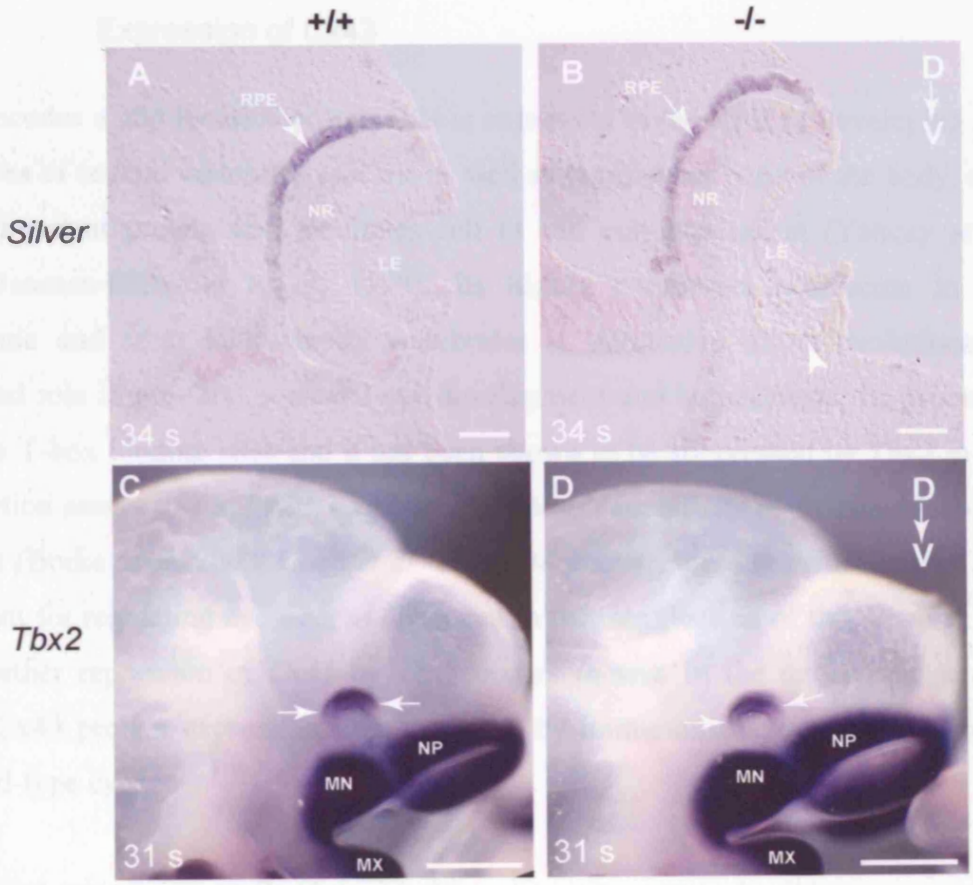
+/+
-/-
Silver
Tbx2
A
RPE
NR
LE
34 s
B
RPE
D
V
NR
LE
34 s
C
NP
MN
MX
31 s
D
D
V
NP
MN
MX
31 s

5.2.4.3 Expression of Cx43

Cx43 encodes a gap junction protein that is expressed in the RPE of developing and adult eyes of several vertebrate species, as well as many other parts of the body, as it is an important protein that facilitates cell to cell communication (Yancey *et al.* 1992; Janssen-Bienhold *et al.* 1998). Its highly conserved expression in the embryonic and adult RPE among vertebrates is suggestive of an evolutionarily preserved role in pre- and postnatal eye development and homeostasis. Its promoter contains T-box binding sites and it has been shown to be suppressed by *Tbx2* in co-transfection assays of *Tbx2* with *Cx43*-driven reporter constructs in an osteoblast-like cell line (Borke *et al.* 2003; Chen *et al.* 2004). Moreover, there is evidence that it is important for regulating eye size, as discussed in the introduction of this Chapter. To test whether repression of *Cx43* by *Tbx2* occurs *in vivo* in the developing neural retina, Cx43 protein expression was compared by immunohistochemistry in $Tbx2^{-/-}$ and wild-type eyes.

The spatial expression of Cx43 in $Tbx2^{-/-}$ and somite matched wild-type eyes was equivalent at 10.5 dpc, with the characteristic punctuate Cx43 expression lining the apical surface (facing the neural retina) of the RPE in a dorsal-high, ventral-low gradient (Fig. 5.12 A-D, G, H; n= 6 eyes per genotype). The ventral presumptive RPE was not positive for Cx43 expression in either mutant or wild-type eyes. Specific Cx43 expression was also detected with an HRP-tagged secondary antibody, in the RPE, but not in control sections without a primary antibody incubation (Fig. 5.12 I,J). As Cx43 expression, which is normally only confined to the RPE in the mouse optic cup, did not extend into the mutant neural retina, correct distinction between the neural retina and the RPE in the dorsal eye was again confirmed in mutants. However, the intensity of Cx43 labelling, reflective of levels of protein, differed between wild-type and mutant eyes. Intense Cx43 labelling was observed in the dorsal peripheral RPE in mutants and weaker labelling was detected in the equivalent region in wild-type eyes (Fig. 5.12 G, H; n= 6 eyes per genotype).

Fig. 5.12 Connexin43 expression in midline sections in *Tbx2*$^{-/-}$ and wild-type eyes at 10.5 dpc detected by immunohistochemistry

All except I-J show pictures show coronally cut frozen sections of 15 μm thickness immuno-labelled with an antibody against Cx43 (green) and counterstained with propidium iodide (red). **(A)** Eye of a wild-type (+/+) embryo at ss 34, showing Cx43 protein localisation to the RPE (arrow) in a dorsal-high, ventral-low gradient. **(B)** Same section as in A, but without the propidium iodide stain. The green fluorescence between the ventral neural retina and presumptive RPE layers and the randomly distributed green circles are non-specific trapping of secondary antibody, as they do not demonstrate the punctate labelling pattern that is characteristic of Cx43 expression and also appear on negative control sections incubated without primary antibody. **(C)** Midline section of the eye of a mutant (-/-) embryo at ss 34. Strong Cx43 expression was detected in the RPE (arrow), in a dorsal-high, ventral-low gradient. The dorsal expression appeared stronger than in wild-type eyes. **(D)** Same section as in C, but without the propidium iodide stain. **(E)** A negative control (10.5 dpc optic cup) showing the non-specific immuno-labelling of the secondary antibody in the absence of the Cx43 antibody. The RPE was completely void of signal. **(F)** Same section as in E without the propidium iodide stain. **(G)** Higher magnification of the dorsal region of the wild-type eye in A. **(H)** Higher magnification of the dorsal region of the mutant eye in C. **(I)** 12 μm thick frozen section of a wild-type embryo at 10.5 dpc immuno-labelled with the same Cx43 antibody as used in A-H, but detected with an HRP-tagged secondary antibody and a colourimetric assay. Section is counterstained with 0.5% Methyl Green. Cx43 expression was detected in the dorsal RPE as in A-D. **(J)** Adjacent section to I treated equally except for the exclusion of the primary antibody. No labelling was seen in the RPE (arrow). Scale bars: A-H, 0.1 mm; I-J, 0.05 mm.

Abbreviations: D, dorsal; LP, lens epithelium; NR, neural retina; RPE, retinal pigmented epithelium; ss, somite stage; V, ventral.

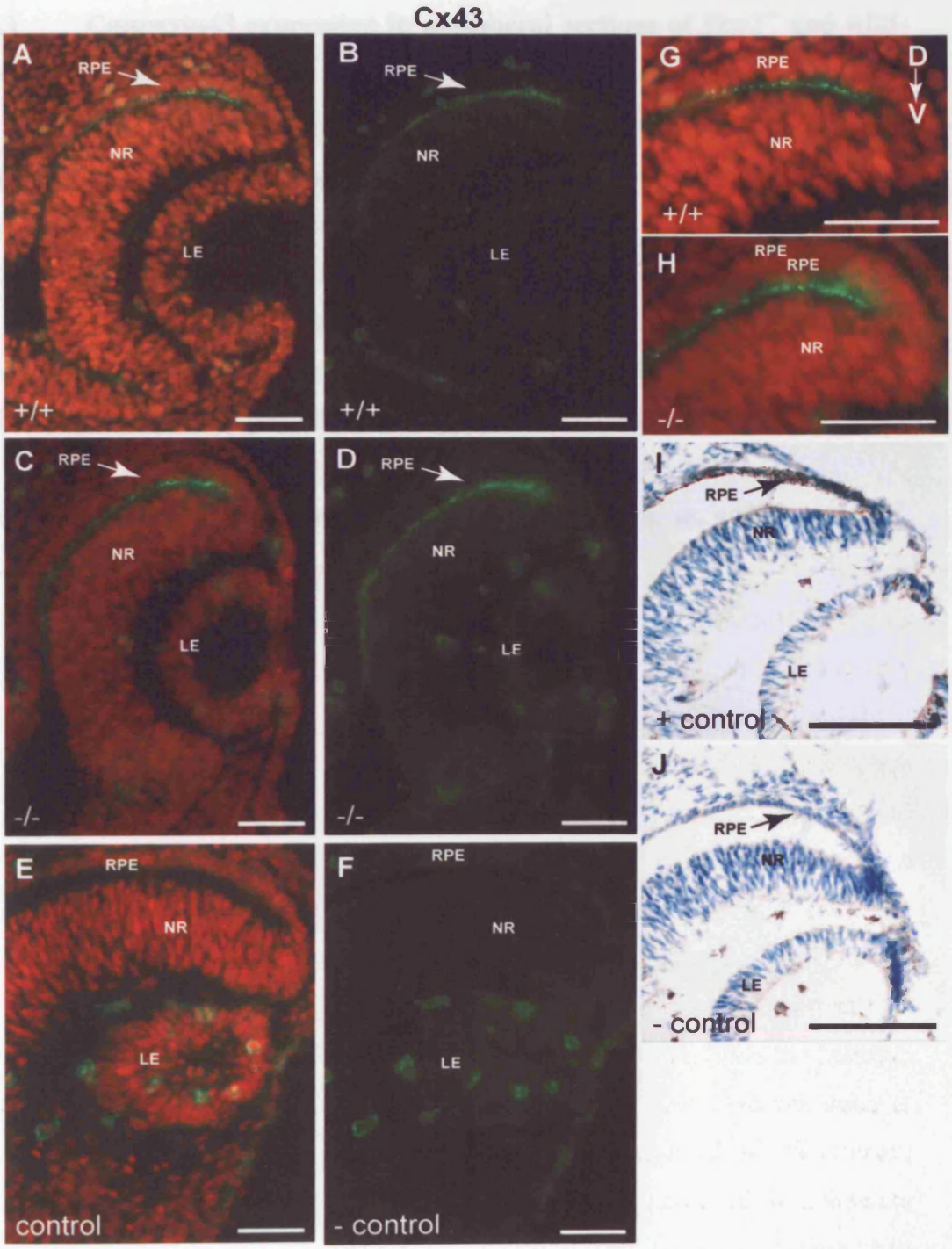
Cx43
A
RPE
NR
LE
+/+
B
RPE
NR
LE
+/+
G
RPE
D
V
NR
+/+
H
RPE
RPE
NR
-/-
C
RPE
NR
LE
-/-
D
RPE
NR
LE
-/-
I
RPE
NR
LE
+ control
J
RPE
NR
LE
- control
E
RPE
NR
LE
control
F
RPE
NR
LE
- control

Fig. 5.13 Connexin43 expression in peripheral sections of *Tbx2*$^{-/-}$ and wild-type eyes at 10.5 dpc detected by immunohistochemistry

Images depict coronally cut frozen sections of 15 μm thickness immuno-labelled with an antibody against Cx43 (green) and counterstained with propidium iodide (red). **(A)** Section of the nasal region of a wild-type eye at ss 34, showing low levels of Cx43 expression in the nasal RPE. **(B)** Same section as A, without propidium iodide. **(C)** Section of the nasal region of a mutant eye at ss 34, showing abnormally high levels of Cx43 expression in the nasal edge of the RPE. **(D)** Same section as shown in C, but without the propidium iodide stain. Scale bars: 50 μm

Abbreviations: D, dorsal; RPE, retinal pigmented epithelium; ss, somite stage; V, ventral.

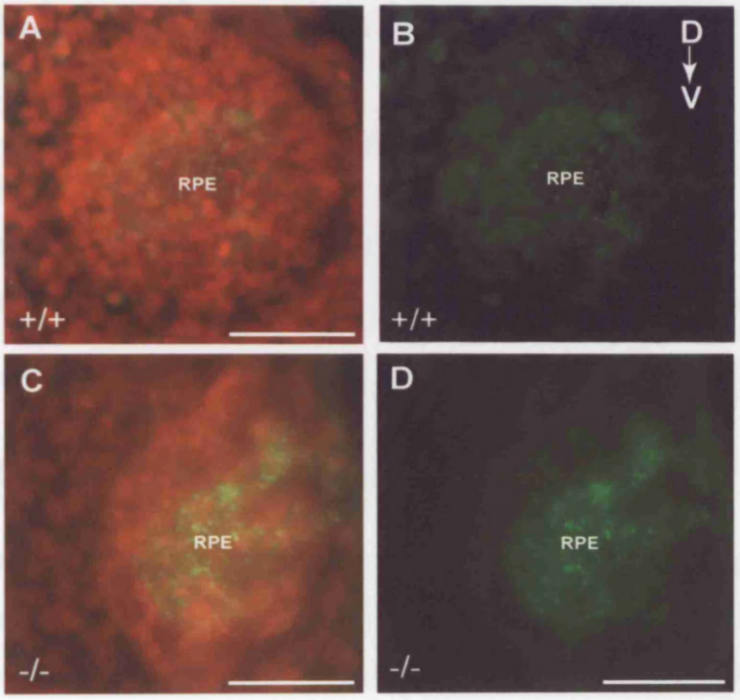
A
RPE
+/+
B
D
V
RPE
+/+
C
RPE
-/-
D
RPE
-/-

Labelling was also highly intense in nasal and temporal peripheral RPE of mutants but barely detectable in equivalent sections from wild-type eyes (Fig. 5.13 A-D)

The difference in Cx43 immuno-labelling intensity between mutant and wild-type eyes is suggestive of higher levels of expression of the protein in the absence of Tbx2 in the dorsal, nasal, and temporal peripheries of the RPE. However, a quantitative approach that measures levels of protein expression would be needed to confirm these results.

5.2.4.4 Differentiation of the neural retina

A reduction in the number of cell divisions undertaken by retinal progenitor cells and early differentiation could cause a small eye size. For example, mice homozygous for a targeted mutation of *Inhibitor of DNA binding 4* (*Id4*) have a small brain size partly due to premature onset of differentiation during early development (Yun *et al.* 2004). To investigate this possibility in *Tbx2*$^{-/-}$ eyes, differentiation was analysed by immunohistochemistry at 12.5 dpc, when the central, but not the peripheral part of the neural retina has normally initiated the differentiation process.

Previous examination of H&E stained sections of mutant eyes at 12.5 dpc (Section 5.2.1) suggested a lack of a nerve fibre layer and a lack of axons projecting through the optic disc in embryos that exhibited the severe phenotype (Fig. 5.3 G). Immuno-labelling with the RMO270 antibody, which labels RGC bodies and processes, revealed an organised nerve fibre layer in the central neural retina, dorsal to the optic disc, in wild-type eyes (Fig. 5.14 A). In mutant eyes, cell bodies and their axons were labelled in the same central region as observed in wild-types and the lack of labelling of axons projecting through the optic disc agreed with observations made previously on H&E sections (n= 2 eyes; Fig. 5.14 B). The absence of labelling in the peripheral neural retina suggests that premature differentiation does not occur at 12.5 dpc in mutants and can thus be excluded as a cause of the small eye phenotype at this stage.

RMO270 labelling also revealed that in mutant retinae, axons were extremely disorganised in comparison to the neat sheet of nerve fibre layer in wild-type retinae (Fig. 5.14 C-J).

Fig. 5.14 Retinal nerve fibre layer genesis and organisation in *Tbx2*$^{-/-}$ and wild-type eyes detected by RMO270 immunohistochemistry

15 μm thick coronal sections of 12.5 dpc eyes immuno-labelled with the RMO270 antibody (green) against intermediate neurofilament-M (160 kDa), and counterstained with propidium iodide (red). **(A)** Midline section through the eye of a wild-type (+/+) embryo at ss 54 showing the existence of a nerve fibre layer on the vitreal surface of the neural retina. Labelling was confined to the central neural retina, dorsal to the optic disc. Arrow points to the optic disc. **(B)** Midline section through the eye of a mutant (-/-) embryo at ss 56 showing the existence of labelled axons in the same region as in the wild-type eye in A. Arrow points to the region where a poorly defined optic disc could be distinguished (see higher magnification in H). **(C)** High power confocal view of the dorsal region of the wild-type optic cup, roughly corresponding to the region highlighted by a solid box in A, although belonging to the adjacent section to A. The nerve fibre layer was orderly arranged on the vitreal surface of the neural retina. Arrow points towards the location of the optic disc, which is not shown in picture. **(D)** High power confocal picture of the dorsal region of the mutant optic cup roughly corresponding to the region highlighted by a solid box in B, although belonging to the adjacent section to B. The nerve fibre layer was disorganised and the axons were protruding into the vitreous chamber. The cells of the neural retina were rounder in appearance than in wild-type. Arrow points towards the optic disc **(E,F)** Same sections as in C and D respectively without the propidium iodide stain. **(G)** High power confocal view of the optic disc region of a wild-type eye (broken box in A). Optic nerve fibres make an orderly exit through the optic disc. **(H)** High power confocal view of the optic disc region of a mutant eye (broken box in B). The axons were disorganised and did not exit the optic cup. Arrow shows the poorly defined optic disc. **(I-J)** Show G-H respectively without the propidium iodide stain. Scale bars: 100 μm in A-B, 20 μm in C-J.

Abbreviations: D, dorsal; L, lens; NR, neural retina; OD, optic disc; RPE, retinal pigmented epithelium; ss, somite stage; V, ventral.

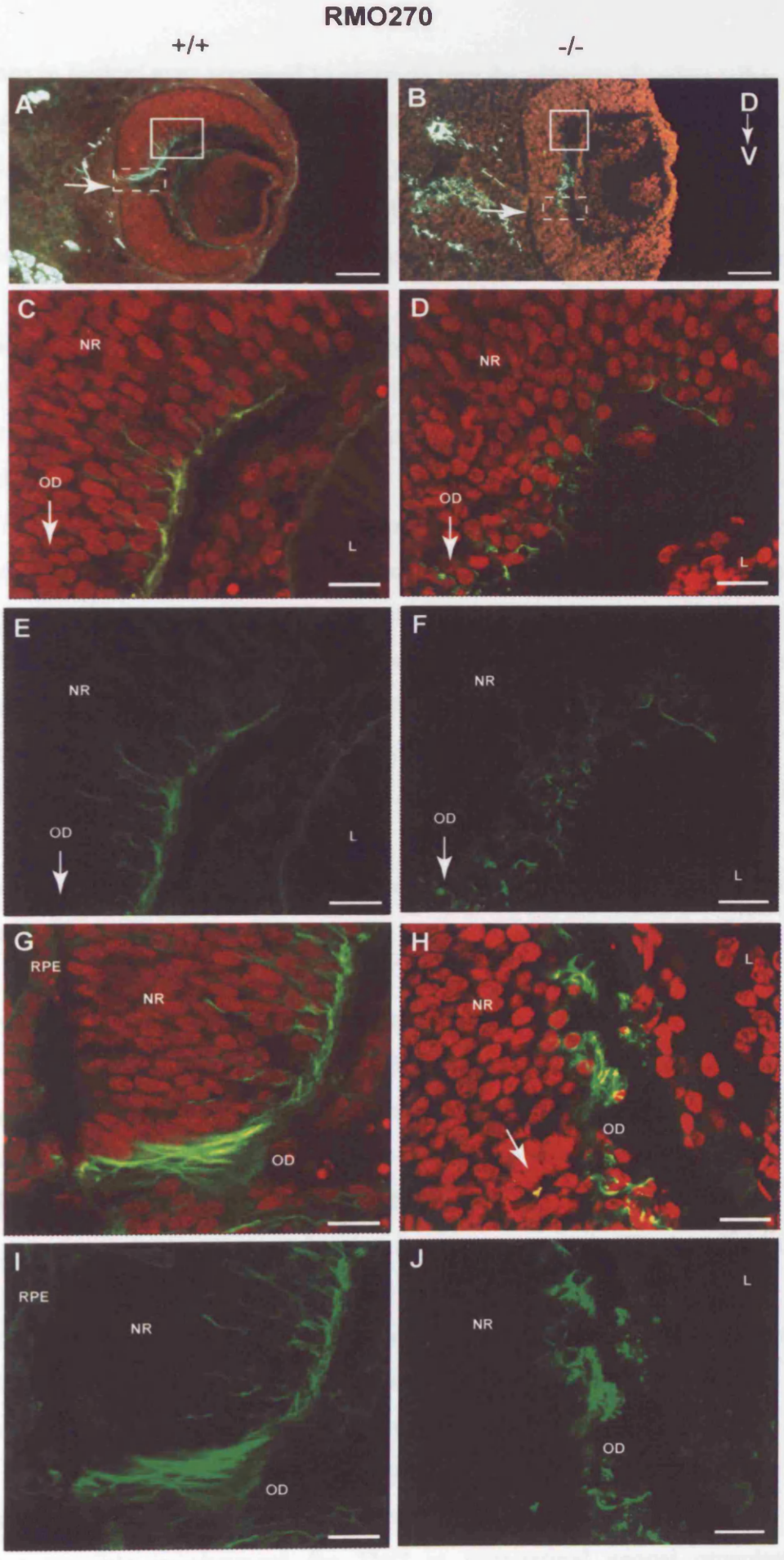
RMO270
+/+
-/-
A
B
D
V
C
NR
OD
L
D
NR
OD
L
E
NR
OD
L
F
NR
OD
L
G
RPE
NR
OD
H
L
NR
OD
I
RPE
NR
OD
J
L
NR
OD

Most axons in mutant eyes appeared to protrude into the vitreous chamber rather than following the vitreal surface of the neural retina These disorganised axons were seen all along the differentiated region of the eye and were not specific to a particular region. The lack of axons exiting the optic disc and a poorly defined optic disc were confirmed in high power views of that region (Fig. 5.14 H, arrow, compare to G).

The embryonic lethality caused by the *Tbx2* mutation prevented further investigations of neurogenesis in *Tbx2*$^{-/-}$ retinae. However, at 12.5 dpc, progenitor cells that will adopt mainly amacrine and horizontal cell fates once postmitotic can be identified by immuno-labelling with the VC1.1 antibody (Alexiades and Cepko 1997). The VC1.1 antibody was used to examine whether commitment to any other cell types apart from the RGC fate could occur in the absence of Tbx2. In both wild-type and mutant retinae, labelling of cell bodies and laminar processes were detected in the central neural retina, dorsal to the optic disc (n= 2 eyes; Fig. 5.15 A-O). In this experiment, it was not possible to distinguish between progenitors and differentiated amacrine/horizontal cells, which are also labelled with the VC1.1 antibody and which start to differentiate at 12.5 dpc (Alexiades and Cepko 1997). The VC1.1 antibody has not been reported to label RGCs and this experiment provides indications of the existence of a progenitor population that is distinct from that giving rise to the RGCs in *Tbx2*$^{-/-}$ eyes.

Surprisingly, strong labelling was also detected in the vitreous chamber of mutant but not wild-type eyes with this antibody, which is raised against an epitope commonly occurring in cell adhesion molecules (see Chapter 2.8.1.1). This labelling site did not particularly coincide within or around cell nuclei and appeared as a fibrous mass that occupied the vitreous chamber (Fig. 5.15 H,K,N). This type of labelling was not seen in wild-type eyes or in the vitreous chamber in negative controls (Fig 5.15 G,J,M,R).

With no evidence for ectopic differentiation, it is concluded that premature differentiation does not cause the small eye phenotype in *Tbx2*$^{-/-}$ embryos by 12.5 dpc. The markers used showed that ganglion cell genesis is initiated in mutant eyes and that at least one other progenitor population exists, which may or may not give rise to amacrine and horizontal cells in the absence of Tbx2. This analysis also revealed a possible involvement for *Tbx2* in intra-retinal axonal organisation.

Fig. 5.15 VC1.1 labelling in *Tbx2*$^{-/-}$ eyes detected by immunohistochemistry

15 μm thick coronal sections of 12.5 dpc eyes immuno-labelled with the VC1.1 antibody (green) against amacrine/horizontal cells and counterstained with propidium iodide (red). **(A)** Section through the eye of a wild-type (+/+) embryo at ss 54, showing labelling within the central region of the neural retina. **(B)** Midline section through the eye of a mutant (-/-) embryo at ss 56, also showing labelling of cells in the central neural retina. Strong labelling was also detected within the vitreous chamber, surrounding the lens (dashed lines). **(C)** A more peripheral section of another mutant eye showing labelled cells within the central neural retina and some labelling in the vitreous surrounding the lens. **(D-F)** Show A-C without propidium iodide staining. **(G)** High power view equivalent to the boxed area in A but in an adjacent section to A. Dorsal is to the right, ventral to the left. VC1.1 labels cell bodies (arrowhead) and laminar processes. **(H,I)** Magnified views of boxed regions in B-C respectively, with arrowhead indicating a labelled cell body. **(J-L)** Show G-I with the propidium iodide stain only. Dashed lines demarcate the region within the vitreous chamber where strong VC1.1 labelling was detected in mutants (in H and K). **(M-O)** Show G-I without the propidium iodide stain. **(P)** Negative control incubated without the VC1.1 antibody, but with the secondary antibody. **(Q)** Adjacent section to P incubated with both primary and secondary antibodies (positive control). **(R)** Another negative control on a section containing the vitreous chamber, showing absence of signal in the vitreous chamber when the VC1.1 antibody was omitted. Scale bars: 50 μm.

Abbreviations: D, dorsal; L, lens; NR, neural retina; ss, somite stage; V, ventral

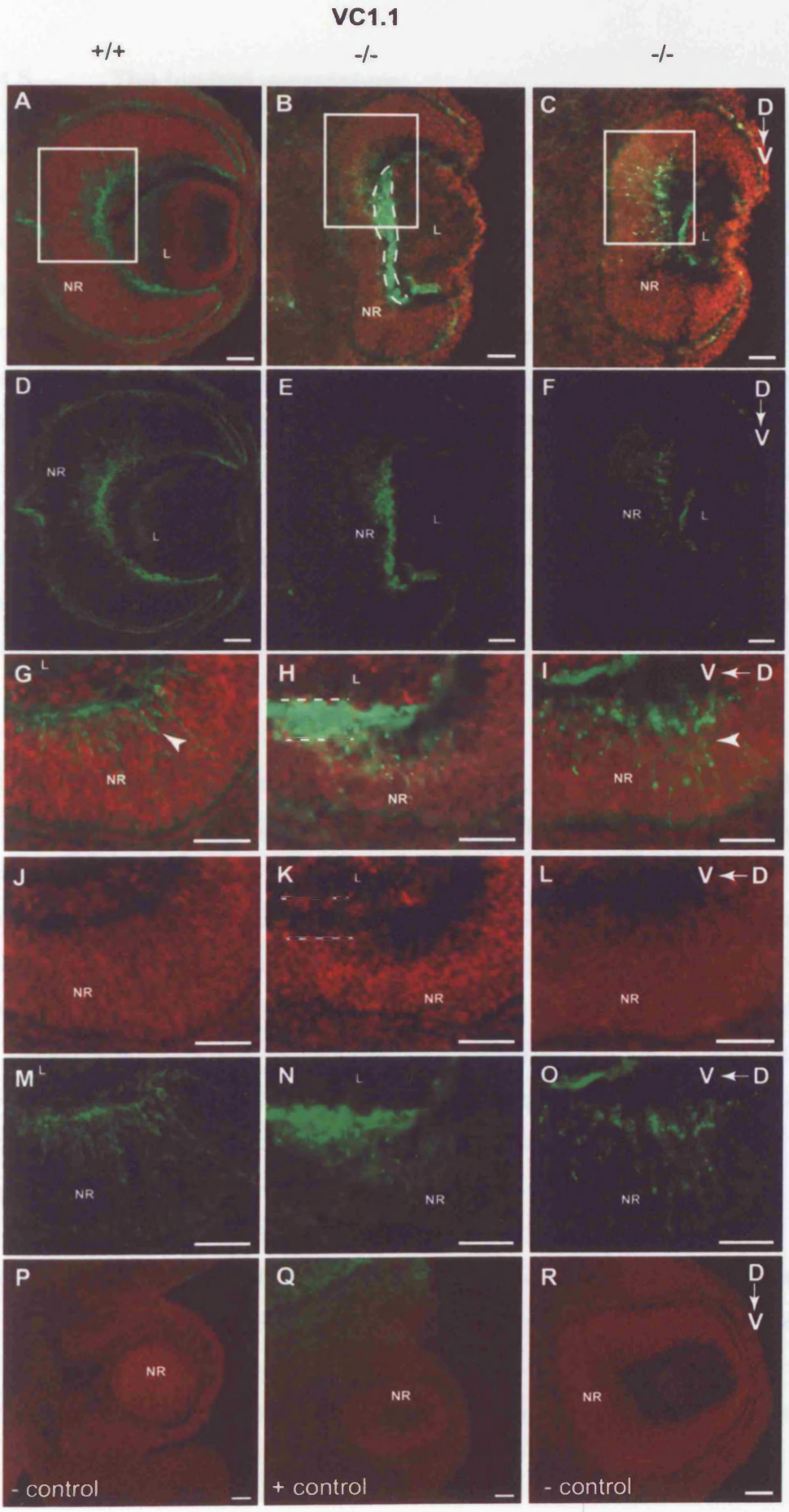
VC1.1
+/+
-/-
-/-
A
B
C
D
V
L
NR
D
E
F
D
V
G
L
H
L
I
V ← D
J
K
L
L
V ← D
M
L
N
L
O
V ← D
P
Q
R
D
V
- control
+ control
- control

5.2.4.5 The hyaloid vasculature

Prior to genotyping of embryos, it was usually possible to identify mutants from wild-types by their abnormally small retinae, but also by a dense manifestation of the vasculature in the region of the optic fissure at 10.5 dpc. Furthermore, histological examination of mutant eyes, described in 5.3.1 also revealed an abnormal hyaloid vasculature in mutants. At 10.5 dpc, the development of the hyaloid vascular system, but not the retinal vasculature, is already underway (Chapter 1.1.1). Relatively little is known about the molecular regulation of hyaloid vasculature formation. At the cellular level however, its formation is pretty well characterised and it is known that mesenchymal cells that enter the optic cup through the optic fissure contribute to its formation. *Tbx2* is expressed in a small number of mesenchymal cells in the ventral region of the optic cup prior to optic fissure closure and could possibly therefore be expressed in cells that later directly become part of the hyaloid vasculature (Fig. 5.16 K).

To further examine the vasculature in mutant eyes, whole embryos were labelled with the endothelial cell specific antibody, Platelet Endothelial Cell Adhesion Molecule 1 (PECAM1; details in Chapter 2.8.1.1), by whole mount immunohistochemistry at 10.5 dpc. Compared to wild-types, PECAM1 immuno-labelling in mutant eyes was more dense in the region of the optic fissure when examined in whole mount view (Fig. 5.16 A,F blue signal; n= 6 eyes), confirming the previous observations of the existence of an abnormal endothelial network during dissections. Sectioning in the transverse plane through labelled eyes showed a larger number of endothelial cells accumulated in the opening of the optic fissure in mutant optic cups compared to wild-types (Fig. 5.16 E,J, yellowish-brown signal).

Jagged1 is also expressed in the same region of the ventral mesenchyme as *Tbx2* (Fig. 5.17 C, E). This site of expression suggested that *Jagged1* may be dependent on *Tbx2* and play a role in the development of the hyaloid vasculature. Together with its other sites of expression in the neural retina and lens, *Jagged1* made an interesting gene to examine in $Tbx2^{-/-}$ embryos.

Fig. 5.16 Comparison of the hyaloid vasculature in *Tbx2*$^{-/-}$ and wild-type eyes at 10.5 dpc labelled by anti PECAM1 whole-mount immunohistochemistry

(A) Eye vasculature at 10.5 dpc in a wild-type embryo immuno-labelled with anti-PECAM1. Endothelial cells were detected in the periphery of the optic cup, encircling the lens and appeared to occupy the optic fissure region (arrow, blue signal). **(B-E)** Complete set of transverse vibratome sections through the eye in A, starting from dorsal shown in B to the ventral most region of the eye shown in E. Endothelial cells were present between the fissure walls (arrow in E, brown signal). **(F)** PECAM1 immuno-labelling in a 10.5 dpc mutant (-/-) embryo somite matched to the embryo in A. Endothelial cells were detected in the periphery of the mutant optic cup but in abnormally clustered pattern, especially in the optic fissure region (arrow, blue signal) and also in the dorsal side of the lens (arrowhead, blue signal). **(G-J)** Complete set of transverse vibratome sections of the eye in F, starting from the dorsal most section shown in G to the ventral most section in J. J shows the large number of endothelial cells populating the fissure region in the mutant eye (arrow, brown signal). **(K)** Vibratome section, showing *Tbx2* expression in mesenchyme ventral to the optic cup (arrowhead). Scale bars: 50 μm.

Abbreviations: D, dorsal; HL, hyaloid vasculature; L, lens; NR, neural retina; OS, optic stalk; ss, somite stage; V, ventral

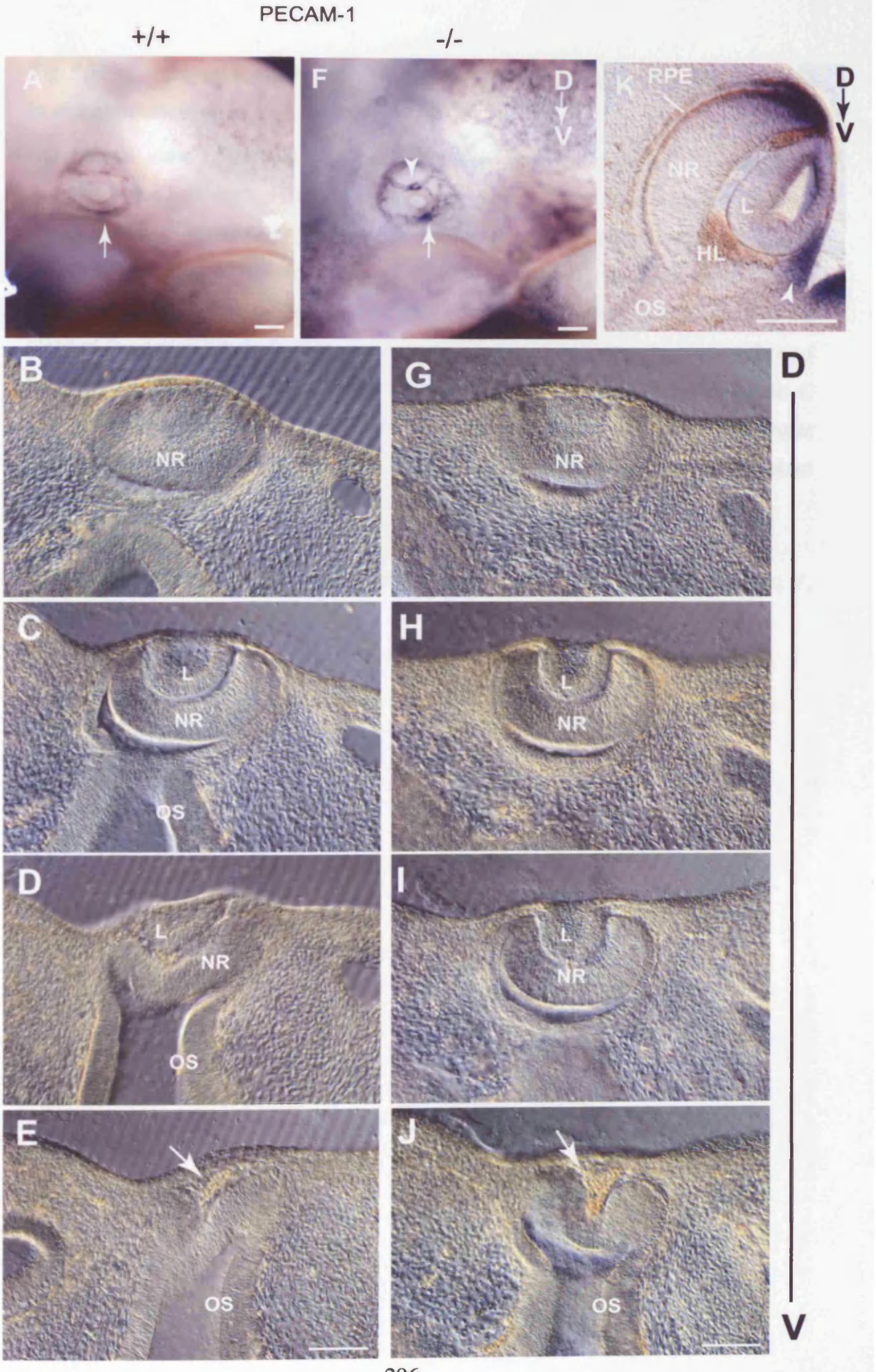
PECAM-1
+/+
-/-
A
F
D
V
K
RPE
D
V
NR
L
HL
OS
B
NR
G
NR
D
C
L
NR
OS
H
L
NR
D
L
NR
OS
I
L
NR
E
OS
J
OS
V

Fig. 5.17 *Jagged1* expression in *Tbx2*$^{-/-}$ and wild-type eyes by whole mount *in situ* hybridisation at 10.5 dpc

(A) Lateral view of a wild-type (+/+) embryo at ss 35 showing expression of *Jagged1* in the lens epithelium and in the neural retina, where it is excluded from the dorsal-most and ventral-most regions. **(B)** Lateral view of a mutant (-/-) embryo at ss 34 showing similar expression to the embryo in A. **(C)** Coronal vibratome section through the plane of the dotted line in A. **(D)** Coronal vibratome section through the plane of the dotted line in B. Expression in the extra-ocular mesenchyme is indicated by arrowheads in C-D. **(E,D)** Higher magnifications of the ventral optic cups in C and D respectively showing the expression of *Jagged1* in the extra-ocular mesenchyme (arrowhead), which was similar between wild-type and mutant embryos. Scale bars: 0.5 mm in A-B, 0.1 mm in C-F.

Abbreviations: D, dorsal; LE, lens epithelium; NR, neural retina; ss, somite stage; V, ventral

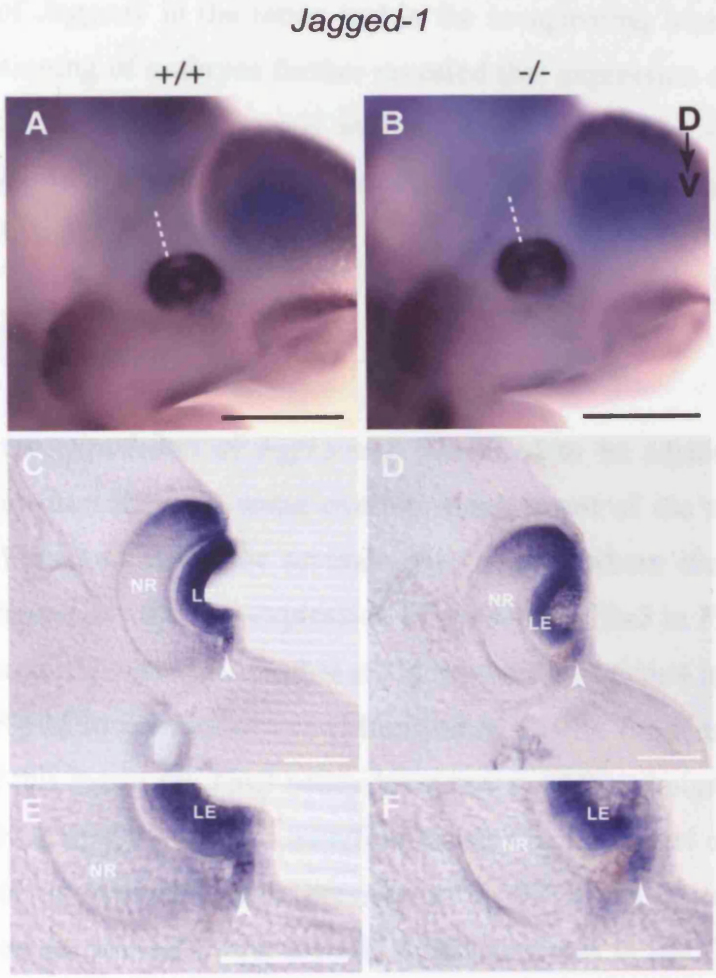
Jagged-1
+/+
-/-
A
B
D
V
C
D
NR
LE
E
F
LE
NR

At 10.5 dpc, somite matched mutant and wild-type embryos showed similar patterns of expression of *Jagged1* in the retina and in the invaginating lens (n= 6 eyes; Fig. 5.17 A,B). Sectioning of embryos further revealed that expression of *Jagged1* in the ventral mesenchyme was also normal in *Tbx2*$^{-/-}$ eyes (Fig. 5.17 C-F). These results exclude *Jagged1* as a downstream target of *Tbx2* in both the neural retina and the ventral mesenchyme.

5.2.5 *Fgf15* expression

In Chapter 3, the expression of *Fgf15* was described to be adjacent to the dorsal *Bmp4* expression domain with some overlap, reminiscent of the spatial pattern of expression of Fgfs and Bmps in several other tissues where they are known to interact (see Chapter 1.4.4). The expression of *Bmp4* and *Tbx2* in *Fgf15*$^{-/-}$ eyes were found to be normal. Meanwhile, another study reported that Bmp4 is essential for the expression of *Fgf15* in the mouse eye (Murali *et al.* 2005). Evidence was presented in Chapter 4 of this thesis for *Tbx2* being downstream of Bmp4 signalling in the eye and being involved in eye growth. I therefore tested whether Bmp4 could act through *Tbx2* to regulate or modulate the expression of *Fgf15* in the central region of the optic cup. Moreover, several of the identified abnormalities in the *Tbx2*$^{-/-}$ mice, such as the abnormal lens, the potentially increased levels of Cx43 in the RPE, as well as the abnormal hyaloid vasculature are suggestive of a non-cell autonomous effect. Therefore, investigation of the expression of an extra-cellular signalling molecule such as *Fgf15* was desired.

Fgf15 expression was examined by *in situ* hybridisation in *Tbx2*$^{-/-}$ embryos. At 10.5 dpc, expression was completely absent in 4/6 eyes (Fig. 5.18 A-C) and the signal intensity was much reduced in the remaining two eyes compared to wild-type somite matched controls (Fig. 5.18 B,D). As in previous experiments, wild-type and mutant embryos were processed in the same tube and therefore treated in exactly the same manner. *Fgf15* expression at other sites in the developing head were similar in all embryos. The presence of *Fgf15* expression in 2/6 mutant eyes, although at reduced signal intensity, suggests that *Tbx2* is not essential for the induction of *Fgf15* expression, but may rather be required for the maintenance of its expression after it has been switched on in the neural retina.

Fig. 5.18 *Fgf15* expression in *Tbx2*$^{-/-}$ and wild-type embryos by whole mount *in situ* hybridisation

Arrows indicate nasal and temporal limits of optic cups. **(A)** Lateral view of two wild-types (+/+) and one mutant (-/-) embryoic heads at ss 35 (10.5 dpc) hybridised with the *Fgf15* probe and treated in the same tube throughout the experiment. *Fgf15* expression was evident in two stripes in the nasal and temporal retina in wild-type embryos but not in the mutant embryo (arrows). **(B)** Higher magnification of the head of a wild-type embryo at ss 35, showing normal *Fgf15* expression (arrows). **(C)** Higher magnification of the head of a mutant embryo at ss 35, showing lack of expression in the eye (arrows) but not the midbrain. **(D)** Lateral view of the head of a mutant embryo at ss 35, showing low levels of *Fgf15* expression in the eye (arrows). This embryo was treated in the same tube as embryo shown in B. **(E)** Lateral view of the head of a mutant embryo at the optic vesicle stage (ss 28), showing *Fgf15* expression in its characteristic two stripes in the nasal and temporal optic vesicle (arrows). Scale bars: 1 mm in A, 0.5 mm in B-E.

Abbreviations: D, dorsal; ss, somite stage; V, ventral

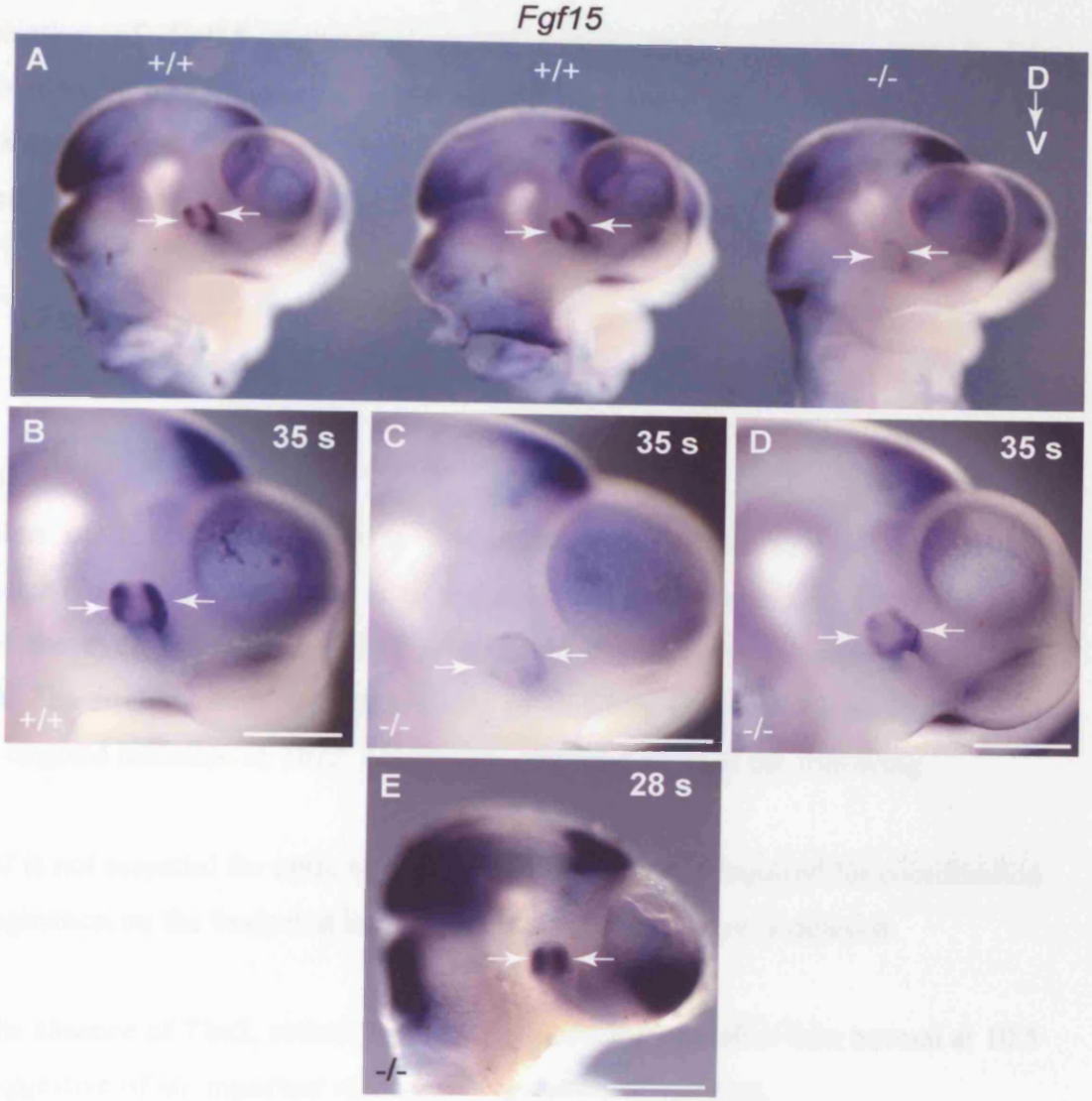
Fgf15
A
+/+
+/+
-/-
D
V
B
35 s
+/+
C
35 s
-/-
D
35 s
-/-
E
28 s
-/-

Examination of *Fgf15* expression at an earlier stage, prior to optic vesicle invagination, in *Tbx2*$^{-/-}$ eyes revealed normal expression (n= 2 eyes; Fig. 5.18 E). This supports the idea that *Tbx2* is important for the maintenance of *Fgf15* expression but not for its induction in the developing mouse eye.

5.3 Discussion

5.3.1 Summary of findings

The aims of this Chapter were to investigate whether the role of the dorsally expressed *Tbx2* in the optic cup is to regulate molecular patterning along the D-V axis of the eye, and whether *Tbx2* is required for early eye morphogenesis and growth. The strategy employed was a loss of function approach by analysing mice with a targeted mutation in *Tbx2*. The results obtained suggest the following:

1) *Tbx2* is not essential for optic vesicle invagination, but is required for coordination of invagination on the basis that invagination of the ventral eye is delayed.

2) In the absence of Tbx2, retinal volume is significantly smaller than normal at 10.5 dpc, suggestive of an important role in the regulation of eye size.

3) A shape change was observed at 12.5 dpc, with the optic cup appearing shorter along the P-Di axis, and protruding much less than in stage matched wild-type eyes.

4) Tbx2 is not essential for the induction of dorsally expressed genes; there is no feed-back regulation of *Bmp4* by *Tbx2* and all genes examined were present. Neither is *Tbx2* essential for the establishment of the dorsal neural retina-RPE border. The expression of several genes are however altered in the absence of *Tbx2* in a way which suggests that Tbx2 may be important for maintaining their correct expression patterns/levels. These include *Tbx5*, *EphrinB2*, *Fgf15*, and Cx43.

5) Investigation of several growth limiting mechanisms as potential causes of the small eye phenotype excluded excessive cell death, precocious cell differentiation,

and expansion of the RPE domain at the expense of the neural retina. Instead, a trend of increased cell proliferation was detected in mutants.

6) A range of other phenotypes were observed including failure of /delayed eye lid groove formation, abnormal lens growth and lens fibre differentiation, disorganised intra-retinal axonal projections, and abnormalities within the vitreous including abnormal development of the hyaloid vasculature.

5.3.2 Tbx2 in eye morphogenesis, early growth, and differentiation of the eye

Analysis of the number of pH3 positive cells in the dorsal eye, revealed a higher number of mitotic cells in mutant eyes at ss 30-31 in comparison to somite matched wild-types. This is in spite of a significant reduction in retinal volume 2-5 somite stages later (ss 33-35). There could be several explanations for this result. Firstly, as the number of pH3 positive cells were low, it is possible that this increase has no significant effect on eye growth, at least not an effect that would be immediately obvious. Because ectopic apoptosis in the dorsal eye was not detected, the effect of increased cell death cannot have counteracted the increased proliferation to yield a small eye. In further support of this conclusion, *in situ* hybridisation using a full-length *Tbx2* RNA probe to detect cells that would have expressed *Tbx2* in mutant embryos, confirmed the presence of this population of cells at apparently normal density in their usual region. Instead, other factors or mechanisms must be responsible for the small eye phenotype. Delayed invagination of the ventral optic cup, which was observed at early 10.5 dpc, when retinal volume measurements were taken, could indeed result in a small eye phenotype. This suggests that two different mechanisms are aberrant in the absence of Tbx2 in the developing eye; one is proliferation of the dorsal neural retina, the other, invagination of the ventral region of the developing eye. An enlarged sub-retinal space in the naso-ventral (and sometimes in the dorsal) side of the developing eye was consistently observed and may represent a true regionally restricted abnormality with a functional significance. Typical coloboma, the most frequent type of coloboma, occurs in the inferio-nasal quadrant of the human eye (Onwochei *et al.* 2000).

An increase in cell proliferation in the absence of Tbx2 correlates well with the role of *Tbx2* elsewhere in embryogenesis. In the developing heart, the expression sites of *Tbx2* in non-chamber myocardium including the AVC and the outflow tract are associated with lower proliferation than the *Tbx2* negative chamber tissue (Cai *et al.* 2005). The chamber tissue in the *Tbx20* targeted mutant mouse, ectopically expresses *Tbx2* and possesses a lower mitotic rate than detected in wild-types, resulting in the formation of a hypoplastic heart. It has been suggested that the cardiac defect in *Tbx20*$^{-/-}$ mice is due to the ectopic expression of *Tbx2* in chamber tissue (Cai *et al.* 2005; Singh *et al.* 2005). Furthermore, *Tbx2* was shown to directly repress the expression of the oncogene *Nmyc1*, which was downregulated in *Tbx20*$^{-/-}$ chamber tissue (Cai *et al.* 2005). In *Tbx2*$^{-/-}$ mice, chamber tissue differentiation occurs at the expense of AVC formation, though when cell proliferation was analysed in whole hearts, no differences were found between mutants and wild-types (Harrelson *et al.* 2004).

There are a lot of reports that link *Tbx2* to the control of the cell cycle, via the inhibition of various CDKIs, including p21 and p19^{ARF}. *In vitro* studies suggest that *Tbx2* acts to promote cell cycle progression/cell division (see Chapter 1.3.5). These reports correlate with reports that *TBX2* is amplified in a subset of primary breast tumours, breast tumour cell lines, and pancreatic cancer cell lines (Jacobs *et al.* 2000; Bärlund *et al.* 2000; Sinclair *et al.* 2002; Mahlamaki *et al.* 2002; Vance *et al.* 2005). However, a similar repression of CDKIs by *Tbx2* during development has not been found. In fact the evidence from the developing heart, and results presented in this Chapter, point towards an opposite role, where *Tbx2* expression is required to slow down proliferation. Analysis of the expression levels of p21, p16^{INK4a}, p15 ^{INK4b}, and p19^{ARF} in the developing heart revealed that these genes are not affected by the lack of Tbx2 during heart development at least (Harrelson *et al.* 2004). Moreover, investigation of a genetic interaction with p53, where the absence of Tbx2 was hypothesised to be compensated for by the absence of p53 in mice doubly homozygous for *Tbx2* and *Trp53*, revealed that these pathways are independent as there was no rescue of the heart phenotype (Harrelson *et al.* 2004). It is still possible that Tbx2 directly regulates cell cycle genes also in development, although these may be a different set of genes than those identified in adult cancer tissues/from adult studies. The identification of *NMyc1* as a target in heart development encourages

future searches for other cell cycle genes that may be regulated by *Tbx2* during embryogenesis.

If additional time and resources were available to me, analysis of more embryos combined with BromodeoxyUridine (BrdU) labelling, which allows tracing of several rounds of cell divisions over a period of time rather than a snap-shot of the state of cell division offered by pH3 immuno-labelling, would be undertaken. This would give a better answer to the effect of loss of *Tbx2* on cell proliferation. Alternatively or in combination, DNA flow cytometry would offer insight into the regulation of the cell cycle in the absence of Tbx2 by detecting the proportion of cells within each phase of the cell cycle in mutant eyes in comparison to wild-types. Finally, pH3 immuno-labelling performed at a later stage would be helpful.

Other avenues responsible for the eye size phenotype were also investigated. Analysis of the RPE specific gene *Silver*, served to address whether Tbx2 is important for setting the dorsal neural retina-RPE boundary. It was shown that this is not the case, as *Silver* was expressed in a normal spatial pattern. Moreover, this experiment together with correct localisation of Cx43 protein to the RPE, showed that the small eye phenotype is unlikely to be due to the expansion of the RPE at the expense of the neural retina, which has been reported to occur in $Chx10^{OrJ/OrJ}$ mice (Horsford *et al.* 2004; Rowan *et al.* 2004). *Chx10*, like *Tbx2* is under the regulation of Bmp signalling in the eye as *Chx10* expression is absent in Bmp receptor compound mutants (Murali *et al.* 2005). *In situ* hybridisation of *Tbx2* in $Chx10^{OrJ/OrJ}$ showed that *Tbx2* expression was normal in the absence of *Chx10*, positioning *Tbx2* in an independent pathway, or perhaps upstream of *Chx10* during mouse eye development. However, several pieces of data presented here argue against the latter. In $Tbx2^{-/-}$ eyes, RPE specific genes do not extend into the neural retina, whereas in $Chx10^{OrJ/OrJ}$ embryos, several RPE genes are ectopically expressed in the neural retina (Horsford *et al.* 2004; Rowan *et al.* 2004). Moreover, differentiation is delayed in $Chx10^{OrJ/OrJ}$ eyes (Burmeister *et al.* 1996), whereas it was detected at 12.5 dpc in $Tbx2^{-/-}$ eyes. Together, these observations suggest that *Tbx2* is likely to be regulating eye size via a different pathway than to *Chx10*.

Interestingly, in a recent study employing morpholino-mediated knockdown of *Tbx2b*, the zebrafish homologue of the mouse *Tbx2* gene, differentiation of all retinal cell types except the RGCs was transiently blocked in the dorsal, but not the ventral neural retina, although the expression of all D-V patterning genes investigated was normal (Gross and Dowling 2005). In *Tbx2*$^{-/-}$ mice it was not possible to examine differentiation past 12.5 dpc. Further analysis and the use of conditional knockout technology to overcome the lethality of the *Tbx2*$^{-}$ allele is needed to investigate whether this is also true in the mouse or whether it is species specific.

5.3.3 Role of *Tbx2* in D-V patterning

Establishment of molecular patterning of the D-V axis of the eye occurs properly in the absence of *Tbx2,* as most asymmetrically expressed genes examined were present at 10.5 dpc. However, *Tbx5* expression was reduced in *Tbx2*$^{-/-}$ eyes. This reduction appeared independent of the reduced eye phenotype of *Tbx2*$^{-/-}$ embryos, as *Msx2*, *Bmp4*, and *Tbx3* expression in the dorsal neural retina were normal in mutants. At 9.5 dpc, *Tbx5* expression is identical in wild-type and mutant embryos (personal communication with Z. Harrelson, Columbia University, NY). These observations suggest that *Tbx2* is not required for the initial expression of *Tbx5*, but rather for its maintenance. Examination of *Tbx5* expression at a later developmental stage would test this hypothesis, because if maintenance of *Tbx5* expression is dependent on *Tbx2*, the expected result would be a loss of *Tbx5* expression in an older embryo.

In Chapter 3 it was shown that Noggin treatment of the optic cup at 11.5 dpc had no effect on D-V patterning including the expressions of *Tbx2* and *Tbx5*, whereas earlier treatment induced changes in these genes. One interpretation of this outcome, as discussed in Chapter 4, is that T-box gene expression as well as overall D-V patterning is dependent on Bmp4 signalling for its induction, but not for its maintenance. In this Chapter, it was found that *Tbx5* expression was reduced, in the absence of a change in expression of *Bmp4* or Bmp signalling, as indicated by the normal expression of the Bmp4 downstream target *Msx2*, suggesting that perhaps Bmp4 induces, while *Tbx2* maintains *Tbx5* expression. That maintenance of *Tbx5* expression may be independent of Bmp signalling and hence its induction, is supported by another study in which *Tbx5* expression is spatially normal when

Noggin is misexpressed in the chick eye at HH 15-18 (Adler and Belecky-Adams 2002). This is one day after *Tbx5* expression is first detected in the chick eye (Koshiba-Takeuchi *et al.* 2000) and a relatively late stage in optic cup morphogenesis; differentiation has already initiated (Martinez-Morales *et al.* 2005).

Vax2 expression in the ventral optic cup also appeared reduced in *Tbx2*$^{-/-}$ mutants. As optic cup formation is particularly delayed in the ventral region, this is likely to be a reflection of the abnormal ventral eye morphogenesis. Analysis of more markers of the ventral optic cup such as *Pax2* or *EphB3* could help to confirm this interpretation. However, it would be possible that *Tbx2* affects the expression of *Vax2* in the ventral eye via a secreted factor.

Analysis of *ephrinB2* expression revealed that even though Tbx2 is not required for the induction of *ephrinB2*, it appears to play a role in regulating its pattern of expression in both the lens and in the neural retina. Expression analysis at later stages combined with quantitative measurement of transcripts are required to verify these data and to determine the quantity of the change in levels of *ephrinB2* expression in *Tbx2*$^{-/-}$ mice.

Although not possible to examine in the *Tbx2*$^{-/-}$ mice, the altered expression of *ephrinB2*, *Tbx5*, and possibly that of *Vax2* is likely to have functional consequences for topographic mapping of RGCs to the superior colliculus, as several studies have shown that these genes are critical for correct topographic mapping (Mann *et al.* 2002; Koshiba-Takeuchi *et al.* 2000; Barbeiri *et al.* 2002). When wild-type *ephrinB2* is overexpressed into the dorsal *Xenopus* neural retina, which normally already expresses high levels of *ephrinB2* and projects axons to the lateral tectum, the dorsally derived axons project even more laterally than normal. Misexpression of a truncated *ephrinB2*, which is thought to act in a dominant negative manner to dilute out the natural ephrinB2 signalling in that region, into the dorsal neural retina causes a medial shift of dorsally derived axons (Mann *et al.* 2002). The incidence of ectopic projections of ventro-temporally derived axons, which normally express high levels of EphB receptors, to more lateral regions of the superior colliculus in *EphB2*$^{+/-}$; *EphB3*$^{-/-}$ compound mutants is lower than the incidence observed in *EphB2*$^{-/-}$; *EphB3*$^{-/-}$ mutants (Hindges *et al.* 2002). Therefore it appears that the ephrinB/EphB receptor

ligands act in a dosage dependent manner to mediate topographic mapping of RGC axons to the brain and that changes in the dosage or pattern of these molecules has a direct functional translation in the form of a shift in axonal projections to ectopic locations.

5.5.4 Cx43

Analysis of the expression of Cx43 in the developing mouse eye at 10.5 dpc, revealed that it is confined to the RPE. In *Tbx2*$^{-/-}$ embryos, Cx43 expression appeared elevated in the RPE. This is indicative of the action of a secreted intermediary, as *Tbx2* itself is never expressed in the RPE.

Cx43 is a gap junction protein which hexamerises to form a hemi-channel. Hemi-channels in neighbouring cells interact to form gap junctions. Gap junctional communication has been implicated in many developmental processes including the control of cell proliferation in the eye (Pearson *et al.* 2005). Previous reports have suggested that gap junctional coupling mediated by Cx43 in the chick retina is positively correlated with retinal cell proliferation, as antisense oligodeoxynucleotide-mediated suppression of Cx43 expression reduces cell proliferation (Becker and Mobbs 1999). The mechanism by which gap junctional communication may affect cell proliferation in the retina has been suggested to be related to the control of interkinetic cell movement of neural progenitor cells. Retinal progenitors migrate to and fro between the vitreal surface and the ventricular surface, which is the site of mitosis (Sidman 1961). Electroporation of dominant-negative Cx43 in chick retinal flat mounts reduces the speed of interkinetic cell movements, while misexpression of Cx43 has been shown to increase this speed compared to controls (Pearson *et al.* 2005). A change in the speed at which proliferating cells reach the ventricular surface, where they appear to receive the signal to undergo mitosis, may result in fewer or more cell divisions. Based on the study of Cx43 in the developing chick eye, if Cx43 is upregulated, increased cell proliferation should occur. Although the difference in mitotic index in the dorsal neural retina between *Tbx2*$^{-/-}$ and wild-type embryos was statistically not significant, the number of mitotic cells were on average doubled, in agreement with increased cell division upon upregulation of Cx43. However, it should be noted that in the older chick retina,

where Cx43 has been studied in relation to retinal cell division, Cx43 was expressed in the RPE but also in the neural retina, mediating coupling between retinal progenitors. At 10.5 dpc, in studies performed here, Cx43 was not detected in the neural retina, and the effect of Cx43 in the RPE at this stage, on retinal cell division, is currently unknown.

Interestingly, during the analysis of Cx43 expression, it was noted that its expression is asymmetrical and distributed in a dorsal-high ventral-low gradient at 10.5 dpc. At this stage the dorsal region of the eye has invaginated and the outer layer is morphologically thinner than the inner layer, although it is not yet pigmented. The ventral portion of the eye is lagging in invagination and the outer layer is still thicker than expected for the RPE.

5.5.5 *Fgf15* as the downstream effector of the non-cell autonomous phenotypes identified in *Tbx2-/-* embryos

The presence of *Fgf15* expression in the optic vesicle but its absence in 4/6 eyes in the optic cup suggest that Tbx2 is required for the maintenance, but not induction, of *Fgf15* expression in the neural retina. The variability in gene expression may reflect the variability in the expressivity of the phenotype, in which case only affected embryos showed the lack of *Fgf15* expression. *Tbx2* and *Fgf15* are not completely co-expressed at 10.5 dpc when *Tbx2* appears to be required for the maintenance of *Fgf15,* suggesting that this regulation is indirect and mediated via another secreted factor. The known secreted factors that are specifically expressed or synthesised in the dorsal optic cup include *Bmp4* and RA. *Bmp4* expression and the expression of its downstream target *Msx2* were directly analysed and shown to be normal in *Tbx2*$^{-/-}$ eyes. On this basis, the most likely intermediary factor to maintain *Fgf15* expression in the eye is RA. *Aldh1a1,* the gene encoding a RA synthesising enzyme, is expressed in the dorsal neural retina but synthesises RA with a lower efficiency than the ventrally expressed *Aldh1a3* (Grün *et al.* 2000), which synthesises RA with a high efficiency. This is thought to account for the lower levels of RA being present in the dorsal eye in comparison to the ventral eye. Interestingly, a middle domain, which is just dorsal to the optic disc but ventral to the expression of *Tbx2* is kept free from RA by the presence of cytochrome P450-linked oxidases encoded by Cyp26

enzymes which degrade RA (Sakai *et al.* 2004). It would be interesting to analyse the expression of RA synthesising and degrading enzymes in *Tbx2*$^{-/-}$ embryos.

Interestingly, many of the phenotypes observed in RA deprived/deficient embryos is similar to those observed n *Tbx2*$^{-/-}$ embryos. RA deficiency in zebrafish embryos results in lack of ventral neural retina formation (Marsh-Armstrong *et al.* 1994). RA deprivation in mammals causes microphthalmia and anophthalmia (Kalter and Warkany 1959), while retroviral driven expression of a dominant negative form of RARα, which is one of the nuclear RA receptors that mediates the RA signal intracellularly, in the developing chick eye results in a small eye phenotype (Sen *et al.* 2005). Other similar abnormalities include shortening of the ventral neural retina, expansion of the ventral extra-ocular mesenchyme, failure of eye lid groove formation, and hyperplasia of the hyaloid vasculature, which were detected in *Aldh1a1; Aldh1a3* compound null mutants (Matt *et al.* 2005).

Fgf15 was identified relatively recently (McWhirter *et al.* 1997). The proposed receptor for Fgf15 is FgfR4 (Xie *et al.* 1999). There is evidence from over/misexpression studies that Fgfs/FgfRs play a role in lens development including induction, proliferation, and differentiation (Faber *et al.* 2001; Lovicu and Overbeek 1998). However, the identity of the Fgfs that convey these effects during normal development is currently unknown, as no mouse mutants have revealed a lens phenotype. Based on the fact that double targeted disruption of the only two Fgfs that are endogenously expressed in the mouse lens vesicle, *Fgf1* and *Fgf2*, does not result in any ocular defects (Miller *et al.* 2000), it has been proposed that an Fgf secreted from the neural retina into the vitreous chamber may be important for lens development, and that it may be Fgf15 (Govindarajan and Overbeek 2001). The chick and human Fgf19 are the closest homologues of the mouse Fgf15 (Xie *et al.* 1999; Wright *et al.* 2004), exhibiting similar but not identical gene expression patterns in the eye (Kurose *et al.* 2004). Electroporation of *Fgf19* in the surface ectoderm overlying the optic vesicle in the chick embryo does not result in any eye defects, although the authors state that perhaps this is due to insufficient levels of overexpression or that Fgf19 may need a synergising partner to induce its effect (Kurose *et al.* 2005). Until more is known about the role of Fgf15 in eye development, the significance of the lack of maintenance of Fgf15 expression is

highly speculative. However, being one of the few secreted factors expressed in the neural retina, it is a good candidate for causing the non-cell autonomous eye defects identified in *Tbx2*$^{-/-}$ embryos.

Fgf15 could also potentially be important for guidance of axons towards the optic disc. A proportion of early axons within the rat retina (13.5 dpc) are severely misrouted when the retina is treated with an FGFR blocking antibody against the extracellular portion of FGFR protein, indicating that FGFR signalling is implicated in intra-retinal organisation and guidance (Brittis *et al.* 1996). The creation of conditional alleles to disrupt *Tbx2* specifically in the developing eye, hence bypassing the heart defect, would allow further characterisation of the disorganised axonal projections observed in the absence of Tbx2. Alternatively, the role of *Tbx2* in intra-retinal axonal projections can be investigated with other *in vivo* manipulation strategies such as misexpression of *Tbx2* or knock-down of Tbx2 using somatic cell gene delivery to the developing eye directly.

5.3.6 Variable expressivity of the phenotype and genetic compensation

The expressivity of the eye phenotype in *Tbx2*$^{-/-}$ mutants was variable. The same was reported for the heart phenotype (Harrelson *et al.* 2004). Two common explanations for such variability include the existence of genetic modifiers, which if true, a more homogenous phenotype is expected on a defined inbred background. The other is stochastic developmental effects. The fact that the *Tbx2* mice are on a mixed genetic background, strain-specific genetic modifiers could potentially explain the variable phenotype. However, Harrelson *et al.* concluded that the expressivity of the phenotype did not change on an inbred background, although their study did not include an analysis of the eye (Harrelson *et al.* 2004). Another explanation offered by Anderson and colleagues, which may be relevant here is natural variation in Bmp signalling (Anderson *et al.* 2002), which was also suggested by Chang and colleagues in their analysis of adult mice heterozygous for *Bmp4* (Chang *et al.* 2001). Downstream targets of Bmp signalling other than *Tbx2*, including *Tbx3* and *Msx2* are normally expressed and could potentially convey the variability in Bmp signalling. If *Tbx3* has the potential to compensate for the *Tbx2*$^{-/-}$ phenotype, then a variation in Bmp signalling between embryos could contribute to the severity of the phenotype.

Tbx2 and *Tbx3* are highly related paralogous genes (Agulnik *et al.* 1996), and are expressed in overlapping or identical regions in the embryo (Chapman *et al.* 1996). They are both implicated in cell cycle control (see Chapter 1.3.5). Therefore, it is likely that they mediate the same or similar effects and can compensate for each other. Furthermore, there is recent evidence of a genetic interaction between *Tbx2* and *Tbx3* in mammary gland development where they also overlap in expression; *Tbx2* heterozygosity does not result in any defects although in combination with *Tbx3* heterozygosity, which itself has an effect on the maintenance of mammary placodes, the *Tbx3* haploinsufficient phenotype of mammary gland aplasia and hypoplasia is enhanced (Jerome-Majewska *et al.* 2005). A similar study for eye development could be carried out once the loss of function *Tbx3* eye phenotype is characterised, which would shed light on the issue of expressivity of phenotype and possible compensation.

CHAPTER 6 Analysis of eye size, retinal cell differentiation, and intra-retinal axonal projections after *Tbx2* misexpression in the developing chick eye

6.1 Introduction

In Chapter 4, eye size was significantly reduced upon rhBMP4 coated bead implantation in the lens vesicle. Although the T-box genes were ectopically expressed in these eyes, the experimental approach was not suitable for addressing the question of whether a particular T-box gene or a combination of the T-box genes regulate eye size. The loss of function approach used in Chapter 5 provided direct evidence that *Tbx2* is indeed implicated in eye size regulation, as *Tbx2*$^{-/-}$ embryos possessed smaller retinal volume than wild-type littermates. My next aims were to directly misexpress *Tbx2* and *Tbx3* in the ventral neural retina in the mouse embryo, first individually and then in combination, during the same developmental period as when rhBMP4 coated bead implantations had been performed. This would allow the investigation of the direct effect of *Tbx2* and *Tbx3* misexpression on eye size. Misexpression studies provide a complementary approach for the analysis of gene function and can be a useful strategy for genes that are co-expressed with their closely related homologues in a tissue, like *Tbx2* and *Tbx3*. It allows the study of the gene of interest in a similar environment, i.e. the tissue of interest, but in the absence of its closely related family members. For example, the ectopic expression of *Tbx2* in the ventral neural retina, where the other T-box genes are not expressed, would allow one to examine the role of *Tbx2* in the context of eye development without the interference of endogenous expression of the other dorsally expressed T-box genes.

Analysis of *Tbx2*$^{-/-}$ embryos also revealed disorganisation of the intra-retinal axonal projections, but further analysis was prevented by the onset of embryonic lethality in these mice. The second aim of this study was therefore to further investigate the role of *Tbx2* in retinal cell differentiation and intra-retinal axonal organisation. RGCs require precise positional information in order to project their axons correctly to their targets in the brain (see Chapter 1.2.2.2). Not only do the RGCs need to know where they reside within the retina, but their axons require positional cues in order to navigate towards the optic disc and beyond after exiting the optic cup. The asymmetrical expression pattern of *Tbx2* along the D-V axis of the neural retina makes it a potential candidate in either providing positional identity to the RGCs or directing the migration of RGC axons from the dorsal neural retina towards the optic

disc via a cell intrinsic or extrinsic mechanism. A role for *Tbx2* in RGC axonal pathfinding has not previously been investigated.

To misexpress the T-box genes, a gene delivery method suitable for targeting the embryonic eye was needed. Current available methods for gene delivery to tissues involve inducing alterations to the property of cell membranes by the application of an electric current, which enables penetration of molecules by opening transient pores through which they enter the cell. This is the method of electroporation. Alternatively gene delivery methods rely on receptor mediated uptake by the cell, which is the basis for viral gene delivery. Other non-viral methods such as microparticle bombardment and lipofection have also been utilised, but electroporation yields the strongest reporter gene expression among non-viral gene delivery methods (Muramatsu *et al.* 1997).

In this Chapter, electroporation was tested for its suitability to deliver plasmid DNA to the embryonic eye. Because one of the aims of the study was to examine eye size, it was important that the experimental procedure itself did not cause non-specific changes to eye morphology, which needed to be retained in an excellent condition. The technique also had to allow good levels of exogenous gene expression in the developing eye. One of the main advantages of electroporation over viral delivery methods is that exogenous gene expression can be detected relatively soon after electroporation (2-5 hrs depending on promoter; Davidson *et al.* 2003; Osumi and Inoue 2001) and that multiple constructs can be co-electroporated simultaneously. Furthermore, insert size is not a limiting factor (Morgan and Fekete 1996).

At the time when experiments described in this Chapter were undertaken, there had only been a few reports of electroporation in the mouse embryo involving targeting of cDNA or morpholinos to gastrula stage embryos, and in older embryos where the developing brain was targeted (Itasaki *et al.* 1999; Swartz *et al.* 2001; Osumi and Inoue 2001; Calegari *et al.* 2002; Mellitzer *et al.* 2002; Davidson *et al.* 2003). However, to date, there have been no reports of gene delivery by electroporation to the embryonic mouse eye. This may partly be due to the existence of other established, although more time consuming, means of genetic manipulation in the mouse, such as targeted mutagenesis in ES cell lines from which genetically altered

mice can be derived, or the creation of transgenic animals. Also other issues such as limited culture period *ex utero* (1-2 days in embryo culture from our own experience and (Martin and Cockroft 1999) or the difficulty of growing embryos *in utero* after manipulations, present technical challenges for the usage of the mouse as a model system in combination with electroporation.

Since culturing of mouse embryos during the period of optic cup formation was successfully performed in Chapter 4, electroporation as a means of gene delivery to the optic cup was explored and different variables were tested in this chapter for the purpose of achieving optimised misexpression of the T-box genes during optic cup formation. Due to difficulties encountered in gene delivery by electroporation to both the developing mouse and chick eyes, the RCASBP retroviral vector was used to misexpress the chick *Tbx2* cDNA in the developing chick eye. Prior to undertaking the misexpression study, the onset of *Tbx2* expression in the chick presumptive ocular tissues and its continued expression in the developing eye until HH 25 was examined, as a detailed analysis had previously not been reported. After *Tbx2* misexpression, eye size, early retinal cell differentiation, and intra-retinal axonal projections were analysed.

6.2 Results

6.2.1 Electroporation as a gene delivery method for the developing eye

6.2.1.1 Mouse electroporation followed by whole embryo culture

The objective of this part of the study was to efficiently deliver and express the pIRES2-EGFP reporter construct in the mouse neural retina at 11.5 dpc without causing damage to the electroporated tissue. Furthermore, survival of the embryo for another ~15-18 hours beyond electroporation was vital.

Previous studies employing electroporation in early post implantation to mid gestation mouse embryos had used currents at 10-40 Volts, which were delivered in up to 5 pulses of 30-50 milliseconds (msec) duration at 1 second (sec) intervals

(Swartz *et al.* 2001; Calegari *et al.* 2002; Davidson *et al.* 2003). With this as a guideline, various experimental parameters were tested, including the strength of the electric field and the number of pulses, the type of electrodes, and the site of DNA injection (Table 6.1). The setup had to be modified depending on the type of electrodes used. These are described in Chapter 2.6.2.4. The level of transfection was assessed by the strength and area of EGFP fluorescent cells in embryos that were successfully cultured overnight. The state of health of embryos pre- and post-culture was assessed as previously described in Chapter 4, and embryos were considered to have shown satisfactory growth if their somite count was increased by six pairs or more after overnight culture (~15-18 hrs) and if they were healthy without morphological deformities. From all experimental parameters that were altered, a change in voltage had the highest impact on EGFP expression and embryo survival.

Table 6.1 Reporter gene expression and embryo survival in mouse electroporation experiments

Electrodes	Voltage	Site of injection	EGFP expression			% showing strong EGFP (n)	% survived culture (n)
			strong	weak	none		
gold	20	vitreous	0	2	0	0% (0/2)	0% (0/2)
	25	N/A*	N/A*	N/A*	N/A*	N/A*	50% (2/4)
	30	N/A*	N/A*	N/A*	N/A*	N/A*	50% (2/4)
	30	vitreous	0	1	1	0% (0/2)	100% (2/2)
gold/tungsten	30	vitreous	1	7	1	11% (1/9)	78% (7/9)
	35	vitreous	0	3	0	0% (0/3)	0% (0/3)
silver	20	vitreous	0	3	0	0% (0/3)	100% (3/3)
	30	vitreous	2	1	0	67% (2/3)	100% (3/3)
	35	vitreous	4	1	1	67% (4/6)	83% (5/6)
	35	SR space	1	4	5	10% (1/10)	70% (7/10)
	40	vitreous	1	0	1	50% (1/2)	100% (2/2)
	40	SR space	1	2	1	25% (1/4)	75% (3/4)

* embryos were electroporated but not injected with DNA.

[DNA]= 1.8 µg/µl. Current was delivered in five pulses of 50 msec duration with 1 sec intervals for all embryos shown in table. Embryos were considered to have grown during overnight culture if they showed an increase of at least 6 somite pairs compared to their pre-culture state. N/A, not applicable; SR space, sub-retinal space.

Fig. 6.1 EGFP expression in 11.5 dpc mouse embryos electroporated with pIRES2-EGFP

Lateral views of post-culture embryos (overnight) injected with 1.88 μg/μl DNA in the vitreous chamber and electroporated using various conditions. **(A)** Embryo injected with 5 pulses at 30 V with the tungsten/gold electrode combination. Low levels of EGFP were expressed in the surface ectoderm surrounding the eye. **(B)** Image in A merged with a brightfield view to show the morphology of the head. **(C)** Embryo electroporated with 5 pulses at 30 V with silver electrodes. Low levels of EGFP expression were detected in the surface ectoderm. **(D)** A brightfield image merged with the picture in C. **(E)** Embryo electroporated with 5 pulses at 35 V with silver electrodes. High levels of EGFP expression were detected. **(F)** A brightfield image merged with the picture in E. EGFP expression was absent in the optic cup. Scale bars: 0.5 mm.

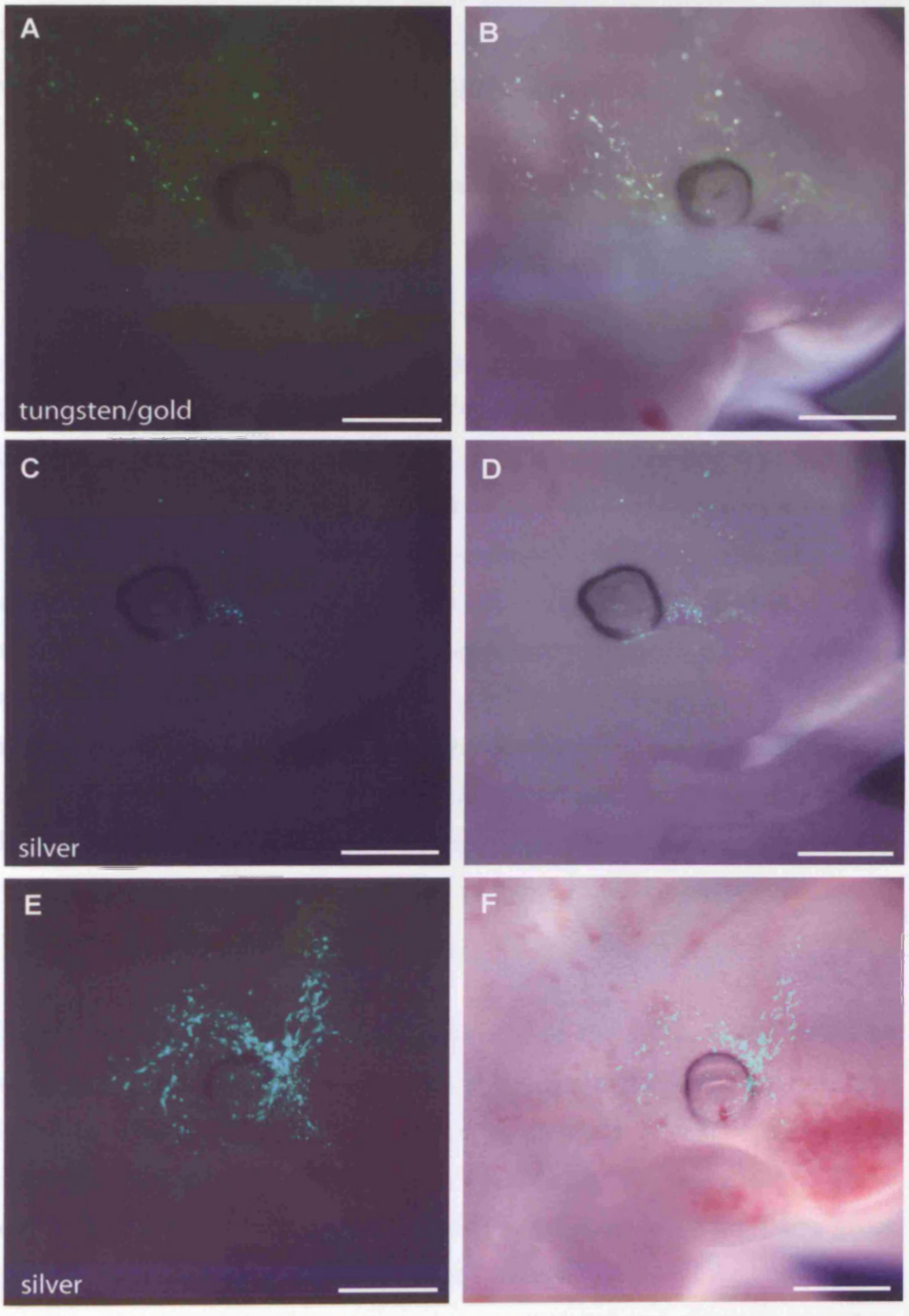
A
tungsten/gold
B
C
silver
D
E
silver
F

Although good levels of EGFP expression were detected in the lens and in the extra-ocular mesenchyme, especially with the silver electrodes, and embryo morphology and survival were good after electroporations, none of the electrodes or varying field strengths tested were successful in driving EGFP expression in the mouse neural retina (Fig. 6.1). Therefore, I decided to test electroporation in the chick embryo, where targeting of the neural retina had been reported in several studies.

6.2.1.2 *In-ovo* chick electroporation

There are several advantages in using the chick embryo for misexpression studies. *In ovo* electroporation is technically much easier to perform than electroporation in the mouse embryo, as the chick embryo is held in place inside of the egg. The little time it takes to prepare the embryo for electroporation also means that far more embryos can be manipulated in each experiment in comparison to an experiment involving mouse embryo culture. In addition, electroporation can be performed at an early embryonic stage and the embryo can be developed until hatching if required, whereas the mouse embryo can only be successfully cultured for 1-2 days *in vitro* as mentioned earlier. This makes the study of later events of eye development, such as retinal cell differentiation and RGC axonal projections, more feasible in the manipulated chick embryo. Furthermore, as well as growing outside of the yolk sac, the early chick embryo lies flat on the surface of the yolk, making it very accessible for manipulations and placement of electrodes.

The objective was to first optimise gene delivery to the chick neural retina by electroporation, in order to achieve high levels of transgene expression, high embryo survival, and no adverse effects on eye size or morphology. Electroporations were performed at HH 9-10, when the primary optic vesicles are first distinguished. These stages were chosen in order to target the eye prior to the stage when the T-box genes are expressed asymmetrically in the dorsal neural retina. Like the mouse electroporation experiments, various parameters were tested and changed, including the electrodes, the setups of which were described in Chapter 2.6.2.5. The reporter constructs used here were pIRES2-EGFP and RCAS-AP (see Chapter 2.6.21 for descriptions), which encodes the human placental alkaline phosphatase in a retroviral vector. After electroporation and a further two days in culture, the percentage

survival of embryos was calculated and EGFP expression, as well as the occurrence of eye abnormalities were scored within survivors (Table. 6.2).

Table 6.2 Reporter gene expression and embryo survival in chick electroporation experiments

Electrodes	pIRES2-EGFP- [μg/μl]	Voltage	% survived* (n)	EGFP expression			% showing abnormal eye morphology (n)
				in survivors % (n)	% strong (n)	% in eye (n)	
Gold	0.88	20	39% (17/44)	82% (14/17)	14% (2/14)	64% (9/14)	30% (5/17)
	1.88	20	44% (16/36)	88% (14/16)	29% (4/14)	21% (3/14)	13% (2/16)
	1.88	15	62% (6/8)	50% (3/6)	33% (1/3)	0% (0/3)	not recorded
gold/tungsten	0.88	20	80% (12/15)	not recorded	not recorded	not recorded	100% (12/12)
	0.88	10	100% (8/8)	50% (4/8)	0% (0/4)	0% (0/4)	50% (4/8)

* % survival 2 days post electroporation.
Current was delivered in five pulses of 50 msec duration with 1 sec intervals for all embryos shown in table.
Abnormal eye morphology included unilateral or bilateral small eye size, absence of optic cup, cyclopia, and in most severe cases, absence of entire forebrain.

These analyses showed that it was possible to deliver DNA at sufficient levels to the optic vesicle in the chick embryo, using the gold plated electrode setup (6.2 A-C). However due to the high incidence of eye and forebrain abnormalities induced by the electroporation procedure (Fig. 6.2 D-F, Table 6.2), this method was deemed inappropriate for the investigation of the effect of T-box gene misexpression on eye size. Instead, it was decided to use retroviral gene delivery, which only involves microinjection of the viral suspension.

Fig. 6.2 Morphology and transgene expression in electroporated chick embryos

(A) Lateral view of an electroporated embryo one day post electroporation at ~HH 17. The embryo is *in ovo* and covered by vascularised membrane. It was injected with 0.88 μg/μl of pIRES2-EGFP and 0.66 μg/μl of RCAS-AP plasmid DNA into the optic vesicle lumen at HH 10 and electroporated with gold plated electrodes at 20 Volts, 5 pulses of 50 msec duration, 1 sec intervals. EGFP expression was detected in the neural retina (arrow). **(B)** Same embryo as in A, two days after electroporation at HH 20. EGFP expression was widely detected in the optic cup (arrow). **(C)** Same embryo as in A-B after the development of the alkaline phosphatase (AP) enzymatic colour reaction. RCAS-AP was expressed in the optic cup, but also in parts of the forebrain. **(D)** Anterior view of the head of an embryo at HH 25 after electroporation with the gold/tungsten combination electrodes with 20 V, 5 pulses of 50 msec duration, 1 sec intervals at HH 9. The embryo appeared cyclopic without a forebrain and had two pigmented optic cups, one much smaller than the other, located at approximately midline (arrows). **(E)** Anterior view of the head of another embryo, treated in the same manner and of the same age as the embryo in D. This embryo had a diencephalon (DI) and one optic cup correctly positioned (arrow), but was completely lacking the second eye. **(F)** Anterior view of the head of another embryo treated in the same way as embryos in D,E. This embryo completely lacked forebrain tissue including eyes, but had two pigmented spots located at midline, presumably where the optic cup tissue should have arisen from (arrows). Scale bars: 0.5 mm.

Abbreviations: DI, diencephalon; FB, forebrain; FL, forelimb; HL, hindlimb; MB, midbrain.

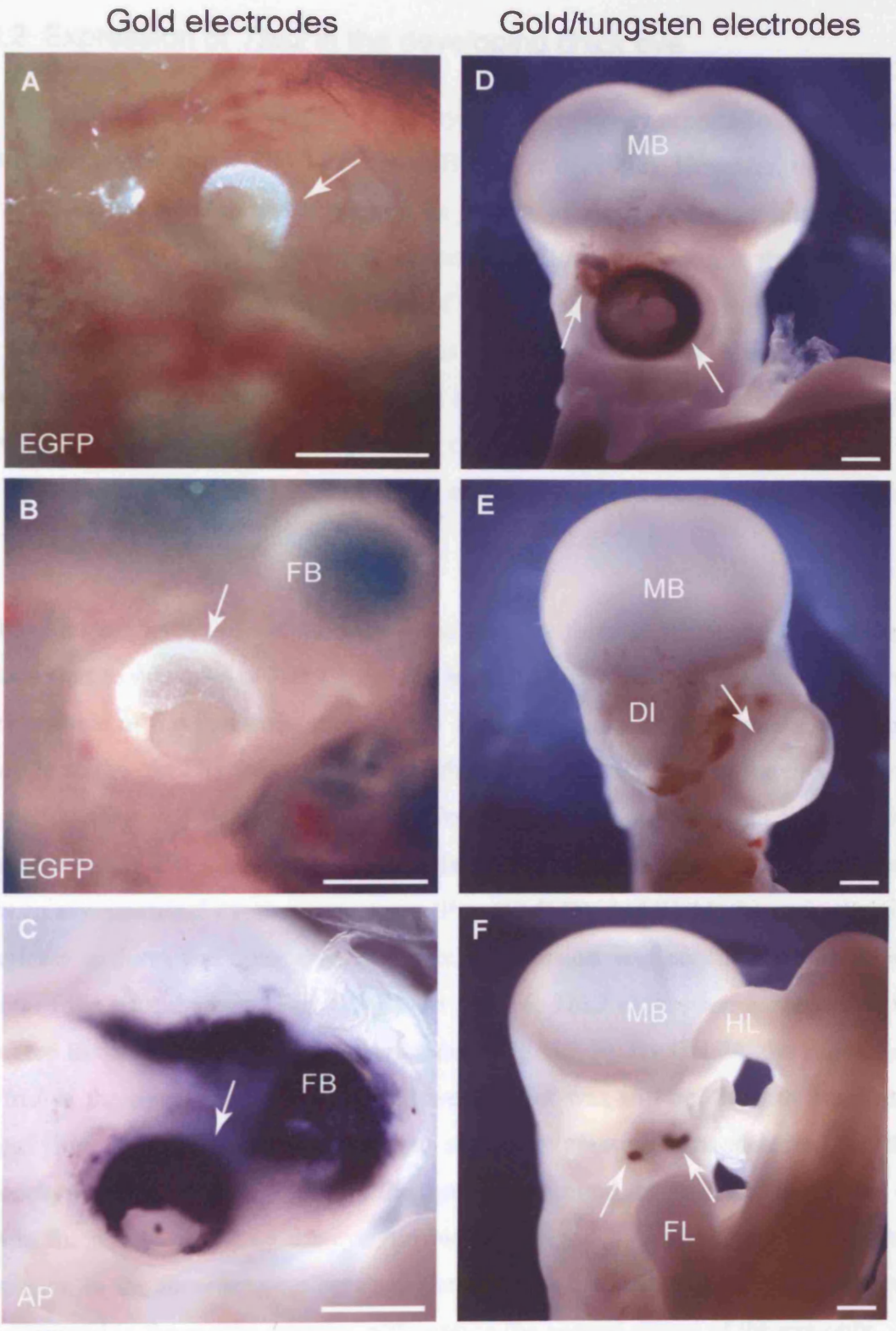
Gold electrodes
Gold/tungsten electrodes
A
EGFP
D
MB
B
FB
EGFP
E
MB
DI
C
FB
AP
F
MB
HL
FL

6.2.2 Expression of *Tbx2* in the developing chick eye

Tbx2 expression in the developing chick eye was previously reported to be localised to the dorsal optic cup at HH 14 (Gibson-Brown *et al.* 1998). However, the onset of *Tbx2* expression prior to this stage and its pattern of expression after this stage has not been reported. Knowledge about the onset of *Tbx2* expression in the developing chick eye was required for the purpose of manipulation of *Tbx2* expression during eye development in subsequent sections of this chapter. It also allowed the comparison of *Tbx2* expression in the eye of the chick embryo to that in the mouse embryo. Spatio-temporal gene expression of *Tbx2* was detected by whole mount *in situ* hybridisation in white Leghorn chick embryos harvested between HH 9-24 (n= 3-4 embryos per stage).

In the chick embryo, the rudimentary optic vesicles form at HH 9 and the proximal regions start to constrict at HH 10, so that by HH 11 two vesicles are clearly distinct on either side of the forebrain, and by HH 12 the proximal regions have shaped into the optic stalks. At HH 9-10, *Tbx2* transcripts were not detected in the presumptive eye region (Fig. 6.3 A,B). At HH 12, *Tbx2* expression was detected in the distal neuroepithelium along the entire D-V axis of the optic vesicle and hence did not show an asymmetrical expression pattern (Fig. 6.3 C,D). At HH 14, the optic vesicles invaginate to form the optic cup, and *Tbx2* expression was confined to the dorsal region of the neural retina (Fig. 6.3 E). At HH 16, *Tbx2* expression continued to be restricted to the dorsal region of the optic cup (Fig. 6.3 F). By HH 24, the expression of *Tbx2* in the optic cup itself appeared weaker but was still confined to the dorsal region (Fig. 6.3 G,H). At this stage, strong expression was detected in the mesenchyme in the ventral region of the optic cup, around the lens, and in a streak of cells in the dorsal region of the eye (arrowheads Fig. 6.3 G and arrow in H). *Tbx2* expression in the mesenchyme between the surface ectoderm and the optic cup was also observed in the mouse embryo, although in the ventral aspect of the eye only.

Fig. 6.3 Expression of *Tbx2* in the developing chick eye detected by *in situ* hybridisation

Images depict lateral views of embryos **(A)** At HH 9 (ss7), *Tbx2* transcripts were absent in the rudimentary optic vesicle (arrow). *Tbx2* was detected in the heart primordia at this stage (arrowhead). **(B)** At HH 10 (ss10) *Tbx2* transcripts were absent from the optic vesicle (arrow), which at this stage had started to undergo constriction in the proximal region (presumptive optic stalk). *Tbx2* expression in the developing heart was restricted to the posterior heart tube (arrowhead). **(C)** At HH 12 (ss16), *Tbx2* was expressed in the entire optic vesicle (arrow). **(D)** Anterior view of the rostral region of the embryo in C. *Tbx2* transcripts were present along the entire D-V axis of the distal region (presumptive neural retina) of the optic vesicle and absent from the overlying ectoderm. Arrows mark the boundaries of expression. Expression was also detected in the ventral midline of the forebrain (arrowhead). **(E)** At HH 14 (ss22), *Tbx2* transcripts were restricted to the dorsal neural retina. Image also shows expression in the mandibular process of the first pharyngeal arch. **(F)** Embryo at HH 16 (ss27) showing *Tbx2* expression in the dorsal optic cup (arrows). Image also shows expression in the nasal primordia, mandibular process, and the atrio-ventricular canal. **(G)** At HH 24, *Tbx2* expression was detected in the dorsal region of the optic cup (arrows), transcripts were absent in the ventral region of the cup. Strong expression was detected in mesenchyme on the ventral surface of the optic cup including in the optic fissure region, and also around the lens and in a streak in the dorsal region of the eye (arrowheads). **(H)** Coronal frozen section of the eye at HH 24 showing *Tbx2* expression, detected by section *in situ* hybridisation, in the dorsal neural retina and the mesenchyme between the ventral optic cup and the surface ectoderm (arrow). Scale bars: 0.5 mm in A-G, 0.1 mm in H

Abbreviations: AVC; atrio-ventricular canal, D, dorsal; Di, distal; H; heart, L; lens, MN; mandibular process, MX; maxillary process, NP; nasal process, P, proximal; Pre. NR; presumptive neural retina, Pre. RPE; presumptive retinal pigmented epithelium; V, ventral

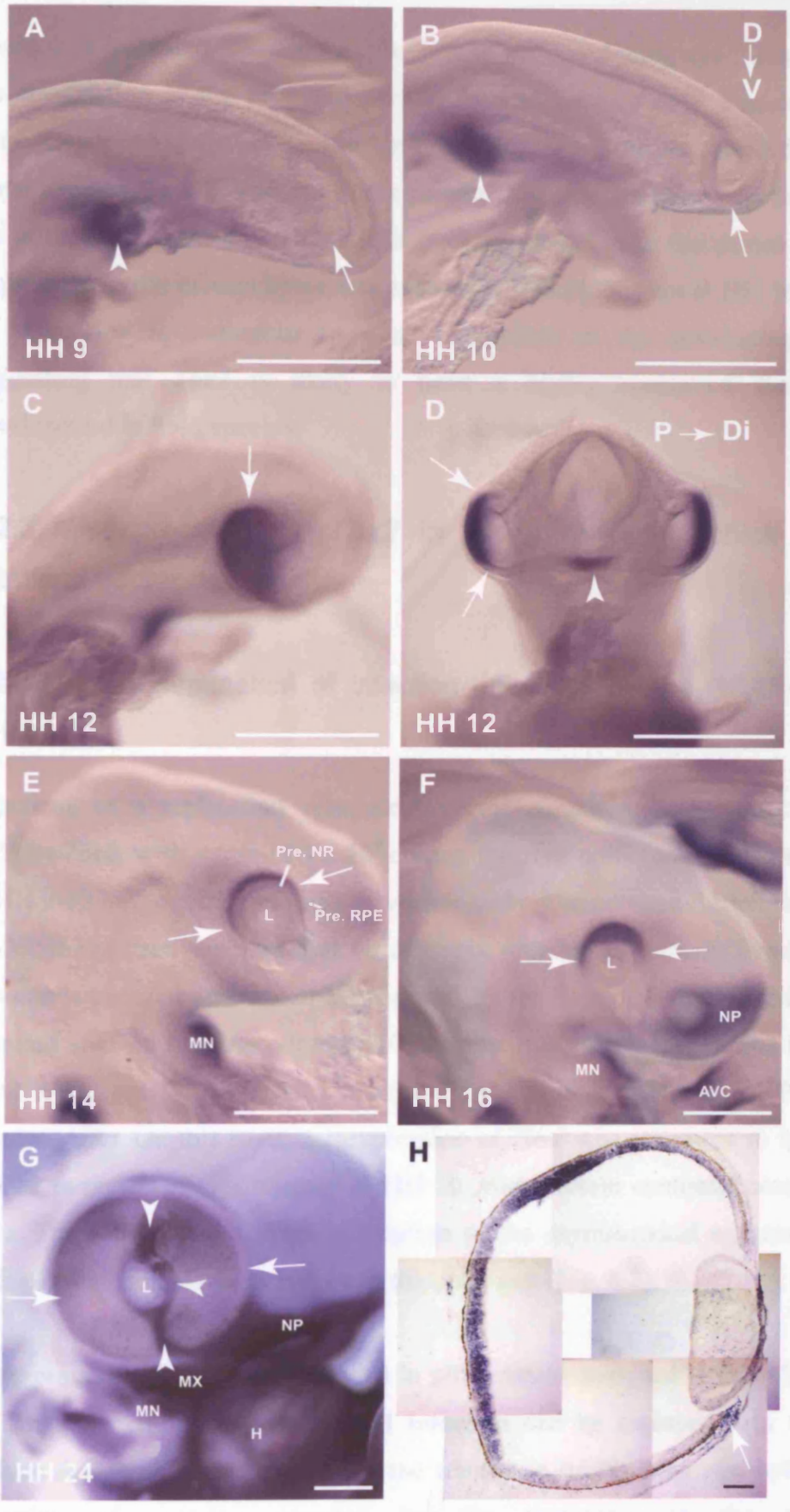
A
HH 9
B
D
V
HH 10
C
HH 12
D
P → Di
HH 12
E
Pre. NR
L
Pre. RPE
MN
HH 14
F
L
NP
MN
AVC
HH 16
G
L
NP
MX
MN
H
HH 24
H

These data indicated that *Tbx2* expression in the developing eye initiated soon after the constriction of the proximal part of the rudimentary optic vesicles, but before optic vesicle invagination. In the optic vesicle, *Tbx2* was expressed throughout the distal neuroepithelium and not in the proximal neuroepithelium (the future RPE), or the optic stalk. After invagination, it became restricted to the dorsal neural retina. Expression in the mesenchyme was evident at HH 24, but not at HH 16. This pattern of expression is analogous to *Tbx2* expression in the developing mouse eye, suggesting that *Tbx2* is likely to have a highly conserved function in eye development in both species.

6.2.3. Misexpression of *Tbx2* in the developing chick eye using retroviral vector delivery

6.2.3.1 Examination of infection efficiency by the RCAS-*cTbx2* virus *in vivo*

Injections of a replication competent vector containing the chick *Tbx2* cDNA, RCAS-*cTbx2,* with a titre of 1 x 10^8 colony forming units (c.f.u)/ml, were performed at HH 9-10 in the primary left optic vesicle and embryos were further cultured to HH 23-25. It has been reported that viral matrix protein, the protein in which the viral genome is encased and which is produced by the host cell after viral integration, is detected after 18 hrs, but not after 10 hrs post infection (Morgan and Fekete 1996). Viral RNA is detected after 12 hrs (personal communication, Dr C. Rallis, NIMR, London, UK). On this basis, misexpression of *Tbx2* was estimated to initiate around HH 12 in optic vesicles injected at HH 10, with protein synthesis occurring shortly after. This would result in the disruption of the asymmetrical expression of *Tbx2*, which is regionalised from HH 14 in the optic cup (Fig. 6.3).

Misexpression of *Tbx2* was assessed in all embryos analysed in this Chapter. There are several methods by which viral infection can be assessed in a tissue. These include detection of viral genes or the transgene itself by *in situ* hybridisation or detection of proteins encoded by the transgene or the virus, using immunohistochemistry. In this study, *in situ* hybridisation was employed using an

antisense probe for *Tbx2* or an antisense probe specific to a 900 bp region of the RCASBP *env* gene called *RSCH* (see Fig. 2.2). Since endogenous *Tbx2* expression is confined to the dorsal region of the developing chick eye after invagination, it was feasible to use the *Tbx2* probe to monitor misexpression in the ventral neural retina.

To assess the level of infection, one of two methods were used, depending on the requirements of subsequent experiments. Either whole mount *in situ* hybridisation of isolated optic cups were carried out, which allowed assessment of infection in the whole retina, or section *in situ* hybridisation of every tenth section of the eye. The frozen sections prepared for the latter approach were of 20 μm thickness, hence examination of every tenth section resulted in a snapshot of the status of targeting in every 200 μm of the eye.

Out of 34 examined eyes at HH 23-25, 22 showed high levels of ectopic *Tbx2* expression, suggesting that infection was successfully achieved in 65% of injections. Fig. 6.4 shows representative examples of control and infected eyes after *in situ* hybridisation. In all 22 infected eyes, *Tbx2* was ectopically expressed in the ventral neural retina (Table 6.3). In some eyes, infection was also confirmed by the detection of *RSCH* on sections adjacent to those hybridised with the *Tbx2* probe (Fig. 6.4 B,C). In most embryos, the lens, surface ectoderm, RPE, and some regions of the brain were also infected, indicating a wide spread of infection from the site of injection, which is likely due to the rapid diffusion of the viral solution when injected into the optic vesicle lumen. *In situ* hybridisation with the *Tbx2* and *RSCH* probes on adjacent sections revealed variable lens expression (Fig. 6.4 B,C). *RSCH* was detected in the dividing cell population in the anterior and equatorial regions of the lens, whereas *Tbx2* was expressed more widely in both dividing and non-dividing (posterior lens) cell populations of the lens. The *RSCH* probe detects a distinct mRNA splice form to the one encoding the transgene (Logan and Tabin 1998). One possible explanation for this is that exogenous *Tbx2* may be inducing ectopic expression of endogenous *Tbx2*, which is detected by the *Tbx2* probe throughout the lens. That the lens is likely to be permissive to *Tbx2* expression is supported by experiments in Chapter 4, where ectopic *Tbx2* expression was induced in the lens vesicle of the mouse embryo implanted with an rhBMP4 coated bead (Fig. 4.4 D).

Fig. 6.4 Examination of infection and morphology of retinae by RCAS-*cTbx2* and RCAS-AP viruses using whole mount and section *in situ* hybridisation and colourimetric detection of alkaline phosphatase activity

A, B, C depict frozen sections cut in the coronal plane at 20μm thickness, whereas D, E, F are retinal flat mounts. *In situ* hybridisation of control and infected samples were performed together under identical conditions. Images are representative of typical levels of infection obtained **(A)** Section of a control eye of a chick embryo at HH 25 showing the normal distribution of *Tbx2* expression in an uninfected retina. *Tbx2* transcripts were not present in the ventral neural retina (arrow). **(B)** Section of the eye of an embryo at HH 24 infected with RCAS-*cTbx2* at HH 10 and hybridised with the *Tbx2* probe. All morphological features expected at HH 24 were present. Ectopic *Tbx2* expression was detected in the ventral neural retina as compared to the control (arrow), and in the lens vesicle. The intensity of *Tbx2* expression was stronger in some areas of the neural retina (white arrowhead). *Tbx2* was also ectopically detected in the diencephalon (grey arrowhead). **(C)** Adjacent section to B, hybridised with a probe specific for part of the viral *env* gene (*RSCH*), indicating infection of the ventral neural retina and lens, as well as the diencephalon (grey arrowhead). **(D)** Flat mounted control retina hybridised with the *Tbx2* probe, showing endogenous *Tbx2* expression at HH 25. Remnants of the extra-ocular mesenchyme account for the blue signal in the ventral region of the retina, which otherwise lacks *Tbx2* expression (arrowhead). **(E)** RCAS-*cTbx2* infected retina at HH 25 hybridised with the *Tbx2* probe. *Tbx2* transcripts were present in large patches of the retina including the ventral region. Areas of strong signal are indicative of higher levels of *Tbx2* expression. **(F)** RCAS-AP infected retina at HH 23. Patchy infection, assayed by AP activity, was detected in all parts of the retina. Scale bars: 0.5 mm.

Abbreviations: D, dorsal; V, ventral.

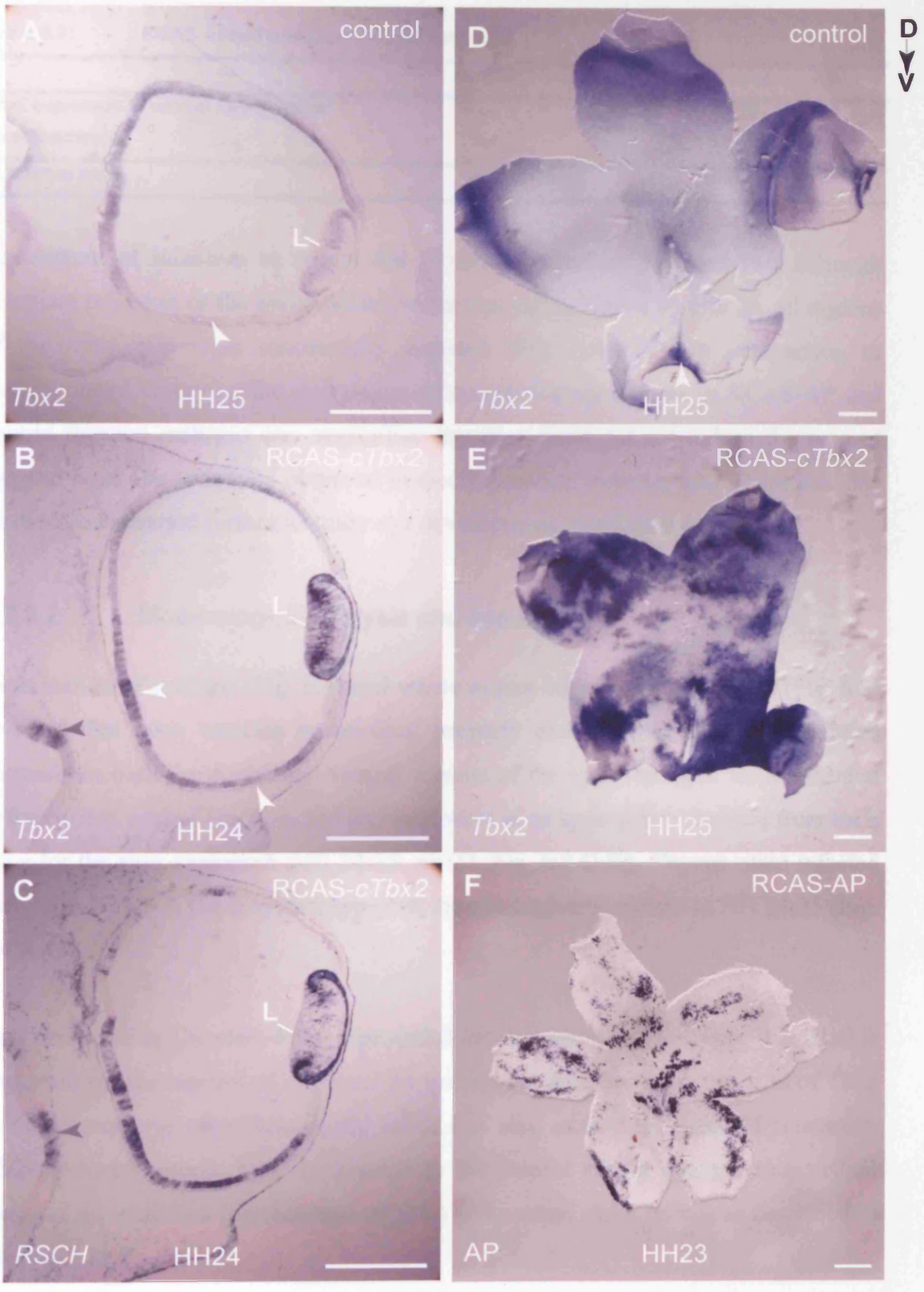
A
control
L
Tbx2
HH25
D
control
D
V
Tbx2
HH25
B
RCAS-cTbx2
L
Tbx2
HH24
E
RCAS-cTbx2
Tbx2
HH25
C
RCAS-cTbx2
L
RSCH
HH24
F
RCAS-AP
AP
HH23

Table 6.3: RCAS-c*Tbx2* infection in injected eyes

	control	virus
Tbx2 expressed in ventral neural retina	0	22
Total examined	10	34
% infected eyes	0 %	65 %

Assessment of infection in retinal flat mount preparations revealed that although complete infection of the entire neural retina was not achieved by HH 25, all regions of the optic cup were successfully targeted (Fig. 6.4 E,F). In comparison to electroporated embryos, the prevalence of morphological defects in RCAS-AP and control injected embryos was negligible. Injection itself did not induce the type of eye and head abnormalities observed in electroporation experiments. Therefore, this method was pursued further to study eye development in infected retinae.

6.2.3.2 Morphological analysis and eye size

Examination of sections (Fig. 6.4) and whole mount views of infected eyes (Fig. 6.5) revealed that optic vesicles invaginated properly and that the RPE differentiated normally in both the dorsal and ventral regions of the eye. The optic fissure formed in the correct ventral position, and its walls were at an appropriate distance from each other for the ages examined (HH 24-25, n= 22, Fig. 6.5 G,H). Though often infected with RCAS-*cTbx2*, the lens also appeared morphologically normal at HH 24-25 (Fig. 6.4 A-C).

Data presented in Chapters 4 and 5 provided indirect and direct evidence that *Tbx2* is important for the control of eye size. To investigate whether misexpression of *Tbx2* in the ventral eye recapitulates the small eye size caused by rhBMP4 treatment, which induced ectopic *Tbx2* expression in the ventral mouse neural retina, retinal area was measured on flat mounted infected and control chick retinae as described in Chapter 2.11.2.

Fig. 6.5 Morphology of RCAS-*cTbx2* infected and stage matched control embryos

Images depict lateral views of embryos unless stated otherwise. **(A)** Control embryo at HH 24. **(B)** RCAS-*cTbx2* infected embryo at HH 24, showing healthy morphology. **(C)** Dorsal view of the head of the control embryo in A. **(D)** Dorsal view of the head of the RCAS-*cTbx2* infected embryo in B. **(E)** Control embryo at HH 25. **(F)** RCAS-*cTbx2* infected embryo at HH 25, showing similar overall morphology to the embryo in E. **(G)** Ventral view of the eyes of the embryo in E. **(H)** Ventral view of the eyes of the embryo in F, showing normal optic fissure development. Arrows in G-H show the optic fissure. Scale bars: 1 mm

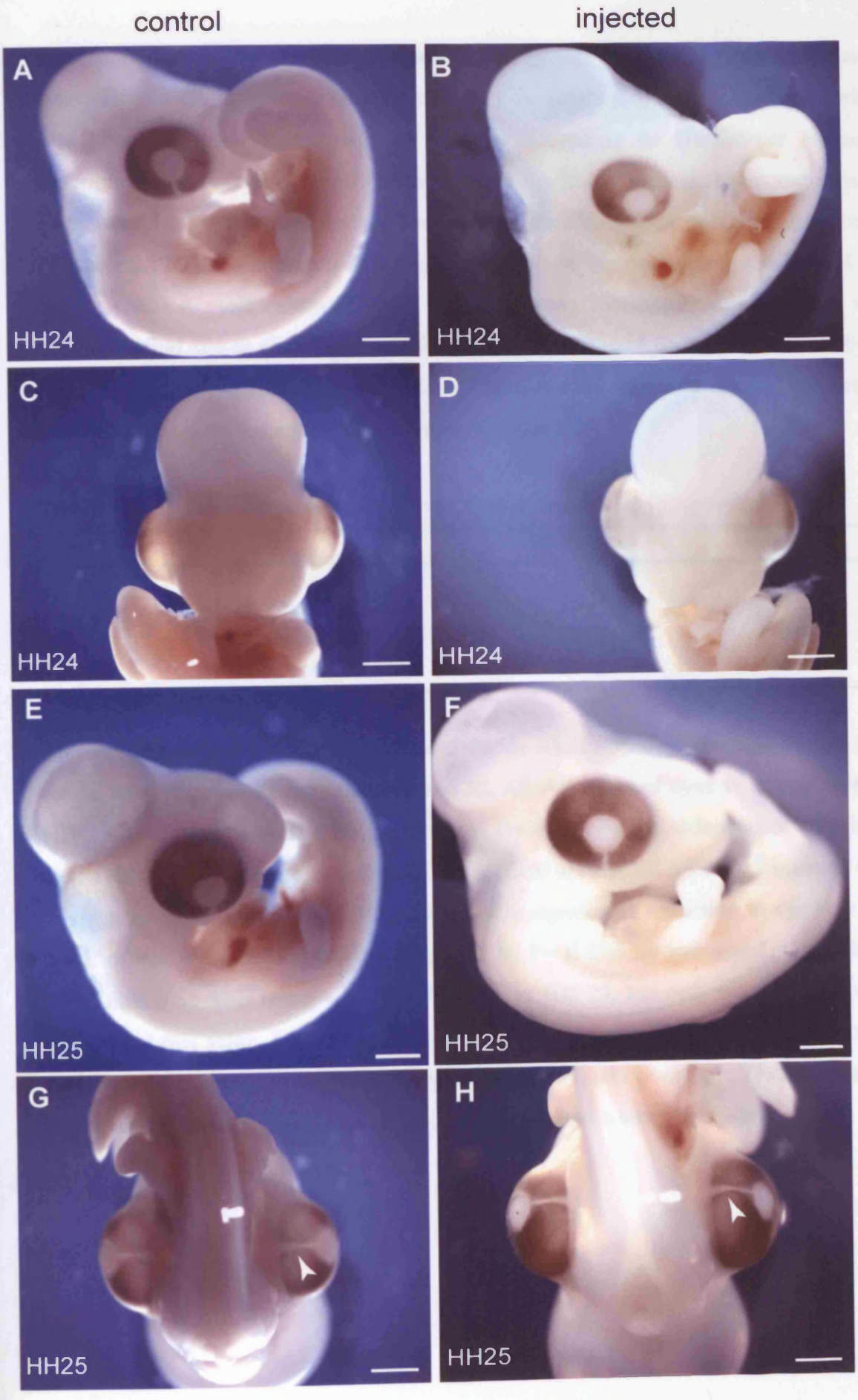
control
injected
A
HH24
B
HH24
C
HH24
D
HH24
E
HH25
F
HH25
G
HH25
H
HH25

First, retinal area was compared between four groups of control embryos between stages HH 23-28, in order to be confident that the method of staging embryos, which was based on their morphological features according to Hamburger Hamilton descriptions, and dissection and flat mounting of retinae were consistent and reliable. Data were Ln transformed to acquire normal distribution as described previously (Chapter 2.12.2). Comparison of retinal area between these age groups with the One-Way ANOVA test showed that retinal area increased significantly with developmental age as also suggested by the bar chart (Fig. 6.6; Table 6.4; $P<0.0001$). Overall, the method used for estimation of retinal area appeared reliable and retinal area increased with the age of the embryo as expected.

Table 6.4 Mean retinal area ± s.d. in HH 23-28 embryos

		n.	Mean (mm^2)	± 1 s.d.
Retinal area	HH 23 control	10	7.29	1.90
	HH 24 control	5	13.60	1.62
	HH 25 control	19	17.12	2.68
	HH 28 control	4	22.14	2.85

To eliminate the possibility that the viral vector itself imposed an effect on eye size, retinal area of control (non-injected) and RCAS-AP injected eyes were compared at HH 23 and found to be similar (Fig. 6.7 A; $P= 0.746$ by the independent samples t-test; Table 6.5). By contrast, comparison of retinal area in RCAS-*cTbx2* infected eyes to stage matched controls at HH 24 revealed a significant reduction in eye size as a result of ectopic *Tbx2* expression (Fig. 6.7 B; $P= 0.006$ by independent samples t-test; Table 6.5). This trend was also observed at HH 23, but only two embryos were analysed at this stage. The reduction in eye size is in accordance with the previously described findings in the mouse embryo (Chapter 4), where ectopic *Tbx2* expression in the ventral neural retina induced by rhBMP4 caused a small eye size.

Fig. 6.6 Comparison of retinal area between control embryos at HH stages 23-28

Bar chart shows Ln mean retinal area ± 1 s.d. for HH 23-28 control embryos. P-value calculated with the One-Way ANOVA test suggests that mean Ln retinal area differs significantly across the age groups. n= number of eyes per group

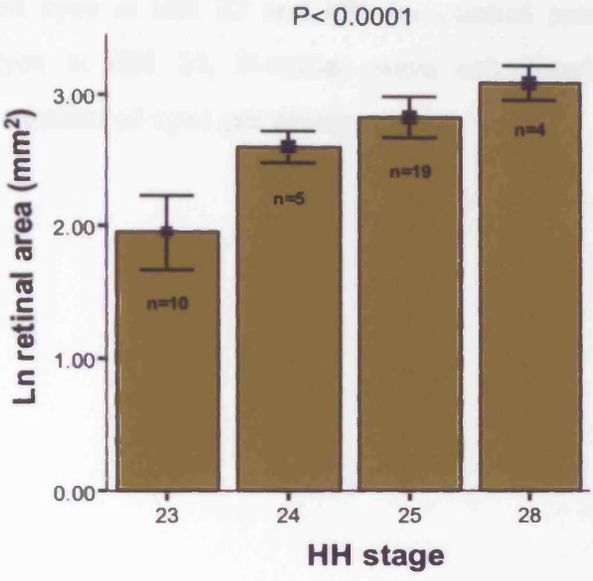
P< 0.0001
Ln retinal area (mm²)
3.00
2.00
1.00
0.00
n=10
n=5
n=19
n=4
23
24
25
28
HH stage

Fig. 6.7 Comparison of retinal area between control, RCAS-AP, and RCAS-*cTbx2* infected embryos

Bar chart shows mean Ln retinal area ± 1 s.d. for **(A)** control (non-injected) and RCAS-AP infected eyes at HH 23 and **(B)** for control (non-injected) and RCAS-*cTbx2* injected eyes at HH 24. P-values were calculated with the independent samples t-test. n= number of eyes per group.

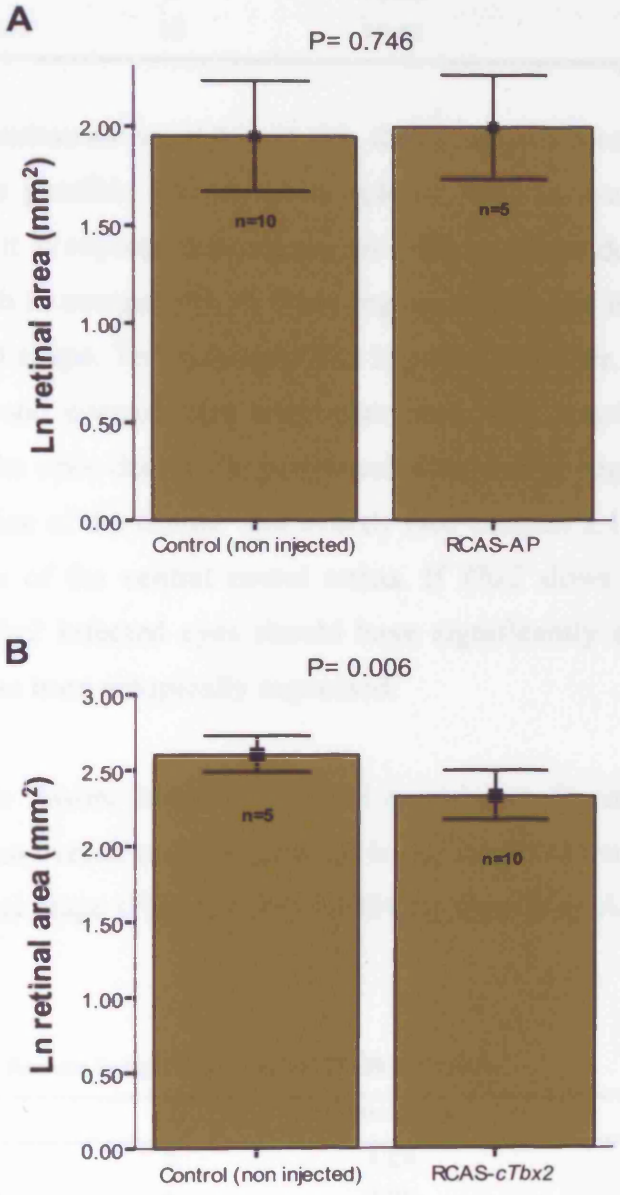
A
P= 0.746
Ln retinal area (mm²)
2.00
1.50
1.00
0.50
0.00
n=10
n=5
Control (non injected)
RCAS-AP
B
P= 0.006
Ln retinal area (mm²)
3.00
2.50
2.00
1.50
1.00
0.50
0.00
n=5
n=10
Control (non injected)
RCAS-cTbx2

Table 6.5 **Mean retinal area ± s.d. in RCAS-*cTbx2* treated and control groups**

		n.	Mean (mm^2)	± 1 s.d.
HH 23	control	10	7.29	1.90
	RCAS-AP	5	7.61	1.81
HH 24	control	5	13.60	1.62
	RCAS-*cTbx2*	10	10.44	1.68

The outcome of the experiments presented in this thesis support a role for *Tbx2* in eye size regulation. It is possible that the early role of *Tbx2* in eye development, during the period when it is expressed in retinal progenitors of the dorsal eye, is to reduce dorsal eye growth in comparison to other regions of the eye in order for the eye to acquire the correct shape. To investigate this hypothesis further, the size of the ventral eye in injected and control eyes were compared. The length of the optic fissure, measured from the optic disc to the peripheral most ventral edge of the neural retina following the outline of the fissure wall exactly (see Chapter 2.11.3), was used as a measure of the size of the ventral neural retina. If *Tbx2* slows growth of the neural retina, RCAS-*cTbx2* infected eyes should have significantly smaller ventral retinae, in which *Tbx2* has been ectopically expressed.

Comparison of the optic fissure length in control (non-injected) embryos at four different stages showed an overall trend of increase in the length of the ventral neural retina with developmental stage (Fig. 6.8; $P < 0.0001$ by One-Way ANOVA; Table 6.6).

Table 6.6 **Mean optic fissure length ± s.d. in HH 23-28 embryos**

		n.	Mean (mm)	± 1 s.d.
Optic fissure length	HH 23	8	1.23	0.27
	HH 24	4	2.05	0.05
	HH 25	17	2.18	0.35
	HH 28	4	2.66	0.39

Fig. 6.8 Comparison of the size of the ventral neural retina between control embryos across HH stages 23-28

Bar chart shows Ln transformed mean optic fissure length ± 1 s.d. in HH 23-28 control embryos. P-value calculated with the One-Way ANOVA test suggests that optic fissure length is significantly different across different age groups. n= number of eyes per group.

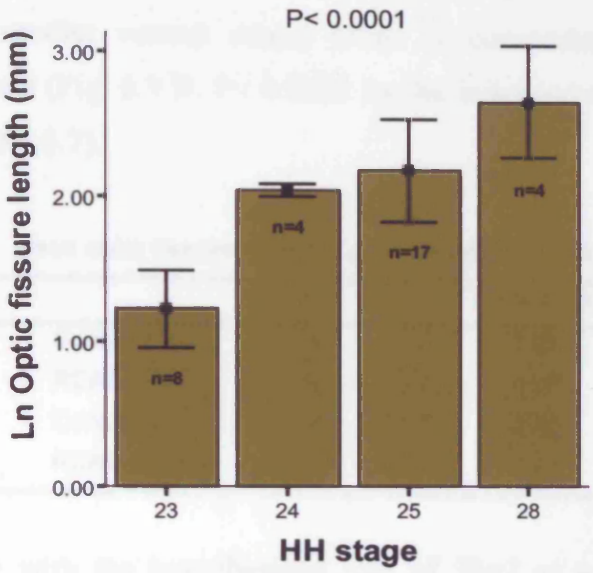
P< 0.0001
Ln Optic fissure length (mm)
3.00
2.00
1.00
0.00
n=8
n=4
n=17
n=4
23
24
25
28
HH stage

Comparison of control (non-injected) and RCAS-AP infected eyes at HH 23 revealed no significant difference in optic fissure length among groups, again confirming that viral infection alone does not perturb eye size (Fig. 6.9 A; P= 0.841 by independent samples t-test; Table 6.7). RCAS-*cTbx2* infected eyes however, at HH 24, showed a significantly smaller ventral neural retina in comparison to stage matched non-injected controls (Fig. 6.9 B; P< 0.0001 by the independent samples t-test, non equal variances; Table 6.7).

Table 6.7 **Mean optic fissure length ± s.d. in RCAS-*cTbx2* treated and control eyes**

		n.	Mean (mm)	± 1 s.d.
HH 23	Control	8	1.23	0.27
	RCAS-AP	4	1.26	0.22
HH 24	Control	4	2.05	0.05
	RCAS-*cTbx2*	8	1.43	0.27

In accordance with the hypothesised role of *Tbx2* as a negative regulator of eye growth, disruption of the asymmetrical expression of *Tbx2* by misexpression in the embryonic chick eye, resulted in eye size that was smaller in infected eyes compared to stage matched controls. The significant decrease in growth of the ventral neural retina can be interpreted as the ventral neural retina adapting the growth rate of the dorsal neural retina, upon *Tbx2* misexpression in this region.

6.2.3.3 Analysis of differentiation in RCAS-*cTbx2* infected eyes

One of the mechanisms that can reduce the growth of a tissue is untimely differentiation of progenitor cells. Growth can be limited if progenitor cells exit the cell cycle prematurely on receiving cues that promote cell cycle exit. This possibility was investigated in RCAS-*cTbx2* infected eyes by immunohistochemistry on frozen sections using the VC1.1 and RMO270 antibodies, used in the previous Chapter, as well as the ßIII-tubulin antibody, which labels early differentiating neurons and their axonal processes (see Chapter 2.8.1.1 for details of antibodies).

Fig. 6.9 Comparison of the size of the ventral neural retina between control (non-injected), RCAS-AP, and RCAS-*cTbx2* infected embryos

Bar charts show mean optic fissure length ± 1 s.d. in **(A)** control (non-injected) and RCAS-AP infected eyes at HH 23 and in **(B)** control (non-injected) and RCAS-*cTbx2* infected eyes at HH 24. P-values were calculated with the independent samples t-test assuming unequal variances in B. n= number of eyes per group.

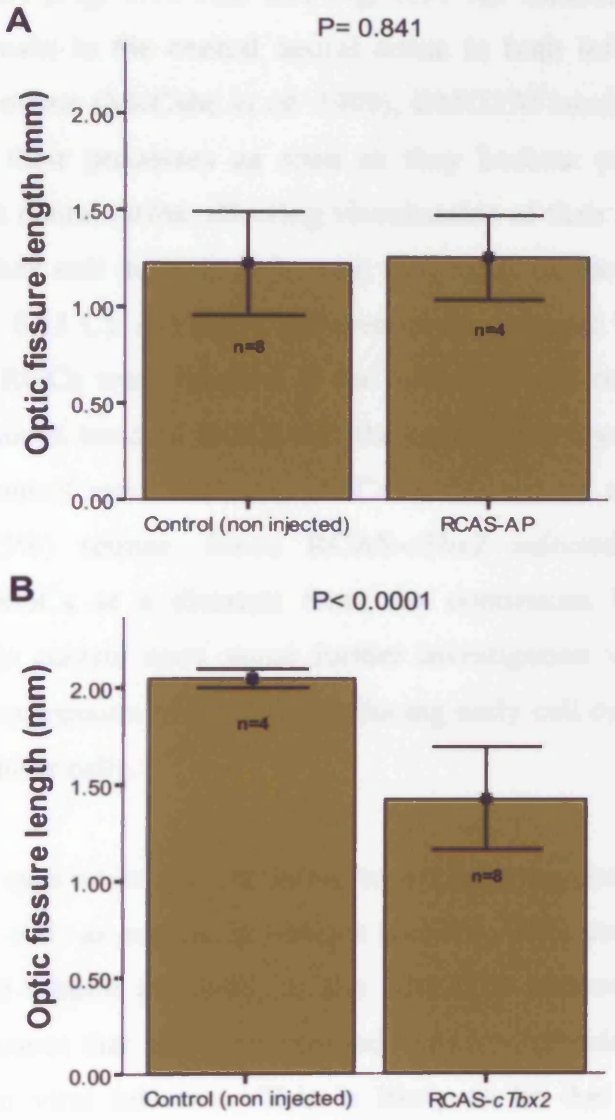
A
P= 0.841
Optic fissure length (mm)
2.00
1.50
1.00
0.50
0.00
n=6
n=4
Control (non injected)
RCAS-AP
B
P< 0.0001
Optic fissure length (mm)
2.00
1.50
1.00
0.50
0.00
n=4
n=8
Control (non injected)
RCAS-cTbx2

Immuno-labelling with the VC1.1 and the RMO270 antibodies revealed no major differences in the pattern of differentiation between control and RCAS-*cTbx2* infected eyes at HH 24 (Fig. 6.10 A,B and Fig. 6.11 A). Labelling was seen in a continuous broad domain in the central neural retina in both infected and control eyes. As reported by others (McCabe *et al.* 1999), RMO270 labelled the cytoplasm of RGC bodies and their processes as soon as they became postmitotic on the ventricular edge of the neural retina, allowing visualisation of their laminar migration from the time when they exit the cell cycle until they settle on the vitreal surface of the neural retina (Fig. 6.11 C). Although, differentiation appeared largely normal, in infected eyes, a few RGCs were labelled in the ventral neural retina at a distance away from the continuous band of RGCs and the nerve fibre layer (6/8, 75%; Fig. 6.11 A, arrow). In control eyes, scattered RGCs in the ventral neural retina were observed in 2/6 (33%) retinae. Since RCAS-*cTbx2* infected eyes contained occasional labelled RGCs at a distance from the continuous band at a higher incidence than seen in control eyes, some further investigation was undertaken to examine whether misexpression of *Tbx2* was inducing early cell cycle exit in ventral infected retinal progenitor cells.

Infected and control eyes were flat mounted, to exclude the possibility of falsely scoring differentiated cells as ectopic in oblique sections. Differentiated RGCs were labelled with the ßIII-tubulin antibody, as the RMO270 antibody was unable to detect its antigen in tissues that had been exposed to *in situ* hybridisation, which was performed to confirm viral infection. This is likely to be due to the failure of preservation of the epitope, which the RMO270 antibody recognises, during the *in situ* hybridisation procedure.

Fig. 6.10 VC1.1 immunohistochemistry in control and RCAS-*cTbx2* infected eyes at HH 24

Images show coronally cut frozen sections (20μm) immuno-labelled with VC1.1 (green) and stained with propidium iodide in red. Insets show high power views of the boxed areas. Arrowheads indicate labelled cell bodies. **(A)** Control eye showing VC1.1 labelling in the central (proximal) neural retina. Arrow shows the dorsal limit of differentiation. **(B)** VC1.1 immuno-labelling in an RCAS-*cTbx2* infected eye. Arrow shows the dorsal limit of differentiation. **(C)** Positive control for VC1.1 labelling in a section through the neural tube. **(D)** Negative control for labelling by the secondary antibody in the absence of the primary antibody. Scale bars: 0.1 mm

Abbreviations: D, dorsal; V, ventral

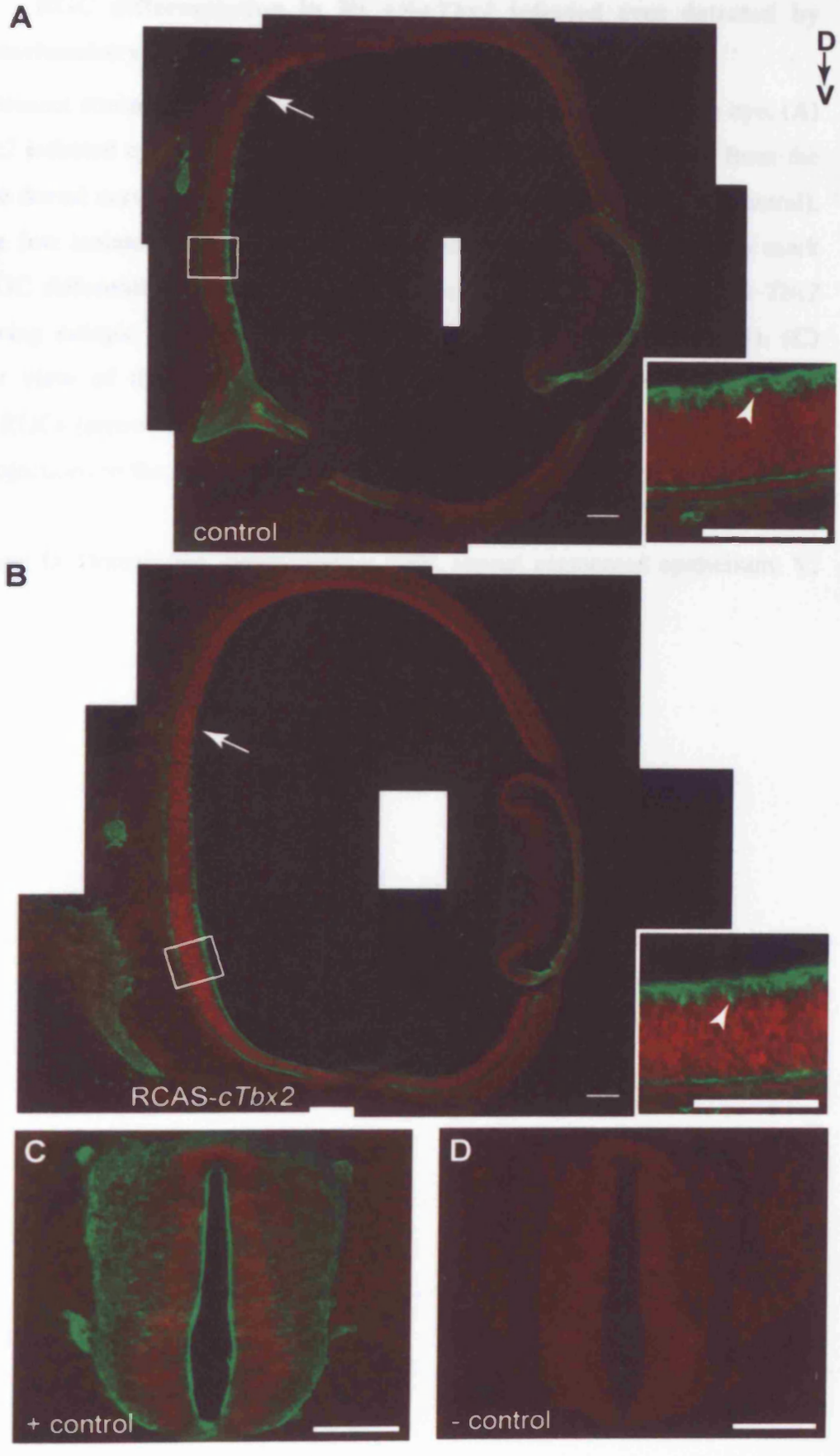
A
D
V
control
B
RCAS-cTbx2
C
+ control
D
- control

Fig. 6.11 RGC differentiation in RCAS-*cTbx2* infected eyes detected by immunohistochemistry using the RMO270 antibody

A and B represent coronal 20 μm frozen sections through the midline of the eye. **(A)** RCAS-*cTbx2* infected eye at HH stage 24 showing labelled RGCs (green) from the region of the dorsal curvature to the optic disc and a short distance beyond (ventral), as well as a few isolated RGCs located in the ventral neural retina. Arrows mark limits of RGC differentiation. **(B)** Adjacent section to A hybridised with the *Tbx2* probe, showing ectopic *Tbx2* expression in the ventral neural retina (arrow). **(C)** High power view of the neural retina in A (boxed area) showing labelling of postmitotic RGCs (arrow) at the ventricular surface (facing RPE) of the neural retina and their projections to the vitreal surface (facing lens). Scale bars: 0.1 mm

Abbreviations: D, Dorsal; NR, neural retina; RPE, retinal pigmented epithelium; V, Ventral

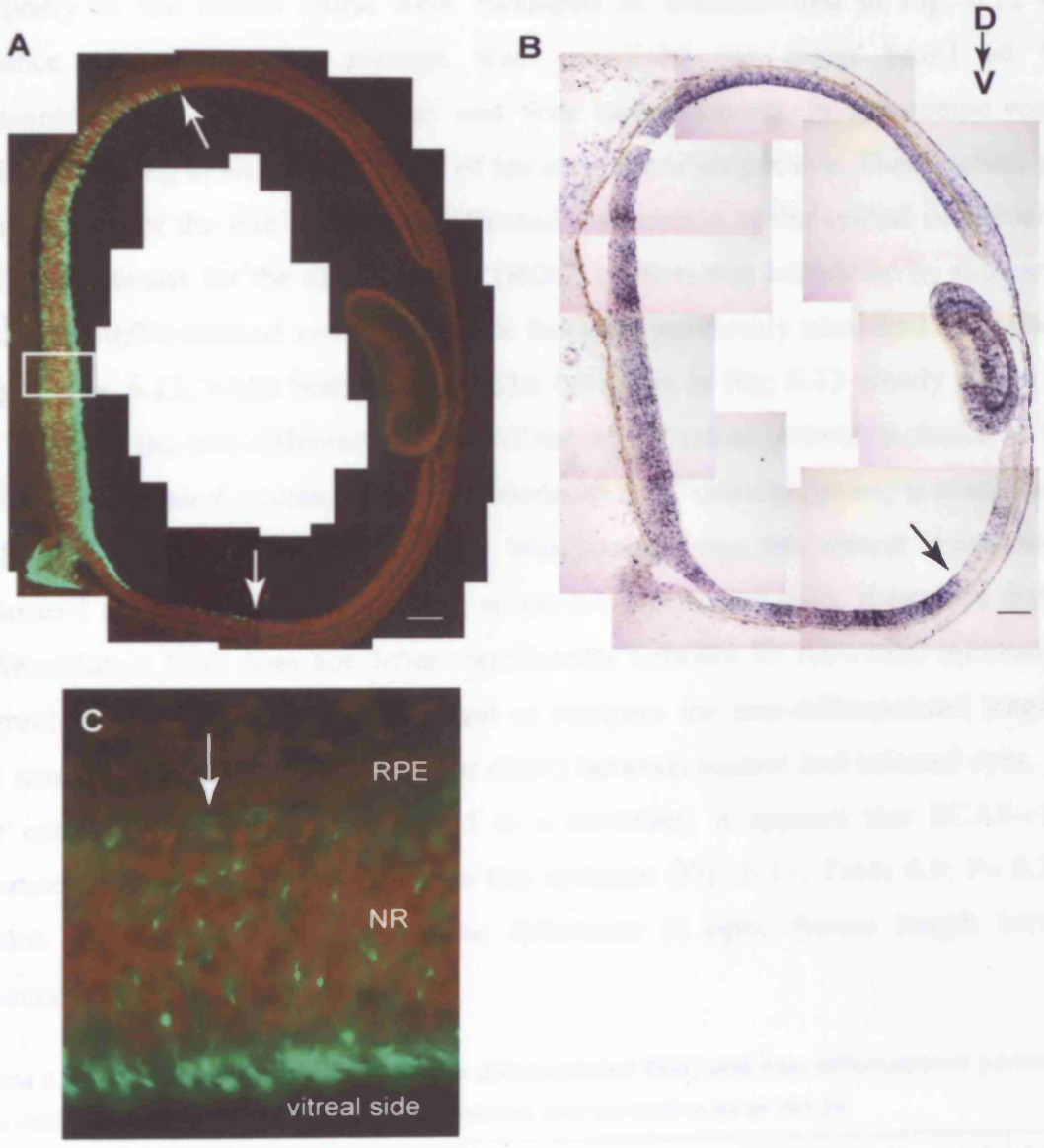
A
B
D
V
C
RPE
NR
vitreal side

The distances between the ventral-most differentiated RGC bodies to the ventral periphery of the neural retina were measured as demonstrated in Fig. 6.12 (the distance of arrows). An average was calculated per retina based on five measurements in the naso-ventral and five measurements in the tempo-ventral regions resulting in an average value of ten measurements per eye. These values gave an indication of the size of the non-differentiated portion of the ventral neural retina, while an estimate for the differentiated (RGC) portion was calculated by subtraction of the non-differentiated average distance from the previously measured optic fissure length (Fig. 6.12, white broken lines). The bar chart in Fig. 6.13 clearly shows that the length of the non-differentiated part of the neural retina (cream) is similar in both infected and control retinae, while differentiated RGC domain (green) is much longer in control retinae (Table 6.8). Taking into account that the ventral neural retina, measured as the optic fissure length, is shorter in infected eyes, it appears that the differentiation front does not differ significantly between RCAS-*cTbx2* infected and control eyes. Using the ANCOVA test to compare the non-differentiated length of the neural retina (cream portion of bar chart) between control and infected eyes, with the optic fissure length incorporated as a covariate, it appears that RCAS-*cTbx2* treatment has no significant effect on this distance (Fig. 6.13; Table 6.9; P= 0.226), which was also not affected by the difference in optic fissure length between treatment groups (P= 0.227).

Table 6.8 Mean length ± s.d. of the differentiated RGC and non-differentiated portions of the ventral neural retina of RCAS-*cTbx2* treated and control eyes at HH 24

		n.	Mean (mm)	± 1 s.d.
RGC front to ventral periphery	control	3	0.76	0.10
	RCAS-*cTbx2*	6	0.73	0.11
Optic disc to ventral RGC front	control	3	1.32	0.13
	RCAS-*cTbx2*	6	0.58	0.19

In contrast to the non-differentiated length of the neural retina, when the distance of the ventral differentiation front (green portion of bar chart) was compared between RCAS-*cTbx2* treated and control retinae using the ANCOVA test, it appeared that the optic fissure length did have a significant effect on this distance as expected (Table 6.10; P= 0.005). However, when this effect was taken into account, the ventral differentiation front was not significantly different between treatment groups (Fig. 6.13; Table 6.10; P= 0.226).

Fig. 6.12 RGC network in flat mounted RCAS-*cTbx2* infected and control retinae at HH 24 detected by immunohistochemistry using the ßIII-tubulin antibody

(A) *Tbx2* expression in a control (non-injected) flat mounted retina detected by whole mount *in situ* hybridisation. The optic disc is in the centre of the dashed circle. Broken black line indicates the length of the optic fissure in the ventral neural retina **(B)** Same retina as in A after whole mount immuno-labelling with the ßIII-tubulin antibody, which labels RGCs and their axonal processes within the retina. Dashed circle shows the optic disc. The arrow indicates the average distance, from 10 measurements, of the ventral-most RGC bodies to the ventral retinal periphery. This is the non-differentiated part of the neural retina. The white broken line extends from the optic disc to the ventral RGC differentiation front, calculated as optic fissure length minus the average distance of the RGC front to the ventral periphery. **(C)** High power merged image of *Tbx2* expression and RGC differentiation in the dorsal neural retina, showing overlap between their expressions. Inset shows a higher power view. **(D)** *Tbx2* expression in an RCAS-*cTbx2* infected flat mounted retina detected by whole mount *in situ* hybridisation. **(E)** Same retina as shown in D after ßIII-tubulin immuno-labelling. The circles, arrow, and dashed lines represent the same as in A and B. **(F)** Merged image of the boxed region in D and E, with inset showing a higher power view. Scale bars: 0.5 mm in A, B, D, E; 0.1 mm in C, F.

Abbreviations: D, dorsal; V, ventral

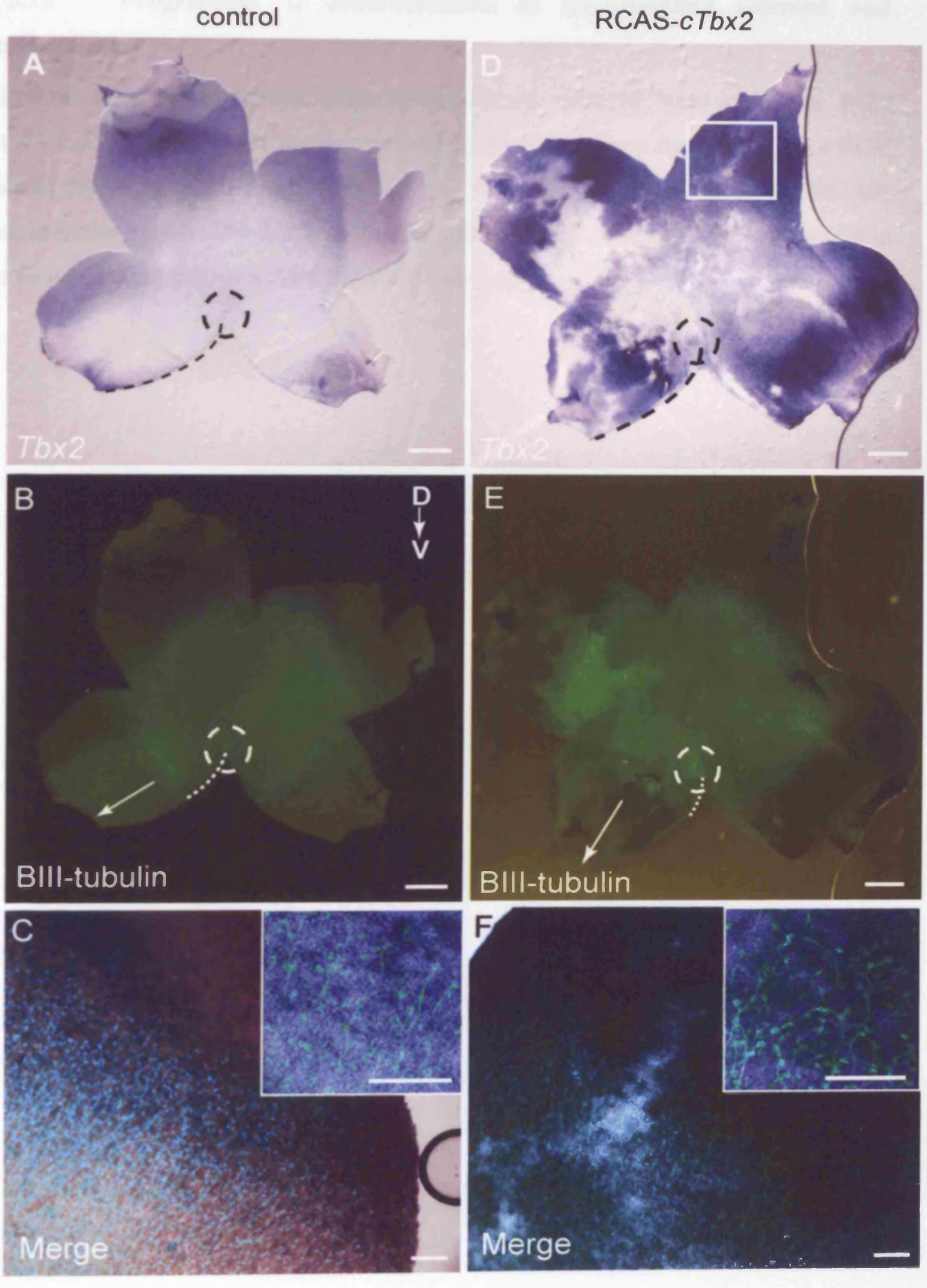
control
RCAS-cTbx2
A
Tbx2
D
Tbx2
B
D
V
BIII-tubulin
E
BIII-tubulin
C
Merge
F
Merge

Fig. 6.13 Progression of differentiation in RCAS-*cTbx2* infected and control retinae

Stacked bar chart represents the mean distance (mm) from the optic disc to the RGC front ± 1 s.d. (green portion) and the mean distance (mm) from the ventral most RGC bodies to the ventral retinal periphery ± 1 s.d. (cream portion) in control and RCAS-*cTbx2* infected eyes at HH 24. Together, the stacked bars represent the difference in optic fissure length between control and infected eyes

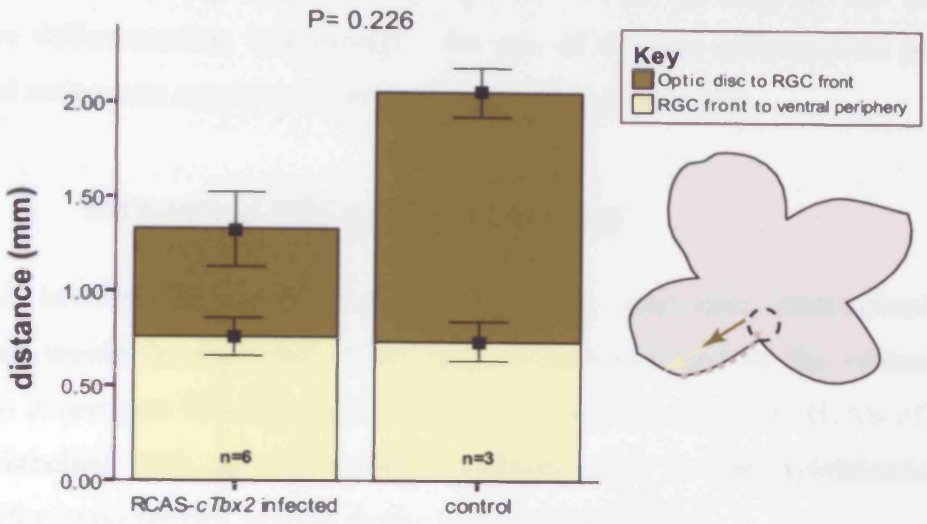

Table 6.9: The ANCOVA table for the analysis of the ventral RGC front to the ventral peripehry (cream portion) in RCAS-*cTbx2* infected and control retinae

Dependent Variable: Average RGC front to ventral periphery (mm)

Source	Type III Sum of Squares	df	Mean Square	F	Sig.
Corrected Model	.018(a)	2	.009	.963	.434
Intercept	.011	1	.011	1.225	.311
Optic fissure length	.017	1	.017	1.810	**.227**
Treatment	.017	1	.017	1.817	**.226**
Error	.056	6	.009		
Total	5.129	9			
Corrected Total	.074	8			

a R Squared = .243 (Adjusted R Squared = -.009)

Table 6.10: The ANCOVA table for the analysis of the distance of the optic disc to the RGC front (green portion) in RCAS-*cTbx2* infected and control retinae

Dependent Variable: Optic disc to average RGC front (mm)

Source	Type III Sum of Squares	df	Mean Square	F	Sig.
Corrected Model	1.272(a)	2	.636	68.260	.000
Intercept	.011	1	.011	1.225	.311
Optic fissure length	.167	1	.167	17.971	**.005**
Treatment	.017	1	.017	1.817	**.226**
Error	.056	6	.009		
Total	7.437	9			
Corrected Total	1.328	8			

a R Squared = .958 (Adjusted R Squared = .944)

These data suggest that misexpression of *Tbx2* in the ventral neural retina is not inducing early differentiation of retinal progenitor cells and therefore the mechanism by which *Tbx2* misexpression reduces growth of the developing eye is not by premature differentiation. Interestingly, the size of the non-differentiated portion of the neural retina was constant regardless of the size of the retina.

6.2.3.4 Intra-retinal RGC axonal projections

If *Tbx2* is involved in axonal routing towards the optic disc, intra-retinal axonal misrouting would be expected when *Tbx2* is misexpressed in the ventral neural retina. To investigate this hypothesis, whole retinae infected with RCAS-*cTbx2* and immuno-labelled with the ßIII-tubulin antibody after *in situ* hybridisation were analysed for irregularities in intra-retinal axonal projections.

In control retinae at HH 24-25, axons labelled with the ßIII-tubulin antibody covered the vitreal surface of the neural retina in radial arrays, which projected towards the optic disc from all areas of the retina (see Fig. 6.12). No axons in dorsal, nasal or temporal regions were seen to migrate outside of the ordered projections towards the optic disc. In the ventral aspect of the neural retina however, mainly in close proximity to the optic fissure, occasionally solitary axons were found outside of the main projection path (Fig. 6.14). Some of these axons belonged to cell bodies positioned within the network, while others originated from cell bodies outside of the network. The number of ectopic axons were however too small for analysis. A preliminary analysis was performed to assess whether the incidence of axonal migration errors was higher in infected eyes as compared to stage matched controls. This is included in Appendix A.

Fig. 6.14 RGC axonal projections in the ventral neural retina of control and RCAS-*cTbx2* infected eyes at HH 24

Images depict flat mounted retinae immuno-labelled with the ßIII-tubulin antibody (green) to show RGC axonal projections in **(A)** control and **(B-E)** several RCAS-*cTbx2* infected eyes. Arrowheads indicate misrouted axons away from the common route towards the optic disc. **(F)** Close-up of the deviated axon in D (arrow). **(G)** Close-up of the deviated axon in C (arrow). Scale bars: 0.1 mm

Abbreviations: OD, optic disc; OF, optic fissure.

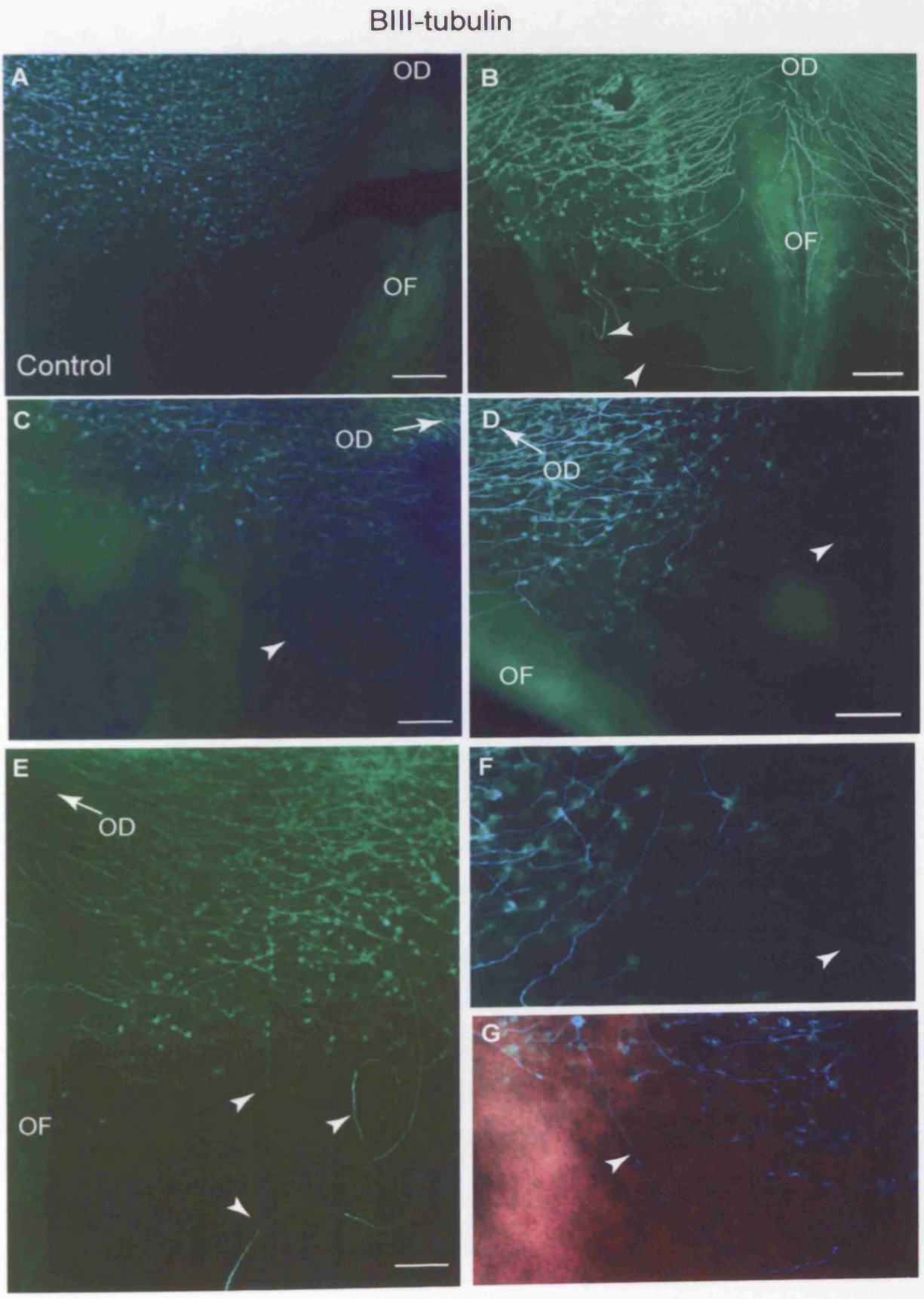
BIII-tubulin
A
OD
OF
Control
B
OD
OF
C
OD
D
OD
OF
E
OD
OF
F
G

6.3 Discussion

6.3.1 Summary of findings

1) Two gene delivery methods were tested for their feasibility and efficiency in delivering exogenous DNA to the embryonic eye. Retroviral mediated gene delivery proved superior than electroporation in terms of success of targeting of the developing eye as well as preservation of eye morphology.

2) *Tbx2* expression in the developing chick eye is first detected at HH 12 in the entire distal neuroepithelium of the optic vesicle but becomes restricted to the dorsal neural retina after optic vesicle invagination, where it persists until at least HH 25. Expression was also detected in the mesenchyme between the optic cup and the surface ectoderm.

3) Retroviral mediated misexpression of *Tbx2* resulted in a small retinal area and particularly a significant decrease in the length of the ventral neural retina, where *Tbx2* was misexpressed.

4) *Tbx2* misexpression did not prevent RGC differentiation.

5) Although the length of the differentiated region of the ventral neural retina of infected eyes was smaller than controls, this decrease was linked to the reduction in the size of the ventral neural retina. The non-differentiated portion of the ventral neural retina however was similar between treatment groups regardless of the difference in eye size.

5) Some intra-retinal axonal misrouting was observed in the ventral region of infected eyes, though a larger analysis is required to establish the involvement of *Tbx2* in this process.

6.3.2 Electroporation as a tool for somatic gene manipulation in the developing eye

Since the first reports of the use of electroporation in *in vivo* systems (e.g. (Muramatsu *et al.* 1997)), this method has been employed by many researchers to address various questions, as it provided a new and promising tool for manipulating gene expression. It is quick, relatively cost-effective, easy to operate, and provides solutions to some of the restrictions posed by earlier existing gene delivery methods, such as the low efficiency of lipofection and microinjection, or the size and host restrictions imposed by viral vectors. Electroporation is now being extensively used in studies involving chick embryos, but its usage for studying mouse development is relatively unexplored. Gene delivery to the developing mouse eye by electroporation has previously not been reported. In this Chapter, I used electroporation to test the feasibility of this method to deliver a reporter construct to the early mouse optic cup followed by whole mouse embryo culture. Various parameters were tested and although plasmid DNA uptake and satisfactory embryo survival were achieved, it was not possible to target the neural retina. DNA injections were performed in the vitreous chamber but also into the subretinal space, as better transfection of the retina was reported to be achieved from this region rather than the vitreal side of the retina in neonatal mice and rats (Matsuda and Cepko 2004). However, in my experience, subretinal injections did not improve embryonic retinal transfection.

The biggest challenge with this method was the difficulty of retaining the DNA solution in the optic cup between injection and the delivery of current. This is because of the small volume of the embryonic eye. Although plasmid DNA was dissolved in sucrose to make the solution more viscous, a superior method appears to be required. Recently, pluronic gels have become available, which retain DNA at the site where they are implanted. DNA is dissolved in the gel, which is then allowed to set and then implanted into the tissue (Becker and Mobbs 1999). Experiments would have to be carried out to determine whether it is feasible to implant the gel within the vitreous or the subretinal space of the embryonic eye, where DNA can be transferred into the retina by the direction of the current. Alternatively, DNA of a higher concentration than used here may improve transfection.

Electroporation was also tested in the chick embryo, as several studies had previously reported successful targeting of the developing chick neural retina. However, as it induced morphological deformities in a high percentage of embryos and affected eye growth, this method was not pursued further. Although several laboratories report using this method successfully, there are mentions in the literature that transfections cannot be achieved based on published parameters. For example, Momose and colleagues could not target the neural retina with the method of Muramatsu and colleagues. Cepko and colleagues could not reproduce the results of Dezawa and colleagues in targeting the RGCs (Matsuda and Cepko 2004). Although it seems possible to optimise electroporation to perhaps achieve a high percentage of successfully targeted specimens, tissue damage in a proportion of the experimental group is unavoidable with this method, and electroporation may therefore not offer the level of reproducibility desired in experiments.

6.3.3 Conservation of *Tbx2* expression and function in vertebrate eye development

In both the mouse and the chick embryo, *Tbx2* is expressed in the optic vesicle, and then in the dorsal optic cup after invagination of the vesicle. Later, both were also detected in mesenchymal cells between the surface ectoderm and the distal tip of the ventral neural retina (In Chapter 3 and here). It therefore appears that, at least during the formation of the optic cup, the spatial expression of *Tbx2* is conserved in these two animal models. Dorsal restriction of *Tbx2* in the optic cup has also been reported in *Xenopus* (Takabatake *et al.* 2002), and zebrafish embryos (Dheen *et al.* 1999), suggesting that dorsal expression of *Tbx2* in the eye serves a highly conserved role in vertebrate species. Despite the conservation of expression in the dorsal optic cup, some differences do exist between *Tbx2* expression in higher and lower vertebrates. In Zebrafish, *Tbx2* (*tbx2b*; *tbxc*) is expressed as early as in the eye field, unlike in the chick and the mouse. In *Xenopus*, *ET*, which is another member of the *Tbx2* subfamily and most closely related to the mouse *Tbx3*, is also expressed in the eye field. This site of expression in lower vertebrates highlights some differences and suggests that perhaps *Tbx2* serves additional early roles in eye development in lower vertebrates.

During the course of this thesis, two studies were reported which addressed the role of *Tbx2* in *Xenopus* and zebrafish eye development, using gain of function and loss of function approaches respectively. Misexpression of *Tbx2* in *Xenopus*, by electroporation in the eye field, was reported to disrupt D-V patterning, by loss of *Pax2* expression in the ventral eye (Takabatake *et al.* 2002). Moreover, pigmentation of the ventral optic cup was absent and the optic stalk appeared shorter than normal. The lack of pigmentation phenotype, was not observed in RCAS-*cTbx2* infected chick eyes presented here. Interestingly and in agreement with results presented here, in the *Xenopus* study, the most severely affected part of the eye was the ventral optic cup, which was absent in embryos with a severe phenotype. The cause of the absence of the ventral optic cup was not investigated. In RCAS-*cTbx2* infected eyes, eye size was reduced and particularly a reduction in the length of the ventral neural retina was detected. Together, these data suggest that *Tbx2*, when misexpressed in the ventral aspects of the developing eye, represses its growth and development.

6.3.4 Small eye size induced by *Tbx2* misexpression in the chick eye provides further support of a role in eye size regulation by *Tbx2*

Quantification of retinal area, as a measure of eye size, in RCAS-*cTbx2* infected retinae revealed that these were significantly smaller than eyes of stage matched controls. Furthermore, measurements of the length of the ventral neural retina showed that this reduction was even more marked in the length of the ventral eye. These observations corroborate the finding in the analysis of *Tbx2*$^{-/-}$ embryos that *Tbx2* is indeed important for the regulation of eye size. Although opposite approaches were used in these two studies, the outcome of both was a small eye phenotype. There are several examples where loss of function and overexpression of genes, transcription factors in particular, cause the same phenotype. For example, submicroscopic duplications of Xq27.1, containing the human *SOX3* transcription factor gene, as well as mutations which reduce the DNA binding activity of *SOX3* result in infundibular hypoplasia and hypopituitarism (Woods *et al.* 2005). Loss of function mutations of *Pax6* as well as transgenic overexpression of multiple copies of *PAX6* cause similar eye phenotypes including a small eye and anterior segment defects (Hill *et al.* 1991; Schedl *et al.* 1996). It has been argued that overexpression

may lead to inhibition of transcriptional activation, in the case of *Pax6*, and therefore result in the same phenotype as loss of expression (Schedl *et al.* 1996).

However, the effect of *Tbx2* homozygosity in mice and *Tbx2* misexpression in the developing chick eye is slightly different to a simple loss of function versus overexpression/increased activation effect of *Pax6* and *SOX3* . This is because *Tbx2* is asymmetrically expressed in the developing eye, so it would be expected that in *Tbx2*$^{-/-}$ eyes, the dorsal eye would be affected by the loss of *Tbx2*, while in the chick eye, although it is probable that the dorsal eye was exposed to higher levels of *Tbx2* expression than normal, the ventral eye was exposed to ectopic *Tbx2* expression, and it would be expected that ventral eye development be more affected. Therefore, the *Tbx2* manipulation studies presented here are not a simple case of loss of/reduced function versus overexpression. Instead, it appears likely that *Tbx2* is required for mediating several different mechanisms, both intrinsic and extrinsic, that affect eye size (see Chapter 7 for a final discussion) and that when the balance of these mechanisms is perturbed, growth of the eye is impaired.

Due to time constraints, infected chick eyes could not be extensively analysed to study mechanisms such as cell death and cell proliferation or molecular changes in gene expression upon *Tbx2* misexpression. Analysis of cell differentiation and quantification of the differentiation front did not reveal an increase in cell differentiation, which is what would be expected if premature cell differentiation was preventing the growth of the eye.

6.3.5 The effect of *Tbx2* misexpression on the differentiation front and intra-retinal axonal projections

A role in tissue specification and differentiation has been demonstrated for several members of the T-box gene family, both during early development and later during organogenesis. For example, *Tbx4* is required for allantois development; loss of *Tbx4* results in failure of expression of allantois differentiation markers (Naiche and Papaioannou 2003).

The effect of Tbx2 misexpression on RGC differentiation and axonal projections were investigated here for two reasons. Firstly, *Tbx2* is one of the few dorsally expressed genes discovered so far and therefore a potential candidate for providing positional information and regulating genes which have been hypothesised to aid in topographic mapping of RGC axons to the brain (Sperry 1963). In support of this idea, misexpression of another dorsally expressed T-box gene, *Tbx5*, in the chick eye causes axonal misprojections to the tectum (Koshiba-Takeuchi *et al.* 2000). Moreover, in *Tbx2*$^{-/-}$ mutants, the RGC axons appeared severely disorganised. The second reason for analysing differentiation was due to a most reason report, in which morpholino-mediated knock-down of *Tbx2b* in zebrafish eyes was described to cause a transient arrest in cell differentiation of dorsal neurons only (Gross and Dowling 2005), suggesting a profound effect on cell differentiation, and most interestingly localised to the dorsal eye.

Differentiation, examined by ßIII-tubulin, VC1.1, and RMO270 immuno-labelling after misexpression of *Tbx2* in the ventral retina, appeared similar to non manipulated eyes at HH 24-25. The length of the differentiation front in the ventral neural retina was reduced in line with the reduction in ventral retinal growth in RCAS-*cTbx2* infected eyes, while the non-differentiated portion of these eyes was similar to stage matched controls. A previous study has reported that the non-differentiated portion remains constant as the neural retina grows; in other words, retinal cell differentiation keeps pace with retinal growth (McCabe *et al.* 1999).

The incidence of ectopically projecting axons was slightly higher after *Tbx2* misexpression, suggesting that ectopic *Tbx2* expression can cause a certain degree of axonal misrouting. Previous studies in which *Tbx5*, *Ventroptin*, and *Bmp4* were misexpressed, or *Bmprlb* or *EphB* receptors were disrupted by targeted mutations also reported a low incidence of axonal misrouting, suggesting that perhaps RGC axons are guided by an array of signals and therefore, the addition of one or lack of one does not overtly affect their projections (Koshiba-Takeuchi *et al.* 2000; Sakuta *et al.* 2001; Birgbauer *et al.* 2000; Liu *et al.* 2003).

CHAPTER 7 Final Discussion

Experiments presented in this thesis aimed to investigate the role of dorsally expressed genes in eye development. Molecular patterning along the D-V axis of the developing eye is remarkably conserved in vertebrates, with *Bmp4*, and several members of the T-box gene family expressed in the dorsal eye, while *Vax2*, *Pax2*, and the Bmp4 antagonist, *Ventroptin* are expressed ventrally (Barbeiri *et al.* 1999; Schulte *et al.* 1999; Mui *et al.* 2002; Barbeiri *et al.* 2002; Nornes *et al.* 1990; Furuta and Hogan 1998; Sakuta *et al.* 2001; Belecky-Adams and Adler 2001; Trousse *et al.* 2001; Papaioannou 2001). In addition, RA signalling, shown by reporter gene expression driven by RA nuclear receptor promoters, is high ventrally and lower dorsally (McCaffery *et al.* 1999; Wagner *et al.* 2000). Members of the EphB/ephrinB families, implicated in topographic mapping of RGC axons to the brain, are also asymmetrically distributed along the D-V axis (Peters and Cepko 2002), and several lines of evidence suggest that these are downstream of the early transcription factors, as loss of function of *Vax2* and manipulation of *Tbx5* result in alterations in the expression of these molecules (Koshiba-Takeuchi *et al.* 2000; Schulte *et al.* 1999; Mui *et al.* 2002; Barbeiri *et al.* 2002). A regulatory hierarchy is starting to emerge where signalling factors induce the expression of transcription factors, which in turn regulate molecules such as the ephrins/EphBs and undoubtedly numerous other cell adhesion, cell cycle, and signalling molecules. Although much remains to be elucidated regarding the role of these asymmetrically expressed genes in eye development and their functional significance, advances have been made in understanding the role of the ventral genes. *Vax2*, together with its closely related homologue *Vax1* serve to establish ventral retina and optic stalk characteristics, and they do so by repressing *Pax6* expression and expansion of neural retinal fate in the optic stalk. This has been nicely demonstrated by analysis of compound mutants for *Vax1*;*Vax2* and several *in vitro* assays which tested *Pax6* binding and repression of activity by the Vax proteins (Mui *et al.* 2005). *Pax2* is important for optic fissure closure and optic nerve development. The loss of both *Pax2* and *Vax2* result in coloboma (Barbeiri *et al.* 2002; Torres *et al.* 1996).

In contrast to the ventrally expressed genes, very little is known about the function of the dorsal genes. In Chapter 4, it was shown that in the developing mouse eye, Bmp4 is upstream of the T-box genes, *Tbx2*, *Tbx3*, and *Tbx5* (Fig. 7.1), regulating the expression of each in a unique manner. A role for Bmp4 signalling in regulating the

spatial domains of gene expression along the D-V axis of the eye and in regulating eye size was demonstrated. The mechanisms by which Bmp4 regulates eye growth include the control of cell proliferation and cell death. These mechanisms appear to require an optimal level of Bmp4 signalling as both increased levels (shown here) and decreased levels (shown by Bmpr conditional knockouts in the eye by Murali *et al.* 2005), result in decreased proliferation and increased cell death.

Although Bmp4 treatment of the eye resulted in a global decrease in cell proliferation, the experimental strategy used in Chapter 4 did not fully resolve the question of whether Bmp4 normally acts to control these cellular events regionally, within the dorsal eye, or whether it has a global effect on cell proliferation and cell death in eye development. In Chapters 5 and 6, the role of *Tbx2* specifically was investigated and it was shown that manipulation of *Tbx2* causes a reduction in eye size, suggesting that a Bmp-Tbx2 pathway is important for the control of early growth of the developing eye. The $Tbx2^{-/-}$ phenotype suggests that *Tbx2* may have both intrinsic and extrinsic effects on eye morphogenesis and growth. Although not statistically significant (P= 0.05), a trend of increased levels of cell division was observed in the dorsal eye specifically, suggesting that *Tbx2* may normally be acting to slow down cell proliferation in the dorsal eye (Fig. 7.1). This role is in agreement with the emerging role of *Tbx2* in negatively controlling growth of other tissues during development.

In the developing heart, the AVC where *Tbx2* is expressed, has a lower rate of cell proliferation in comparison to the chamber tissue (Cai *et al.* 2005). It has been suggested that *Tbx2* represses chamber differentiation in the presumptive AVC, where it acts regionally to induce lower rates of proliferation by repressing the expression of *Nmyc1* and chamber tissue markers (Harrelson *et al.* 2004; Cai *et al.* 2005). The functional significance of this regionalisation is that it allows the division of the atrial and ventricular compartments by the AVC cushion tissue, which form the valves. Moreover, the AVC has a lower conduction velocity in comparison to the chamber tissue, and imposes a delay, allowing contraction of the atria to be completed before ventricular filling (Stennard and Harvey 2005). Evidence for Tbx2 as a repressor of tissue growth has also come to light in an organ that is homologous to the vertebrate eye, namely the *Drosophila* compound eye. *Omb*, which is the

orthologue of mouse *Tbx2* (Bollag *et al.* 1994), is expressed in the *Drosophila* eye disc (Pflugfelder *et al.* 1992a), where it appears to be repressing eye growth. *Omb* null mutants display an increase in ommatidial number, while a dominant gain of function allele of *omb* results in a reduction of ommatidial number (unpublished data presented at the 1st European T-box meeting, November 2005, by G. O. Pflugfelder, Mainz University, Germany).

Despite the increased trend in cell proliferation in the dorsal neural retinae of *Tbx2*$^{-/-}$ mutants, they displayed a small retinal volume. The question arises as to how a role for *Tbx2* as a repressor of eye growth is compatible with the small eye phenotype in the mutants. The abnormal morphogenesis of mutant eyes offers a plausible answer to this question. A delay in morphogenesis in the ventral neural retina was observed in mutants compared to wild-types at 10.5 dpc, with the ventral neural retina appearing smaller and less invaginated. Abnormal ventral invagination of the optic cup could lead to a smaller retinal volume despite an increase in dorsal cell division. An effect on ventral invagination by the lack of a dorsally expressed transcription factor is suggestive of misregulation of signalling molecules, which could convey the signal to the ventral eye. The morphological analysis of *Tbx2*$^{-/-}$ eyes provided several indications that *Tbx2* plays a cell extrinsic role in eye development. As well as delayed ventral optic cup morphogenesis, this was evident in the absence of lens fibre elongation at 12.5 dpc, and abnormal hyaloid vasculature development at 10.5 dpc. *Tbx2* misexpression in the developing chick eye, in Chapter 6, resulted in reduced eye size, which was more marked in the ventral neural retina, although the mechanisms by which this occurred were not investigated due to time constraints, it supports a role for *Tbx2* as a negative regulator of eye growth.

The proposed model is that a Bmp4 signalling gradient restricts *Tbx2* expression in the dorsal eye, which slows the growth of the dorsal neural retina, by an intrinsic mechanism (Fig. 7.1). *Tbx2* also regulates morphogenesis of the ventral eye via a/multiple secreted factor(s). This would suggest that perhaps there is cross-talk between the dorsal and the ventral regions of the eye, which act in a synchronous manner to direct eye morphogenesis and growth. During eye morphogenesis, the dorsal neural retina invaginates first followed by the ventral neural retina, so that initially, the dorsal part appears larger and the optic stalk is positioned ventrally.

Therefore, for the eye to acquire the globe shape that is apparent from 13.5 dpc in the mouse, when the optic fissure has closed and the optic disc and nerve are positioned approximately in the centre of the globe as opposed to ventrally, the ventral neural retina must grow at a faster pace than the dorsal region between the onset of invagination and completion of optic cup formation (around 13.5 dpc in mouse). Analysis of cell proliferation in the dorsal versus the ventral neural retina in the chick embryo at HH 14, which is when the optic vesicle has just invaginated, supports this idea. In the chick, the mitotic index is higher in the ventral optic cup than in the dorsal optic cup at this stage and this trend continues until HH 17, although it is not as significant as at HH 14 (Calvente *et al.* 1988). This difference has also been detected in the mouse optic cup at 10.5 dpc (J.Morcillo; J.C. Sowden *et al.* manuscript submitted). The idea that *Tbx2* may act to reduce growth in the eye is also supported by the expression pattern of *Tbx2*. In Chapter 6, it was demonstrated that at optic vesicle stage, *Tbx2* is expressed along the entire D-V length of the distal neuroepithelium in the chick embryo, which is still thin in appearance. Upon invagination, the distal layer undergoes a concomitant increase in cell number and becomes thicker than the proximal layer which goes on to form the thin RPE. During this process, *Tbx2* becomes localised to the dorsal optic cup, where it may continue to act to reduce growth so that the ventral optic cup can 'catch up'. This interpretation would suggest that *Tbx2* functions to slow down the neural retina-specified distal layer of the optic vesicle; upon invagination and restriction of *Tbx2* to the dorsal optic cup, it continues to serve this function dorsally, allowing the rest of the cup to acquire a higher rate of division.

Fig. 7.1 Schematic diagram illustrating the proposed model for the role of *Tbx2* in the regulation of gene expression and growth along the D-V axis of the eye

This schematic builds on the one presented in Chapter 1 (Fig. 1.4). Findings of this thesis are shown by red arrows and lines, hypotheses are marked by grey. A dorsal-high, ventral-low Bmp4 signalling gradient restricts the expression of the dorsal genes *Tbx2*, *Tbx3*, and *Tbx5*, in distinct yet overlapping domains, while repressing *Vax2* (refer to Fig. 3.9 for illustration of the domains).

The role of *Tbx2* in D-V patterning: *Tbx2* positively maintains the expression of *Tbx5*, *Fgf15*, while negatively regulating Cx43 and *ephrinB2*.

The proposed role of *Tbx2* in early growth and morphogenesis: *Tbx2* has a dual role in regulation of eye growth and morphogenesis. 1) It acts intrinsically in the dorsal neural retina to negatively regulate cell division (see invaginating optic cup). Evidence supporting such a role was provided by the increase in the trend of cell division in *Tbx2*$^{-/-}$ embryos in the dorsal eye specifically. Moreover, growth of the ventral neural retina was reduced in rhBmp4 treated eyes in which *Tbx2* was ectopically expressed, as well as in the ventral region of chick eyes infected with RCAS-*cTbx2*. 2) *Tbx2* positively affects growth and morphogenesis of the ventral eye via secreted factors. Evidence for this was provided by the delayed invagination of the ventral optic cup in *Tbx2*$^{-/-}$ eyes. *Tbx2* regulation of RA or Fgf15 could potentially convey this effect. *Fgf15* was absent in *Tbx2*$^{-/-}$ eyes at 10.5 dpc. Based on reports regarding the role of Fgf signalling in lens development, Fgf15 is a potential candidate for regulating the development of the lens, which was perturbed in *Tbx2*$^{-/-}$ embryos.

Abbreviations: D, dorsal; V, ventral

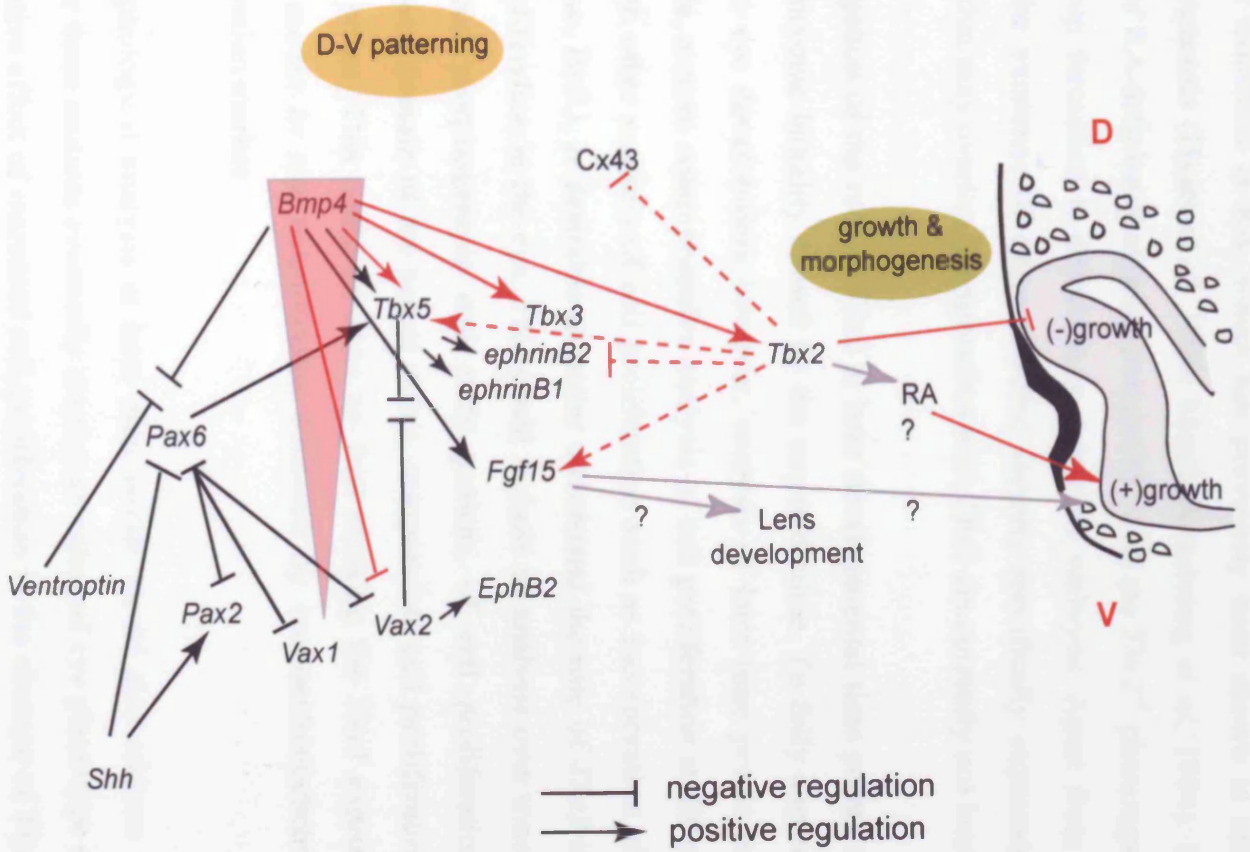
D-V patterning
Cx43
Bmp4
growth &
morphogenesis
D
Tbx5
Tbx3
ephrinB2
ephrinB1
Tbx2
(-)growth
RA
?
Pax6
Fgf15
(+)growth
?
?
Lens
development
Ventroptin
Pax2
Vax1
Vax2
EphB2
V
Shh
negative regulation
positive regulation

As described, the *Tbx2*$^{-/-}$ phenotype, suggests a dual mechanism of growth control in the eye, both of which were affected by the loss of Tbx2. How is *Tbx2* affecting ventral optic cup morphogenesis? In Chapter 5, it was shown that *Fgf15*, encoding a secreted factor expressed in the neural retina, is not maintained in *Tbx2*$^{-/-}$ mice and could potentially be the signal that conveys this effect. As discussed in Chapter 5, another candidate is RA, which has previously been shown to affect ventral eye morphogenesis (Hyatt *et al.* 1996; Marsh-Armstrong *et al.* 1994). Specifically, the effect of RA deficiency appears compatible with the *Tbx2*$^{-/-}$ phenotype, where ventral optic cup formation is defective in zebrafish embryos. Apart from one other Fgf, Fgf9, the existence of other secreted factors, specifically expressed in the neural retina, that may overlap in expression with *Tbx2* are currently not known.

Investigation of the role of *Tbx2* at later developmental time points was impeded by the embryonic lethality caused by the targeted allele. To fully appreciate the role of *Tbx2* in eye development however, analysis of later time points is necessary. For example, a more comprehensive analysis of cell proliferation at different time points and with other markers of cell proliferation such as incorporation of the Thymidine analogue, BrdU, is desirable to better understand the role of *Tbx2* in the control of cell proliferation in the eye. This could include an analysis over time, during normal optic cup morphogenesis and early growth, of cell proliferation in the *Tbx2* expression domain of the neural retina, compared to cell proliferation in the ventral neural retina. This could be done by first marking the *Tbx2* expressing region by whole mount *in situ* hybridisation followed by immunohistochemistry for a cell proliferation marker.

A morphological analysis at later time points would also address the question of whether these mutants eventually display an enlarged eye phenotype as the result of a cumulative effect of increased cell proliferation in the absence of Tbx2, like the *omb* null mutants, or whether other mechanisms still would prevent eye growth. It would also be interesting to find out if lens fibre elongation does eventually occur in mutants or remains abnormal. Other phenotypes that may be expected are anterior segment defects, because *Tbx2* is expressed in the corneal ectoderm from 14.5 dpc in mouse (Sowden *et al.* 2001). Furthermore, as the lens is essential for the

development of the anterior segment, an abnormal lens would likely also result in abnormalities in the anterior segment.

Although *Tbx2* misexpression did not have a profound effect on intra-retinal RGC projections, the disorganisation of the axons in *Tbx2*$^{-/-}$ mice was an interesting phenotype, and merits further investigation. It would be necessary to establish whether these persist in later development and if so, which molecules may be affected that are not expressed/over expressed and are responsible for this defect. Currently, it cannot be excluded that this phenotype occurs due to the cardiac problems of these mutants, as it was detected at 12.5 dpc when the rate of lethality is high. Although it should be noted, that all embryos analysed were healthy with heart beat and circulation and did not reveal cardiac distress such as edema. The questions posed here can only be answered with the establishment of other experimental strategies as mentioned before, such as the creation of conditional mutants.

At the molecular level, analysis of the expression of *Tbx5*, *Vax2*, and *ephrinB2* at later developmental time points would answer the question of whether *Tbx2* is indeed needed to maintain their correct localisation. Analyses in Chapter 5 suggest that it does, as these were altered, but a complete lack of *Tbx5* expression and further expansion of *ephrinB2* would further corroborate these findings. Several other downstream candidates are also deserving of analysis. These include Cyp26 enzymes, to investigate the regulation of RA degradation and therefore signalling in the absence of Tbx2 for the reasons mentioned before. Analysis of additional markers of the ventral neural retina such as *Pax2* and *EphB3* would clarify whether the reduction in *Vax2* expression, detected at 10.5 dpc, is due to a reduction in gene expression or the smaller ventral neural retina in mutants.

With regards to the regulation of the T-box genes by Bmp4, there are several experiments that could be conducted to answer specific questions that have arisen as the result of the findings presented in Chapter 4. Firstly, the normal distribution of Bmp signalling, detected by an antibody against phosphorylated Smads, which convey the Bmp signal to the nucleus where they, in conjunction with other factors, activate or repress gene expression, could be analysed. This may help to determine the extent of Bmp signalling away from the source. Secondly, the direct/indirect

effect of Bmp4 bead implantation on T-box gene expression could be determined by bead implantation into the lens vesicle of mutant embryos that lack functional Bmprs in the neural retina followed by embryo culture. Conditional inactivation of these receptors in the neural retina has recently been reported (Murali *et al.* 2005). If bead implantation in the lens vesicle, which retains Bmpr expression and therefore is capable of receiving the Bmp signal, still induces ectopic T-box gene expression in the neural retina, in which Bmprs have been inactivated, it would suggest that the effect is indirect and that intermediaries are involved. Conversely, if ectopic T-box gene expression is not induced, it indicates that the effect of Bmp4 is mediated by its direct action on the neural retina. Alternatively, the method of transgenic expression of a modified Bmp4 hybrid protein, bearing a transmembrane motif, which targets and tethers Bmp4 to the plasma membrane in the lens vesicle, hence preventing it from diffusing, could be explored. This was discussed in Chapter 4. These methods may however be technically difficult and hampered by a number of issues, such as failure to tether the Bmp4 protein to the cell membrane, or the loss of functional activity with the Bmp fusion protein after the modification. The use of the conditional compound Bmpr mutants would be restricted to a small window of development, as the neural retina has been reported to degenerate in these mice (Murali *et al.* 2005). Although it would still be feasible to do the suggested experiment, with an overnight culture period. The effect of increased levels of Bmp signalling on the spatial distribution of D-V markers could be further tested using the bead implantation and whole embryo culture system, by varying the concentration of the protein on beads. Experiments in Chapter 4, showed that beads soaked in high levels of Bmp4, induced more cell death in the dorsal eye than beads soaked in less protein. Using beads with a high concentration of Bmp4, it could be tested whether *Tbx5*, normally restricted to D1, could be expanded not only into D2, as observed in experiments presented in Chapter 4, but also in the ventral neural retina (V3 and V4).

The significance of D-V patterning of the eye by the early asymmetrical expression of various genes is not yet fully understood. The importance of patterning along this axis for topographic mapping of RGC axons to the brain is well established (McLaughlin *et al.* 2003a). It is likely that D-V patterning is important for additional functions. Here, data was presented which suggests that an additional role for this asymmetry is to control the growth of the eye in order to sculpt the shape of the

globe. This thesis has provided new insights into the role of *Tbx2* in eye development and the regulation of T-box genes by Bmp4 signalling in the mammalian eye. A role for *Tbx2* in eye morphogenesis and early growth has been identified. The research has also opened up several avenues to be further explored and new questions to be answered. It is hoped that subsequent studies will be able to build upon these findings and further characterise the role of *Tbx2* but also those of *Tbx3* and *Tbx5* in eye development.

Appendix A

Analysis of intra-retinal RGC axonal projections in RCAS-*cTbx2* infected and control retinae

The analysis described here was performed on chick retinae infected at HH 9-10 with RCAS-*cTbx2* virus and harvested at HH 24-25. Intra-retinal axonal projections were visualised with ßIII-tubulin whole mount immunohistochemistry, after which retinae were flat mounted for analysis. Table A.1 shows the number of eyes in which 'ectopic' axons were detected in the ventral neural retina in infected and stage matched control eyes. The percentage of eyes containing 'ectopic' axons was higher in the RCAS-*cTbx2* infected group compared to the control group (60% versus 47% respectively).

Table A.1: Incidence of ectopic axons and projection errors in RCAS-*cTbx2* infected and control retinae at HH 24-25

		Treatment	
		RCAS-*cTbx2* infected	Control
n. eyes	with ectopic axons	6	14
	without ectopic axons	4	16
	Total	10	30
	%	60%	47%
n. axons	0° deviation	5	3
	≤90° deviation	8	16
	>90° deviation	3	1
	Total	16	20
	%	19%	5%

The angle at which the ectopic axons deviated from the common route taken by their neighbours was measured by assigning the common route of axons as the 0° horizontal axis, while the optic disc and fissure were assigned the 90° vertical axis. An axon perpendicular to the common route (0°), which extended parallel to the optic fissure towards the ventral periphery would be described as having a 90° deviation. An axon not following the common route, but still projecting towards the optic fissure would be described as having <90° deviation, while an axon projecting away from the common route and away from the optic fissure would have >90° deviation. Hence, three categories were created to describe these deviations. 0°, for axons

outside of the network but projecting in the same manner, ≤90°, for axons projecting away from the network but towards the optic fissure and never away from it including those perpendicular to the network, >90°, for axons projecting away from the network and away from the optic fissure. Fig. A1 illustrates the criteria for assigning axon deviation angles.

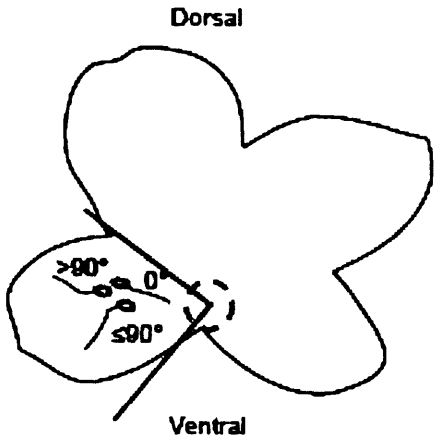

Fig. A1 Schematic diagram of the categorisation of 'ectopic' axonal projections

Picture illustrates a retinal flat mount (grey) with the area of the optic disc highlighted by a dashed circle. The three different types of RGC axonal deviations observed are categorised into 0°, ≤90°, and >90°, with respect to the common route of axons (0°) in the ventral aspects of the retina and the optic fissure (90°).

In control retinae, which contained deviated axons, only 5% (1/20) of these axons deviated more than 90°. By contrast, in RCAS-*cTbx2* infected eyes, 19% (3/16) of the 'ectopic' axons deviated more than 90° (Table A1). The incidence of axonal migration errors was slightly higher in RCAS-*cTbx2* infected eyes and among axons that extended in the wrong direction, the percentage of axons deviating severely from the common route (>90°) was four times higher in infected eyes than observed in stage matched controls (19% versus 5%), suggesting that *Tbx2* misexpression in the

ventral retina may be causing higher than normal axonal misrouting. For these observations to be validated, a larger data set is required.

References

References

Abzhanov, A., Protas, M., Grant, B.R., Grant, P.R., and Tabin, C.J. (2004). *Bmp4* and morphological variation of beaks in Darwin's Finches. *Science*. **305**, 1462-1465.

Achiron, R., Kreiser, D., and Achiron, A. (2000). Axial growth of the fetal eye and evaluation of the hyaloid artery: *in utero* ultrasonographic study. *Prenat.Diagn.* **20**, 894-899.

Adams, R.H., Wilkinson, G.A., Weiss, C., Diella, F., Gale, N.W., Deutsch, U., Risau, W., and Klein, R. (1999). Roles of ephrinB ligands and EphB receptors in cardiovascular development: demarcation of arterial/venous domains, vascular morphogenesis, and sprouting angiogenesis. *Genes Dev.* **13**, 295-306.

Adler, R. and Belecky-Adams, T.L. (2002). The role of bone morphogenetic proteins in the differentiation of the ventral optic cup. *Development*. **129**, 3161-3171.

Agulnik, S.I., Garvey, N., Hancock, S., Ruvinsky, I., Chapman, D.L., Agulnik, I., Bollag, R., Papaioannou, V., and Silver, L.M. (1996). Evolution of mouse T-box genes by tandem duplication and cluster dispersion. *Genetics*. **144**, 249-254.

Alexiades, M.R. and Cepko, C.L. (1997). Subsets of retinal progenitors display temporally regulated and distinct biases in the fates of their progeny. *Development*. **124**, 1119-1131.

Anderson, R.M., Lawrence, A.R., Stottmann, R.W., Bachiller, D., and Klingensmith, J. (2002). Chordin and noggin promote organizing centers of forebrain development in the mouse. *Development*. **129**, 4975-4987.

Ang, SL., Jin, O., Rhinn, M., Daigle, N., Stevenson, L., and Rossant, J. (1996). A targeted mouse *Otx2* mutation leads to severe defects in gastrulation and formation of axial mesoderm and to deletion of rostral brain. *Development*. **122**, 243-252.

Atfi, A., Djelloul, S., Chastre, E., Davis, R., and Gespach, C. (1997). Evidence for a role of Rho-like GTPases and stress-activated protein kinase/c-Jun N-terminal kinase (SAPK/JNK) in transforming growth factor ß-mediated signaling. *J.Biol.Chem.* **272**, 1429-1432.

Avilion, A.A., Nicolis, S.K., Pevny, L.H., Perez, L., Vivian, N., and Lovell-Badge, R. (2003). Multipotent cell lineages in early mouse development depend on *Sox2* function. *Genes Dev.* **17**, 126-140.

Bachiller, D., Klingensmith, J., Kemp, C., Belo, J.A., Anderson, R.M., May, S.R., McMahon, J.A., McMahon, A.P., Harland, R.M., Rossant, J., and De Robertis, E.M. (2000). The organizer factors Chordin and Noggin are required for mouse forebrain development. *Nature.* **403**, 658-661.

Bamshad, M., Lin, R.C., Law, D.J., Watkins, W.C., Krakowiak, P.A., Moore, M.E., Franceschini, P., Lala, R., Holmes, L.B., Gebuhr, T.C., Bruneau, B.G., Schinzel, A., Seidman, J.G., Seidman, C.E., and Jorde, L.B. (1997). Mutations in human TBX3 alter limb, apocrine and genital development in ulnar-mammary syndrome. *Nat.Genet.* **16**, 311-315.

Bao, Z. and Cepko, C.L. (1997). The expression and function of *Notch* pathway genes in the developing rat eye. *J.Neurosci.* **17**, 1425-1434.

Bar-Yosef, U., Abuelaish, I., Harel, T., Hendler, N., Ofir, R., and Birk, O.S. (2004). *CHX10* mutations cause non-syndromic microphthalmia/anophthalmia I Arab and Jewish kindreds. *Hum.Genet.* **115**, 302-309.

Barbeiri, A., Lupo, G., Bulfone, A., Andreazzoli, M., Mariani, M., Fougerousse, F., Consalez, G., Borsani, G., Beckmann, J.S., Barsacchi, G., Ballabio, A., and Banfi, S. (1999). A homeobox gene, vax2, controls the patterning of the eye dorsoventral axis. *Proc.Natl.Acad.Sci.U.S.A.* **96**, 10729-10734.

Barbeiri, A., Broccoli, V., Bovolenta, P., Alfano, G., Marchitiello, A., Mocchetti, C., Crippa, L., Bulfone, A., Marigo, V., Ballabio, A., and Banfi, S. (2002). Vax2 inactivation in mouse determines alteration of the eye dorsal-ventral axis, misrouting of the optic fibres and eye coloboma. *Development.* **129**, 805-813.

Bärlund, M., Monni, O., Kononen, J., Cornelison, R., Torhorst, J., Sauter, G., Kallioniemi, O.-P., and Kallioniemi, A. (2000). Multiple genes at 17q23 undergo amplification and overexpression in breast cancer. *Cancer Res.* **60**, 5340-5344.

Barth, K.A., Kishimoto, Y., Rohr, K.B., Seydler, C., Schulte-Merker, S., and Wilson, S.W. (1999). Bmp activity establishes a gradient of positional information throughout the entire neural plate. *Development.* **126**, 4977-4987.

Basson, C.T., Bachinsky, D.R., Lin, R.C., Levi, T., Elkins, J.A., Soults, J., Grayzel, D., Kroumpouzou, E., Traill, T.A., Leblanc-Straceski, J., Renault, B., Kucherlapati, R., Seidman, J.G., and Seidman, C.E. (1997). Mutations in human TBX5 [corrected] cause limb and cardiac malformation in Holt-Oram syndrome. *Nat.Genet.* **15**, 30-35.

Bäumer, N., Marquardt, T., Stoykova, A., Ashery-Padan, R., Chowdhury, K., and Gruss, P. (2002). *Pax6* is required for establishing naso-temporal and dorsal characteristics of the optic vesicle. *Development.* **129**, 4535-4545.

Baxter, L.L. and Pavan, W.J. (2003). *Pmel17* expression is *Mitf*-dependent and reveals cranial melanoblast migration during murine development. *Gene Expr.Patterns.* **3**, 703-707.

Becker, D.L. and Mobbs, P. (1999). Connexin α1 and cell proliferation in the developing chick retina. *Exp.Neurol.* **156**, 326-332.

Beebe, D.C. and Coats, J.M. (2000). The lens organizes the anterior segment: specification of neural crest cell differentiation in the avian eye. *Dev.Biol.* **220**, 424-431.

Belecky-Adams, T. and Adler, R. (2001). Developmental expression patterns of Bone morphogenetic proteins, receptors, and binding proteins in the chick retina. *J.Comp Neurol.* **430**, 562-572.

Beppu, H., Kawabata, M., Hamamoto, T., Chytil, A., Minowa, O., Noda, T., and Miyazono, K. (2000). BMP type II receptor is required for gastrulation and early development of mouse embryos. *Dev.Biol.* **221**, 249-258.

Bertuzzi, S., Hindges, R., Mui, S.H., O'Leary, D.D., and Lemke, G. (1999). The homeodomain protein vax1 is required for axon guidance and major tract formation in the developing forebrain. *Genes Dev.* **13**, 3092-3105.

Birgbauer, E., Cowan, C.A., Sretavan, D.W., and Henkemeyer, M. (2000). Kinase independent function of EphB receptors in retinal axon pathfinding to the optic disc from dorsal but not ventral retina. *Development.* **127**, 1231-1241.

Bollag, R.J., Siegfried, Z., Cebra-Thomas, J.A., Garvey, N., Davison, E.M., and Silver, L.M. (1994). An ancient family of embryonically expressed mouse genes sharing a conserved protein motif with the T locus. *Nat.Genet.* **7**, 383-389.

Borke, J.L., Chen, J.R., Yu, J.C., Bollag, R.J., Orellana, M.F., and Islas, C.M. (2003). Negative transcriptional regulation of connexin 43 by Tbx2 in rat immature coronal sutures and ROS 17/2.8 cells in culture. *Cleft Palate Craniofac.J.* **40**, 284-290.

Botchkarev, V.A. (2003). Bone morphogenetic proteins and their antagonists in skin and hair follicle biology. *J.Invest Dermatol.* **120**, 36-47.

Braisted, J.E., McLaughlin, T., Wang, H.U., Friedman, G.C., Anderson, D.J., and O'Leary, D.D.M. (1997). Graded and lamina-specific distributions of ligands of EphB receptor tyrosine kinases in the developing retinotectal system. *Dev.Biol.*, 14-28.

Briscoe, J., Chen, Y., Jessell, T.M., and Struhl, G. (2001). A hedgehog-insensitive form of patched provides evidence for direct long-range morphogen activity of sonic hedgehog in the neural tube. *Mol.Cell.* **7**, 1279-1291.

Briscoe, J., Pierani, A., Jessell, T.M., and Ericson, J. (2000). A homeodomain protein code specifies progenitor cell identity and neuronal fate in the ventral neural tube. *Cell.* **101**, 435-445.

Brittis, P.A., Silver, J., Walsh, F.S., and Doherty, P. (1996). Fibroblast Growth Factor receptor function is required for the orderly projection of ganglion cell axons in the developing mammalian retina. *Mol.Cell.Neurosci.* **8**, 120-128.

Brown, N.A. (1990). Routine assessment of morphology and growth: scoring systems and measurements of size. 93-108.

Bruhn, S.L. and Cepko, C.L. (1996). Development of the pattern of photoreceptors in the chick retina. *J.Neurosci.* **16**, 1430-1439.

Buckland, R.A., Collinson, J.M., Graham, E., Davidson, D.R., and Hill, R.E. (1998). Antagonistic effects of FGF4 on BMP induction of apoptosis and chondrogenesis in the chick limb bud. *Mech.Dev.* **71**, 143-150.

Bumsted, K.M. and Barnstable, C.J. (2000). Dorsal retinal pigment epithelium differentiates as neural retina in *Microphthalmia (mi/mi)* mouse. *Invest Ophthalmol.Vis.Sci.* **41**, 903-908.

Burmeister, M., Novak, J., Liang, M.Y., Basu, S., Ploder, L., Hawes, N.L., Vidgen, D., Hoover, F., Goldman, D., Kalnins, V.I., Roderick, T.H., Taylor, B.A., Hankin, M.H., and McInnes, R.R. (1996). Ocular retardation mouse caused by *Chx10* homeobox null allele: impaired retinal progenitor proliferation and bipolar cell differentiation. *Nat.Genet.* **12**, 376-384.

Bussen, M., Petry, M., Schuster-Gossler, K., Leitges, M., Gossler, A., and Kispert, A. (2004). The T-box transcription factor Tbx18 maintains the separation of anterior and posterior somite compartments. *Genes Dev.* **15**, 1209-1221.

Cai, C.L., Zhou, W., Yang, L., Qyang, Y., Zhang, X., Li, X., Rosenfeld, M.G., Chen, J., and Evans, S. (2005). T-box genes coordinate regional rates of proliferation and regional specification during cardiogenesis. *Development.* **132**, 2475-2487.

Calegari, F., Haubensak, W., Yang, D., Huttner, W.B., and Buchholz, F. (2002). Tissue-specific RNA interference in postimplantation mouse embryos with endoribonuclease-prepared short interfering RNA. *Proc.Natl.Acad.Sci.U.S.A.* **99**, 14236-14240.

Calvente, R., Carmona, R., Abadía-Molina, F., and Abadía-Fenoll, F. (1988). Stereological study on the mode of optic cup expansion and the accumulation of mitoses in the early stages of chick embryo development. *The Anatomical Record.* **222**, 401-407.

Carlson, H., Ota, S., Campbell, C.E., and Hurlin, P.J. (2001). A dominant repression domain in Tbx3 mediates transcriptional repression and cell immortalization. *Hum.Mol.Genet.* **10**, 2413.

Carlson, H., Ota, S., Song, Y., Chen, Y., and Hurlin, P.J. (2002). Tbx3 impinges on the p53 pathway to suppress apoptosis, facilitate cell transformation and block myogenic differentiation. *Oncogene.* **21**, 3827-3835.

Carreira, S., Dexter, T.J., Yavuzer, U., Easty, D.J., and Goding, C.R. (1998). Brachyury-related transcription factor Tbx2 and repression of the melanocyte-specific TRP-1 promoter. *Mol.Cell Biol.* **18**, 5099-5108.

Carreira, S., Liu, B., and Goding, C.R. (2000). The gene encoding the T-box factor *Tbx2* is a target for the Microphthalmia-associated transcription factor in melanocytes. *J.Biol.Chem.* **275**, 21920-21927.

Cepko, C.L., Austin, C.P., Yang, X., Alexiades, M., and Ezzeddine, D. (1996). Cell fate determination in the vertebrate retina. *Proc.Natl.Acad.Sci.U.S.A.* **93**, 589-595.

Chang Chuang, J. and Raymond, P.A. (2001). Zebrafish genes *rx1* and *rx2* help define the region of forebrain that gives rise to retina. *Dev.Biol.* **231**, 13-30.

Chang, B., Smith, R.S., Peters, M.A., Savinova, O.V., Hawes, N.L., Zabaleta, A., Nusinowitz, S., Martin, J.E., Davisson, M.L., Cepko, C.L., Hogan, B.L., and John, S.W.M. (2001). Haploinsufficient *Bmp4* ocular phenotypes include anterior segment dysgenesis with elevated intraocular pressure. *BMC Genetics.* **2**, 18.

Chapman, D.L., Garvey, N., Hancock, S., Alexiou, M., Agulnik, S.I., Gibson-Brown, J.J., Cebra-Thomas, J., Bollag, R.J., Silver, L.M., and Papaioannou, V.E. (1996). Expression of the T-box family genes, Tbx1-Tbx5, during early mouse development. *Dev.Dyn.* **206**, 379-390.

Chapman, D.L. and Papaioannou, V.E. (1998). Three neural tubes in mouse embryos with mutations in the T-box gene Tbx6. *Nature.* **391**, 695-697.

Chen, J., Zhong, Q., Wang, J., Cameron, R.S., Borke, J.L., Isales, C.M., and Bollag, R.J. (2001). Microarray analysis of Tbx2-directed gene expression: a possible role in osteogenesis. *Mol.Cell Endocrinol.* **177**, 43-54.

Chen, J.R., Chatterjee, B., Meyer, R., Yu, J.C., Borke, J.L., Isales, C.M., Kirby, M.L., Lo, C.W., and Bollag, R.J. (2004). Tbx2 represses expression of Connexin43 in osteoblastic-like cells. *Calcif.Tissue.Int.* **74**, 561-573.

Chiang, C., Litingtung, Y., Lee, E., Young, K.E., Corden, J.L., Westphal, H., and Beachy, P.A. (1996). Cyclopia and defective axial patterning in mice lacking Sonic hedgehog gene function. *Nature.* **383**, 407-413.

Chin, L., Pomerantz, J., and DePinho, R.A. (1998). The INK4a/ARF tumor suppressor. One gene-two products-two pathways. *Trends Biochem.Sci.* **23**, 291-296.

Chow, R.L. and Lang, R.A. (2001). Early eye development in vertebrates. *Annu.Rev.Cell Dev.Biol.* **17**, 255-296.

Christoffels, V.M., Hoogaars, W.M., Tessari, A., Clout, D.E., Moorman, A.F.M., and Campione, M. (2004). T-box transcription factor Tbx2 represses differentiation and formation of the cardiac chambers. *Dev.Dyn.* **229**, 763-770.

Cockroft, D.L. (1990). Dissection and culture of postimplantation embryos. 15-40.

Coll, M., Seidman, J.G., and Muller, C.W. (2002). Structure of the DNA-bound T-box domain of human TBX3, a transcription factor responsible for ulnar-mammary syndrome. *Structure.* **10**, 343-356.

Colvin, J.S., Feldman, B., Nadeau, J.H., Goldfarb, M., and Ornitz, D.M. (1999). Genomic organization and embryonic expression of the mouse fibroblast growth factor 9 gene. *Dev.Dyn.* **216**, 72-88.

Conlon, F.L., Fairclough, L., Price, B.M.J., Casey, E.S., and Smith, J.C. (2001). Determinants of T-box protein specificity. *Development.* **128**, 3749-3758.

Connor, R.J., Menzel, P., and Pasquale, E.B. (1998). Expression and tyrosine phosphorylation of Eph receptors suggest multiple mechanisms in patterning of the visual system. *Dev.Biol.*, 21-35.

Coulombre, A.J. (1965). The eye. *Organogenesis*, New York: Holt, Rinehart and Winston, 219-251.

Crossley, P.H. and Martin, G.R. (1995). The mouse Fgf8 gene encodes a family of polypeptides and is expressed in regions that direct outgrowth and patterning in the developing embryo. *Development.* **121**, 439-451.

Crossley, P.H., Martinez, S., Ohkubo, Y., and Rubenstein, J.L. (2001). Coordinate expression of Fgf8, Otx2, Bmp4, and Shh in the rostral prosencephalon during development of the telencephalic and optic vesicles. *Neuroscience.* **108**, 183-206.

Cunliffe, V. and Smith, J.C. (1992). Ectopic mesoderm formation in Xenopus embryos caused by widespread expression of a Brachyury homologue. *Nature.* **358**, 427-430.

Curcio, C.A., Sloan, K.R., Kalina, R.E., and Hendrickson, A.E. (1990). Human photoreceptor topography. *J.Comp Neurol.* **292**, 497-523.

Dakubo, G.D., Wang, Y.P., Mazerolle, C., Campsall, K., McMahon, A.P., and Wallace, V.A. (2003). Retinal ganglion cell-derived sonic hedgehog signaling is required for optic disc and stalk neuroepithelial cell development. *Development.* **130**, 2967-2980.

Dattani, M.T., Martinez-Barbera, JP., Thomas, P.Q., Brickman, J.M., Gupta, R., Mårtensson, IL., Toresson, H., Fox, M., Wales, J.K.H., Hindmarsh, P.C., Krauss, S., Beddington, R.S., and Robinson, I.C.A.F. (1998). Mutations in the homeobox gene *HESX1/Hesx1* associated with septo-optic dysplasia in human and mouse. *Nat.Genet.* **19**, 125-133.

Davidson, B.P., Tsang, T.E., Khoo, P., Gad, J.M., and Tam, P.P.L. (2003). Introduction of cell markers into germ layer tissues of the mouse gastrula by whole embryo electroporation. *Genesis.* **35**, 57-62.

Dheen, T., Sleptsova-Friedrich, I., Xu, Y., Clark, M., Lehrach, H., Gong, Z., and Korzh, V. (1999). Zebrafish *tbx-c* functions during formation of midline structures. *Development.* **126**, 2703-2713.

Dolk, H., Busby, A., Armstrong, B.G., and Walls, P.H. (1998). Geographical variation in anophthalmia and microphthalmia in England, 1988-94. *BMJ.* **317**, 905-910.

Dominguez, M. and Casares, F. (2005). Organ specification-growth control connection: New in-*sights* from the *Drosophila* eye-antennal disc. *Dev.Dyn.* **232**, 673-684.

Dräger, U.C. (1985). Birth dates of retinal ganglion cells giving rise to the crossed and uncrossed optic projections in the mouse. *Proc.R.Soc.Lond.B.* **224**, 57-77.

Dudley, A.T., Lyons, K.M., and Robertson, E.J. (1995). A requirement for bone morphogenetic protein-7 during development of the mammalian kidney and eye. *Genes Dev.* **9**, 2795-2807.

Dudley, A.T. and Robertson, E.J. (1997). Overlapping expression domains of bone morphogenetic protein family members potentially account for limited tissue defects in BMP7 deficient embryos. *Dev.Dyn.* **208**, 349-362.

Duester, G. (2000). Families of retinoid dehydrogenases regulating vitamin A function. Production of visual pigment and retinoic acid. *Eur.J.Biochem.* **267**, 4315-4324.

Dunn, N.R., Winnier, G.E., Hargett, L.K., Schrick, J.L., Fogo, A.B., and Hogan, B.L. (1997). Haploinsufficient phenotypes in *Bmp4* heterozygous null mice and modification by mutations in *Gli3* and *Alx4*. *Dev.Biol.* **188**, 235-247.

Duprez, D., Bell, E.J., Richardson, M.K., Archer, C.W., Wolpert, L., Brickell, P.M., and Francis-West, P.H. (1996). Overexpression of Bmp-2 and Bmp-4 alters the size and shape of developing skeletal elements in the chick limb. *Mech.Dev.* **57**, 145-157.

Dütting, D. and Thanos, S. (1995). Early establishment of nasal-temporal retinotopic specificity in the eye anlage of the chick embryo. *Dev.Biol.* **167**, 263-281.

Eccles, M.R. and Schimmenti, L.A. (1999). Renal-coloboma syndrome: a multi-system developmental disorder caused by *PAX2* mutations. *Clin.Genet.* **56**, 1-9.

Echelard, Y., Epstein, D.J., St-Jacques, B., Shen, L., Mohler, J., McMahon, J.A., and McMahon, A.P. (1993). Sonic hedgehog, a member of a family of putative signaling molecules, is implicated in the regulation of CNS polarity. *Cell.* **75**, 1417-1430.

Ericson, J., Rashbass, P., Schedl, A., Brenner-Morton, S., Kawakami, A., van Heyningen, V., Jessell, T.M., and Briscoe, J. (1997). *Pax6* controls progenitor cell identity and neuronal fate in response to graded Shh signaling. *Cell.* **90**, 169-180.

Faber, S.C., Dimanlig, P., Makarenkova, H.P., Shitke, S., Ko, K., and Lang, R.A. (2001). Fgf receptor signaling plays a role in lens induction. *Development.* **128**, 4425-4438.

Faber, S.C., Robinson, M.L., Makarenkova, H.P., and Lang, R.A. (2002). Bmp signaling is required for development of primary lens fiber cells. *Development.* **129**, 3727-3737.

Fantes, J., Ragge, N.K., Lynch, SA., McGill, N.I., Collin, R.O., Howard-Peebles, P.N., Hayward, C., Vivian, A.J., Williamson, K., van Heyningen, V., and FitzPatrick, D.R. (2003). Mutations in *SOX2* cause anophthalmia. *Nat.Genet.* **33**, 1-2.

Feldman, B., Gates, M.A., Egan, E.S., Dougan, S.T., Rennebeck, G., Sirotkin, H.I., Schier, A.F., and Talbot, W.S. (1998). Zebrafish organizer development and germ-layer formation require nodal-related signals. *Nature.* **395**, 181-185.

Ferda Percin, E., Ploder, L.A., Yu, J.J., Arici, K., Horsford, D.J., Rutherford, A., Bapat, B., Cox, D.W., Duncan, A.M., Kalnins, V.I., Kocak-Altintas, A., Sowden, J.C., Traboulsi, E., Sarfarazi, M., and McInnes, R.R. (2000). Human microphthalmia associated with mutations in the retinal homeobox gene *CHX10*. *Nat.Genet.* **25**, 397-401.

Francis, P.H., Richardson, M.K., Brickell, P., and Tickle, C. (1994). Bone morphogenetic proteins and a signalling pathway that controls patterning in the developing chick limb. *Development.* **120**, 209-218.

Fuhrmann, S., Levine, E.M., and Reh, T.A. (2000). Extraocular mesenchyme patterns the optic vesicle during early eye development in the embryonic chick. *Development.* **127**, 4599-4609.

Furimsky, M. and Wallace, V.A. (2005). Complementary Gli activity mediates early patterning of the mouse visual system. *Dev Dyn.*

Furukawa, T., Kozak, C.A., and Cepko, C.L. (1997). *rax*, a novel paired-type homeobox gene, shows expression in the anterior neural fold and developing retina. *Proc.Natl.Acad.Sci.U.S.A.* **94**, 3088-3093.

Furuta, Y. and Hogan, B.L. (1998). BMP4 is essential for lens induction in the mouse embryo. *Genes Dev.* **12**, 3764-3775.

Furuta, Y., Piston, D.W., and Hogan, B.L. (1997). Bone morphogenetic proteins (BMPs) as regulators of dorsal forebrain development. *Development.* **124**, 2203-2212.

Gage, P.J., Rhoades, W., Prucka, S.K., and Hjalt, T. (2005). Fate maps of neural crest and mesoderm in the mammalian eye. *Invest Ophthalmol.Vis.Sci.* **46**, 4200-4208.

Gallardo, M.E., Lopez-Rios, J., Fernaud-Espinosa, I., Granadino, B., Sanz, R., Ramos, C., Ayuso, C., Seller, M.J., Brunner, H.G., Bovolenta, P., and Rodríguez de Córdoba, S. (1999). Genomic cloning and characteriztion of the human homeobox gene *SIX6* reveals a cluster of SIX genes in chromosome 14 and associates *SIX6* hemizygosity with bilateral anophthalmia and pituitary anomalies. *Genomics.* **61**, 82-91.

Gallardo, M.E., Schneider, A.S., Ayuso, C., and Bovolenta, P. (2004). Analysis of the developmental *SIX6* homeobox gene in patients with anophthalmia/microphthalmia. *Am.J.Med.Genet.* **129A**, 92-94.

Gibson-Brown, J.J., Agulnik, S.I., Silver, L.M., and Papaioannou, V. (1998). Expression of T-box genes *Tbx2-Tbx5* during chick organogenesis. *Mechanisms of Development.* **74**, 165-169.

Glaser, T., Walton, D.S., and Maas, R.L. (1992). Genomic structure, evolutionary conservation and aniridia mutations in the human PAX6 gene. *Nat.Genet.* **2**, 232-239.

Godin, R.E., Takaesu, N.T., Robertson, E.J., and Dudley, A.T. (1998). Regulation of BMP7 expression during kidney development. *Development.* **125**, 3473-3482.

Goldberg, S. (1976). Polarization of the avian retina. Ocular transplantation studies. *J.Comp.Neurol.* **168**, 379-392.

Golden, J.A., Bracilovic, A., McFadden, K.A., Beesley, J., Rubenstein, J.L., and Grinspan, J.B. (1999). Ectopic bone morphogenetic proteins 5 and 4 in the chicken forebrain lead to cyclopia and holoprosencephaly. *Proc.Natl.Acad.Sci.U.S.A.* **96**, 2439-2444.

Govindarajan, V. and Overbeek, P.A. (2001). Secreted FGFR3, but not FGFR1, inhibits lens fiber differentiation. *Development.* **128**, 1617-1627.

Graham, A., Francis-West, P., Brickell, P., and Lumsden, A. (1994). The signalling molecule BMP4 mediates apoptosis in the rhombencephalic neural crest. *Nature.* **372**, 684-686.

Graw, J. (2003). The genetic and molecular basis of congenital eye defects. *Nat.Genet.Reviews.* **4**, 876-888.

Greene, N.D. and Copp, A.J. (1997). Inositol prevents folate-resistant neural tube defects in the mouse. *Nat.Med.* **3**, 60-66.

Gregory-Evans, C.Y., Williams, M.J., Halford, S., and Gregory-Evans, K. (2004). Ocular coloboma: a reassessment in the age of molecular neuroscience. *J.Med.Genet.* **41**, 881-891.

Grimm, S. and Pflugfelder, G.O. (1996). Control of the gene optomotor-blind in Drosophila wing development by decapentaplegic and wingless. *Science.* **271**, 1601-1604.

Grindley, J.C., Davidson, D.R., and Hill, R.E. (1995). The role of *Pax-6* in eye and nasal development. *Development.* **121**, 1433-1442.

Gross, J.M. and Dowling, J.E. (2005). Tbx2b is essential for neuronal differentiation along the dorsal/ventral axis of the zebrafish retina. *Proc.Natl.Acad.Sci.U.S.A.* **102**, 4371-4376.

Grün, F., Hirose, Y., Kawauchi, S., Ogura, T., and Umesono, K. (2000). Aldehyde dehydrogenase 6, a cytosolic retinaldehyde dehydrogenase prominently expressed in sensory neuroepithelia during development. *J.Biol.Chem.* **275**, 41210-41218.

Gu, Z., Reynolds, E.M., Song, J., Lei, H., Feijen, A., Yu, L., He, W., MacLaughlin, D.T., van den Eijnden-van Raaij, Donahoe, P.K., and Li, E. (1999). The type I serine/threonine kinase receptor ActRIA (ALK2) is required for gastrulation of the mouse embryo. *Development.* **126**, 2551-2561.

Gurdon, J.B., Mitchell, A., and Mahony, D. (1995). Direct and continuous assessment by cells of their position in a morphogen gradient. *Nature.* **376**, 520-521.

Habets, P.E.M.H., Moorman, A.F.M., Clout, D.E.W., van Roon, M.A., Lingbeek, M., van Lohuizen, M., Campione, M., and Christoffels, V.M. (2002). Cooperative action of Tbx2 and Nkx2.5 inhibits ANF expression in the atrioventricular canal: implications for cardiac chamber formation. *Genes Dev.* **16**, 1234-1246.

Hallonet, M., Hollemann, T., Pieler, T., and Gruss, P. (1999). Vax1, a novel homeobox-containing gene, directs development of the basal forebrain and visual system. *Genes Dev.* **13**, 3106-3114.

Hamburger, V. and Hamilton, H.L. (1992). A series of normal stages in the development of the chick embryo. *Dev.Dyn.* **195**, 231-272.

Hammond, C.J., Andrew, T., Mak, Y.T., and Spector, T.D. (2004). A susceptibility locus for myopia in the normal population is linked to the *PAX6* gene region on chromosome 11: a genomewide scan of dizygotic twins. *Am.J.Hum.Genet.* **75**, 294-304.

Harrelson, Z., Kelly, R.G., Goldin, S.N., Gibson-Brown, J.J., Bollag, R., Silver, L.M., and Papaioannou, V.E. (2004). Tbx2 is essential for patterning the atrioventricular canal and for morphogenesis of the outflow tract during heart development. *Development.* **131**, 5041-5052.

Hatakeyama, J. and Kageyama, R. (2004). Retinal cell fate determination and bHLH factors. *Semin.Cell Dev.Biol.* **15**, 83-89.

Hatini, V., Tao, W., and Lai, E. (1994). Expression of winged helix genes, *BF-1* and *BF-2*, define adjacent domains within the developing forebrain and retina. *J.Neurobiol.* **25**, 1293-1309.

He, M.L., Chen, Y., Peng, Y., Jin, D., Du, D., Wu, J., Lu, P., Lin, M.C., and Kung, H.F. (2002). Induction of apoptosis and inhibition of cell growth by developmental regulator hTBX5. *Biochem.Biophys.Res.Commun.* **297**, 185-192.

Herrmann, B.G., Labeit, S., Poustka, A., King, T.R., and Lehrach, H. (1990). Cloning of the T gene required in mesoderm formation in the mouse. *Nature.* **343**, 617-622.

Hetherington, C.M., Doe, B., and Hay, D. (2000). Mouse care and husbandry. *Mouse genetics and transgenetics*, New York: Oxford University Press Inc. 1-25.

Hill, R.E., Favor, J., Hogan, B.L., Ton, C.C.T., Saunders, G.F., Hanson, I.M., Prosser, J., Jordan, T., Hastie, N.D., and van Heyningen, V. (1991). Mouse *Small eye* results from mutations in a paired-like homeobox-containing gene. *Nature.* **354**, 522-525.

Hindges, R., McLaughlin, T., Genoud, N., Henkemeyer, M., and O'Leary, D.D.M. (2002). EphB forward signaling controls directional branch extension and arborization required for dorsal-ventral retinotopic mapping. *Neuron.* **35**, 475-487.

Hiroi, Y., Kudoh, S., Monzen, K., Ikeda, Y., Yazaki, Y., Nagai, R., and Komuro, I. (2001). Tbx5 associates with Nkx2-5 and synergistically promotes cardiomyocyte differentiation. *Nat.Genet.* **28**, 276-280.

Hodgkinson, C.A., Moore, K.J., Nakayama, A., Steingrimsson, E., Copeland, N.G., Jenkins, N.A., and Arnheiter, H. (1993). Mutations at the mouse microphthalmia locus are associated with defects in a gene encoding a novel basic-helix-loop-helix zipper protein. *Cell.* **74**, 395-404.

Hofmann, C. (2003). Somite and Axial Development in Vertebrates. *Patterning in vertebrate development*, New York: Oxford University Press, 48-76.

Holash, J.A. and Pasquale, E.B. (1995). Polarized expression of the receptor protein tyrosine kinase Cek5 in the developing avian visual system. *Dev.Biol.* **172**, 683-693.

Holash, J.A., Soans, C., Chong, L.D., Shao, H., Dixit, V.M., and Pasquale, E.B. (1997). Reciprocal expression of the Eph receptor Cek5 and its ligand(s) in the early retina. *Dev.Biol.* **182**, 256-269.

Holme, R.H., Thomson, S.J., and Davidson, D.R. (2000). Ectopic expression of *Msx2* in chick retinal pigmented epithelium cultures suggests a role in patterning the optic vesicle. *Mech.Dev.* **91**, 175-187.

Holt, C. (1980). Cell movements in *Xenopus* eye development. *Nature.* **287**, 850-852.

Holt, C.E., Bertsch, T.W., Ellis, H.M., and Harris, W.A. (1988). Cellular determination in the Xenopus retina is independent of lineage and birth date. *Neuron.* **1**, 26.

Holt, J.K.L. (2003). An analysis of the role of T-box genes in development of the mammalian retina. PhD Thesis.

Horsford, D.J., Nguyen, M.T., Sellar, G.C., Kothary, R., Arnheiter, H., and McInnes, R.R. (2004). *Chx10* repression of *Mitf* is required for the maintenance of mammalian neuroretinal identity. *Development.* **132**, 177-187.

Hsu, D.R., Economides, A.N., Wang, X., Eimon, P.M., and Harland, R.M. (1998). The Xenopus dorsalizing factor Gremlin identifies a novel family of secreted proteins that antagonize BMP activities. *Mol.Cell.* **1**, 673-683.

Hu, Q., Ueno, N., and Behringer, R.R. (2004). Restriction of BMP4 activity domains in the developing neural tube of the mouse embryo. *EMBO reports.* **5**, 734-739.

Huh, S., Hatini, V., Marcus, R.C., Li, S.C., and Lai, E. (1999). Dorsal-ventral patterning defects in the eye of BF-1-deficient mice associated with a restricted loss of shh expression. *Dev.Biol.* **211**, 53-63.

Hyatt, G.A., Schmitt, E.A., Marsh-Armstrong, N., and Dowling, J.E. (1992). Retinoic acid-induced duplication of the zebrafish retina. *Proc.Natl.Acad.Sci.U.S.A.* **89**, 8293-8297.

Hyatt, G.A., Schmitt, E.A., Marsh-Armstrong, N., McCaffery, P., Drager, U.C., and Dowling, J.E. (1996). Retinoic acid establishes ventral retinal characteristics. *Development.* **122**, 195-204.

Hyer, J., Kuhlman, J., Afif, E., and Mikawa, T. (2003). Optic cup morphogenesis requires pre-lens ectoderm but not lens differentiation. *Dev.Biol.* **259**, 351-363.

Hyer, J., Mima, T., and Mikawa, T. (1998). FGF1 patterns the optic vesicle by directing the placement of the neural retina domain. *Development.* **125**, 869-877.

Ingham, P.W. and McMahon, A.P. (2001). Hedgeog signaling in animal development: paradigms and principles. *Genes Dev.* **15**, 3059-3087.

Inoue, H., Nojima, H., and Okayama, H. (1990). High efficiency transformation of Escherichia coli with plasmids. *Gene.* **96**, 23-28.

Inoue, T., Nakamura, S., and Osumi, N. (2000). Fate mapping of the mouse prosencephalic neural plate. *Dev.Biol.* **219**, 373-383.

Itasaki, N., Bel-Vialar, S., and Krumlauf, R. (1999). 'Shocking' developments in chick embryology: electroporation and *in ovo* gene expression. *Nat.Cell Biol.* **1**, E203-E207.

Ito, M. and Yoshioka, M. (1999). Regression of the hyaloid vessels and pupillary membrane of the mouse. *Anat.Embryol.* **200**, 403-411.

Jacobi, F.K., Zrenner, E., Broghammer, M., and Pusch, C.M. (2005). A genetic perspective on myopia. *Cell Mol.Life Sci.* **62**, 800-808.

Jacobs, J.J., Keblusek, P., Robanus-Maandag, E., Kristel, P., Lingbeek, M., Nederlof, P.M., van Welsem, T., van de Vijver, M.J., Koh, E.Y., Daley, G.Q., and van Lohuizen, M. (2000). Senescence bypass screen identifies TBX2, which represses Cdkn2a (p19(ARF)) and is amplified in a subset of human breast cancers. *Nat.Genet.* **26**, 291-299.

Janssen-Bienhold, U., Dermietzel, R., and Weiler, R. (1998). Distribution of Connexin43 immunoreactivity in the retinas of different vertebrates. *J.Comp Neurol.* **396**, 310-321.

Jean, D., Bernier, G., and Gruss, P. (1999). *Six6* (*Optx2*) is a novel murine *Six3*-related homeobox gene that demarcates the presumptive pituitary/hypothalamic axis and the ventral optic stalk. *Mech.Dev.* **84**, 31-40.

Jeffery, G. (1997). The albino retina: an abnormality that provides insight into normal retinal development. *Trends Neurosci.* **20**, 169.

Jena, N., Martin-Seisdedos, C., McCue, P., and Croce, C.M. (1997). BMP7 null mutation in mice: developmental defects in skeleton, kidney, and eye. *Exp.Cell Res.* **230**, 28-37.

Jerome-Majewska, L.A., Jenkins, G.P., Ernstoff, E., Zindy, F., Sherr, C.J., and Papaioannou, V.E. (2005). *Tbx3*, the Ulnar-Mammary syndrome gene, and *Tbx2* interact in mammary gland development through a $p19^{Arf}$/p53-independent pathway. *Dev.Dyn.* **234**, 922-933.

Jessell, T.M. (2000). Neuronal specification in the spinal cord: inductive signals and transcriptional codes. *Nat.Rev.Genet.* **1**, 20-29.

Jones, C.M., Armes, N., and Smith, J.C. (1996). Signalling by TGF-ß family members: short-range effects of Xnr-2 and BMP-4 contrast with the long-range effects of activin. *Curr.Biol.* **6**, 1468-1475.

Jordan, T., Hanson, I., Zaletayev, D., Hodgson, S., Prosser, J., Seawright, A., Hastie, N., and van Heyningen, V. (1992). The human PAX6 gene is mutated in two patients with aniridia. *Nat.Genet.* **1**, 328-332.

Kalter, H. and Warkany, J. (1959). Experimental production of congenital malformations in mammals by metabolic procedure. *Physiol.Rev.* **39**, 69-115.

Kamachi, Y., Uchikawa, M., Collignon, J., Lovell-Badge, R., and Kondoh, H. (1998). Involvement of *Sox1*, *2*, and *3* in the early and subsequent molecular events of lens induction. *Development.* **125**, 2521-2532.

Kaufman, M.H. (1992). *The atlas of mouse development*. London: Academic Press Ltd.

Khokha, M.K., Hsu, D., Brunet, L.J., Dionne, M.S., and Harland, R.M. (2003). Gremlin is the BMP antagonist required for maintenance of Shh and Fgf signals during limb patterning. *Nat.Genet.* **34**, 303-307.

Kimura, N., Matsuo, R., Shibuya, H., Nakashima, K., and Taga, T. (2000). BMP2-induced apoptosis is mediated by activation of the TAK1-p38 kinase pathway that is negatively regulated by Smad6. *J.Biol.Chem.* **275**, 17647-17652.

Kjaer, K.W., Hansen, L., Eiberg, H., Leicht, P., Opitz, J.M., and Tommerup, N. (2004). Novel *Connexin 43 (GJA1)* mutation causes oculo-dento-digital dysplasia with curly hair. *Am.J.Med.Genet.* **127A**, 152-157.

Koshiba-Takeuchi, K., Takeuchi, J.K., Matsumoto, K., Momose, T., Uno, K., Hoepker, V., Ogura, K., Takahashi, N., Nakamura, H., Yasuda, K., and Ogura, T. (2000). Tbx5 and the retinotectum projection. *Science.* **287**, 134-137.

Kraus, F., Haenig, B., and Kispert, A. (2001). Cloning and expression analysis of the mouse T-box gene tbx20. *Mech.Dev.* **100**, 87-91.

Kubo, F., Takeichi, M., and Nakagawa, S. (2003). Wnt2b controls retinal cell differentiation at the ciliary marginal zone. *Development.* **130**, 587-598.

Kubota, R., McGuire, C., Dierks, B., and Reh, T. (2004). Identification of ciliary epithelial-specific genes using subtractive libraries and cDNA arrays in the avian eye. *Dev.Dyn.* **229**, 529-540.

Kurose, H., Bito, T., Adachi, T., Shimizu, M., Noji, S., and Ohuchi, H. (2004). Expression of *Fibroblast growth factor 19 (Fgf19)* during chicken embryogenesis and eye development, compared with *Fgf15* expression in the mouse. *Gene Expr.Patterns.* **4**, 687-693.

Kurose, H., Okamoto, M., Shimizu, M., Bito, T., Marcelle, C., Noji, S., and Ohuchi, H. (2005). FGF19-FGFR4 signaling elaborates lens induction with the FGF8-L-Maf cascade in the chick embryo. *Develop.Growth Differ.* **47**, 213-223.

Lagutin, O.V., Zhu, C.C., Kobayashi, D., Topczewski, J., Shimamura, K., Puelles, L., Russell, H.R.C., McKinnon, P.J., Solnica-Krezel, L., and Oliver, G. (2003). *Six3* repression of Wnt signaling in the anterior neuroectoderm is essential for vertebrate forebrain development. *Genes Dev.* **17**, 368-379.

Larsen, W.J. (2001). Development of the head, the neck, the eyes, and the ears. *Human embryology*, Philadelphia: Churchill Livingstone, 349-417.

Laufer, E., Nelson, C.E., Johnson, R.L., Morgan, B.A., and Tabin, C. (1994). *Sonic hedgehog* and *Fgf-4* act through a signaling cascade and feedback loop to integrate growth and patterning of the developing limb bud. *Cell.* **79**, 993-1003.

Leconte, L., Lecoin, L., Martin, P., and Saule, S. (2004). Pax6 interacts with cVax and Tbx5 to establish the dorsoventral boundary of the developing eye. *J.Biol.Chem.* **279**, 47272-47277.

Lecuit, T., Brook, W.J., Ng, M., Calleja, M., Sun, H., and Cohen, S.M. (1996). Two distinct mechanisms for long-range patterning by Decapentaplegic in the *Drosophila* wing. *Nature.* **381**, 387-393.

Lee, C.S., May, N.R., and Fan, C.M. (2001a). Transdifferentiation of the ventral retinal pigmented epithelium to neural retina in the growth arrest specific gene 1 mutant. *Dev Biol.* **236**, 17-29.

Lee, H.Y., Wroblewski, E., Philips, G.T., Stair, C.N., Conley, K., Reedy, M., Mastick, G.S., and Brown, N.L. (2005). Multiple requirements for *Hes1* during early eye formation. *Dev.Biol.* **284**, 464-478.

Lee, K.J. and Jessell, T.M. (1999). The specification of dorsal cell fates in the vertebrate central nervous system. *Annu.Rev.Neurosci.* **22**, 261-294.

Lee, S.H., Fu, K.K., Hui, J.N., and Richman, J.M. (2001b). Noggin and retinoic acid transform the identity of avian facial prominences. *Nature.* **414**, 909-912.

Li, H., Wagner, E., McCaffery, P., Smith, D., Andreadis, A., and Dräger, U.C. (2000). A retinoic acid synthesizing enzyme in ventral retina and telencephalon of the embryonic mouse. *Mech.Dev.* **95**, 283-289.

Li, Q.Y., Newbury-Ecob, R.A., Terrett, J.A., Wilson, D.I., Curtis, A.R., Yi, C.H., Gebuhr, T., Bullen, P.J., Robson, S.C., Strachan, T., Bonnet, D., Lyonnet, S., Young, I.D., Raeburn, J.A., Buckler, A.J., Law, D.J., and Brook, J.D. (1997). Holt-Oram syndrome is caused by mutations in TBX5, a member of the Brachyury (T) gene family. *Nat.Genet.* **15**, 21-29.

Li, X., Perissi, V., Liu, F., Rose, D.W., and Rosenfeld, M.G. (2002). Tissue-specific regulation of retinal and pituitary precursor cell proliferation. *Science.* **297**, 1180-1183.

Liberatore, C.M., Searcy-Schrick, R.D., and Yutzey, K.E. (2000). Ventricular expression of tbx5 inhibits normal heart chamber development. *Dev.Biol.* **223**, 169-180.

Lindsell, C.E., Boulter, J., diSibio, G., Gossler, A., and Weinmaster, G. (1996). Expression patterns of *Jagged, Delta1, Notch1, Notch2*, and *Notch3* genes identify ligand-receptor pairs that may function in neural development. *Mol.Cell.Neurosci.* **8**, 14-27.

Lingbeek, M.E., Jacobs, J.J., and van Lohuizen, M. (2002). The T-box repressors TBX2 and TBX3 specifically regulate the tumor suppressor gene p14ARF via a variant T-site in the initiator. *J.Biol.Chem.* **277**, 26120-26127.

Liu, I.S.C., Chen, J., Ploder, L., Vidgen, D., van der Kooy, D., Kalnins, V.I., and McInnes, R.R. (1994). Developmental expression of a novel murine homeobox gene (*Chx10*): Evidence for roles in determination of the neuroretina and inner nuclear layer. *Neuron.* **13**, 377-393.

Liu, J., Wilson, S., and Reh, T. (2003). BMP receptor 1b is required for axon guidance and cell survival in the developing retina. *Dev.Biol.* **256**, 34-48.

Logan, M. and Tabin, C.J. (1998). Targeted gene misexpression in chick limb buds using avian replication-competent retroviruses. *Methods.* **14**, 407-420.

López-Ríos, J., Gallardo, M.E., Rodríguez de Córdoba, S., and Bovolenta, P. (1999). *Six9* (*Optx2*), a new ember of the Six gene family of transcription factors, is

expressed at early stages of vertebrate ocular and pituitary development. *Mech.Dev.* **83**, 155-159.

Lovicu, F.J. and Overbeek, P.A. (1998). Overlapping effects of different members of the FGF family on lens fiber differentiation in transgenic mice. *Development.* **125**, 3365-3377.

Luo, G., Hofmann, C., Bronckers, A.L., Sohocki, M., Bradley, A., and Karsenty, G. (1995). BMP-7 is an inducer of nephrogenesis, and is also required for eye development and skeletal patterning. *Genes Dev.* **15**, 2808-2820.

Lupo, G., Liu, Y., Qiu, R., Chandraratna, R.A.S., Barsacchi, G., He, R., and Harris, W.A. (2005). Dorsoventral patterning of the *Xenopus* eye: a collaboration of Retinoid, Hedgehog and Fgf receptor signalling. *Development.* **132**, 1737-1748.

Macdonald, R., Barth, K.A., Xu, Q., Holder, N., Mikkola, I., and Wilson, S.W. (1995). Midline signalling is required for Pax gene regulation and patterning of the eyes. *Development.* **121**, 3267-3278.

Mahlamaki, E.H., Bärlund, M., Tanner, M., Gorunova, L., Höglund, M., Karhu, R., and Kallioniemi, A. (2002). Frequent amplification of 8q24, 11q, 17q, and 20q-specific genes in pancreatic cancer. *Gene Chrom.Cancer.* **35**, 353-358.

Mann, F., Ray, S., Harris, W.A., and Holt, C.E. (2002). Topographic mapping in dorsoventral axis of the *Xenopus* retinotectal system depends on signaling through Ephrin-B ligands. *Neuron.* **35**, 461-473.

Manson, F.D.C., Trump, D., Read, A.P., and Black, G.C.M. (2005). Inherited eye disease: cause and late effect. *Trends Mol.Med.* **11**, 449-455.

Marcus, R.C., Gale, N.W., Morrison, M.E., Mason, C.A., and Yancopoulos, G.D. (1996). Eph Family Receptors and Their Ligands Distribute in Opposing Gradients in the Developing Mouse Retina. *Dev.Biol.* **180**, 786-789.

Marigo, V., Davey, R.A., Zuo, Y., Cunningham, J.M., and Tabin, C.J. (1996). Biochemical evidence that patched is the Hedgehog receptor. *Nature.* **384**, 176-179.

Marsh-Armstrong, N., McCaffery, P., Gilbert, W., Dowling, J.E., and Drager, U.C. (1994). Retinoic acid is necessary for development of the ventral retina in zebrafish. *Proc.Natl.Acad.Sci.U.S.A.* **91**, 7286-7290.

Martin, P. and Cockroft, D.L. (1999). Culture of postimplantation mouse embryos. *Methods Mol.Biol.* **97**, 7-22.

Martinez-Morales, J.R., Del Bene, F., Nica, G., Hammerschmidt, M., Bovolenta, P., and Wittbrodt, J. (2005). Differentaition of the Vertebrate Retina Is Coordinated by an FGF Signaling Center. *Developmental Cell.* **8**, 565-574.

Massague, J. and Chen, YG. (2000). Controlling TGF-ß signaling. *Genes Dev.* **14**, 627-644.

Mathers, P.H., Grinberg, A., Mahon, K.A., and Jamrich, M. (1997). The Rx homeobox gene is essential for vertebrate eye development. *Nature.* **387**, 603-607.

Matsuda, T. and Cepko, C.L. (2004). Electroporation and RNA interference in the rodent retina *in vivo* and *in vitro*. *Proc.Natl.Acad.Sci.U.S.A.* **101**, 16-22.

Matsuo, I., Kuratani, S., Kimura, C., Takeda, N., and Aizawa, S. (1995). Mouse Otx2 functions in the formation and patterning of rostral head. *Genes Dev.* **9**, 2646-2658.

Matt, N., Dupé, V., Garnier, JM., Dennefeld, C., Chambon, P., Mark, M., and Ghyselinck, N.B. (2005). Retinoic acid-dependent eye morphogenesis is orchestrated by neural crest cells. *Development.* **132**, 4789-4800.

McAvoy, J.W. (1980). Cytoplasmic processes interconnect lens placode and optic vesicle during eye morphogenesis. *Exp.Eye Res.* **31**, 527-534.

McCabe, K.L., Gunther, E.C., and Reh, T.A. (1999). The development of the pattern of retinal ganglion cells in the chick retina: mechanisms that control differentiation. *Development.* **126**, 5713-5724.

McCaffery, P., Mi-Ock, L., Wagner, E., Sladek, N.E., and Dräger, U.C. (1992). Asymmetrical retinoic acid synthesis in the dorsoventral axis of the retina. *Development.* **115**, 371-382.

McCaffery, P., Tempst, P., Lara, G., and Dräger, U.C. (1991). Aldehyde dehydrogenase is a positional marker in the retina. *Development.* **112**, 693-702.

McCaffery, P., Wagner, E., O'Neil, J., Petkovich, M., and Drager, U.C. (1999). Dorsal and ventral rentinoic territories defined by retinoic acid synthesis, break-down and nuclear receptor expression. *Mech.Dev.* **85**, 203-214.

McDowell, N., Zorn, A.M., Crease, D.J., and Gurdon, J.B. (1997). Activin has direct long-range signalling activity and can form a concentration gradient by diffusion. *Curr.Biol.* **7**, 671-681.

McLaughlin, T., Hindges, R., and O'Leary, D.D. (2003a). Regulation of axial patterning of the retina and its topographic mapping in the brain. *Curr.Opin.Neurobiol.* **13**, 57-69.

McLaughlin, T., Hindges, R., Yates, P.A., and O'Leary, D.D. (2003b). Bifunctional action of ephrin-B1 as a repellent and attractant to control bidirectional branch extension in dorsal-ventral retinotopic mapping. *Development.* **130**, 2407-2418.

McMahon, J.A., Takada, S., Zimmerman, L.B., Fan, C.M., Harland, R.M., and McMahon, A.P. (1998). Noggin-mediated antagonism of BMP signaling is required for growth and patterning of the neural tube and somite. *Genes Dev.* **12**, 1438-1452.

McWhirter, J.R., Goulding, M., Weiner, J.A., Chun, J., and Murre, C. (1997). A novel fibroblast growth factor gene expressed in the developing nervous system is a downstream target of the chimeric homeodomain oncoprotein E2A-Pbx1. *Development.* **124**, 3221-3232.

Mehler, M.F., Mabie, P.C., Zhang, D., and Kessler, J.A. (1997). Bone morphogenetic proteins in the nervous system. *Trends Neurosci.* **20**, 309-317.

Mellitzer, G., Hallonet, M., Chen, L., and Ang, S. (2002). Spatial and temporal 'knock down' of gene expression by electroporation of double-stranded RNA and morpholinos into early postimplantation mouse embryos. *Mech.Dev.* **118**, 57-63.

Mey, J., McCaffery, P., and Klemeit, M. (2001). Sources and sink of retinoic acid in the embryonic chick retina: distribution of aldehyde dehydrogenase activities, CRABP-I, and sites of retinoic acid inactivation. *Dev.Brain.Res.* **127**, 135-148.

Mey, J. and Thanos, S. (2000). Development of the visual system of the chick: I. Cell differentiation and histogenesis. *Brain Res.Reviews.* **32**, 379.

Miller, D.L., Ortega, S., Bashayan, O., Basch, R., and Basilico, C. (2000). Compensation by Fibroblast growth factor 1 (FGF1) does not account for the mild phenotypic defects observed in FGF2 null mice. *Mol.Cell Biol.* **20**, 2260-2268.

Mishina, Y., Suzuki, A., Ueno, N., and Behringer, R.R. (1995). Bmpr encodes a type I bone morphogenetic protein receptor that is essential for gastrulation during mouse embryogenesis. *Genes Dev.* **9**, 3027-3037.

Mitchell, C.A., Risau, W., and Drexler, H.C.A. (1998). Regression of vessels in the Tunica Vasculosa Lentis is initiated by coordinated endothelial apoptosis: A role for vascular endothelial growth factor as a survival factor for endothelium. *Dev.Dyn.* **213**, 322-333.

Mitsiadis, T.A., Henrique, D., Thesleff, I., and Lendahl, U. (1997). Mouse Serrate-1 (Jagged-1): expression in the developing tooth is regulated by epithelial-mesenchymal interactions and fibroblast growth factor-4. *Development.* **124**, 1473-1483.

Mochii, M., Mazaki, Y., Mizuno, N., Hayashi, H., and Eguchi, G. (1998). Role of Mitf in differentiation and transdifferentiation of chicken pigmented epithelial cell. *Dev.Biol.* **193**, 47-62.

Momose, T., Tonegawa, A., Takeuchi, J., Ogawa, H., Umesono, K., and Yasuda, K. (1999). Efficient targeting of gene expression in chick embryos by microelectroporation. *Dev.Growth Differ.* **41**, 335-344.

Monaghan, A.P., Davidson, D.R., Sime, C., Graham, E., Baldock, R., Bhattacharya, S.S., and Hill, R.E. (1991). The *Msh*-like homeobox genes define domains in the developing vertebrate eye. *Development.* **112**, 1053-1061.

Morcillo,J.,Martinez-Morales,J.R., Trousse,F. Sowden,J.C., Bovolenta,P. Proper patterning of the retinal fissure requires the sequential activity of BMP7 and SHH. Submitted publication. Cajal Institute, Spain.

Morgan, B.A. and Fekete, D.M. (1996). Manipulating gene expression with replication-competent retroviruses. *Methods Cell Biol.* **51**, 185-218.

Moriguchi, T., Kuroyanagi, N., Yamaguchi, K., Gotoh, Y., Irie, K., Kano, T., Shirakabe, K., Muro, Y., Shibuya, H., Matsumoto, K., Nishida, E., and Hagiwara, M. (1996). A novel kinase cascade mediated by mitogen-activated protein kinase kinase 6 and MKK3. *J.Biol.Chem.* **271**, 13675-13679.

Mozer, B.A. (2001). Dominant *Drop* mutants are gain-of-function alleles of the *muscle segment homeobox* gene (*msh*) whose overexpression leads to the arrest of eye development. *Dev.Biol.* **233**, 380-393.

Mui, S.H., Hindges, R., O'Leary, D.D.M., Lemke, G., and Bertuzzi, S. (2002). The homeodomain protein Vax2 patterns the dorsoventral and nasotemporal axes of the eye. *Development.* **129**, 797-804.

Mui, S.H., Kim, J.W., Lemke, G., and Bertuzzi, S. (2005). Vax genes ventralize the embryonic eye. *Genes Dev.* **19**, 1249-1259.

Muller, C.W. and Herrmann, B.G. (1997). Crystallographic structure of the T domain-DNA complex of the Brachyury transcription factor. *Nature.* **389**, 884-888.

Murali, D., Yoshikawa, S., Corrigan, R.R., Plas, D.J., Crair, M.C., Oliver, G., Lyons, K.M., Mishina, Y., and Furuta, Y. (2005). Distinct developmental programs require different levels of Bmp signaling during mouse retinal development. *Development.* **132**, 913-923.

Muramatsu, T., Mizutani, Y., Ohmori, Y., and Okumura, J. (1997). Comparison of three nonviral transfection methods for foreign gene expression in early chicken embryos *in ovo*. *Biochem.Biophys.Res.Commun.* **230**, 376-380.

Mutti, D.O., Mitchell, G.L., Moeschberger, M.L., Jones, L.A., and Zadnik, K. (2002). Parental Myopia, Near Work, School Achievement, and Children's Refractive Error. *Investigative Ophthalmology Visual Science.* **43**, 3633-3640.

Naegele, J.R. and Barnstable, C.J. (1991). A carbohydrate epitope defined by monoclonal antibody VC1.1 is found on N-CAM and other cell adhesion molecules. *Brain Res.* **559**, 118-129.

Naiche, L.A., Harrelson, Z., Kelly, R.G., and Papaioannou, V.E. (2005). T-box genes in vertebrate development. *Annu.Rev.Genet.* **39**, 219-239.

Naiche, L.A. and Papaioannou, V.E. (2003). Loss of Tbx4 blocks hindlimb development and affects vascularization and fusion of the allantois. *Development.* **130**, 2681-2693.

Nellen, D., Burke, R., Struhl, G., and Basler, K. (1996). Direct and long-range action of a DPP morphogen gradient. *Cell.* **85**, 357-368.

Newbury-Ecob, R.A., Leanage, R., Raeburn, J.A., and Young, I.D. (1996). Holt-Oram syndrome: a clinical genetic study. *J.Med.Genet.* **33**, 300-307.

Nguyen, M. and Arnheiter, H. (2000). Signaling and transcriptional regulation in early mammalian eye development: a link between FGF and MITF. *Development.* **127**, 3581-3591.

Nguyen, V.H., Trout, J., Connors, S.A., Andermann, P., Weinberg, E., and Mullins, M.C. (2000). Dorsal and intermediate neuronal cell types of the spinal cord are established by a BMP signaling pathway. *Development.* **127**, 1209-1220.

Niswander, L., Jeffrey, S., Martin, G.R., and Tickle, C. (1994). A positive feedback loop coordinates growth and patterning in the vertebrate limb. *Nature.* **371**, 609-612.

Niswander, L. and Martin, G.R. (1993). FGF-4 and BMP-2 have opposite effects on limb growth. *Nature.* **361**, 68-71.

Nornes, H.O., Dressler, G.R., Knapik, E.W., Deutsch, U., and Gruss, P. (1990). Spatially and temporally restricted expression of *Pax2* during murine neurogenesis. *Development.* **109**, 797-809.

Nurse, P. (2000). A long twentieth century of the cell cycle and beyond. *Cell.* **100**, 71-78.

O'Leary, D.D.M., Yates, P.A., and McLaughlin, T. (1999). Molecular development of sensory maps: Representing sights and smells in the brain. *Cell.* **96**, 255-269.

Ogita, J., Isogai, E., Sudo, H., Sakiyama, S., Nakagawara, A., and Koseki, H. (2001). Expression of the Dan gene during chicken embryonic development. *Mech.Dev.* **109**, 363-365.

Ohkawara, B., Iemura, S., Ten Dijke, P., and Ueno, N. (2002). Action range of BMP is defined by its N-terminal basic amino acid core. *Curr.Biol.* **12**, 205-209.

Ohkubo, Y., Chiang, C., and Rubenstein, J.L. (2002). Coordinate regulation and synergistic actions of BMP4, SHH and FGF8 in the rostral prosencephalon regulate morphogenesis of the telencephalic and optic vesicles. *Neuroscience.* **111**, 1-17.

Oka, C., Tsujimoto, R., Kajikawa, M., Koshiba-Takeuchi, K., Ina, J., Masato, Y., Tsuchiya, A., Ueta, Y., Soma, A., Kanda, H., Matsumoto, M., and Kawaichi, M. (2003). HtrA1 serine protease inhibits signaling mediated by TGFß family proteins. *Development.* **131**, 1041-1053.

Oliver, G., Mailhos, A., Wehr, R., Copeland, N.G., Jenkins, N.A., and Gruss, P. (1995). *Six3*, a murine homologue of the *sine oculis* gene, demarcates the most anterior border of the developing neural plate and is expressed during eye development. *Development.* **121**, 4045-4055.

Onwochei, B.C., Simon, J.W., Bateman, J.B., Couture, K.C., and Mir, E. (2000). Ocular Colobomata. *Surv.Ophthalmol.* **45**, 175-194.

Oster, S.F., Deiner, M., Birgbauer, E., and Sretavan, D.W. (2004). Ganglion cell axon pathfinding in the retina and optic nerve. *Semin.Cell Dev.Biol.* **15**, 125-136.

Osumi, N. and Inoue, T. (2001). Gene transfer into cultured mammalian embryos by electroporation. *Methods.* **24**, 35-42.

Oyster, C.W. (1999). Formation of the human eye. *The human eye*, Sunderland Massachusetts: Sinauer Associates Inc. 57-75.

Packham, E.A. and Brook, J.D. (2003). T-box genes in human disorders. *Hum.Mol.Genet.* **12**, R37-R44.

Papaioannou, V.E. (1998). The coming of age of the transgenic era. *Int.J.Dev.Biol.* **42**, 841-846.

Papaioannou, V.E. (2001). T-box genes in development: from hydra to humans. *Int.Rev.Cytol.* **207**, 1-70.

Papapetrou, C., Edwards, Y.H., and Sowden, J.C. (1997). The T transcription factor functions as a dimer and exhibits a common human polymorphism Gly-177-Asp in the conserved DNA-binding domain. *FEBS Lett.* **409**, 201-206.

Paxton, C., Zhao, H., Chin, Y., Langner, K., and Reecy, J. (2002). Murine Tbx2 contains domains that activate and repress gene transcription. *Gene.* **283**, 117-124.

Paznekas, W.A., Boyadjiev, S.A., Shapiro, R.E., Daniels, O., Wollnik, B., Keegan, C.E., Innis, J.W., Dinulos, M.B., Christian, C., Hannibal, M.C., and Wang Jabs, E. (2003). *Connexin 43 (GJA1)* mutations cause the pleiotropic phenotype of oculodentodigital dysplasia. *Am.J.Hum.Genet.* **72**, 408-418.

Pearson, R.A., Lüneborg, N.L., Becker, D.L., and Mobbs, P. (2005). Gap junctions modulate interkinetik nuclear movement in retinal progenitor cells. *J.Neurosci.* **25**, 10803-10814.

Peters, M.A. and Cepko, C.L. (2002). The dorsal-ventral axis of the neural retina is divided into multiple domains of restricted gene expression which exhibit features of lineage compartments. *Dev.Biol.* **251**, 59-73.

Pflugfelder, G.O., Roth, H., and Poeck, B. (1992a). A homology domain shared between Drosophila optomotor-blind and mouse Brachyury is involved in DNA binding. *Biochem.Biophys.Res.Commun.* **186**, 918-925.

Pflugfelder, G.O., Roth, H., Poeck, B., Kerscher, S., Schwarz, H., Jonschker, B., and Heisenberg, M. (1992b). The lethal(1)optomotor-blind gene of Drosophila melanogaster is a major organizer of optic lobe development: isolation and characterization of the gene. *Proc.Natl.Acad.Sci.U.S.A.* **89**, 1199-1203.

Piccolo, S., Sasai, Y., Lu, B., and De Robertis, E.M. (1996). Dorsoventral patterning in Xenopus: inhibition of ventral signals by direct binding of chordin to BMP-4. *Cell.* **86**, 589-599.

Pittack, C., Grunwald, G.B., and Reh, T.A. (1997). Fibroblast growth factors are necessary for neural retina but not pigmented epithelium differentiation in chick embryos. *Development.* **124**, 805-816.

Pizette, S. and Niswander, L. (1999). BMPs negatively regulate structure and function of the limb apical ectodermal ridge. *Development.* **126**, 883-894.

Poeck, B., Hofbauer, A., and Pflugfelder, G.O. (1993). Expression of the *Drosophila optomotor-blind* gene transcript in neuronal and glial cells of the developing nervous system. *Development.* **117**, 1017-1029.

Porter, F.D., Drago, J., Xu, Y., Cheema, S.S., Wassif, C., Huang, S.P., Lee, E., Grinberg, A., Massalas, J.S., Bodine, D., Alt, F., and Westphal, H. (1997). Lhx2, a LIM homeobox gene, is required for eye, forebrain, and definitive erythrocyte development. *Development.* **124**, 2935-2944.

Prada, C., Puga, J., Perez-Mendez, L., Lopez, R., and Ramirez, G. (1991). Spatial and temporal patterns of neurogenesis in the chick retina. *Eur J Neurosci.* **3**, 559-569.

Prince, S., Carreira, S., Vance, K.W., Abraham, S., and Godin, R.E. (2004). Tbx2 directly represses the expression of the p21(WAF1) cyclin-dependent kinase inhibitor. *Cancer Res.* **64**, 1669-1674.

Ragge, N.K., Brown, A.G., Poloschek, C.M., Lorenz, B., Henderson, R.A., Clarke, M.P., Russell-Eggitt, I., Fielder, A., Gerrelli, D., Martinez-Barbera, JP., Ruddle, P., Hurst, J., O'Collin, J.R., Salt, A., Cooper, S.T., Thompson, P.J., Sisodiya, S.M., Williamson, K.A., FitzPatrick, D.R., van Heyningen, V., and Hanson, I.M. (2005). Heterozygous mutations of *OTX2* cause severe ocular malformations. *Am.J.Hum.Genet.* **76**, 1008-1022.

Rahi, J.S., Gilbert, C.E., Foster, A., and Minassia, D. (1999). Measuring the burden of childhood blindness. *Br.J.Ophthalmol.* **83**, 387-388.

Rebagliati, M.R., Toyama, R., Haffter, P., and Dawid, I.B. (1998). cyclops encodes a nodal-related factor involved in midline signaling. *Proc.Natl.Acad.Sci.U.S.A.* **95**, 9932-9937.

Reese, A.B. (1955). Persistent hyperplastic primary vitreous. *Am.J.Ophthalmol.* **40**, 317-331.

Reifers, F., Böhli, H., Walsh, E.C., Crossley, P.H., Stainier, D.Y.R., and Brand, M. (1998). *Fgf8* is mutated in zebrafish *acerebellar (ace)* mutants and is required for maintenance of midbrain-hindbrain boundary development and somitogenesis. *Development.* **125**, 2381-2395.

Robinson, S.R. (1991). Development of the mammalian retina. *Neuroanatomy of the visual pathways and their development*, London: The McMillan Press Ltd. 69-128.

Roessler, E., Belloni, E., Gaudenz, K., Jay, P., Berta, P., Scherer, S.W., Tsui, L.C., and Muenke, M. (1996). Mutations in the human Sonic Hedgehog gene cause holoprosencephaly. *Nat.Genet.* **14**, 357-360.

Romanoff, A.L. (1960). The organ of special sence. *The avian embryo: structural and functional development*, New York: The McMillan Company, 363-427.

Rowan, S., Chen, C.M.A., Young, T.L., Fisher, D.E., and Cepko, C.L. (2004). Transdifferentiation of the retina into pigmented cells in ocular retardation mice defines a new function of the homeodomain gene *Chx10*. *Development.* **131**, 5139-5152.

Saint-Geniez, M. and D'Amore, P.A. (2004). Development and pathology of the hyaloid, choroidal and retinal vasculature. *Int.J.Dev.Biol.* **48**, 1045-1058.

Sakai, Y., Luo, T., McCaffery, P., Hamada, H., and Dräger, U.C. (2004). CYP26A1 and CYP26C1 cooperate in degrading retinoic acid within the equatorial retina during later eye development. *Dev.Biol.* **276**, 143-157.

Sakuta, H., Suzuki, R., Takahashi, H., Kato, A., Shintani, T., Iemura, S., Yamamoto, T.S., Ueno, N., and Noda, M. (2001). Ventroptin: a BMP-4 antagonist expressed in a double-gradient pattern in the retina. *Science.* **293**, 111-115.

Sampath, K., Rubinstein, A.L., Cheng, A.M., Liang, J.O., Fekany, K., Solnica-Krezel, L., Korzh, V., Halpern, M.E., and Wright, C.V. (1998). Induction of the zebrafish ventral brain and floorplate requires cyclops/nodal signalling. *Nature*. **395**, 185-189.

Sasagawa, S., Takabatake, T., Takabatake, Y., Muramatsu, T., and Takeshima, K. (2002). Axes establishment during eye morphogenesis in Xenopus by coordinate and antagonistic actions of BMP4, Shh, and RA. *Genesis*. **33**, 86-96.

Schedl, A., Ross, A., Lee, M., Engelkamp, D., Rashbass, P., van Heyningen, V., and Hastie, N.D. (1996). Influence of *PAX6* gene dosage on development: overexpression causes severe eye abnormalities. *Cell*. **86**, 71-82.

Schimmenti, L.A., de la Cruz, J., Lewis, R.A., Karkera, J.D., Manligas, G.S., Roessler, E., and Muenke, M. (2003). Novel mutation in Sonic hedgehog in non-syndromic colobomatous microphthalmia. *Am.J.Med.Genet.* **116A**, 215-221.

Scholtz, C.L. and Chan, K.K. (1987). Complicated colobomatous microphthalmia in the microphthalmic (*mi/mi*) mouse. *Development*. **99**, 501-508.

Schook, P. (1980a). A spatial analysis of the localisation of cell division and cell death in relationship with the morphogenesis of the chick optic cup. *Acta Morphol.Neerl.-Scand.* **18**, 213-229.

Schook, P. (1980b). Morphogenetic movements during the early development of the chick eye. *Acta Morphol.Neerl.-Scand.* **18**, 1-30.

Schulte, D., Furukawa, T., Peters, M.A., Kozak, C.A., and Cepko, C.L. (1999). Misexpression of the Emx-related homeobox genes *cVax* and *mVax2* ventralizes the retina and perturbs the retinotectal map. *Neuron*. **24**, 541-553.

Schulte, D., Peters, M.A., Sen, J., and Cepko, C.L. (2005). The rod photoreceptor pattern is set at the optic vesicle stage and requires spatially restricted cVax expression. *J.Neurosci.* **25**, 2823-2831.

Schwarz, M., Cecconi, F., Bernier, G., Andrejewski, N., Kammandel, B., Wagner, M., and Gruss, P. (2000). Spatial specification of mammalian eye territories by

reciprocal transcriptional repression of *Pax2* and *Pax6*. *Development*. **127**, 4325-4334.

Sen, J., Harpavat, S., Peters, M.A., and Cepko, C.L. (2005). Retinoic acid regulates the expression of dorsoventral topographic guidance molecules in the chick retina. *Development*. **132**, 5147-5159.

Shi, Y. and Massague, J. (2003). Mechanisms of TGF-ß signaling from cell membrane to the nucleus. *Cell*. **113**, 685-700.

Shintani, T., Kato, A., Yuasa-Kawada, J., Sakuta, H., Takahashi, M., Suzuki, R., Ohkawara, T., Takahashi, H., and Noda, M. (2004). Large-scale identification and characterization of genes with asymmetric expression patterns in the developing chick retina. *J.Neurobiol.* **59**, 34-47.

Sidman, R.L. (1961). Histogenesis of mouse retina studied with Thymidine-H^3. *The structure of the eye*, New York: Academic Press, 487-506.

Simeone, A., Acampora, D., Mallamaci, A., Stornaiuolo, A., D'Apice, M.R., Nigro, V., and Boncinelli, E. (1993). A vertebrate gene related to *orthodenticle* contains a homeodomain of the *bicoid* class and demarcates anterior neuroectoderm in the gastrulating mouse embryo. *The EMBO J.* **12**, 2735-2747.

Sinclair, C.S., Adem, C., Naderi, A., Soderberg, C.L., Hohnson, M., Wu, K., Wadum, L., Couch, V.L., Sellers, T.A., Schaid, D., Slezak, J., Fredericksen, Z., Ingle, J.N., Hartmann, L., Jenkins, R.B., and Couch, F.J. (2002). TBX2 is preferentially amplified in BRCA1- and BRCA2- related breast tumors. *Cancer Res.* **62**, 3587-3591.

Singh, M.K., Christoffels, V.M., Dias, J.M., Trowe, MO., Petry, M., Schuster-Gossler, K., Bürger, A., Ericson, J., and Kispert, A. (2005). *Tbx20* is essential for cardiac chamber differentiation and repression of *Tbx2*. *Development*. **132**, 2697-2707.

Sinha, S., Abraham, S., Gronostajski, R.M., and Campbell, C.E. (2000). Differential DNA binding and transcription modulation by three T-box proteins, T, TBX1 and TBX2. *Gene*. **258**, 15-29.

Snow, R.L. and Robson, J.A. (1995). Migration and differentiation of neurons in the retina and optic tectum of the chick. *Exp.Neurol.* **134**, 13-24.

Sowden, J.C., Holt, J.K., Meins, M., Smith, H.K., and Bhattacharya, S.S. (2001). Expression of Drosophila omb-related T-box genes in the developing human and mouse neural retina. *Invest Ophthalmol.Vis.Sci.* **42**, 3095-3102.

Sperry, R.W. (1963). Chemoaffinity in the orderly growth of nerve fiber patterns and connections. *Proc.Natl.Acad.Sci.U.S.A.* **50**, 703-710.

Stanley, E., Biben, C., Kotecha, S., Fabri, L., Tajbaksh, S., Wang, CC., Hatzistavrou, T., Roberts, B., Drinkwater, C., Lah, M., Buckingham, M., Hilton, D., Nash, A., Mohun, T., and Harvey, R.P. (1998). DAN is a secreted glycoprotein related to *Xenopus* cerberus. *Mech.Dev.* **77**, 173-184.

Steingrimsson, E., Moore, K.J., Lamoreaux, M.L., Ferré-D'Amaré, A.R., Burley, S.K., Sanders Zimring, D.C., Skow, L.C., Hodgkinson, C.A., Arnheiter, H., Copeland, N.G., and Jenkins, N.A. (1994). Molecular basis of mouse *microphthalmia (mi)* mutations helps explain their developmental and phenotypic consequences. *Nat.Genet.* **8**, 256-263.

Stennard, F.A. and Harvey, R.P. (2005). T-box transcription factors and their roles in regulatory hierarchies in the developing heart. *Development.* **132**, 4897-4910.

Stern, C.D. (1993). Avian embryos. *Essential Developmental Biology*, Oxford: Oxford University Press, 45-54.

Streit, A. and Stern, C.D. (2001). Combined whole-mount *in situ* hybridisation and immunohistochemistry in avian embryos. *Methods.* **23**, 339-344.

Sundin, O.H., Leppert, G.S., Silva, E.D., Yang, J.M., Dharmaraj, S., Maumenee, I.H., Santos, L.C., Parsa, C.F., Traboulsi, E.I., Broman, K.W., Dibernardo, C., Sunness, J.S., Toy, J., and Weinberg, E.M. (2005). Extreme hyperopia is the result of null mutations in MFRP, which encodes a Frizzled-related protein. *Proc.Natl.Acad.Sci.U.S.A.* **102**, 9553-9558.

Suzuki, R., Shintani, T., Sakuta, H., Kato, A., Ohkawara, T., Osumi, N., and Noda, M. (2000). Identification of RALDH-3, a novel retinaldehyde dehydrogenase, expressed in the ventral region of the retina. *Mech.Dev.* **98**, 37-50.

Swartz, M., Eberhart, J., Mastick, G.S., and Krull, C.E. (2001). Sparking new frontiers: using *in vivo* electroporation for genetic manipulations. *Dev.Biol.* **233**, 13-21.

Szél, Á., Röhlich, P., Caffé, A.R., Juliusson, B., Aguirre, G., and Van Veen, T. (1992). Unique topographic separation of two spectral classes of cones in the mouse retina. *J.Comp Neurol.* **325**, 327-342.

Tada, M. and Smith, J.C. (2001). T-targets: clues to understanding the functions of T-box proteins. *Dev.Growth Differ.* **43**, 1-11.

Takabatake, Y., Takabatake, T., Sasagawa, S., and Takeshima, K. (2002). Conserved expression control and shared activity between cognate T-box genes Tbx2 and Tbx3 in connection with Sonic hedgehog signaling during Xenopus eye development. *Dev.Growth Differ.* **44**, 257-271.

Take-uchi, M., Clarke, J.D.W., and Wilson, S.W. (2003). Hedgehog signalling maintains the optic stalk-retinal interface through the regulation of Vax gene activity. *Development.* **130**, 955-968.

Tassabehji, M., Newton, V.E., and Read, A.P. (1994). Waardenburg syndrome type 2 caused by mutations in the human microphthalmia (MITF) gene. *Nat.Genet.* **8**, 251-255.

Tejedor, J. and de la Villa, P. (2003). Refractive changes induced by form deprivation in the mouse eye. *Investigative Ophthalmology Visual Science.* **44**, 32-36.

Thomas, P. and Beddington, R.S. (1996). Anterior primitive endoderm may be responsible for patterning the anterior neural plate in the mouse embryo. *Curr.Biol.* **6**, 1487-1496.

Thomas, P.Q., Dattani, M.T., Brickman, J.M., McNay, D., Warne, G., Zacharin, M., Cameron, F., Hurst, J., Woods, K., Dunger, D., Stanhope, R., Forrest, S., Robinson, I.C.A.F., and Beddington, R.S. (2001). Heterozygous *HESX1* mutations associated with isolated congenital pituitary hypoplasia and septo-optic dysplasia. *Hum.Mol.Genet.* **10**, 39-45.

Tickle, C. (2002). Molecular basis of vertebrate limb patterning. *Am.J.Med.Genet.* **112**, 250-255.

Tomita, K., Ishibashi, M., Nakahara, K., Ang, SL., Nakanishi, S., Guillemot, F., and Kageyama, R. (1996). Mammalian *hairy* and *Enhancer of Split* homolog 1 regulates differentiation of retinal neurons and is essential for eye morphogenesis. *Neuron.* **16**, 723-734.

Torres, M., Gomez-Pardo, E., and Gruss, P. (1996). Pax2 contributes to inner ear patterning and optic nerve trajectory. *Development.* **122**, 3381-3391.

Toy, J. and Sundin, O. (1999). Expression of the *Optx2* homeobox gene during mouse development. *Mech.Dev.* **83**, 183-186.

Trousse, F., Esteve, P., and Bovolenta, P. (2001). Bmp4 mediates apoptotic cell death in the developing chick eye. *J.Neurosci.* **21**, 1292-1301.

Tumpel, S., Sanz-Ezquerro, J.J., Isaac, A., Eblaghie, M.C., Dobson, J., and Tickle, C. (2002). Regulation of Tbx3 expression by anteroposterior signalling in vertebrate limb development. *Dev.Biol.* **250**, 251-262.

Turner, D.L. and Cepko, C.L. (1987). A common progenitor for neurons and glia persists in rat retina late in development. *Nature.* **328**, 131-136.

Turner, D.L., Snyder, E.Y., and Cepko, C.L. (1990). Lineage-independent determination of cell type in the embryonic mouse retina. *Neuron.* **4**, 833-845.

Uemonsa, T., Sakagami, K., Yasuda, K., and Araki, M. (2002). Development of dorsal-ventral polarity in the optic vesicle and its presumptive role in eye morphogenesis as shown by embryonic transplantation and *in ovo* explant culturing. *Dev.Biol.* **248**, 319-330.

Unoki, K., Ohba, N., and Hoyt, W.F. (2002). Optical coherence tomography of superior segmental optic hypoplasia. *Br.J.Ophthalmol.* **86**, 910-914.

Vance, K.W., Carreira, S., Brosch, G., and Goding, C.R. (2005). Tbx2 is overexpressed and plays an important role in maintaining proliferation and suppression of senescence in melanomas. *Cancer Res.* **65**, 2260-2268.

Vecchi, A., Garlanda, C., Lamugnani, M.G., Renati, M., Matteucci, C., Stoppacciaro, A., Schnurch, H., Risau, W., Ruco, L., Mantovani, A., and *et al.* (1994). Monoclonal antibodies specific for endothelial cells of mouse blood vessels. Their application in the identification of adult and embryonic endothelium. *Eur.J.Cell Biol.* **63**, 247-254.

Vincent, JP. and Briscoe, J. (2001). Morphogens. *Curr.Biol.* **11**, R851-R854.

Vitiello, C., D'Adamo, P., Gentile, F., Vingolo, E.M., Gasparini, P., and Banfi, S. (2005). A novel *GJA1* mutation causes oculodentodigital dysplasia without syndactyly. *Am.J.Med.Genet.* **133A**, 58-60.

Vogel-Hopker, A., Momose, T., Rohrer, H., Yasuda, K., Ishihara, L., and Rapaport, D.H. (2000). Multiple functions of fibroblast growth factor-8 (FGF-8) in chick eye development. *Mech.Dev.* **94**, 25-36.

Voronina, V.A., Kozhemyakina, E.A., O'Kernick, C.M., Kahn, N.D., Wenger, S.L., Linberg, J.V., Schneider, A.S., and Mathers, P.H. (2004). Mutations in the human *RAX* homeobox gene in a patient with anophthalmia and sclerocornea. *Hum.Mol.Genet.* **13**, 315-322.

Wagner, E., McCaffery, P., and Drager, U.C. (2000). Retinoic acid in the formation of the dorsoventral retina and its central projections. *Dev.Biol.* **222**, 460-470.

Wallis, D.E., Roessler, E., Hehr, U., Nanni, L., Wiltshire, T., Richieri-Costa, A., Gillessen-Kaesbach, G., Zackai, E.H., Rommens, J., and Muenke, M. (1999). Mutations in the homeodomain of the human SIX3 gene cause holoprosencephaly. *Nat.Genet.* **22**, 196-198.

Wallman, J. and Winawer, J. (2004). Homeostasis of eye growth and the question of myopia. *Neuron.* **43**, 447-468.

Walther, C. and Gruss, P. (1991). *Pax-6*, a murine paired box gene, is expressed in the developing CNS. *Development.* **113**, 1435-1449.

Watterson, R.L. (1965). Structure and mitotic behavior of the early neural tube. *Organogenesis*, New York: Rinehart and Winston, 129-159.

Wawersik, S., Purcell, P., Rauchman, M., Dudley, A.T., Robertson, E.J., and Maas, R. (1999). BMP7 acts in murine lens placode development. *Dev.Biol.* **207**, 176-188.

Wetts, R. and Fraser, S.E. (1988). Multipotent precursors can give rise to all major cell types of the frog retina. *Science.* **239**, 1142-1145.

White, T.W., Sellitto, C., Paul, D.L., and Goodenough, D.A. (2001). Prenatal lens development in Connexin43 and Connexin50 double knockout mice. *Invest Ophthalmol.Vis.Sci.* **42**, 2916-2923.

Wilkie, A.O., Tang, Z., Elanko, N., Walsh, S., Twigg, S.R., Hurst, J.A., Wall, S.A., Chrzanowska, K.H., and Maxson, RE. (2000). Functional haploinsufficiency of the human homeobox gene MSX2 causes defects in skull ossification. *Nat.Genet.* **24**, 330-331.

Wilkinson, D.G. (1992). *In situ hybridisation.* Oxford; Oxford University Press.

Wilkinson, D.G. (2001). Multiple roles of EPH receptors and ephrins in neural development. *Nat.Rev.Neurosci.* **2**, 155-164.

Winnier, G., Blessing, M., Labosky, P.A., and Hogan, B.L. (1995). Bone morphogenetic protein-4 is required for mesoderm formation and patterning in the mouse. *Genes Dev.* **9**, 2105-2116.

Wolpert, L. (1969). Positional information and the spatial pattern of cellular differentiation. *J.Theoret.Biol.* **25**, 1-47.

Wolpert, L. and Kerszberg, M. (2003). Patterning and positional information. *Patterning in vertebrate development.* New York, Oxford University Press, 1-9.

Woods, K.S., Cundall, M., Turton, J., Rizotti, K., Mehta, A., Palmer, R., Wong, J., Chong, W.K., Al-Zyoud, M., El-Ali, M., Otonkoski, T., Martinez-Barbera, JP.,

Thomas, P.Q., Robinson, I.C., Lovell-Badge, R., Woodward, K., and Dattani, M.T. (2005). Over- and underdosage of SOX3 is associated with infundibular hypoplasia and hypopituitarism. *Am.J.Hum.Genet.* **76**, 833-849.

Woollard, A. and Hodgkin, J. (2000). The caenorhabditis elegans fate-determining gene mab-9 encodes a T-box protein required to pattern the posterior hindgut. *Genes Dev.* **14**, 596-603.

Wright, C.S., Becker, D.L., Lin, J.S., Warner, A.E., and Hardy, K. (2001). Stage-specific and differential expression of gap junctions in the mouse ovary: connexin-specific roles in follicular regulation. *Reproduction.* **121**, 77-88.

Wright, T.J., Ladher, R., McWhirter, J., Murre, C., Scoenwolf, G.C., and Mansour, S.L. (2004). Mouse FGF15 is the orthologue of human and chick FGF19, but is not uniquely required for otic induction. *Dev.Biol.* **269**, 264-275.

Wu, L.Y., Li, M., Hinton, D.R., Guo, L., Jiang, S., Wang, J.T., Zeng, A., Xie, J.B., Snead, M., Shuler, C., Maxson, RE., and Liu, Y.H. (2003). Microphthalmia resulting from MSX2-induced apoptosis in the optic vesicle. *Investigative Ophthalmology Visual Science.* **44**, 2404-2412.

Wu, P., Jiang, TX., Suksaweang, S., Widelitz, R.B., and Chuong, CM. (2004). Molecular shaping of the beak. *Science.* **305**, 1465-1466.

Wuyts, W., Reardon, W., Preis, S., Homfray, T., Rasore-Quartino, A., Christians, H., Willems, P.J., and Van Hul, W. (2000). Identification of mutations in the MSX2 homeobox gene in families affected with foramina parietalia permagna. *Hum.Mol.Genet.* **9**, 1251-1255.

Xie, M.H., Holcomb, I., Deuel, B., Dowd, P., Huang, A., Vagts, A., Foster, J., Liang, J., Brush, J., Gu, Q., Hillan, K., Goddard, A., and Gurney, A.L. (1999). FGF-19, a novel fibroblast growth factor with unique specificity for FGFR4. *Cytokine.* **11**, 729-735.

Yamada, M., Revelli, J.P., Eichele, G., Barron, M., and Schwartz, R.J. (2000). Expression of chick Tbx-2, Tbx-3, and Tbx-5 genes during early heart development: evidence for BMP2 induction of Tbx2. *Dev.Biol.* **228**, 95-105.

Yamaguchi, K., Shirakabe, K., Shibuya, H., Irie, K., Oishi, I., Ueno, N., Taniguchi, T., Nishida, E., and Matsumoto, K. (1995). Identification of a member of the MAPKKK family as a potential mediator of TGF-ß signal transduction. *Science*. **270**, 2008-2011.

Yamashita, H., Ten Dijke, P., Heldin, C.H., and Miyazono, K. (1996). Bone morphogenetic protein receptors. *Bone*. **19**, 569-574.

Yancey, S.B., Biswal, S., and Revel, JP. (1992). Spatial and temporal patterns of distribution of the gap junction protein connexin43 during mouse gastrulation and organogenesis. *Development*. **114**, 203-212.

Yasuda, K., Momose, T., and Takahashi, Y. (2000). Applications of microelectroporation for studies of chick embryogenesis. *Dev.Growth Differ*. **42**, 203-206.

Yoshikawa, S.I., Aota, S., Shirayoshi, Y., and Okazaki, K. (2000). The ActR-I activin receptor protein is expressed in notochord, lens placode and pituitary primordium cells in the mouse embryo. *Mech.Dev*. **91**, 439-444.

Yun, K., Mantani, A., Garel, S., Rubenstein, J., and Israel, M.A. (2004). *Id4* regulates neural progenitor proliferation and differentiation in vivo. *Development*. **131**, 5441-5448.

Zakin, L. and De Robertis, E.M. (2004). Inactivation of mouse *Twisted gastrulation* reveals its role in promoting *Bmp4* activity during forebrain development. *Development*. **131**, 413-424.

Zecca, M., Basler, K., and Struhl, G. (1995). Sequential organizing activities of engrailed, hedgehog and decapentaplegic in the *Drosophila* wing. *Development*. **121**, 2265-2278.

Zecca, M., Basler, K., and Struhl, G. (1996). Direct and long-range action of a wingless morphogen gradient. *Cell*. **87**, 833-844.

Zhang, X.M. and Yang, X.J. (2001). Temporal and spatial effects of Sonic hedgehog signaling in chick eye morphogenesis. *Dev.Biol*. **233**, 271-290.

Zhao, S., Hung, F.C., Colvin, J.S., White, A., Dai, W., Lovicu, F.J., Ornitz, D.M., and Overbeek, P.A. (2001). Patterning the optic neuroepithelium by FGF signaling and Ras activation. *Development*. **128**, 5051-5060.

Zhao, S., Thornquist, S.C., and Barnstable, C.J. (1995). In vitro transdifferentiation of embryonic rat retinal pigment epithelium to neural retina. *Brain Res.* **677**, 300-310.

Zimmerman, L.B., De Jesus-Escobar, J.M., and Harland, R.M. (1996). The spemann organizer signal noggin binds and inactivates bone morphogenetic protein 4. *Cell.* **86**, 599-606.

Zuber, M.E., Perron, M., Philpott, A., Bang, A., and Harris, W.A. (1999). Giant eyes in *Xenopus laevis* by overexpression of *XOptx2*. *Cell.* **98**, 341-352.

Zúñiga, A., Haramis, AP.G., McMahon, A.P., and Zeller, R. (1999). Signal relay by Bmp antagonsim controls the SHH/FGF4 feedback loop in vertebrate limb buds. *Nature*. **401**, 598-602.